Development of ROS-responsive Turn-on Fluorogenic Prodrugs for the Delivery of Anti-inflammatory and Anti-cancer Drugs along with Hydrogen Sulfide

A Thesis

Submitted in Partial Fulfilment of the

Requirements for the Degree of

Doctor of Philosophy

by

Abu Sufian

Department of Chemistry

Indian Institute of Technology Guwahati

Assam – 781039, India

August 2023

TH-3161_176122050

TH-3161_176122050

Development of ROS-responsive Turn-on Fluorogenic Prodrugs for the Delivery of Anti-inflammatory and Anti-cancer Drugs along with Hydrogen Sulfide

A Thesis

Submitted in Partial Fulfilment of the

Requirements for the Degree of

Doctor of Philosophy

By

Abu Sufian

Roll no. - 176122050

Department of Chemistry

Indian Institute of Technology Guwahati

Assam – 781039, India

August 2023

TH-3161_176122050

TH-3161_176122050

Dedicated To

My Parents and Family Members

TH-3161_176122050

TH-3161_176122050

Indian Institute of Technology Guwahati

Department of Chemistry

Guwahati

Assam – 781039

STATEMENT

I hereby declare that the research work described in the thesis entitled "***Development of ROS-responsive Turn-on Fluorogenic Prodrugs for the Delivery of Anti-inflammatory and Anti-cancer Drugs along with Hydrogen Sulfide***" is the outcome of investigations carried out by me under the supervision of **Dr. Krishna P. Bhabak** at Department of Chemistry, Indian Institute of Technology Guwahati, India, for the award of degree of Doctor of Philosophy.

In keeping with the general practice of reporting scientific observations, due acknowledgements have been made wherever the work described in this thesis is based on the findings of other investigators. Any omission that might have occurred by oversight or mistake is unintentional and gravely regretted.

_____

Abu Sufian

Roll No: 176122050

TH-3161_176122050

TH-3161_176122050

Indian Intitute of Technology Guwahati
Department of Chemistry
Guwahati
Assam – 781039

CERTIFICATE

This is to certify that the research work presented in the thesis entitled "***Development of ROS-responsive Turn-on Fluorogenic Prodrugs for the Delivery of Anti-inflammatory and Anti-cancer Drugs along with Hydrogen Sulfide***" by **Mr. Abu Sufian** (Roll no: 176122050) for the award of the degree of Doctor of Philosophy is an authentic record of the results obtained from the research work carried out under my supervision at Department of Chemistry, Indian Institute of Technology Guwahati, India. The research work reported in his thesis is original and the same has not been submitted elsewhere for a degree.

Dr. Krishna P. Bhabak

(Supervisor)

Associate Professor
Department of Chemistry
Indian Institute of Technology Guwahati
Assam – 781039

TH-3161_176122050

TH-3161_176122050

Acknowledgements

I would like to take this opportunity to appreciate the kind help and support of all the people around me to make the journey a very memorable one. Without their help, it would not have been possible to achieve this goal.

First and foremost, I would like to express my deepest gratitude towards my thesis supervisor **Dr. Krishna P. Bhabak** for his constant and persistent support, motivation and guidance throughout the entire tenure of my research work. His perseverant support, unparalleled efforts and never-ending patience, even in the midst of COVID-19 pandemic, proved to be extremely important for fulfilling this goal. Moreover, his mindful scrutiny and scrupulous suggestions of manuscripts were invaluable assets in this journey. Under his close supervision, the ideals of a true researcher have been inculcated within me. It has been, indeed, a very nice and pleasant experience in working with him.

I would like to extend my acknowledgement to my doctoral committee members **Prof. Abu Taleb Khan** (Chairman), **Dr. Animesh Das** (Member) and **Prof. Shankar Prasad Kanaujia** (Member) for taking their time out of their busy schedule to review my progress and also to share their knowledge, provide invaluable suggestions to overall improve my research.

I am thankful to **Indian Institute of Technology Guwahati** for providing me fellowship, and to the **Department of Chemistry**, **Central Instruments Facility** (**CIF**) for providing me with instrumental facilities such as nuclear magnetic resonance (NMR), ESI-MS, and other instruments. Additionally, I would like to acknowledge all the instrument operators and non-teaching staffs of Department of Chemistry, Administrative Building, IIT Guwahati for extending their kind help in whichever ways, as applicable.

I would like to specially acknowledge my colleague **Dr. Kaustav Banerjee**, **Dr. Debojit Bhattacherjee** for their homely care, other professional help and moral support in every academic and personal perspectives, during the ups and downs of my PhD journey. I am forever grateful and thankful towards other lab members **Dr. Sulendar K. Mahato**, **Ms. Shivani Marandi**, **Ms. Pallavi Barman**, **Mr. Rahul Kesarwani**, **Mr. Roopjyoti Misra**, **Mr. MD. Badirujjaman, Ms. Nikita Pal**, and **Mr. Samanaway Das** for bearing with me throughout the entirety of my research journey.

TH-3161_176122050

Next I would like to thank all the project students **Ms. Tripti Mishra**, **Mr. Abhay Srivastava**, **Mr. Tushar Kanti Roy**, and **Mr. Ashes Roy** for their contributions towards my research work.

I would like to specially acknowledge my labmates **Dr. Debojit Bhattacherjee**, **Ms. Pallavi Barman**, and **Mr. MD. Badirujjaman** for their active collaborative effort for cellular studies.

I would like to extend my thanks to all of my batch mates and friends specially **Ms. Rupa Bai Addanki**, **Mr. Tipu Alam**, **Mr. Paresh K. Behera** for their homely care and moral support in every academic and personal perspectives, during the ups and downs of my PhD journey.

Next, most importantly I would like to thank my family. I would like to mention my father **Mr. Rustum Ali** and my mother **Mrs. Bibi Fultan Nesha** and my grandfather **Haji Makbul Hussain** for raising me into who I am. Last but not the least, I must acknowledge the unparalleled motivation and constant encouragement I received from **Mst. Sarifa Sarmin** and **Dr. Nasim Akhtar** during my difficult times. Finally, I would like to thank the Almighty God for making this journey possible and giving me the strength, perseverance and determination to work.

Sd/-_____

Abu Sufian

TH-3161_176122050

Table of Contents

TH-3161_176122050

TH-3161_176122050

TH-3161_176122050

TH-3161_176122050

TH-3161_176122050

TH-3161_176122050

Abbreviations

ATP	Adenosine triphosphate
ACN	Acetonitrile
AIBN	Azobisisobutyronitrile
B_2pin_2	Bis(pinacolato)diboron
Bcl2	B-cell lymphoma 2
Conc.	Concentrated
Calcd.	Calculated
CS_2	Carbondisulfide
CA	Carbonic anhydrase
CAT	Cysteine amino transferase
CBS	Cystathionine-β-synthase
$CDCl_3$	Chloroform-d_3
COS	Carbonyl sulfide
COX-2	Cyclooxygenase-2
CSE	Cystathionine-γ-lyase
Cum-OOH	Cumene hydroperoxide
CYP	Cytochrome P450
Cys	L-Cysteine
DADS	Diallyl disulfide
DAO	Diamine oxidase
DMF	*N*,*N*-Dimethylformamide
DCM	Dichloromethane
DATS	Diallyl trisulfide
DIPEA	Diisopropylethylamine
DBU	1,8-Diazabicyclo[5.4.0]undec-7-ene
DIBAL-H	Diisobutylaluminium hydride
DBTS	Dibenzyl trisulfide
DCFH-DA	Dichloro-dihydro-fluorescein diacetate
DMEM	Dulbecco's modified Eagle medium
DMSO	Dimethyl sulfoxide
DPBS	Dulbecco's phosphate buffered saline

TH-3161_176122050

DTT	1,4-Dithiothreitol
DTTS	Diallyl tetrasulfide
ESI-MS	Electrospray ionization mass spectroscopy
EtOAc	Ethyl acetate
EtOH	Ethanol
FBS	Fetal bovine serum
g	Gram
GAPDH	Glyceraldehyde-3-phosphate dehydrogenase
GSH	Glutathione reduced
GSSG	Glutathione disulfide
h	Hour(s)
HCl	Hydrochloric acid
H_2S	Hydrogen sulfide
H_2SO_4	Sulfuric acid
HOCl	Hypochlorus acid
H_2O_2	Hydrogen peroxide
HPLC	High performance liquid chromatography
HS^-	Hydrosulfide
IC_{50}	Inhibitory concentration 50%
KO_2	Potassium dioxide
KOAc	Potassium acetate
LOD	Limit of detection
M	Molar
MeOH	Methanol
M.P.	Melting point
MB	Methylene blue
MeI	Methyl iodide
MCF-7	Michigan cancer foundation-7
Min	Minute(s)
mL	Millilitre
mM	Milimolar
mm	Millimetre
mmol	Milimole

TH-3161_176122050

3-MST	3-Mercaptopyruvate sulfurtransferase
MTT	(3-(4,5-Dimethylthiazol-2-yl)-2,5-diphenyltetrazolium bromide)
$NaHCO_3$	Sodium bicarbonate
Na_2SO_4	Sodium sulfite
NaOMe	Sodium methoxide
Na_2S	Sodium sulfide
NBS	*N*-bromosuccinimide
NAC	*N*-acetyl L-cysteine
$NADP^+$	Nicotinamide adenine dinucleotide phosphate oxidized
NADPH	Nicotinamide adenine dinucleotide phosphate reduced
NaSH	Sodium hydrosulfide
NMR	Nuclear magnetic resonance
NO	Nitric oxide
Nrf2	Nuclear factor erythroid 2-releated factor 2
NSAIDs	Non-steroidal anti-inflammatory drugs
ºC	Degree Celsius
OSCs	Organosulfur compounds
PAG	*D,L*-Propargyl glycine
PBS	Phosphate Buffer Saline
PBr_3	Phosphorus bromide
Pet. Ether	Petroleum ether (60 – 80)
Py	Pyridine
ppm	Parts per million
Q-TOF	Quadrupole time-of-flight
RIPA	Radio-immunoprecipitation assay P (Lysis buffer)
RNS	Reactive nitrogen species
ROS	Reactive oxygen species
rt/RT	Room temperature
TLC	Thin layer chromatography
TEA	Triethylamine
THF	Tetrahydrofuran
TFA	Trifluoroacetic acid

TH-3161_176122050

TNBC	Triple-negative breast cancer
TNF-α	Tissue necrosis factor-α
t-Bu-OOH	*tert*-Butyl hydroperoxide
UV-Vis	Ultra-violet visible
δ	Chemical shift (ppm)
ΔOD	Difference in optical density
μg	Microgram
μL	Microliter
μM	Micromolar

TH-3161_176122050

Reactive oxygen species (ROS) play important roles in physiological as well as pathological conditions. These are chemically reactive oxygen-containing species such as hydrogen peroxide (H_2O_2), superoxide (O_2^-), hydroxyl radical ($^{\cdot}OH$), hypochlorite (OCl^-), and singlet oxygen ($^1O_2$).[1] H_2O_2 is comparatively less reactive and relatively more stable among all the ROS. Therefore, it can translocate from one organelle to other organelles of the cells and acts as a signalling molecule.[2] Moreover, H_2O_2 plays a crucial role in physiological functions when levels of ROS are optimum.[3] However, H_2O_2 plays a major role in the production of more toxic hydroxyl radicals ($^{\cdot}OH$) in the presence of iron metal (Fe^{2+}). Hydroxyl radical is defined as the most reactive oxidizing species and has an extremely short half-life.[4] Therefore, it reacts with biological membranes, proteins, and lipids, which leads to a condition known as oxidative stress.[5] Furthermore, oxidative stress is the cause of oxidative damage of DNA, biological membranes, proteins, and lipids, which induces various diseases, including neurodegenerative disorders, inflammatory diseases, thyroid diseases, cardiovascular diseases, and cancer.[6] To protect the cells from different pathogens, GSH plays a crucial role as an antioxidant to detoxify the ROS.[7] It is to be noted that hydrogen sulfide (H_2S) is indirectly involved in synthesizing the GSH, which is a more abundant non-enzymatic anti-oxidant in the cells.[8] Although several drugs marketed for the treatment of ROS-related diseases specially cancer and inflammatory diseases. However, these drugs have several side-effects and limitations. Therefore, ROS-responsive prodrugs of anti-cancer drugs developed over time to overcome the side-effects of corresponding conventional drugs. Further, ROS-responsive prodrugs of anti-cancer and anti-inflammatory drugs with co-delivery of H_2S are necessary to develop for overcoming the side-effects of conventional drugs effectively.

The present thesis, entitled "***Development of ROS-responsive Turn-on Fluorogenic Prodrugs for the Delivery of Anti-inflammatory and Anti-cancer Drugs along with Hydrogen Sulfide***" consists of five chapters, based on the results of experimental works performed during the complete course of PhD research tenure.

Chapter 1: Introduction

A general introduction relevant to ROS, H_2S, and their pharmacological functions have been discussed in chapter 1. The introduction has been divided into five sections; firstly, the production of ROS (intracellular and extracellular sources) and its detoxification

TH-3161_176122050

process has been discussed elaborately. Secondly, the development of ROS-responsive prodrugs of anti-inflammatory and anti-cancer drugs (**1**-**4**) has been reviewed thoroughly (Figure 1).[9-12]

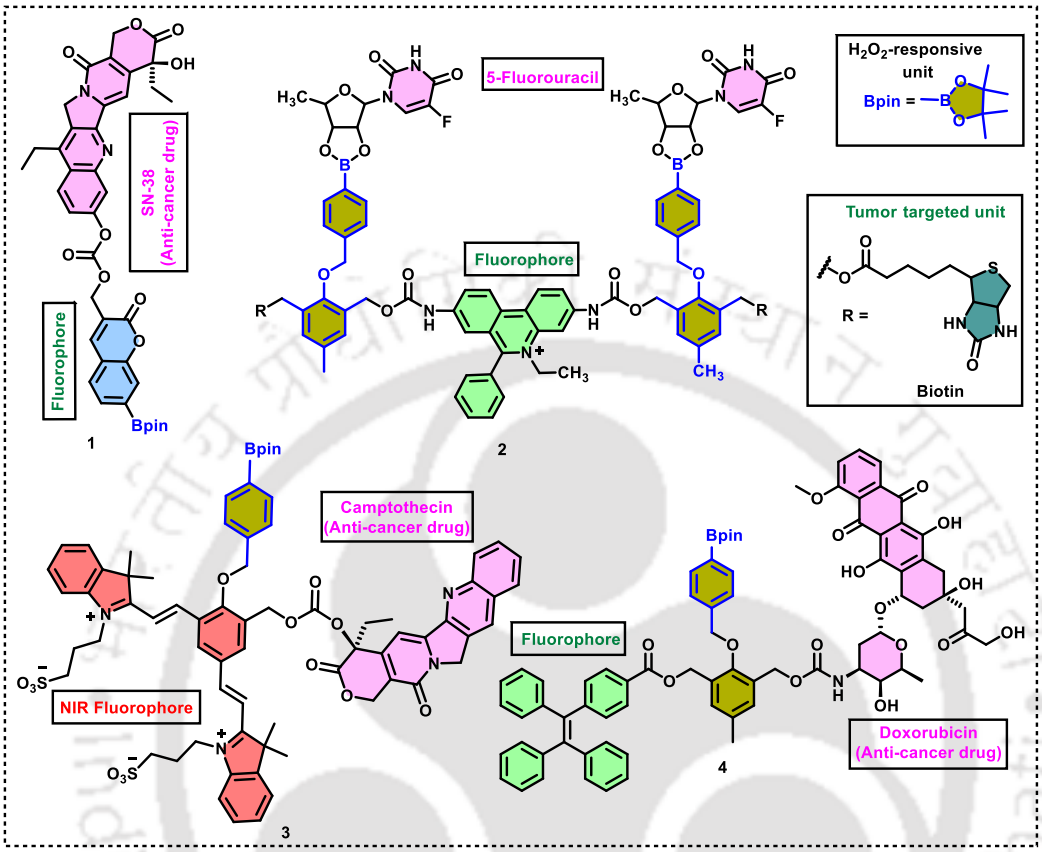

Figure 1. Chemical structures of some representative H_2O_2-responsive fluorogenic prodrugs.

Thirdly, the biological functions of H_2S and its correlation with ROS have been elaborated (Figure 2A). Fourthly, owing to the emergence of H_2S research in medical science, methods for accurate and quantitative detection of H_2S in biological samples have been discussed. Finally, along with intracellular and dietary sources of H_2S, a discussion has been made on the development of various stimuli-triggered organic donors of H_2S, such as (i) hydrolysis-based H_2S donors, (ii) biothiol-triggered H_2S donors, (iii) ROS-responsive H_2S donors etc. (Figure 2A).[13-16] Furthermore, a brief discussion has been made on the importance of H_2S delivery with anti-inflammatory drug as H_2S-NSAID conjugates as reported in the literature, which are non-fluorogenic (Figure 2B).[17-19]

TH-3161_176122050

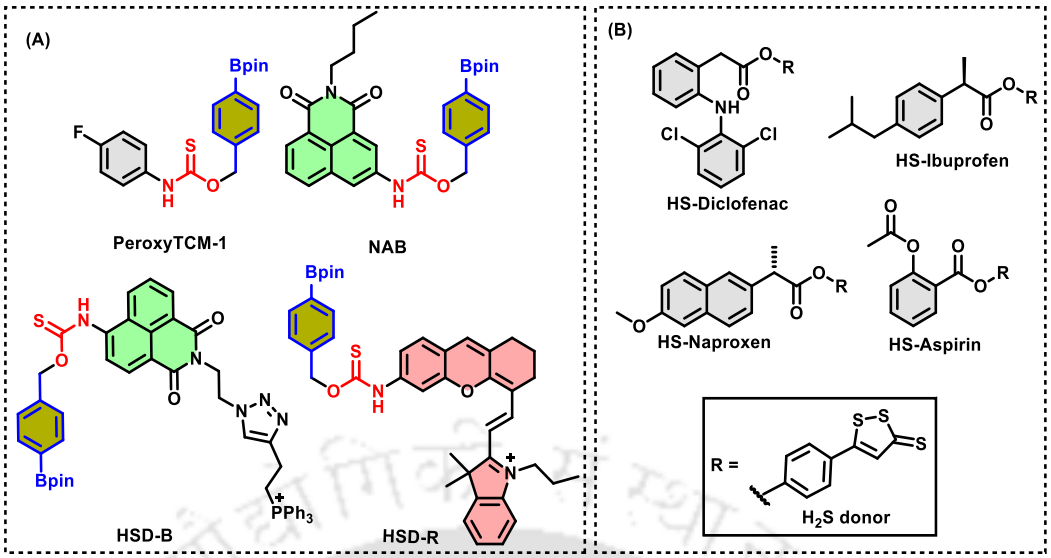

Figure 2. Chemical structures of some representative (A) H_2O_2-responsive fluorogenic H_2S donors and (B) H_2S-NSAID hybrids.

Inspired by the previous reports on ROS-responsive turn-on fluorogenic prodrugs of anti-cancer drugs and peroxide-triggered fluorogenic H_2S donors, we developed the interest in designing ROS-responsive fluorogenic prodrugs of anti-inflammatory and anti-cancer drugs along with H_2S delivery. The current thesis explored the following possibilities:

1. It is unclear which types of linkers will be chosen for developing boronate ester-coupled ROS-responsive probes for sensing H_2O_2 or prodrugs for sustained drug delivery. Therefore, a proper investigation is necessary to understand the importance of fluorophores as well as linkers.
2. A ROS-responsive fluorogenic prodrug of anti-inflammatory drugs, which is necessary for delivering the drug selectively towards inflammatory sites over normal sites and real-time monitoring of drug release, has not been developed yet.
3. Although a non-fluorogenic H_2S-NSAID conjugated system has been developed to reduce the side-effects of NSAIDs, stimuli-triggered fluorogenic prodrugs of NSAIDs are still missing.
4. ROS-responsive turn-on fluorogenic prodrugs of anti-cancer drugs have been developed; however, ROS-responsive fluorogenic prodrugs of anti-cancer drugs with concomitant release of H_2S are yet to be developed.

Chapter 2: Peroxide-responsive boronate ester-containing turn-on fluorogenic probes: impact of the self-immolative linkers on peroxide-triggered sustained drug delivery

TH-3161_176122050

As discussed in chapter 1, several ROS-responsive non-fluorogenic as well as fluorogenic prodrugs have been developed over time; however, a proper rationalization is missing in understanding the importance of different linkers for connecting the boronate ester moiety with different fluorophores. In order to achieve our objective, we designed and synthesized nine probes where boronate ester was coupled *via* three different linkers (direct, ether, and carbonate) with three different fluorophores (coumarin, naphthalimide, and fluorescein units) (Scheme 1).

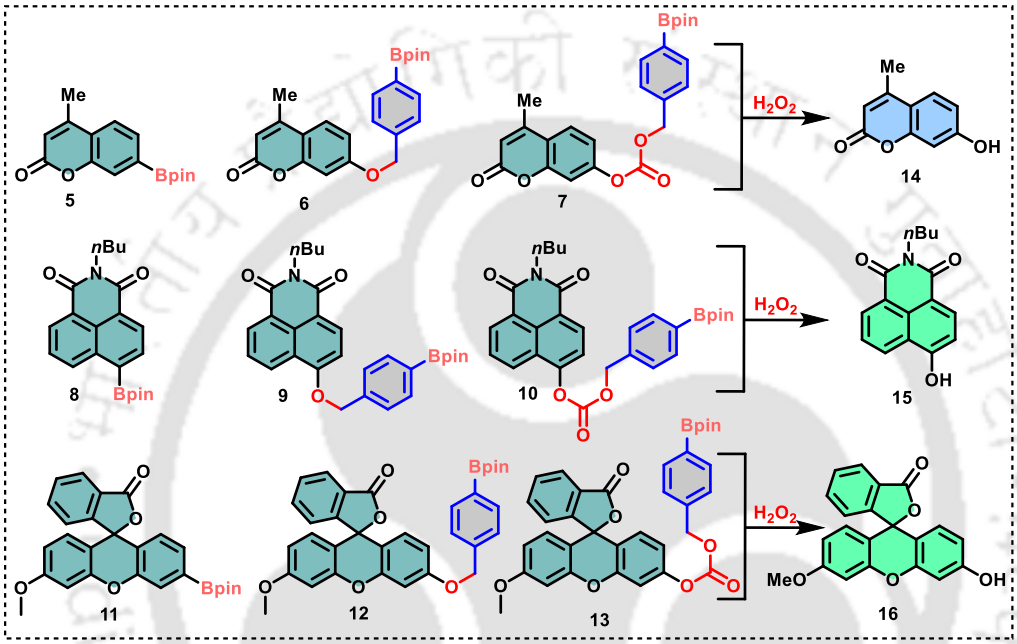

Scheme 1. Chemical structures of the designed turn-on fluorogenic probes and the schematic representation for fluorophore release in the presence of H_2O_2.

Furthermore, we thoroughly carried out spectroscopic studies, HPLC, and cellular studies to understand the importance of different linkers. We observed in spectroscopic studies that, as compared to the ether- or carbonate-linked probes, directly connected boronate ester probes **5**, **8**, and **11** exhibited strong sensitivities towards H_2O_2 (Figure 3A-C). Furthermore, we noticed that all three probes **11-13** are compatible with cellular conditions, and they detected the endogenous level of H_2O_2 (Figure 3D). However, a higher emission response in the green channel was observed for probe **11** as compared to probes **12** and **13**, indicating the higher sensitivity of the directly linked probe **11**. It can be concluded that a directly coupled boronate ester probe is capable of detecting very trace amounts of H_2O_2. However, a sustained drug delivery system will be an additional benefit from the self-immolative probes.

TH-3161_176122050

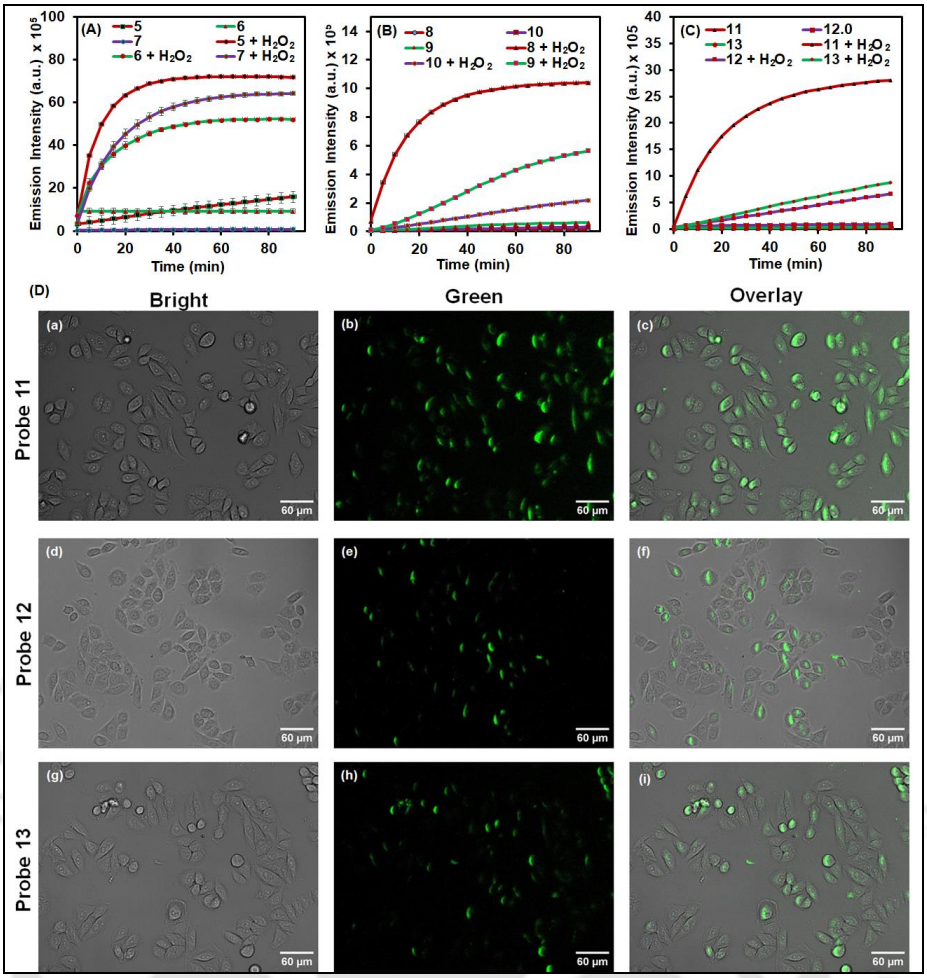

Figure 3. Emission spectra of (A) coumarin-, (B) naphthalimide- and (C) fluorescein-based probes (10 µM) with and without H_2O_2 (200 µM) over 90 min in phosphate buffer (20 mM) of pH 7.5. (D) Fluorescence microscopy images (bright field, green channel, and overlay) of HeLa cells in the presence of fluorescein-based probes **11-13** for the detection of the endogenous level of H_2O_2.

Chapter 3: Peroxide-responsive prodrug of non-steroidal anti-inflammatory drug diclofenac: sustained drug release with turn-on near-infrared fluorescence

As we observed in chapter 2, self-immolative boronate ester-coupled ROS-responsive fluorogenic probes will be suitable for developing a prodrug for sustained delivery of the drug. Therefore, we developed a unique peroxide-responsive fluorogenic prodrug (**DCI-ROS**) of NSAID diclofenac (**DCF**) using NIR-fluorophore (**DCI-OH**) in such a way that the drug will be released sustainably (Figure 4). In addition, a negative control prodrug (**DCI-Con**) was also synthesized without any H_2O_2-triggering unit to understand the role of boronate ester moiety in activating the drug release.

TH-3161_176122050

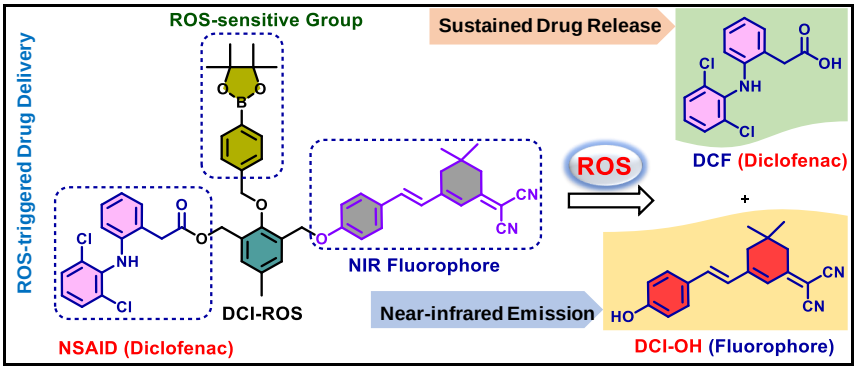

Figure 4. Schematic representation of our rationally designed ROS-responsive prodrug of diclofenac (**DCI-ROS**).

Preliminary spectroscopic studies indicated the release of the fluorophore in the presence of H_2O_2 (Figure 5A). Moreover, the fluorophore was released from the prodrug continuously throughout 10 h and became saturated, which validated our hypothesis of sustained drug release (Figure 5B). Since the fluorophore release was increased with increasing the concentration of H_2O_2, more amounts of drugs per mole will be released in regions with elevated levels of H_2O_2 (inflammatory sites) (Figure 5C). In addition, the prodrug **DCI-ROS** was found to be non-toxic towards triple-negative breast cancer cells MDA-MB-231 and macrophage cells RAW 264.7 (Figure 5D and 5E). Furthermore, we observed the LPS pre-treated RAW 264.7 cells showed significant enhancement in red emission compared to those without treating LPS, indicating the LPS-induced ROS production, which results in higher fluorophore release from inflamed cells. (Figure 5F). This result indicates that more amount of drugs per mole would be released from the prodrug in inflammatory sites over normal tissues. To study the anti-inflammatory activity, COX-2 was overexpressed in RAW 264.7 cells using lipopolysaccharide (LPS) followed by prodrug **DCI-ROS** was treated dose-dependently (50 and 100 µM). Interestingly, 100 µM of the prodrug downregulated COX-2 significantly, which is consistent with the activity of free diclofenac (Figure 5G). This outcome amply the release of the drug from the prodrug and showed its anti-inflammatory activity.

TH-3161_176122050

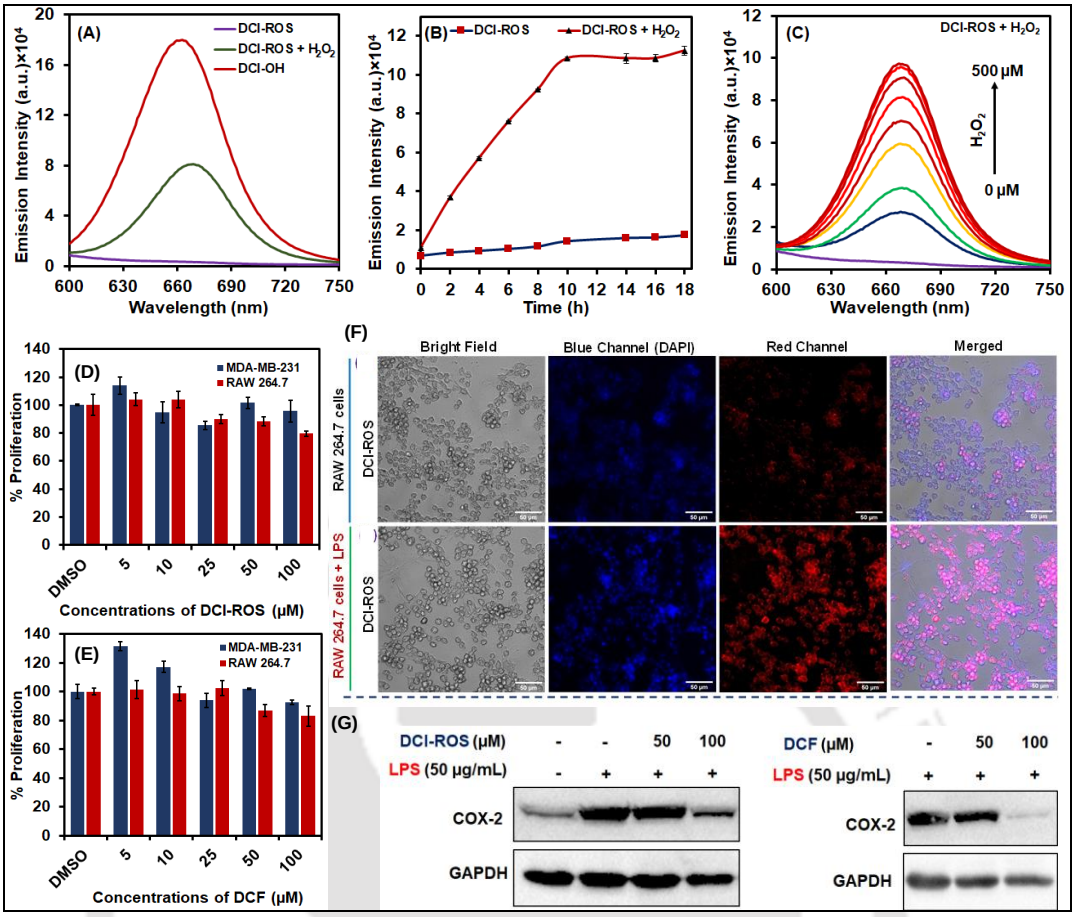

Figure 5. (A) Emission spectrum of prodrug **DCI-ROS** (10 µM) with and without H_2O_2 (200 µM) along with the emission spectrum of pure **DCI-OH** (10 µM). The emission spectra of **DCI-ROS** + H_2O_2 was recorded after 14 h; (B) Emission spectra of **DCI-ROS** (10 µM) in the absence and presence of H_2O_2 (200 µM) with variable time (0-18 h); (C) Emission spectra of **DCI-ROS** (10 µM) with variable concentration of H_2O_2 (0-500 µM) with a fixed incubation time of 14 h; Phosphate buffer (20 mM, pH 7.5, with 50% DMSO v/v). λ_{ex} = 550 nm, λ_{em} = 670 nm. Cellular *via*bility of MDA-MB-231 and RAW 264.7 cells in the presence of (D) **DCI-ROS** and (E) **DCF**. (F). Fluorescence microscopy images (bright field, blue channel, red channel, and merged) of RAW 264.7 cells in the presence of **DCI-ROS** (50 µM) for endogenous ROS-triggered and LPS-induced ROS-triggered fluorogenic drug release. RAW 264.7 cells were pre-incubated with LPS (50 µgmL-1) for 14 h to elevate the ROS level. DAPI (blue channel) was used for the nuclear staining of cells. Scale bar: 50 µm. (G). Anti-inflammatory activity of the prodrug **DCI-ROS** as well as the **DCF** in RAW 264.7 cells. Western blot analysis for COX-2 protein expression level in RAW 264.7 cells and the effect of **DCI-ROS** (50 and 100 µM) and pure **DCF** in the LPS (50 µg/mL) pre-treated cells. GAPDH was used as a housekeeping gene.

TH-3161_176122050

Chapter 4: Peroxide-activatable turn-on fluorogenic prodrug of diclofenac: adjuvant drug delivery with hydrogen sulfide

We observed in chapter 3 that ROS-responsive prodrug **DCI-ROS** was capable of delivering the active drug in a sustainable manner and showed similar anti-inflammatory properties as the parent drug. However, the side-effects (gastrointestinal damage) of non-selective COX-2 inhibitors (NSAIDs) could be overcome by delivering the H_2S along with the NSAID. Therefore, we developed a peroxide-responsive fluorogenic prodrug (**DCF-HS**) of diclofenac and H_2S to deliver H_2S along with the drug diclofenac in a sustained manner and it may reduce the side-effects of the drug (Figure 6).

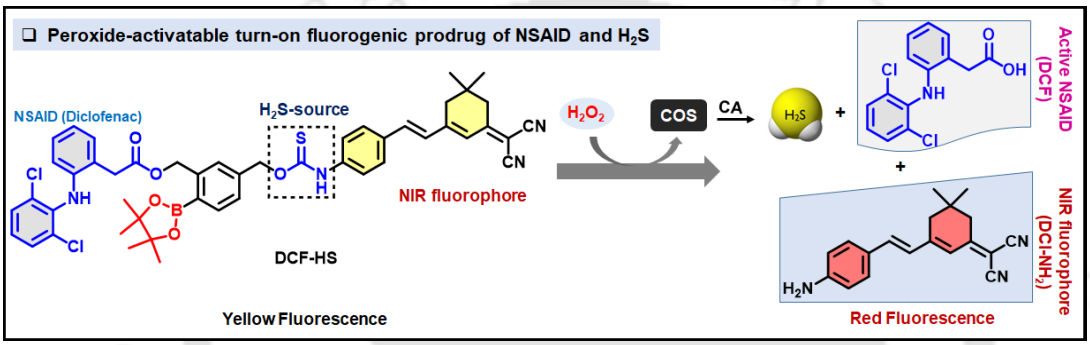

Figure 6. Schematic representation of our rationally designed ROS-responsive prodrug of diclofenac and delivery of H_2S (**DCF-HS**).

Upon synthesizing the prodrug **DCF-HS**, spectroscopic, HPLC, and cellular studies were carried out to investigate the sustained release of the drug and H_2S and its anti-inflammatory activity. From spectroscopic studies, we found that the drug was released from the prodrug **DCF-HS** in the presence of H_2O_2 (Figure 7A and 7B). Since the fluorophore release was increased with increasing the concentration of H_2O_2, more amounts of drugs per mole will be released in regions with elevated levels of H_2O_2 (inflammatory sites) (Figure 7C). Interestingly, the prodrug **DCF-HS** was found to be non-toxic up to 100 µM in cancer cells (HeLa) as well as normal cells (HEK-293) (Figure 7D). To investigate the H_2S release from the prodrug **DCF-HS**, HeLa cells were pre-treated with H_2S-triggered probe **WSP2**, followed by prodrug **DCF-HS** (Fluorophore was connected through thiocarbamate linker) or control prodrug **DCF-Con** (fluorophore was connected through carbamate linker) were treated (Figure 7E). Interestingly, blue fluorescence was observed for **DCF-HS**-treated cells due to the release of umbelliferone in the presence of released H_2S from the prodrug **DCF-HS**. Furthermore, the anti-inflammatory property of **DCF-HS** was analyzed in COX-2-overexpressed (LPS pre-

TH-3161_176122050

treated) RAW 264.7 cells (Figure 7F). Interestingly, 100 µM of the prodrug **DCF-HS** downregulated COX-2 significantly, which is consistent with the activity of free diclofenac (Figure 7F). This outcome amply the release of the drug from the prodrug and showed its anti-inflammatory activity.

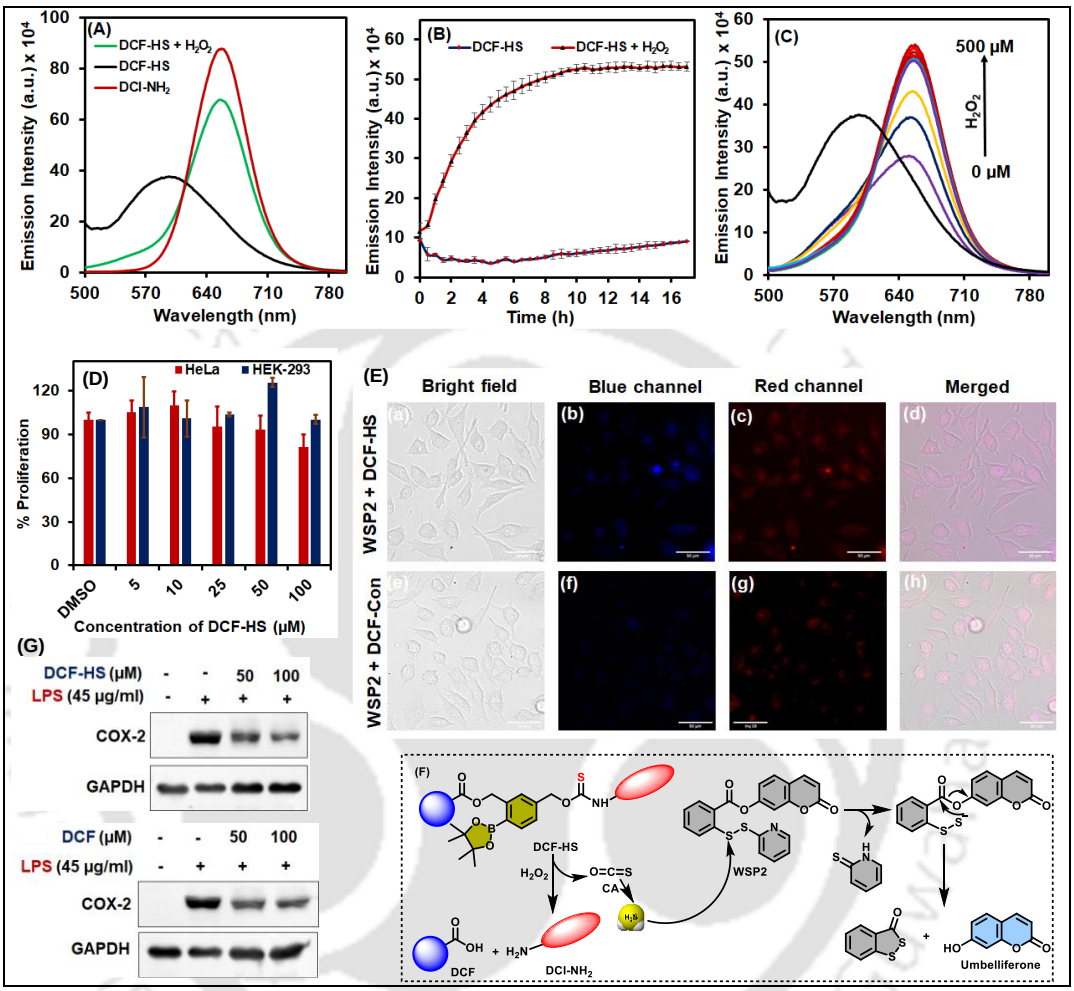

Figure 7. (A) Emission spectrum of prodrug **DCF-HS** (5 µM) with and without H_2O_2 (200 µM) along with the emission spectrum of pure **DCI-NH₂** (10 µM). The emission spectra of **DCF-HS** + H_2O_2 were recorded after 10 h. (B) Emission spectra of **DCF-HS** (5 µM) in the absence and presence of H_2O_2 (200 µM) with variable time (0-17 h). (C) Emission spectra of **DCF-HS** (5 µM) with variable concentration of H_2O_2 (0-500 µM) with a fixed incubation time of 10 h. The experiments were carried out in PBS (20 mM, pH 7.4, with 50% DMSO v/v). λ_{ex} = 472 nm. (D). Cellular viability of HeLa and HEK-293 cells in the presence of **DCF-HS** (E). Fluorescence microscopy images (bright field, blue channel, red channel, and merged) of HeLa cells in the presence of **DCF-HS** (50 µM) for the detection of released H_2S from the **DCF-HS** using the H_2S-selective turn-on fluorogenic probe **WSP2**. (F) Schematic representation for the detection of released H_2S from **DCF-HS** using H_2S-selective turn-on fluorogenic probe **WSP2**. (G). Anti-inflammatory activity

of the prodrug **DCF-HS** in RAW 264.7 cells. Western blot analysis for COX-2 protein expression level in RAW 264.7 cells and the effect of **DCF-HS** and pure **DCF** in the LPS pre-treated cells. GAPDH was used as a housekeeping gene.

Chapter 5: Peroxide-responsive turn-on fluorogenic prodrug of the anti-cancer drug amonafide: adjuvant drug delivery with hydrogen sulfide

ROS-responsive fluorogenic prodrugs of anti-cancer drugs developed over time to reduce the side-effects of conventional drugs and drug release were monitored using turn-on fluorophore. Since H_2S has several pharmacological properties, including antioxidant, anti-inflammatory and cytoprotective properties, the side-effects of anti-cancer drugs might be overcome by delivering H_2S with anti-cancer drugs. Therefore, we developed a peroxide-responsive turn-on fluorogenic prodrug of anti-cancer drug amonafide and delivery of H_2S along with it (Figure 8).

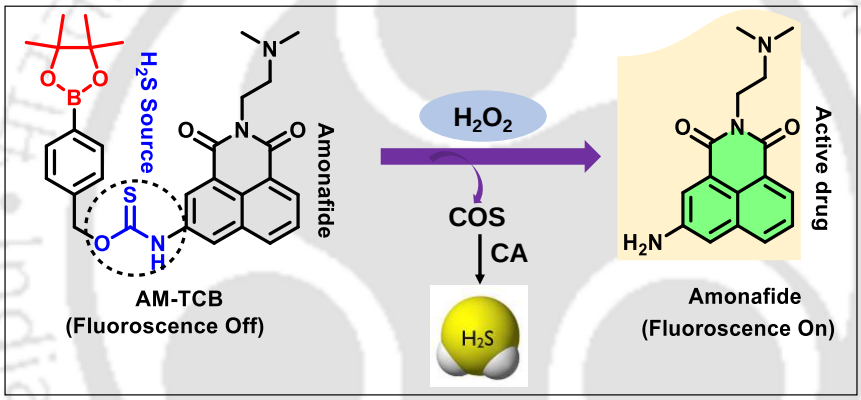

Figure 8. Schematic representation of peroxide-responsive turn-on fluorogenic prodrug for the co-delivery of amonafide and H_2S.

Upon synthesizing the designed prodrug **AM-TCB**, spectroscopic, HPLC, and cellular studies were carried out to investigate the drug and H_2S release from the prodrug. The spectroscopic results indicated that amonafide was released in the presence of H_2O_2 slowly over time and the amount of drug release increased gradually with increasing the concentration of H_2O_2 (Figure 9A and 9B). Moreover, the release of H_2S was confirmed by fluorescence spectroscopy using an H_2S-responsive fluorogenic probe **WSP2** (Figure 9C). At 450 nm, emission intensity increased when **AM-TCB** reacted with H_2O_2, followed by the addition of carbonic anhydrase and **WSP2** probe (green line), further confirmed with free umbelliferone (red line). In addition, cell viability was analyzed for normal cell line (HEK-293) (Figure 9D) and the cancer cell line (HeLa) (Figure 9E) against prodrug **AM-TCB** and drug amonafide. Interestingly, the prodrug **AM-TCB**

TH-3161_176122050

exhibited cytoprotective properties for normal cells compared to drug amonafide and showed similar anti- cancer activity as the parent drug for cancer cells HeLa.

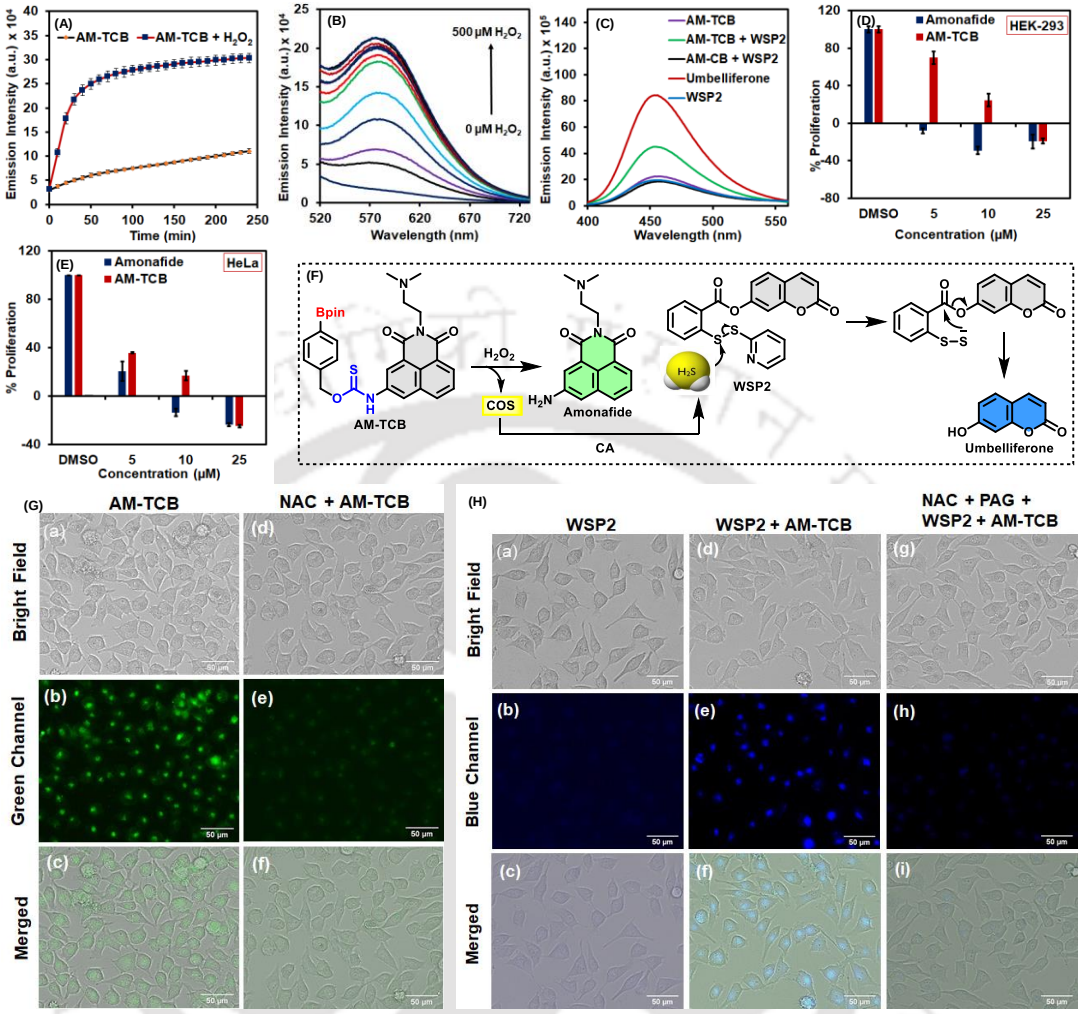

Figure 9.(A) Emission spectra of **AM-TCB** (5 μM) in the absence and presence of H_2O_2 (200 μM) with variable time (0-240 min); (B) Emission spectra of **AM-TCB** (5 μM) with variable concentration of H_2O_2 (0-500 μM) with a fixed incubation time of 90 min. Phosphate buffer (20 mM, pH 7.4). λ_{ex} = 405 nm. Cellular viability of HEK-293 (D) and HeLa (E) cells in the presence of **AM-TCB** and Amonafide. (F) Schematic representation for the detection of released H_2S from **AM-TCB** using H_2S-selective turn-on fluorogenic probe **WSP2**. (G) Fluorescence microscopy images (bright field, green channel, and merged) of HeLa cells in the presence of **AM-TCB** (25 μM) for detection of the drug release. (H) Fluorescence microscopy images (bright field, blue channel, and merged) of HeLa cells in the presence of **AM-TCB** (25 μM) for the detection of released H_2S from the **AM-TCB** using the H_2S-selective turn-on fluorogenic probe **WSP2**.

TH-3161_176122050

The plausible mechanism of umbelliferone from the **WSP2** probe in the presence of H_2S, which was released from the prodrug is shown in Figure 9F. Moreover, strong green emission was observed for **AM-TCB**-treated HeLa cells, indicating the drug release in the presence of endogenous ROS (Figure 9G). Finally, H_2S release from the prodrug was analyzed under a cellular medium (Figure 9H). Very negligible blue fluorescence was observed when **WSP2** treated alone. Interestingly, strong blue fluorescence was observed due to the release of umbelliferone when cells were post-treated with **AM-TCB**, which indicated the release of H_2S from the prodrug **AM-TCB**. Additionally, to understand the interference of cellular H_2S for showing the blue fluorescence, cells were pre-treated with *N*-acetyl cysteine (NAC) as a ROS quencher and DL-propargyl glycine (PAG) as an inhibitor of cystathionine-γ-lyase (H_2S producer enzyme) followed by **WSP2** and **AM-TCB** were treated. The resulting negligible emission indicated that H_2S was not released from the prodrug **AM-TCB** in the absence of ROS

Conclusions

In summary, we analyzed the importance of different linkers for connecting the boronate ester unit to the fluorophore for developing peroxide-responsive fluorogenic prodrug for the delivery of drugs in a sustained manner. Moreover, a peroxide-responsive turn-on fluorogenic prodrug of the anti-inflammatory drug diclofenac (**DCI-ROS**) was developed for real-time monitoring of the drug diclofenac release. In addition, we developed a peroxide-triggered fluorogenic prodrug of diclofenac (**DCF-HS**) for the delivery of active drug diclofenac and H_2S concomitantly from the prodrug. Finally, we developed a peroxide-responsive turn-on fluorogenic prodrug (**AM-TCB**) for the adjuvant delivery of the anti-cancer drug amonafide and H_2S.

References

1. D. B. Zorov, M. Juhaszova and S. J. Sollott, *Physiol. Rev.*, 2014, **94**, 909-950.
2. T. Finkel, *Curr. Opin. Cell Biol.*, 2003, **15**, 247-254.
3. D. E. Handy and J. Loscalzo, *Antioxid. Redox Signaling*, 2012, **16**, 1323-1367.
4. M. Schieber and N. S. Chandel, *Curr. Biol.*, 2014, **24**, R453-R462.
5. Y. Yang, S. Karakhanova, J. Werner and A. V Bazhin, *Curr. Med. Chem.*, 2013, **20**, 3677-3692.
6. V. Vallyathan and X. Shi, *Environ. Health Perspect.*, 1997, **105**, 165-177.

TH-3161_176122050

7. H. J. Shields, A. Traa and J. M. Van Raamsdonk, *Front. Cell Dev. Biol.*, 2021, **9**, 181.
8. M. Giorgio, M. Trinei, E. Migliaccio and P. G. Pelicci, *Nat. Rev. Mol. Cell Biol.*, 2007, **8**, 722-728.
9. E.J. Kim, S. Bhuniya, H. Lee, H. M. Kim, C. Cheong, S. Maiti, K. S. Hong and J. S. Kim, *J. Am. Chem. Soc.*, 2014, **136**, 13888-13894.
10. R. Kumar, J. Han, H.-J. Lim, W. X. Ren, J.-Y. Lim, J.-H. Kim and J. S. Kim, *J. Am. Chem. Soc.*, 2014, **136**, 17836-17843.
11. O. Redy-Keisar, S. Ferber, R. Satchi-Fainaro and D. Shabat, *ChemMedChem*, 2015, **10**, 999-1007.
12. X. Gao, J. Cao, Y. Song, X. Shu, J. Liu, J. Z. Sun, B. Liu and B. Z. Tang, *RSC Adv.*, 2018, **8**, 10975-10979.
13. Y. Zhao and M. D. Pluth, *Angew. Chem., Int. Ed.*, 2016, **128**, 14858-14862.
14. Y. Hu, X. Li, Y. Fang, W. Shi, X. Li, W. Chen, M. Xian and H. Ma, *Chem. Sci.*, 2019, **10**, 7690-7694.
15. N. Zhang, P. Hu, Y. Wang, Q. Tang, Q. Zheng, Z. Wang and Y. He, *ACS sensors*, 2020, **5**, 319-326.
16. M. Yao, Y. Lu, L. Shi, Y. Huang, Q. Zhang, J. Tan, P. Hu, J. Zhang, G. Luo and N. Zhang, *Bioact. Mater.*, 2022, **9**, 168-182.
17. L. Li, G. Rossoni, A. Sparatore, L. C. Lee, P. Del Soldato and P. K. Moore, *Free Radic. Biol. Med.*, 2007, **42**, 706-719.
18. M. Chattopadhyay, R. Kodela, N. Nath, Y. M. Dastagirzada, C. A. Velázquez-Martínez, D. Boring and K. Kashfi, *Biochem. Pharmacol.* , 2012, **83**, 715-722.
19. M. V. Chan and J. L. Wallace, *Am. J. Physiol. Gastrointest. Liver Physiol.*, 2013, **305**, G467-G473.

TH-3161_176122050

TH-3161_176122050

Introduction

TH-3161_176122050

TH-3161_176122050

1.1 Reactive oxygen species (ROS)

Reactive oxygen species (ROS) are highly reactive oxygen-containing molecules. They are generated either by the partial reduction of molecular oxygen in the cells or from external sources such as smoking, radiation, cytotoxic chemicals, and so on.[1] Free radical ROS, including hypochlorite (OCl^-), superoxide ($O_2^{-\bullet}$), hydroxyl radical ($^{\bullet}OH$), and singlet oxygen ($^1O_2$) are short-lived species due to their high reactivity. Therefore, they cannot leave the intracellular location from their site of generation.[2] In contrast, non-radical ROS, specifically hydrogen peroxide (H_2O_2) is relatively less reactive and more stable than radical ROS. Therefore, it can leave the intracellular location and acts as a signaling molecule. Both radical and non-radical ROS are interconvertible in the presence of metals or enzymes.[1] In addition, ROS known as potent oxidants and play a crucial role in physiological processes.[2-4] ROS are scavenged by antioxidants in a regulated manner to prevent them from rising above the physiological threshold level. The failure of antioxidants to quench the ROS leads to a situation where the rate of its production and detoxification is imbalanced, thus leading to oxidative stress. Furthermore, oxidative stress causes of damage to DNA, biological membrane, proteins, and lipids, which induces various diseases such as neurodegenerative disorders, inflammatory diseases, thyroid, cardiovascular diseases, and cancer.[1, 5, 6]

1.1.1. The biological function of ROS

ROS play a crucial role in several biological processes based on their concentration. When the intracellular level of ROS is optimum, these interact with cysteine (Cys) residues in proteins to maintain and regulate physiological functions.[7] For example, H_2O_2 oxidize the cysteine residues ($Cys\text{-}S^-$) to their sulfenic acid form (Cys-SOH) at physiological pH that changes the structure and function of the targeted proteins (Figure 1.1A). These changes in protein function caused by the redox process can affect transcription, phosphorylation, and other important signaling events. They can also change the metabolic fluxes and reactions in cells by modulating the enzymatic characteristics of the proteins. According to research, ROS are necessary for the release of pro-inflammatory cytokines such as interleukin 1β (IL-1β), tumor necrosis factor α (TNF-α), and interferon β (IFN-β), which are essential for regulating the immunological responses.[8] However, high levels of ROS can oxidize the intracellular macromolecules such as proteins, nucleic acids, and phospholipids, which further leads to many diseases such as diabetes, inflammatory diseases, cancer, neurodegenerative disorders,

TH-3161_176122050

and so on.[9] Moreover, cytostasis is a cellular condition when the intracellular level of ROS is lower than optimal. It suppresses cell proliferation and negatively impacts cellular differentiation and immunity (Figure 1.1B).[8] Therefore, maintaining an optimal basal level of ROS between cytostasis and cytotoxic allows correct redox biology reactions. Since ROS are beneficial as well as harmful for our body based on their concentration, it is important to know the sources of ROS intracellularly and extracellularly.

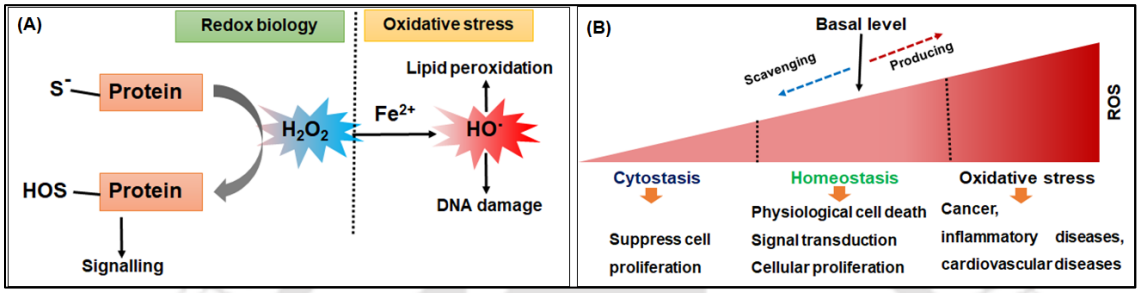

Figure 1.1. (A) Schematic representation of ROS and redox biology. (B) The effect of different ROS levels on the regulation of different cellular processes.

1.1.2. Generation of ROS

ROS are continuously produced in living cells and are often advantageous for metabolic processes. The principal sources of endogenous ROS generation in the biological system are mitochondria, endoplasmic reticulum, microsomes, endothelial cells, phagocytic cells, and nuclei. Among these, mitochondria is the important organelle for the production of endogenous ROS during the typical metabolic processes such as oxidative phosphorylation process. This process occurs in the mitochondria where adenosine triphosphate (ATP) is produced using oxygen and carbohydrates. During this process, mitochondrial ROS (mROS) is produced through the electron transport chain (ETC) in the mitochondria.[10] In ETC process, O_2 is reduced partially to $O_2^{\cdot-}$ because of leaking electrons from the complex I and III. Approximately, (0.2-2.0)% of O_2 consumed by mitochondria is converted into $O_2^{\cdot-}$ during the ETC process (Figure 1.2A).[11] The produced $O_2^{\cdot-}$ is converted into less reactive ROS H_2O_2 in the presence of superoxide dismutase (SOD) enzyme, which could be transformed further into a more stable molecule H_2O in the presence of catalase.

Multiple non-mitochondrial processes are involved in producing ROS, including NADPH oxidase, cytochrome P450 oxidase, and xanthine oxidase (Figure 1.2B). In all cases, $O_2^{\cdot-}$ is produced first, then it is further converted into either H_2O_2 in the presence of SOD or reactive

TH-3161_176122050

nitrogen species ($ONOO^-$) in the presence nitroxyl radical ($NO^{\cdot}$). Additionally, other ROS such as $^{\cdot}OH$, and HOCl are produced from H_2O_2 in the presence of Fe^{2+} (Fenton reaction) and myeloperoxidase (MPO), respectively (Figure 1.2B). The produced HOCl is further converted to $^1O_2$ by reacting with H_2O_2.

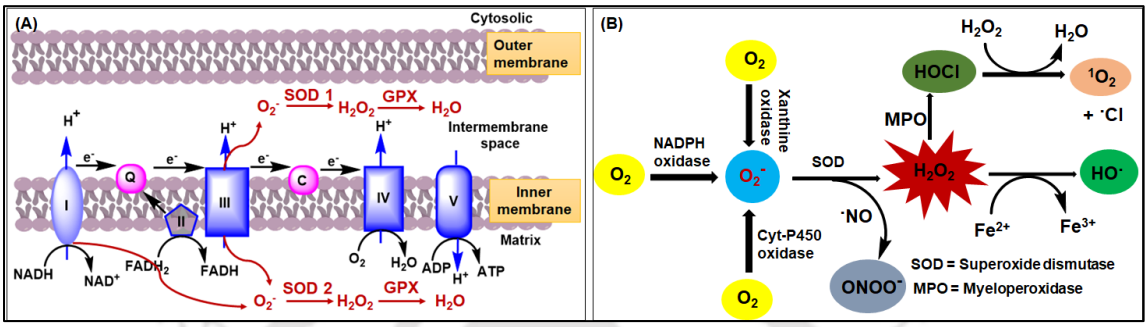

Figure 1.2. Schematic representation of ROS generation at mitochondria (A) and non-mitochondria sources (B).

In addition, ROS are produced in biological processes from a variety of exogenous sources such as tobacco, smoking, harmful gases, radiation, chemicals, dust particulates, and poisonous ambient air. Moreover, industrial processes, congested metropolitan areas, and automobile emissions can also cause oxidative stress in cells leading to several ROS-related diseases.[12] Since the overproduction of ROS leads to several diseases, detoxification of ROS is necessary to maintain homeostasis in cells keeping the biological function normal and preventing ROS-related diseases.

1.1.3. Detoxification of ROS

Maintaining a homeostatic level of ROS is essential for protecting the cells from oxidative damage and retaining an optimal redox environment for the physiological process. Therefore, the overproduction of ROS are detoxified in a regulated manner by antioxidants. ROS are neutralized by antioxidants (enzymatic and non-enzymatic) through several processes enabling the conversion of highly reactive ROS into less reactive ROS or stable molecules.[13] ROS are quenched by several enzymatic antioxidants, such as peroxiredoxin (Prx), superoxide dismutase (SOD), glutathione peroxidase (GPx), catalase (CAT), and thioredoxin (Trx) to maintain the homeostasis in the cells (Figure 1.3). In addition, non-enzymatic antioxidants such as glutathione (GSH), *N*-acetyl cysteine (NAC), flavonoids, vitamin C,

TH-3161_176122050

vitamin E, and dietary nutrients, such as vegetables and fruits also quench the ROS in the cells.[14]

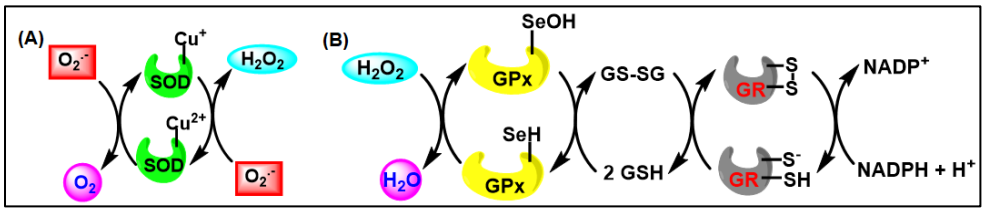

Figure 1.3. Schematic pathway of ROS quenching by the enzymatic antioxidants, SOD (A) and GPx (B).

Due to several reasons, intracellular and extracellular antioxidants fail to detoxify the overproduction of ROS effectively, which leads to oxidative stress. Since H_2O_2 is the relatively more stable ROS among all, the concentration of intracellular H_2O_2 can be monitored easily by administering the small molecules containing H_2O_2-sensitive functional groups, which are discussed in the next section.

1.2. H_2O_2-sensitive functional groups

Since H_2O_2 has a relatively lower cellular reactivity and exists at a substantially higher concentration than other ROS, it is easy to estimate the level of H_2O_2 in diseased cells. Therefore, various probes and prodrugs were developed using different H_2O_2-sensitive function groups over time.[15,16] There are several H_2O_2-responsive functional groups such as boronic acid, boronate ester, thioether, selenium, tellurium, aryl oxalate, and thioketal, which are used for the development of probes and prodrugs (Scheme 1.1).[17] Among different H_2O_2-responsive functional groups, boronate ester and boronic acid are most widely used to develop the ROS-responsive probes and prodrugs.[18, 19]

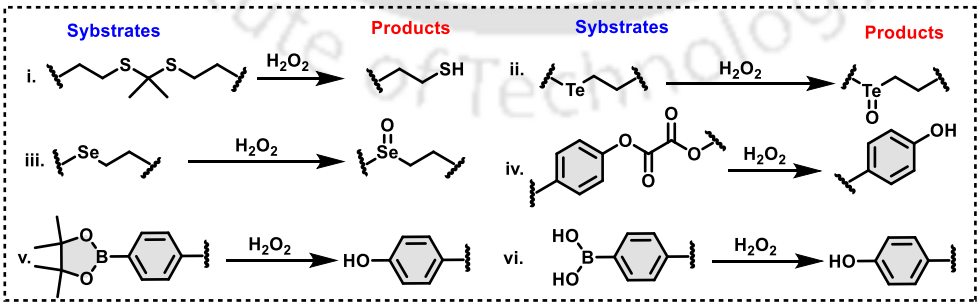

Scheme 1.1. Schematic representation of the reaction of different H_2O_2-responsive functional groups with H_2O_2.

TH-3161_176122050

1.3. Activation mechanism of the boronate ester-based probes and prodrugs

Boronate ester or boronic acid is connected to a substrate (fluorophore or drug) to synthesize the H_2O_2-responsive probes and prodrugs. The boron atom in boronate has a vacant p-orbital, which acts as an electrophilic center and it is attacked by the nucleophile like H_2O_2. The phenolic hydroxyl group is generated because of a subsequent rearrangement followed by hydrolysis. In the case of directly connected boronate ester probes, the fluorophore/drug is released once it is generated the phenolic hydroxyl group. However, self-immolative processes are required to release the fluorophore/drug from the linker-based boronate ester probes or prodrugs.[20] As shown in Scheme 1.2A, H_2O_2 or its conjugate base (HOO^-) attacks the boron center of the probe **1.1a** to form a tetrahedral boronate intermediate **1.1b**. In the next step, 1,2-rearrangement reaction leads to the formation of the borate intermediate **1.1c**. Under physiological conditions, the borate intermediate **1.1c** undergoes hydrolysis into a boric acid/ester to form the phenolic intermediate **1.1d**. It is interesting to note that **1.1a** is entirely converted to **1.1d** within a shorter period.[21]

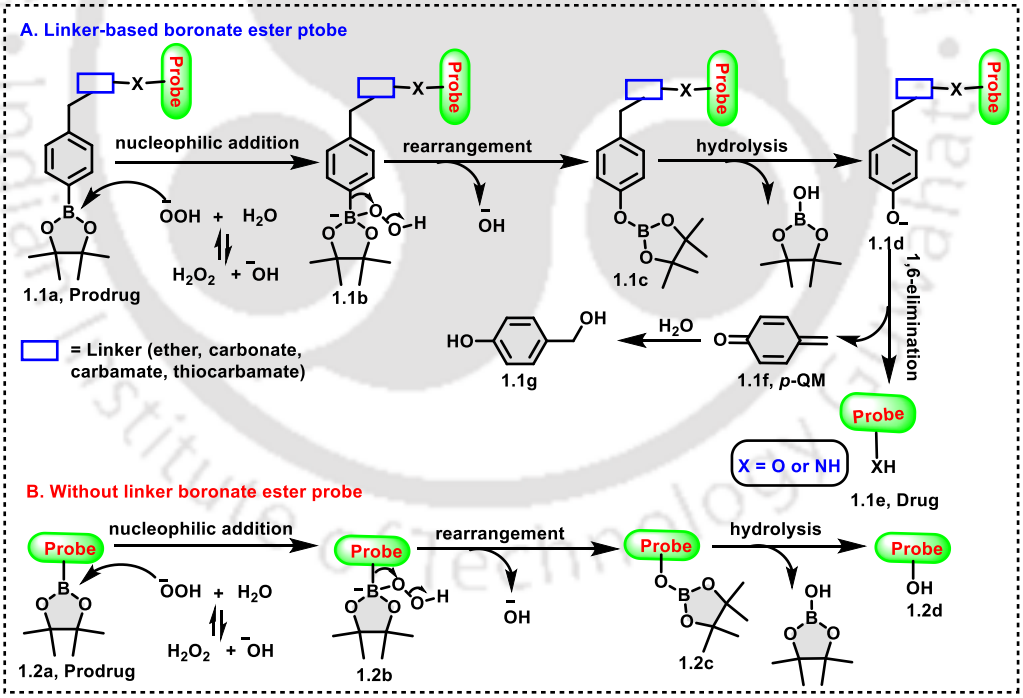

Scheme 1.2. Proposed mechanism for the release of drug/fluorophore from the H_2O_2-responsive prodrugs/probes.

The intermediate **1.1d** undergoes a spontaneous 1,6-elimination process to release the parent compound **1.1e** and *p*-benzoquinone methide (*p*-QM) (**1.1f**). The highly reactive *p*-QM

TH-3161_176122050

undergoes rapid hydrolysis to form *p*-hydroxybenzyl alcohol (**1.1g**) as shown in Scheme1.2A. However, the release of fluorophore/drug from the H_2O_2-responsive probes without any linker follows a similar mechanism as Scheme 1.2A except the 1,6-elimination process as shown in Scheme 1.2B. The active fluorophore/drug (**1.2d**) is released upon hydrolysis of intermediate **1.2c**.

It is to be mentioned that boronate ester moiety is also reactive towards $ONOO^-$ and $O_2^{\cdot-}$ partially. However, these bio-analytes are not stable enough as H_2O_2 in the cells. Since the diseased cells have higher levels of H_2O_2 than normal cells, researchers have developed H_2O_2-responsive probes, prodrugs, and theranostic prodrugs over time for the treatment and diagnosis of the ROS-related disorders accurately [22, 23] H_2O_2-responsive probes can be categorized into two types such as non-fluorogenic and fluorogenic prodrugs. Both types of H_2O_2-responsive prodrugs have been discussed in the next sections elaborately.

1.4. H_2O_2-responsive non-fluorogenic prodrugs

Since anti-inflammatory drugs have several limitations such as poor bioavailability, selectivity towards inflammatory tissues over normal tissues, and so on, it is important to develop their prodrugs to overcome limitations. As described above, oxidative stress is the key feature of inflammatory diseases.[24] Intracellular H_2O_2 levels are observed to be almost 100-times higher in the inflammatory sites than in the normal tissues.[25, 26] Taking it as an advantage, H_2O_2-responsive anti-inflammatory prodrugs were developed over the years. In 2015, Khang and co-workers developed the H_2O_2-responsive prodrug **1.3** from *p*-hydroxybenzyl alcohol (**HBA**) (Figure 1.4).[27] Upon the reaction with intracellular H_2O_2, **HBA** released from the prodrug and showed potent antioxidant and anti-inflammatory activities. In addition, the released component **HBA** suppressed the pro-inflammatory cytokine TNF-α. Prodrug **1.3** showed a significant protective effect against hepatic and cardiac ischemia-reperfusion (I/R) injury at less than 5 mg/kg, while free drug **HBA** required at least 25 mg/kg to provide similar therapeutic activity. These results indicated that the H_2O_2-responsive prodrug would be beneficial over conventional drugs. In 2018, the Clausen group developed ROS-responsive prodrug (**1.4**) of methotrexate (**MTX**), a potent anti-inflammatory drug for the treatment of arthritis (Figure 1.4).[28] Interestingly, the group of mice treated with prodrug **1.4** showed no side effects such as losing body weight. However, the group receiving **MTX** directly, experienced a considerable drop in body weight. These

TH-3161_176122050

results suggested that the H_2O_2-responsive prodrugs could be synthesized from the corresponding anti-inflammatory drugs to enhance the effectiveness of the drug. In addition, cancer is the most dangerous malady among all the diseases associated with oxidative stress in cells. It contributes to around 13% of all fatalities worldwide and is the second biggest cause of mortality in the entire world.[29] There are several ways to treat cancers such as surgery, radiotherapy, and chemotherapy. Among different processes, chemotherapy is the most convenient choice of treatment for cancers because of its high efficiency. However, it shows several limitations such as poor bioavailability, several side-effects, lack of selectivity (*i.e.*, failure to differentiate between healthy and cancerous cells), and multidrug resistance (MDR) of tumor cells.[30] To overcome the problems associated with chemotherapy, it is desirable to develop a drug delivery approach with known anti-cancer drugs with improved survival rates, bioavailability, and reduced side-effects. Provided that, as cancer cells produce more H_2O_2 than healthy cells do, converting anticancer drugs into prodrugs by incorporating H_2O_2-responsive moieties will be an appealing strategy for enhancing the action of non-selective anti-cancer drugs.[31]

In 2011, Peng and co-workers developed the H_2O_2-responsive anticancer prodrugs **1.5** and **1.6** (Figure 1.4) of nitrogen mustard.[32] They observed that both the prodrugs are selectively reactive toward H_2O_2 over other relevant bio-analytes. The cytotoxicity of nitrogen mustard was greatly increased in cancer cells when phenylboronic acid or phenylboronate prodrugs of it were treated in the lung (NCI-H460), leukemia (SR), and renal (CAKI-1 and SN12C) cancer cell lines, although the intrinsic toxicity of the prodrugs was decreased significantly. In normal lymphocytes under the same cell circumstances, both the prodrugs did not induce apoptosis, whereas showed promising *in vitro* early safety profiles. In 2014, Peng and co-workers performed extensive research with several electron-withdrawing linkers and discovered potent anticancer prodrugs **1.7** and **1.8** by connecting boronate ester unit as the electron-withdrawing group with the drug nitrogen mustard *via* directly or carbamate linker (Figure 1.4).[33] *In vitro* cytotoxicity studies with the prodrugs **1.7** and **1.8** revealed substantial inhibitory activity against several cancer cell lines, including lung, breast, leukemia, and renal cancers with GI_{50} values under 1 μM. Moreover, the formation of the cytotoxic aziridinium intermediate was suppressed because of decreasing the electron density of the aromatic ring. Interestingly, the prodrug was converted to electron-rich aromatic nitrogen mustard in the

TH-3161_176122050

presence of H_2O_2 and showed the highest cellular activity *in vitro* due to increased cell permeability and solubility. These outcomes indicated that H_2O_2-responsive anticancer prodrugs would be a useful technique to minimize the side-effects of conventional anti-cancer drugs. Moreover, in 2018, Wang and co-workers developed an H_2O_2-responsive anti-cancer prodrug of the histone deacetylase inhibitor (HDACI) belinostat, **1.9**.[34] In the prodrug, the H_2O_2-responsive moiety boronate ester was used to mask the hydroxamic acid zinc-binding domain of HDACI. Interestingly, prodrug **1.9** showed lower efficacy than the parent drug against breast (MDA-MB-231), lung (A549 and NCI-H460), and skin (SK-MEL-28) cancer cells. Due to the partial release of the active drug from the prodrug **1.9** *in vitro*, unexpected results were obtained. Despite of this unexpected result, they extended their studies in a mouse breast xenograft model (MCF-7) based on their previous experience. It is interesting to note that both the free drug (belinostat) and the prodrug **1.9** showed prevention of tumor formation significantly in an *in vivo* assay. These results validated the enhancement of biocompatibility and bioavailability of the prodrug **1.9**.

A first-line drug for treating pancreatic cancer is gemcitabine.[35] However, its clinical use was restricted because of its serious side-effects like myelosuppression. In the year of 2019, a novel prodrug of gemcitabine, **1.10** was developed by Matsushita and co-workers to reduce the off-target side-effects of gemcitabine (Figure 1.4).[36] Since the cancer cells were found to be at high levels of H_2O_2, the active drug was released effectively from the prodrug **1.10** in the presence of H_2O_2 and showed a significant anti-cancer effect as the parent drug. Importantly, the side-effect of gemcitabine, myelosuppression was diminished significantly upon the administration of the prodrug **1.10** *in vivo* because of its activation in cancer cells specifically.

However, the drug release was monitored for the non-fluorogenic prodrugs using either NMR spectroscopy, mass spectrometry, or analytical HPLC method, which are not sensitive enough. In addition, it is difficult to monitor the drug release as well as the drug metabolism in the cellular medium. Nevertheless, the molecular mechanisms of H_2O_2 generation, accumulation, trafficking, and function remain poorly analyzed, even in the most basic eukaryotic species.[37] Therefore, it is very important to develop a new tool to investigate the physiological and pathological effects of H_2O_2 and associated ROS in living systems.

TH-3161_176122050

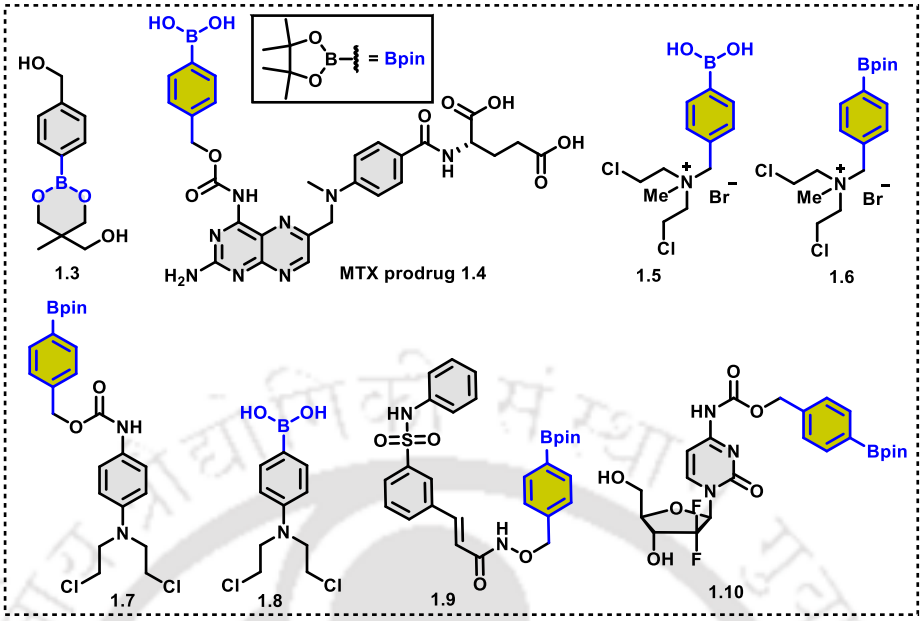

Figure 1.4. Chemical structures of H_2O_2-responsive non-fluorogenic anti-inflammatory and anti-cancer prodrugs.

1.5. H_2O_2-responsive fluorogenic probes

Fluorogenic probes are well-adapted tools to fulfill the requirement of examining the biological chemistry of H_2O_2 in cells. Developing water-soluble fluorescent probes that measure H_2O_2 selectively over competing biological ROS and lipid alkyl peroxides was a big challenge in reaching this goal. Such probes can be synthesized using small synthetic molecules and many other reagents evaluated for H_2O_2 detection. In 1965, Ketson and co-workers developed the most frequently used fluorescent probe 2',7'-dichlorodihydrofluorescein diacetate (H_2DCFDA), to detect the intracellular ROS.[38] Apart from this, dihydroethidium (DHE) is also used for the detection of ROS. H_2DCFDA shows very negligible fluorescence emission in the absence of ROS. Once it is incubated in a cellular medium, the H_2DCFDA is converted into H_2DCF by cleaving the ester group in the presence of intracellular esterase followed by the oxidation occurs in the presence of ROS, and shows strong fluorescence emission (Scheme 1.3).[39]

However, these compounds take part in non-specific redox reactions, which result in the formation of a distinct but comparable fluorescent adduct. Therefore, it is difficult to distinguish from fluorescent products produced by the interactions with ROS. Most

TH-3161_176122050

importantly, these are not selective towards H_2O_2 only. Therefore, several scientific groups developed selective H_2O_2-sensing probes over time.

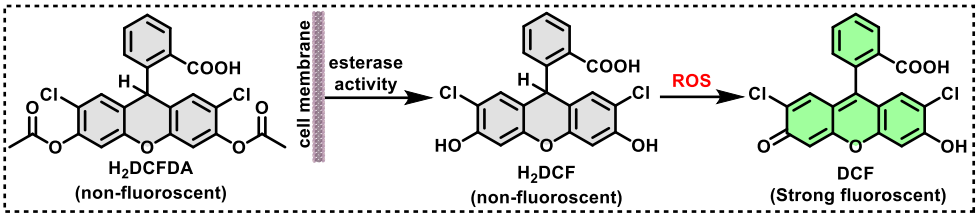

Scheme 1.3. Schematic representation of fluorescent changes of DCF indicator in the presence of ROS.

1.6. ROS-responsive directly-coupled boronate ester-based fluorogenic probes

Due to the great sensitivity of boronate ester for the primary ROS in cells under pathological as well as physiological conditions, researchers paid attention to developing the boronate ester-based probes to achieve ROS-specific imaging.[40, 41] In 2004, peroxyfluor-1 (**1.11**), a new boronate-based fluorescent probe was developed by Chang and co-workers for imaging the intracellular H_2O_2 in cells (Figure 1.5).[42] In comparison with the previously reported probes, compound **1.11** exhibited a 10-100 times enhancement in emission in the presence of H_2O_2 selectivity. Moreover, probe **1.11** showed selectivity towards H_2O_2 over other competing bio-analytes. Next year in 2005, the same group developed peroxy resorufin-1 (**1.12**) and peroxy xanthone-1 (**1.13**) probes, and both of the probes displayed outstanding selectivity for the intracellular H_2O_2.[43] Additionally, these probes are suitable for monitoring the micromolar changes in H_2O_2 in living cells. However, earlier reported probes showed the fluorescence emission in the presence of H_2O_2 through the intramolecular charge transfer (ICT) mechanism. In this process, donors and acceptors are present in the same molecule. In 2006, the same group developed a fluorescence resonance energy transfer (FRET)-based probe **1.14** for the detection of H_2O_2 ratiometrically. In the FRET system, two fluorophores are connected using a rigid spacer in such a way that one fluorophore acts as a donor and the other fluorophore acts as an acceptor. Moreover, the emission wavelength of the donor should be overlapped with the excitation wavelength of the acceptor for showing FRET properties. In probe **1.14**, the coumarin unit acts as a donor, and fluorescein moiety acts as an acceptor. FRET was off in the absence of H_2O_2 and showed only blue fluorescence emission corresponding to the coumarin unit. Interestingly, fluorescence emission red-shifted (blue to green) gradually in the presence of H_2O_2. Moreover, this probe was capable of quantifying

TH-3161_176122050

the H_2O_2 concentration more accurately than other probes. However, all the probes were developed by connecting two boronate esters unit in a single fluorophore. In 2007, Chang and co-workers developed boronate ester-based probes such as peroxy green 1 (**1.15**) and peroxy crimson 1 (**1.16)** (Figure 1.5) to detect the H_2O_2.[44] Both the probes showed high selectivity towards H_2O_2 over other bio-analytes and were suitable for detecting intracellular H_2O_2. However, as previously discussed all the fluorescent probes inadequate for detecting the H_2O_2 in specific organelles such as mitochondria, lysosome, endoplasmic reticulum, etc. Since mitochondria are the main sources of H_2O_2 production in cells, it is important to develop mitochondria-targeting fluorescent probes. To monitor endogenous H_2O_2 changes in mitochondria, numerous probes were developed over time. Since the mitochondrial membrane (180 mV) is negatively charged, generally the positively charged molecules such as triphenylphosphonium (TPP) or quaternary ammonium salts were connected to the fluorophore for developing the mitochondria-targeting probes. In this regard, in 2008, Chang and co-workers developed a mitochondrial-targeting fluorescent probe (**1.17**) for imaging H_2O_2 in mitochondria (Figure 1.5).[45] Arylboronate ester was connected to dihydrorhodamine (DHR) as the turn-on fluorescent reporter to synthesize the probe **1.17** for sensing ROS, and TPP moiety was connected to target the mitochondria. Interestingly, probe **1.17** detected H_2O_2 selectively compared to other ROS. The probe showed mitochondria-targeting properties in cells, which was confirmed by co-localizing with MitoTracker^{TM} Red.[45] However, the utility of probe **1.17** in deep tissue imaging was constrained by its shallow penetration depth (<80 μm) and relatively shorter emission wavelengths (510 nm). It was important to develop fluorescent probes with higher excitation/emission wavelength to address this issue, which can easily penetrate the tissue without harming the cells. Near-infrared (NIR) fluorescent probes are exhibited exceptional performance and evolved as a viable tool in bio-imaging because of their special qualities, including deeper tissue penetration power, least damage to bio-samples, and minimum auto-fluorescence interferences.[46] In 2016, Peng and co-workers developed a near-infrared (NIR) fluorescence probe (**1.18**) for detecting H_2O_2 *in vivo* that targets mitochondria (Figure 1.5).[47] Aarylboronate moiety was used for sensing H_2O_2 and a quaternary ammonium group was connected to target the mitochondria. Importantly, the probe was excited with 635 nm and emission was observed in the 700-750 nm range in the presence of H_2O_2. For the first time,

TH-3161_176122050

probe **1.18** was used to detect the intracellular H_2O_2 associated with an autophagy process *in vivo*.

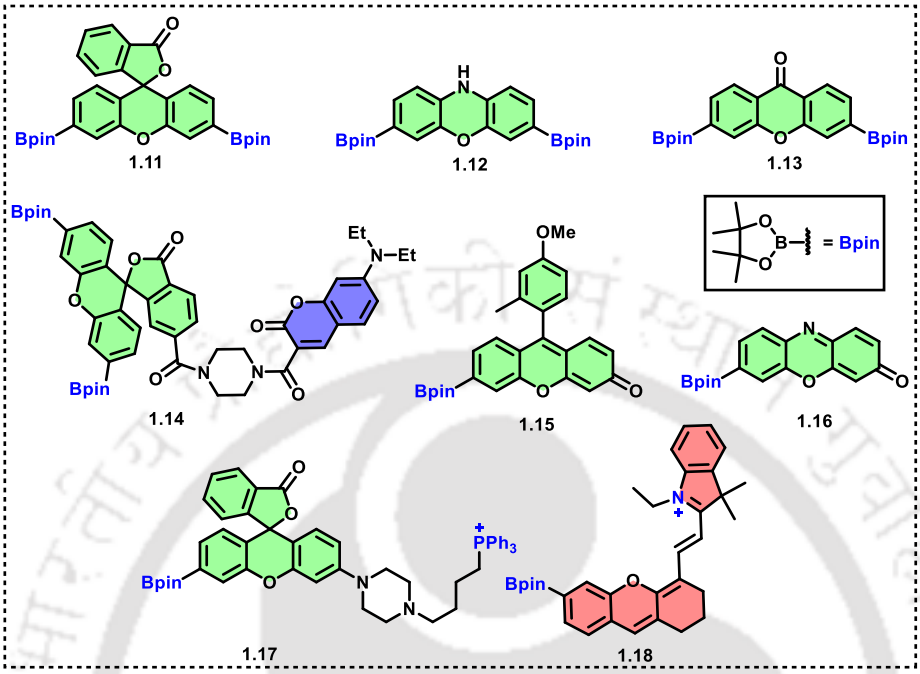

Figure 1.5. Chemical structures of the H_2O_2-responsive directly connected boronate ester fluorescent probes.

So far, all the fluorescent probes were developed by connecting the boronate ester moiety directly to the fluorophore, known as intensity-based probes. However, the intensity-based probes are limited by variations in excitation and emission efficiency, sample environment, and probe distribution, which can make them difficult to utilize in the quantitative measurement of H_2O_2. To overcome these limitations, ratiometric probes provide the advantage of having built-in corrections for these variabilities because they permit the simultaneous detection of two signals originating from the reacted and unreacted forms of the probe in the same sample.[48]

1.7. ROS-responsive linker-based fluorogenic probes

In 2008, Chang and co-workers developed the H_2O_2-responsive ratiometric fluorescent probe **1.19** for the first time.[49] Boronate ester moiety was connected with the corresponding fluorophore *via* a carbamate linker in this probe. It is to be noted that probe **1.19** showed blue fluorescence emission at 475 nm in the absence of H_2O_2. Interestingly, fluorescence emission red-shifted to 540 nm (green emission) in the presence of H_2O_2. In addition, this probe

TH-3161_176122050

showed selectivity towards H_2O_2 over other bio-analytes. However, this ratiometric probe **1.19** was incompatible with measuring the organelle-specific H_2O_2 concentration in cells due to the absence of any organelle-targeting moiety in the probe. Therefore, in 2012, Kim and co-workers developed a mitochondria-targeting probe **1.20** where the TPP moiety served as the mitochondria-targeting unit. The aryl boronate ester was connected to the fluorophore *via* carbamate linker to detect H_2O_2 and aminonaphthenyl benzothiazole was taken as a two-photon fluorescence reporter. (Figure 1.6).[50] Probe **1.20** exhibited a significant emission change (red-shifted) in the presence of H_2O_2. It showed outstanding stability under physiological conditions. It is important to be noted that probe **1.20** detected H_2O_2 quantitatively in living tissues and showed a penetration depth of 100-180 μm.[50] Additionally, in 2013, Cohen and co-workers developed a benzyl ether linkage boronate ester probe **1.21** for sensing the H_2O_2.[51] Probe **1.21** was synthesized just in a one-step reaction where fluorescein was reacted with boronate benzyl bromide in the presence of cesium carbonate. However, a weak emission under the green channel was observed while the RAW 264.7 cells were treated with 50 μM of **1.21**, which is quite a high concentration. Moreover, in 2014, Zhang and co-workers developed an ether linkage probe **1.22**, where the naphthalimide unit was connected with the H_2O_2-responsive unit boronate ester *via* an ether linkage.[52] This probe also acted as a ratiometric fluorescent probe and exhibited 100 nm red-shifted accompanied by the color changes from colorless to yellow upon addition of H_2O_2. Therefore, probe **1.22** can serve as a "naked-eye" probe for detecting H_2O_2. Lysosomes are organelles with a single membrane layer that are acidic (pH 4.5–5.0) and responsible for recycling and degrading cell components.[53] The accumulation of considerable amounts of proteins and peroxidized lipids in lysosomes as a result of lysosomal disruption brought on by the elevated ROS levels, which is linked to several diseases, including inflammation, cancer, and neurodegenerative disorders.[53, 54] Therefore, developing lysosome-targeting H_2O_2-responsive fluorogenic probes are very important. A basic moiety, such as morpholine or *N*,*N*-diethyl/methyl moiety is frequently utilized as a lysosome-targeting group for the development of lysosome-targeting probes or prodrugs.[55]

In 2015, Yoon and co-workers developed a boronate-based probe **1.23** where H_2O_2-responsive moiety boronate ester was connected to naphthalimide fluorophore through carbamate linker and morpholine was connected to target the lysosome, which showed high

TH-3161_176122050

selectivity towards H_2O_2 both in the solution and in living cells (Figure 1.6). The outcomes of the cell imaging study indicated that probe **1.23** could be utilized to monitor both intracellular and extracellular H_2O_2.[55] Probe **1.23** showed extremely weak emission without the addition of H_2O_2 externally in HeLa cells; however, significant enhancement of red emission was observed while cells were pretreated with 100 μM of H_2O_2. Despite the advantages of carbamate and ether linkage-based probes, carbonate linkage-based probes also will be interesting as H_2O_2-responsive linker-based fluorescent probes. In 2016, Floreancig and co-workers developed a carbonate linkage-based probe **1.24** using a non-toxic and water-soluble fluorophore coumarin unit.[56] Same year in 2016, Zhao and co-workers developed a ROS-responsive lysosome targeting fluorogenic probe **1.25** for detection and quantification of the intracellular H_2O_2 (Figure 1.6).[57] Probe **1.25** showed very negligible fluorescence emission in the absence of H_2O_2. Interestingly, fluorescence emission increased significantly in the presence of H_2O_2. The protonated form showed increased fluorescence emission at low pH. However, the deprotonated form showed weak emission, indicating a significant selectivity of the probe toward acidic lysosomes in cells. Moreover, in 2017, the same group developed another lysosome-targeting fluorescent probe (**1.26**) for detecting endogenous H_2O_2 in the lysosome of HeLa cells by connecting the morpholine moiety. The designed fluorescent probe **1.26** has many advantages such as quick response time, high sensitivity, high selectivity, optimal *p*Ka for lysosomal surroundings, and effective lysosome-localizing ability. In addition, having a great cell-membrane permeability, benzorhodol fluorophores are easily dissolved in water.[58] Moreover, in 2018, Zhang and co-workers designed a coumarin-based fluorescent probe **1.27** with the use of the pyridinium cation, that may specifically target the mitochondria.[59] The probe showed extremely good sensitivity, selectivity, and quantitative H_2O_2 detection abilities. When the probe detected H_2O_2, it particularly displayed a selective strong emission change with a 105 nm shift and an associated color change from red to green (blue shift).

However, different linkers (direct, carbamate, ether, and carbonate) were chosen for developing H_2O_2-responsive fluorescent probes randomly without any proper study. Therefore, proper rationalization is required to understand the reason behind choosing a linker for developing a probe/prodrug for sensing H_2O_2. Since the concentration of H_2O_2 is

TH-3161_176122050

higher in oxidative-stressed cells than in normal cells, H_2O_2-responsive fluorescent probes can be utilized further for delivering the drug selectively in diseased cells over normal cells.

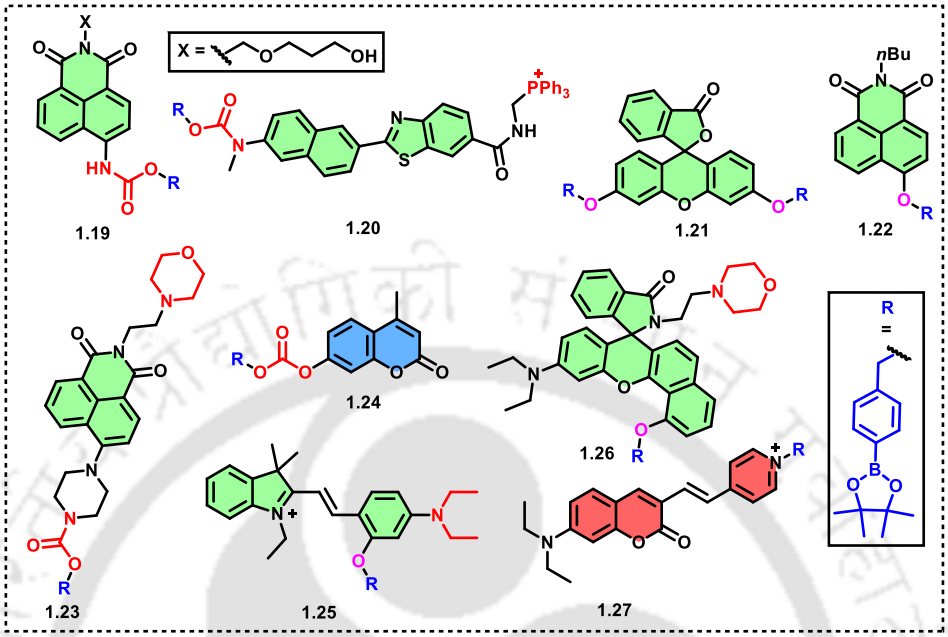

Figure 1.6. Chemical structures of H_2O_2-responsive linker-based boronate ester probes.

1.8. H_2O_2-responsive fluorogenic prodrugs

Theranostic prodrugs are a new and interesting prodrug technique that has the potential to diagnose diseases in their early stages while administering drugs to the affected site. It is suitable for evaluating the phase of disease progression and monitoring the kinetics of the drug release. Therefore, the patient can receive precise, efficient, and quick therapies owing to this one-step approach.[60] The general scheme for the H_2O_2-responsive theranostic prodrugs is shown in Scheme 1.4. In this system, fluorescence emission is either weak or turn-off for the prodrug in the absence of H_2O_2. Upon the treatment with H_2O_2, the boronate ester moiety is oxidized and releases the active drug as well as the fluorophore *via* self-immolative processes. The released fluorophore shows turned-on fluorescence emission and helps to monitor the drug release in a real-time manner.

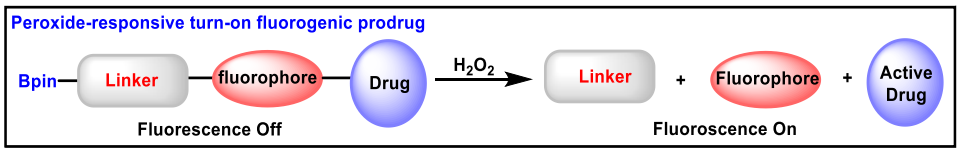

Scheme 1.4. Schematic representation of the delivery of H_2O_2-sensitive theranostic prodrug using fluorescence turn-off/on strategy.

TH-3161_176122050

Several H_2O_2-responsive non-fluorogenic prodrugs for the treatment of cancers as well as inflammatory diseases reported over time and discussed in the earlier section. However, theranostic prodrug approach utilized for the development of anti-cancer prodrugs not for anti-inflammatory prodrugs until now. Utilizing this concept, glutathione (GSH)-responsive theranostic prodrugs for the treatment of cancers developed by several scientific groups over time.[61-64] There was no report on H_2O_2-responsive theranostic prodrugs for cancer treatments until 2014. In 2014, Kim and co-workers developed the H_2O_2-triggered theranostic prodrug (**1.28**) for the treatment of metastatic malignancies (Figure 1.7).[65] Prodrug **1.28** was designed using three components, these are the boronate ester moiety serves as an H_2O_2-responsive unit; the potent anticancer drug **SN-38**; and a coumarin unit serves as a self-immolative linker as well as a fluorescent reporter to track the release of **SN-38**. A high level of H_2O_2 in cancer cells helped to activate the prodrug **1.28** for releasing the anti-cancer drug **SN-38** selectively towards cancer cells over normal cells. Therefore, it showed significant cytotoxicity towards cancer cells whereas less toxic to normal cells and inhibited the cell growth of tumors selectively. The drug release process was monitored conveniently by the increase in emission intensity at 456 nm due to the release of the free coumarin unit. However, prodrug **1.28** was incompatible with delivering the active drug into a specific organelle in the cells, as there is no organelle-targeting unit in the prodrug. In addition, due to the shorter excitation wavelength of the coumarin, it was difficult to monitor the drug release *in vivo*. Considering the limitations of the prodrug **1.28**, in that year itself, they developed the H_2O_2-responsive another theranostic prodrug (**1.29**) of 5-fluorouracil (**5-FU**) with mitochondria targeting property (Figure 1.7).[66] Prodrug **1.29** was designed using four different ligands such as boronate ester as an H_2O_2-responsive moiety, ethidium bromide as a fluorophore, biotin as a tumor-targeting unit, and **5-FU** as an anti-cancer drug. Upon reaction with the high level of H_2O_2 in tumor tissues, 5'-deoxy-5-fluorouracil is released, which is further converted to the parent anticancer drug **5-FU** upon reaction with thymidine phosphorylase, which is present in high concentration in the carcinoma cells. Moreover, the self-immolative process releases the mitochondria-targeting fluorophore ethidium bromide, which is weakly fluorescent in an aqueous solution and strongly fluorescent (λ_{em} = 590 nm) on intercalating with the DNA of the mitochondria. Prodrug **1.29** improved the anti-cancer activity effectively in cancer cells and reduced the cytotoxicity of the normal cells as compared to **5-FU**. The prodrug (**1.29**)

TH-3161_176122050

showed almost seven times higher fluorescence emission in the tumor cells over the normal cells because of the biotin. Moreover, a study in A549-inoculated xenograft mice showed that the prodrug **1.29** inhibited tumor growth significantly during the eight weeks of treatment.

However, both the prodrugs **1.28** and **1.29** were designed with shorter excitation wavelength-based fluorophores such as coumarin and ethidium bromide, respectively, which were incompatible for *in vivo* study. The limitations of the shorter excitation-based fluorophores could be overcome using the NIR fluorophore, which exhibits a longer excitation wavelength. Therefore, Shabat and co-workers developed the H_2O_2-responsive cyanine-based prodrug **1.30** in 2015 (Figure 1.7).[67] The fluorescence emission at 720 nm enhanced significantly upon the reaction with H_2O_2, indicating the release of cyanine moiety (NIR fluorophore) that confirmed the co-release of active drug camptothecin. Moreover, the released active drug camptothecin from the prodrug **1.30** showed similar anti-cancer activity as the parent drug. Furthermore, in 2018, Tang and co-workers developed a theranostic prodrug **1.31** of doxorubicin using a FRET-based fluorophore (Figure 1.7).[68] Upon reaction with H_2O_2, fluorophore and doxorubicin were released from the prodrug, which was confirmed by spectroscopy as well as cellular studies. To analyze the cytotoxicity of the released drug from the prodrug **1.31**, HeLa cells were treated with the prodrug **1.31** and observed negligible cytotoxicity upto 10 µM, indicated that the drug was not released completely in the presence of endogenous H_2O_2. Therefore, cells were pretreated with the ROS-inducer Pherol-12-Myristate-13-Acetate (PMA), and then prodrug **1.31** was incubated for 48 h. Cell viability decreased dose-dependently and exhibited IC_{50} at around 1.5 µM as the parent drug. This result indicates the release of an active drug (Dox) in the presence of a higher level of H_2O_2 and showed cytotoxicity toward HeLa cells.

It is to be noted that H_2O_2-responsive theranostic prodrugs showed great achievements in the prodrug strategy by releasing the active drug in cancerous cells over normal cells selectively and monitoring it using fluorophore in living cells. In addition, the drug release profile was monitored *in vivo* efficiently by connecting NIR-fluorophore in the theranostic prodrug. Despite the advantages of above discussed theranostic prodrugs, the design of the prodrug further can be improved by adding hydrogen sulfide (H_2S) sources along with the active drug (co-delivery of H_2S with the drug), which may help to improve the activity of the drug and

TH-3161_176122050

can be reduced the off-target side effects of the corresponding drug. It is to be noted that H_2S shows several pharmacological effects such as cytoprotective effects, anti-inflammatory effects, anti-cancer effects, etc.[69, 70]

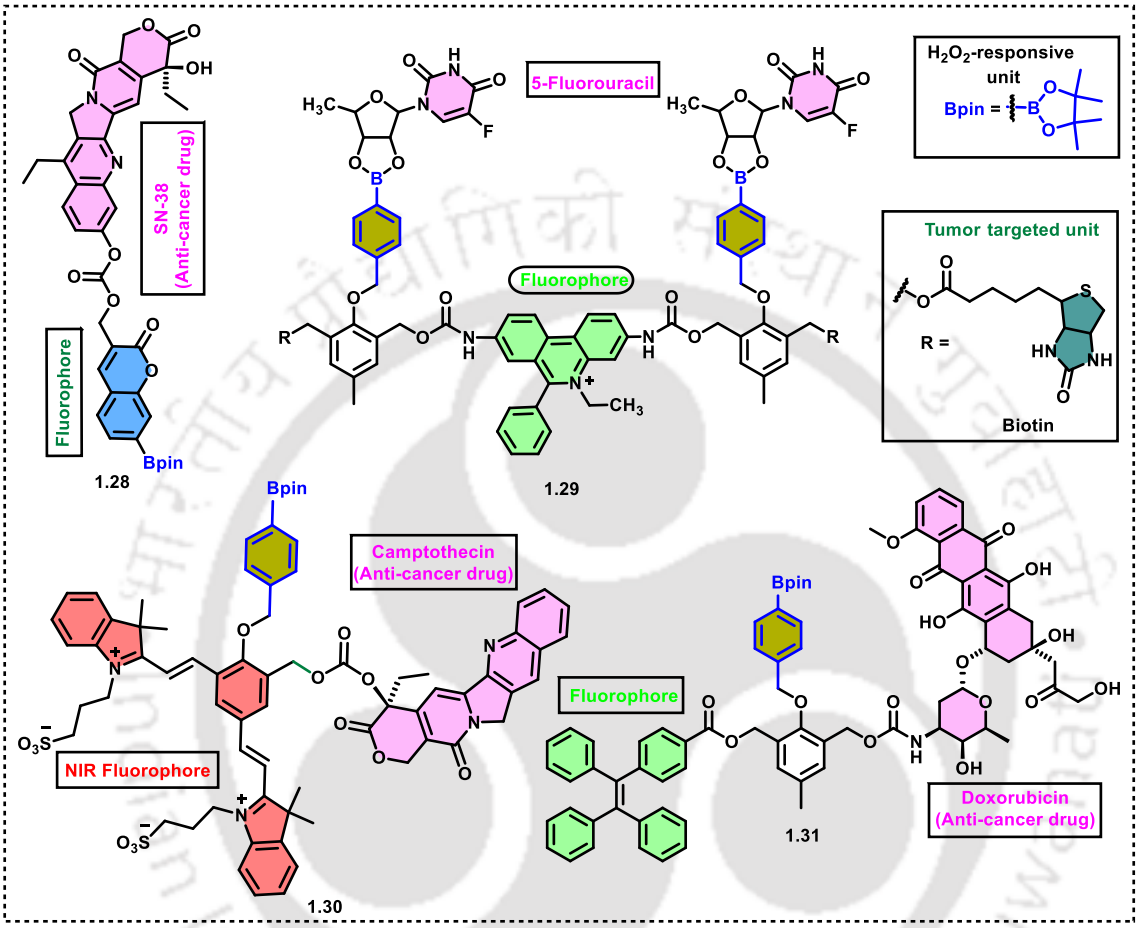

Figure 1.7. Chemical structures of some representative H_2O_2-responsive fluorogenic prodrugs.

1.9. ROS and H_2S

As described in the earlier section, the overproduction of ROS is responsible for oxidative stress, which leads to several diseases. To protect the cells from different pathogens, GSH plays a crucial role as an antioxidant to detoxify the ROS. It is to be noted that H_2S is indirectly involved to synthesize the GSH, which is a more abundant antioxidant in the cells. H_2S is a colorless gaseous chemical that emits a potent rotten-egg odor at ambient temperatures. It is also known as the third member of the family of gasotransmitters after carbon monoxide (CO) and nitric oxide (NO) with a wide range of biological applications. H_2S is also involved to activate the SOD enzyme, which detoxifies the $O_2^{\cdot-}$.[71] Furthermore,

TH-3161_176122050

H_2S inhibits mitochondrial ROS production through the sulfhydration of pro-apoptotic protein, p66Shc.[72]

1.10. Biological functions of H_2S

H_2S exhibits several biological effects, such as antioxidant, anti-cancer, anti-inflammatory, cytoprotective, neuroprotective, and vasodilatory effects (Figure 1.8).[69, 70, 73, 74] H_2S plays a crucial role in scavenging the ROS by interacting with the SOD enzyme (enzymatic antioxidant).[70] In 1995, Searcy and co-workers reported that H_2S is the important substrate of SOD and binds to the Cu-core of it catalytically.[75] The rate of scavenging $O_2^{\cdot-}$ increased synergistically when HS^- interacted with SOD. Moreover, similar to NO, H_2S also relaxes blood vessels *via* modifying K^+ channel function and increase the guanosine 3',5'-cyclic monophosphate (cGMP) levels in vascular smooth muscle cells (SMCs).[73] In the year of 2008, Li and co-workers studied the effect of H_2S in the cardiovascular system using a well-known slow H_2S donor, morpholin-4-ium 4-methoxyphenyl(morpholino) phosphinodithioate (GYY4137).[76] The acute vasorelaxant effects of GYY4137 were investigated in rat aortic rings, perfused rat kidneys *in vitro* and the anesthetized rat (male Sprague-Dawley) *in vivo*. Interestingly, GYY4137 showed slow relaxation of rat aortic rings dilates the perfused renal vasculature by activating K_{ATP} channels of vascular smooth muscle cells.[76]

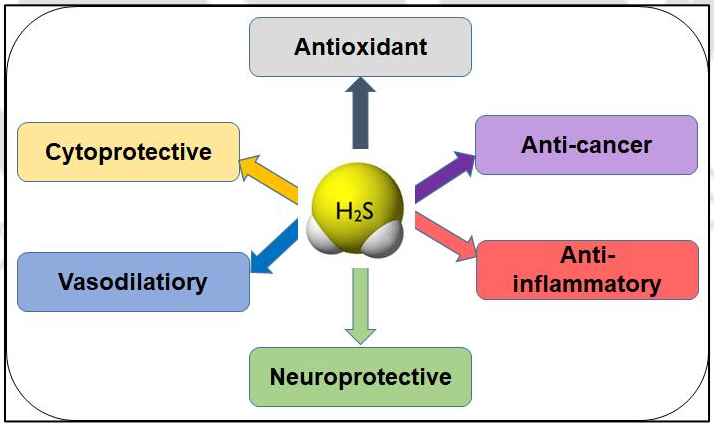

Figure 1.8. Some of the pharmacological effects of H_2S.

In addition, H_2S shows anti-inflammatory effect by reducing the expression of several pro-inflammatory cytokines such as interleukin 1-β (IL-1β), tumor necrosis factor α (TNF-α), and so on. It inhibits the expression of the pro-inflammatory cytokines by suppressing the activity of nuclear factor κB (NF-κB), which is a protein complex that controls the production of cytokines and transcription of DNA. Furthermore, H_2S shows cytoprotective effect

TH-3161_176122050

through an anti-apoptotic mechanism. Although H_2S has anti-apoptotic effects in several organs, many researchers focused on I/R injury to the heart. It has been found that H_2S inhibited myocardial I/R-induced cardiac myocyte apoptosis.[77] Sivarajah *et al.* shown that the decrease in cardiac myocyte apoptosis and caspase-9 activity brought on by H_2S was eliminated by the administration of 5-hydroxy decanoate (5-HD), a K_{ATP} channel blocker.[78] In addition to decreasing the activity of caspase-9, H_2S improved the expression of the Bcl-2 protein brought on by localized myocardial I/R, which was suppressed by 5-HD. These results suggest that H_2S inhibits apoptosis significantly, possibly as a result of the opening of putative mitochondrial K_{ATP} channels.[78].Therefore, several pharmacological effects of H_2S encouraged us to explore its sources.

1.11. Detection of H_2S

Since H_2S shows several pharmacological effects in mammalian cells under normal as well as pathological conditions, it is very important to estimate the level of H_2S under both conditions. Therefore, several methods such as the spectrophotometric method, electrochemical method, and fluorogenic method were developed over time.[79, 80] Among many H_2S detection spectrophotometric methods, methylene blue (MB) assay is a very convenient method for the detection of H_2S using UV-Vis spectroscopy. In this method, MB dye is formed from *p*-(dimethylamino)aniline (**1.32**) in the presence of H_2S under an acidic conditions, which exhibits a typical absorbance pattern at 670 nm (Scheme 1.5A).[81]

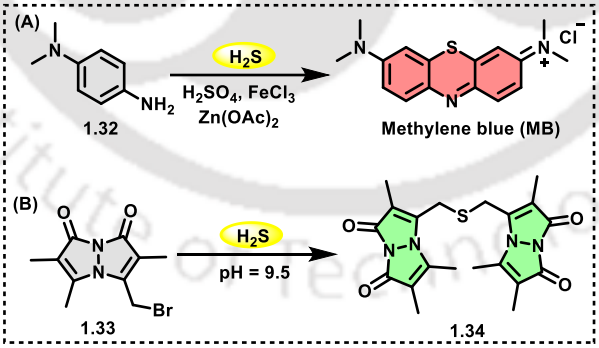

Scheme 1.5. (a) Schematic representation for the formation of MB dye from **1.32** under an acidic medium; (b) the reaction of H_2S with **1.33** with the formation of monosulfide **1.34**, used for the detection and quantification of H_2S.

However, the limit of detection (LOD) is quite high (~1.0 μM) and the assay is performed under acidic conditions, which may restrict its application in the cellular medium.[82] As an

TH-3161_176122050

alternative method, monobromobimane (**1.33**) is reacted with H_2S under alkaline conditions and forms a highly fluorescent compound **1.34**, which is measured using fluorescence spectroscopy (Scheme 1.5B).[81] However, non-specific reaction with other thiols is one of the limitations of this method.

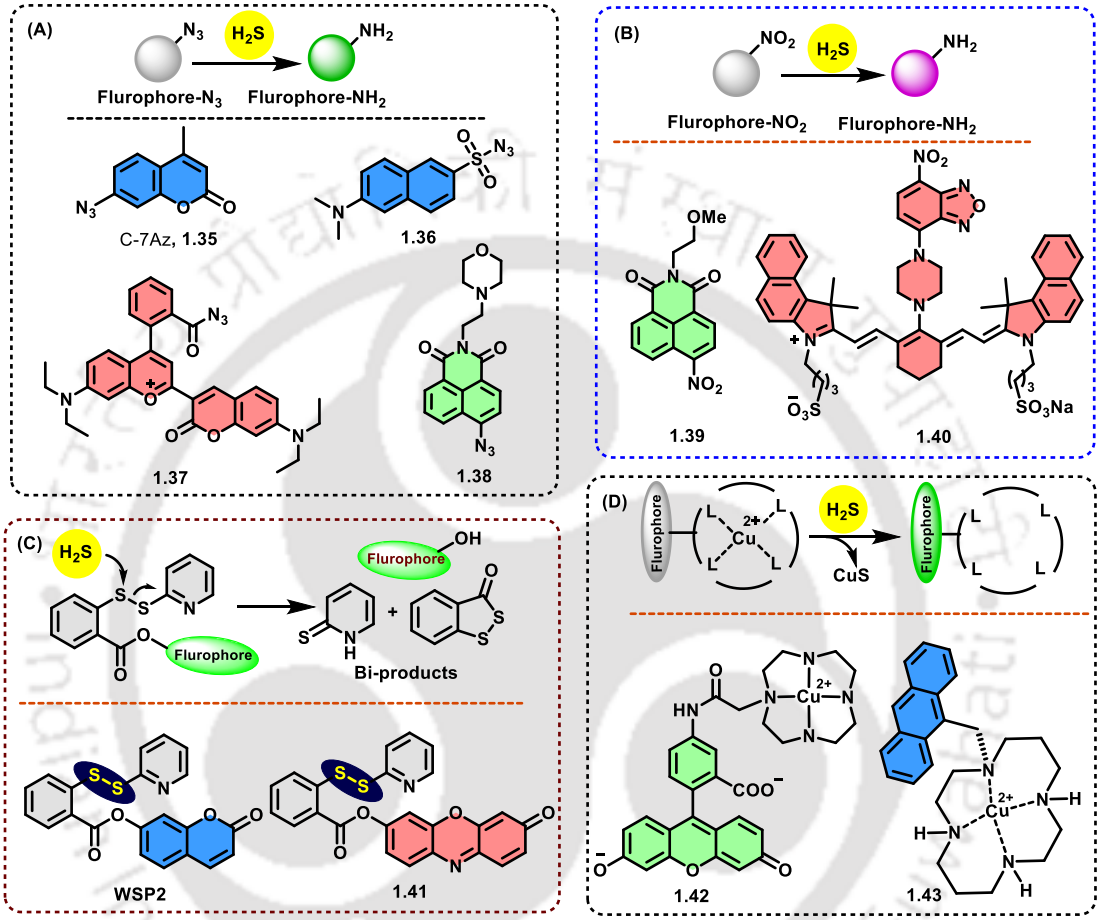

Figure 1.9. Chemical structures of different classes of turn-on fluorogenic probes for detecting H_2S.

The development of response-based probes for the detection of H_2S has attracted a lot of attention in recent years. Such probes were often designed with some H_2S-sensitive functional groups. However, this chemical process is typically irreversible, and can only measure the ultimate accumulated product not the dynamics of H_2S in real-time.[81] Despite these limitations, fluorogenic probes are very helpful for detecting endogenous H_2S in mammalian cells and tissues at sub-micromolar levels.

TH-3161_176122050

Most of the azido-based (**1.35-1.38**) and nitro-based (**1.39** and **1.40**) probes were designed in such a way that these probes showed very negligible fluorescence emission in the absence of H_2S and exhibited strong emission in the presence of H_2S (Figure 1.9A and B).[83-86]

However, these probes were interfered with other thiols also and showed turned-on fluorescence emission. For selective detection of H_2S, researchers developed **WSP2** and probe **1.41**, which showed a turned-on fluorescence signal upon the nucleophilic attack followed by cyclization in the presence of H_2S specifically (Figure 1.9C).[87, 88] In addition, turn-on fluorogenic organometallic compounds (**1.42** and **1.43**) for the specific detection of H_2S developed over time (Figure 1.9D).[89] The insoluble metal sulfide is precipitated out when the metal ion reacts with H_2S and showed strong emission.

1.12. Sources of H_2S

1.12.1. Dietary sources of H_2S

The allium and cruciferous family of vegetables such as garlic, onion, broccoli, and asparagus contain many organosulfur compounds (OSCs), which metabolize further in our body to produce the H_2S (Figure 1.10A). In garlic alone, more than 33 distinct OSCs have been found. Garlic contains several polar OSCs such as allicin, alliin, methyl-allyl thiosulfinate, and S-allyl cysteine. Moreover, allylic sulfides such as diallyl sulfide (DAS), diallyl disulfide (DADS), and diallyl trisulfide (DATS) are reported to be the active constituents of crushed garlic (Figure 1.10B).[90] These are well-investigated for their antioxidant and anti-cancer activities.[91]

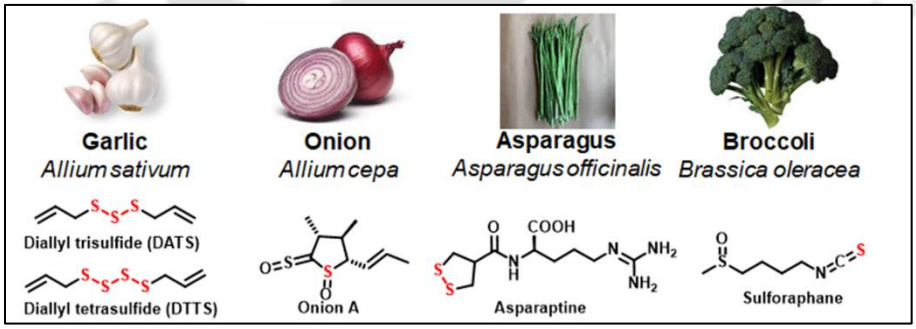

Figure 1.10. Examples of some representative allium cruciferous vegetables and chemical structures of some key OSCs present in those vegetables.

Sulforaphane has been found in cruciferous vegetables such as Brussels sprouts, broccoli, and cabbages. It activates the expression of the protein nuclear factor erythroid 2-related factor 2 (Nrf2), which has a promising impact on chemoprotection.[90] A popular nutritional

TH-3161_176122050

item consumed throughout the world is onion, which contains a variety of phytochemicals such as polysaccharides, saponins, phenolic compounds, and OSCs. Notably, OSCs in onion such as onionin A, cycloalliin, methiin, and propiin have antioxidant, anti-inflammatory, and anti-cancer effects.[92] Asparaptine, a recently identified chemical found in asparagus, acts as a potent inhibitor of the angiotensin-converting enzyme (ACE).[93]

1.12.2. Biosynthesis of H_2S

In addition to dietary sources of H_2S, it produces in our body enzymatically in the presence of different enzymes, including cystathionine-γ-lyase (CSE), cystathionine-β-synthase (CBS), and cysteine aminotransferase (CAT) in combination with 3-mercaptopyruvate sulfurtransferase (3-MST) (Figure 1.11).[94] Recent research has shown that D-amino acid oxidase (DAO) and 3-MST can produce H_2S when D-cysteine is used as the substrate.[95] It has been found that 3-MST is responsible for 90% of the H_2S generation in the brain. It is interesting to note that 3-MST is mostly present in mitochondria and uses the metabolism of CAT to produce H_2S from α-ketoglutarate and L-cysteine.[96] A significant portion of the H_2S synthesis in brain is dependent on 3-MST in neurons.[97]

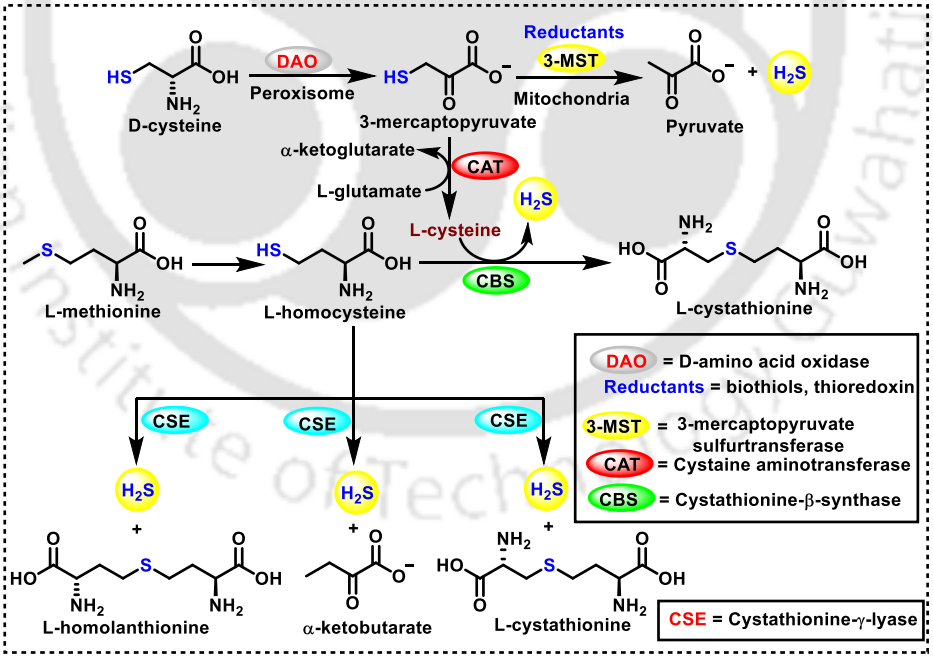

Figure 1.11. Biosynthetic pathways of H_2S production in mammalian cells.

H_2S has been found to control the metabolic demand in mitochondria like nitric oxide (NO).[98] However, the generation of H_2S is exclusively controlled in the cytoplasm and further utilized

TH-3161_176122050

in the mitochondria through oxidation. Moreover, it has been demonstrated that H_2S protects mitochondria and controls several processes including respiration, redox balance, and metabolism.[99] Current studies shows that using low concentrations of sulfide (as an energy substrate) to treat human colon cancer is safe and effective.[100] It is interesting to note that Abe and Kimura's seminal 1996 article highlighted the role of endogenously produced H_2S in cell signaling and cellular process regulation.[101] For cellular homeostasis and redox equilibrium, H_2S biosynthesis is essential. The quantity of H_2S is dysregulated in many diseases.[102] Therefore, in the case of a cellular H_2S deficiency, exogenous H_2S donation is required to maintain its ideal cellular concentration. Several exogenous H_2S donors such as hydrolysis-based, thiol-triggered, ROS-responsive, etc. were developed over time.

1.12.3. Hydrolysis-based H_2S donors

Sulfide salts like sodium hydrosulfide (NaSH) and sodium sulfide (Na_2S) are the most often used inorganic donors of H_2S in the biological system. Sulfide salts were used extensively as a therapeutic tool to comprehend the signaling pathways of H_2S. The sulfide salts tend to create an equilibrium between H_2S, HS^-, and S^{2-} species. However, H_2S can produce instantly after administration and evaporation can occur rapidly. As a result, using inorganic salts as H_2S donors make it difficult to obtain the necessary concentration of H_2S.[103] Therefore, the development of slow H_2S donors were necessary, which might be useful against various disease models.[103] Several hydrolysis-based H_2S donors developed over time as shown in Figure 1.12.[104] For instance, a Lawesson's reagent (LR) is a commercially available sustained donor of H_2S that can release H_2S for a prolonged period. In addition, it was found that a water-soluble LR derivative called GYY4137 produced H_2S continuously under physiological conditions. It is interesting to note that an aqueous solution of GYY4137 caused plasma sulfide levels to considerably increase after 30 minutes of treatment and remain elevated for the following two hours.[76] A different class of H_2S donors based on hydrolysis are 1,2-dithiol-3-thiones (DTTs) and derivatives. It is noteworthy that an analog of DTT called **ADT-OH** is employed during chemotherapy for certain forms of aggressive malignancies.[105]

TH-3161_176122050

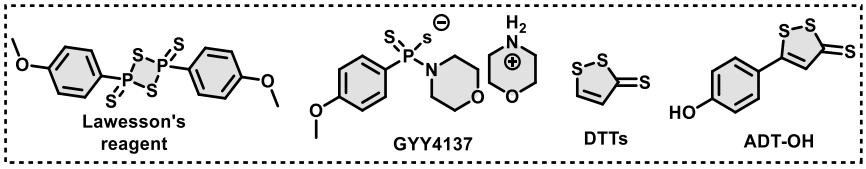

Figure 1.12. Chemical structures of some representative hydrolysis-triggered H_2S donors.

1.12.4. Bio-thiol-triggering H_2S donors

Since bio-thiols (glutathione, L-cysteine, and L-homocysteine) are more abundant in the mammalian cellular environment, thiol-triggered H_2S donors would be more advantageous over other chemical donors. In the presence of bio-thiols, garlic-derived polysulfides (DATS and DTTS) are well-known as H_2S donors. However, these are volatile and difficult to handle. Therefore, in 2017, Pluth and co-workers reported synthetic phenyl analogs of DTTS (**S-tetrasulfides**) (Figure 1.13).[106] They observed that the synthesized tetrasulfides release more H_2S per molecule than DATS or DTTS in the presence of glutathione (GSH). Moreover, in 2020, Bhabak and co-workers developed thiol-triggered non-fluorogenic (**DBTS**) and trisulfide-linked fluorogenic donors of H_2S (**UTS-1** and **UTS-2**) (Figure 1.13).[107] Both the probes are suitable for releasing H_2S in the presence of GSH significantly and monitored the release of H_2S using MB assay. It is to be noted that the lysosome targeting moiety morpholine was connected in **UTS-2** to track the release of intracellular H_2S and its subsequent trafficking to the lysosomes.

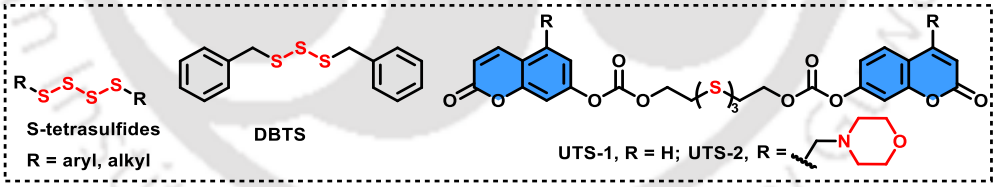

Figure 1.13. Chemical structures of some representative bio-thiol-triggering H_2S donors.

1.12.5. H_2O_2-responsive H_2S donors

Hydrogen sulfide exhibits strong anti-inflammatory effects in cells and antioxidant properties, protective benefits against ROS.[108] H_2S also protects against myocardial ischemia-reperfusion (MI/R) injury by consuming ROS produced by mitochondria and maintains heart activity.[109] Biomarker-responsive thiocarbamate linker-based probes are also another class of substance that release H_2S. When the triggering unit reacts with the biomarker, carbonyl sulfide (COS) is released through self-immolation, and further transform into H_2S in the presence of carbonic anhydrase (CA) enzyme.

TH-3161_176122050

In 2016, Pluth and co-workers developed the first H_2O_2-responsive H_2S donor **PeroxyTCM-1**, where boronate ester was connected to the other substrate *via* thiocarbamate unit (Figure 1.14).[110] Interestingly, the donor showed dose-dependent cytoprotective properties (10–50 μM) in HeLa cells against H_2O_2-induced toxicity. This result indicates that boronate esters reacted with intracellular H_2O_2 and generated the COS, which further transformed into H_2S and protected the cells from oxidative damage. Fluorescence spectroscopy has received a lot of interest, which offers superior spatial and temporal sampling capacities and great sensitivity. Therefore, fluorogenic H_2S donors will be extremely useful for monitoring the H_2S in a real-time manner in biological systems. In 2019, Xian and co-workers developed the first H_2O_2-triggered fluorogenic H_2S donor **NAB** (Figure 1.14).[111] To get this probe, H_2O_2-triggering moiety aryl boronate was connected to the fluorophore, 3-amino-*N*-butyl-1,8-naphthalimide (**NAH**) *via* thiocarbamate. When **NAB** released COS and **NAH** in the presence of H_2O_2 through a self-immolative process. The ubiquitous enzyme CA then converted COS rapidly to H_2S. Most significantly, **NAB** showed a cytoprotective effect against ROS in RAW 264.7 cells. Since H_2O_2 is generated in mitochondria, in 2020, He and co-workers developed mitochondria-targeted H_2O_2-responsive fluorogenic H_2S donor **HSD-B**.[112] In addition to precisely targeting mitochondria, **HSD-B** exhibited ratiometric fluorescence for the visualization and measurement of H_2S release. Furthermore, the released H_2S exhibited protective properties in a cellular model of cardiac I/R injury. Nevertheless, because of its shorter emission wavelength (455 nm), **HSD-B** was incompatible to provide the desired *in vivo* self-reporting fluorescence. To overcome the aforementioned crucial problems, in 2021, Luo-Zhang and co-workers developed a novel H_2S donor **HSD-R** by incorporating a NIR fluorophore (λ_{em} = 705 nm) with an H_2O_2-responsive moiety *via* thiocarbamate linker.[113] Since the NIR fluorophore have high cell penetration power and minimum interference with biomolecules, the distribution profiles and release kinetics of H_2S measured *in vivo* using this probe.

TH-3161_176122050

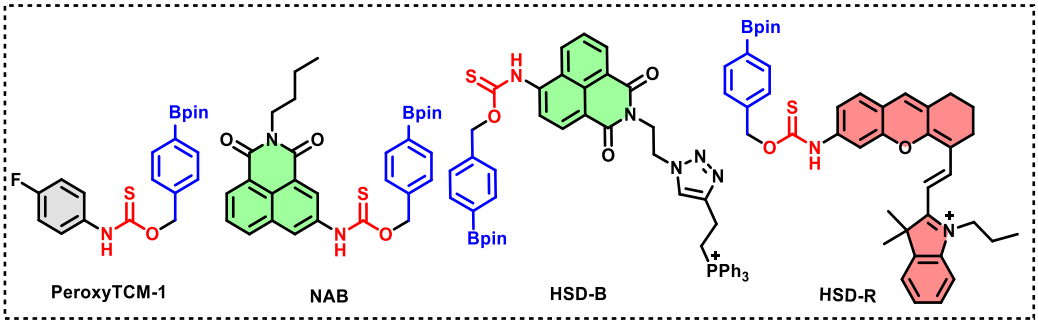

Figure 1.14. Chemical structures of some representative H_2O_2-responsive H_2S donors

1.13. H_2S-conjugated anti-inflammatory prodrugs

Non-steroidal anti-inflammatory drugs (NSAIDs) are primarily available over the counter and frequently used to treat both acute and chronic inflammation.[114] Over 30 million people worldwide take NSAIDs regularly to alleviate pain, fever, and various inflammatory conditions such as rheumatoid arthritis (RA), osteoarthritis, migraine, gout, and oral infections.[115] Injured tissues release an excessive amount of prostaglandins, which are linked to the signs and symptoms of acute inflammation.[115] Cyclooxygenase (COX-1 and COX-2) enzymes play a major role in the biosynthesis of prostaglandins from arachidonic acid, and their reversible inhibition by NSAIDs is a significant contributor to their anti-inflammatory actions.[115, 116] The COX-2 isoform is induced at inflammatory sites and promotes inflammation and pain, whereas COX-1 expression is constitutive and related to protecting the gastric mucosa.[117] To control inflammation and other disorders, it is crucial to reduce COX-2 overexpression selectively. However, because of an elevated risk of heart attacks and strokes, the selective COX-2 inhibitors (the coxib family) except celecoxib have been removed from the market.[118] The carboxylic acid group in drugs like aspirin, ibuprofen, and diclofenac, as well as the acidic enolic group in oxicams like piroxicam, are additional factors that contribute to the gastrointestinal side effects of non-selective COX inhibitors. These acidic groups of NSAIDs produce local irritation, resulting in gastrointestinal side effects either on their own or in conjunction with the inhibition of the COX-1 enzyme.[119, 120] Moreover, The use of NSAIDs involves an unacceptable risk of gastrointestinal bleeding and ulceration.[121] The effectiveness of H_2S to minimize the gastrointestinal (GI) tract damage is remarkable, especially cytoprotective action also prevents the severe bleeding and injury that can be carried in the small intestine by continuous NSAID treatment.[122] To address these

TH-3161_176122050

issues, DTTs, and ADT-OH coupled with NSAIDs to develop hydrogen sulfide and NSAIDs hybrid prodrug (HS-NSAIDs) (Figure 1.15).

In 2007, Moore and co-workers developed HS-NSAID-hybrid prodrug HS-Diclofenac, where ADT-OH was coupled to diclofenac in an attempt to improve the anti-inflammatory effects of the prodrug.[123] It is interesting to note that the oral administration of HS-Diclofenac decreased COX-1 and COX-2 activity dose-dependently and the effectiveness was comparable to that of diclofenac. Moreover, pretreatment with HS-Diclofenac and diclofenac resulted in a decrease in the volume of carrageenan-induced paw edema. The treatment with HS-diclofenac at 10 mmol/kg reduced the production of edema in a manner comparable to that observed following diclofenac at 30 mmol/kg. The release of H_2S from HS-Diclofenac was largely responsible for this improved potency. Several HS-NSAIDs, such as HS-Sulindac, HA-Aspirin, HS-Ibuprofen, and HS-Naproxen developed to exhibit anti-proliferative effects against human colon, breast, pancreatic, prostate, lung, and leukemia cancer cell lines in addition to their anti-inflammatory effects.[124] Interestingly, they exhibited a notable decrease in gastro-intestinal damage compared to the parent NSAIDs.[125] Also, the anti-inflammatory effects of HS-NSAIDs are enhanced compared to their NSAID counterparts.

However, it is not clear whether the active drug was released or activity was observed from the modified NSAIDs, which were formed after hydrolysis of DTT to release the H_2S. Additionally, the drug delivery is not specific and selective towards inflammatory sites. Therefore, the development of ROS-responsive prodrugs of NSAIDs is very important, which may overcome the limitations of existing drugs as well as prodrugs. However, in comparison to non-fluorogenic prodrugs, the strategies of turn-on fluorogenic prodrugs have extra advantages for real-time monitoring of the drug release, suitable for the *in vitro* and *in vivo* applications.

TH-3161_176122050

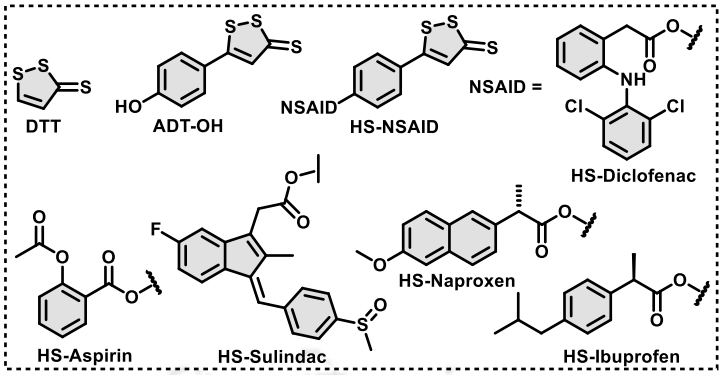

Figure 1.15. Chemical structures of some representative **HS-NSAID** hybrids.

1.14. Thesis Objectives

From the above reported literatures, we found that several H_2O_2-responsive fluorogenic probes were developed over time to measure or detect the most abundant cellular ROS (H_2O_2) *in vitro* as well as *in vivo*. However, the linkers to connect the fluorophore with the H_2O_2-responsive unit were chosen randomly. Therefore, a solid rationalization is necessary for the sensitivity and reactivity of the probes to the target analyte (H_2O_2), which may help to choose the proper linker for the development of probes/prodrugs for sensing H_2O_2 for the delivery of drugs in a sustainable way. It is to be mentioned that NIR fluorophore is the best choice for the development of different H_2O_2-responsive fluorescent probes or theranostic prodrugs because of its high cell penetrating power, and minimum interference with different biomolecules. Since anti-inflammatory drugs have several serious side-effects, the development of anti-inflammatory prodrugs is very important in recent days. However, very few reports are there on the H_2O_2-responsive non-fluorogenic prodrug of anti-inflammatory drugs. Therefore, H_2O_2-responsive fluorogenic prodrugs of anti-inflammatory drugs need to be developed further for monitoring the drug release in real-time in living cells. From the previous literature reports, several H_2S-conjugated non-steroidal anti-inflammatory drugs (NSAIDs) prodrugs developed over time to reduce the side effects of NSAIDs and to improve the anti-inflammatory activity. Despite showing enhancement in anti-inflammatory activity and reducing side effects of NSAIDs by these prodrugs, the active drug is not released from the prodrug due to the absence of any triggering unit to activate the prodrug. Additionally, these prodrugs are inadequate to monitor the drug as well as H_2S release in real-time manner in living cells. Therefore, it is very important to develop an H_2O_2-responsive theranostic

TH-3161_176122050

prodrug of anti-inflammatory drugs with co-delivery of H_2S. Furthermore, peroxide-responsive fluorogenic anti-cancer prodrug can be developed for adjuvant delivery of the anti-cancer drug with H_2S to reduce the side-effects of corresponding anti-cancer drug.

1.15. Thesis overview

The thesis comprised five chapters. **Chapter 1** highlighted the basic information about ROS generation and its biological roles in the body. Moreover, in this chapter, we discussed the development of H_2O_2-responsive probes, non-fluorogenic prodrugs, and fluorogenic prodrugs for cancer and inflammatory diseases. Furthermore, we discussed on the importance of H_2S in the biological system and elucidated the development of external H_2S donors and their corresponding applications. In **chapter 2**, we rationally designed and synthesized H_2O_2-responsive probes using three different fluorophores, which were connected to an H_2O_2-responsive unit boronate ester *via* three different linkers (direct, ether, and carbonate) to understand the suitable linker for sustained drug delivery. From the spectroscopic studies and *in vitro* studies, we observed that directly connected boronate ester probes were found to be appropriate for sensing H_2O_2 effectively. However, the self-immolating linker-based probes may find wider application in H_2O_2-responsive prodrug development, which requires a sustained and regulated drug release profile. As we observed in **chapter 2**, self-immolative linked boronate ester probes are suitable for sustained drug delivery; therefore, H_2O_2-responsive turn-on fluorogenic prodrug (**DCI-ROS**) of an NSAID (diclofenac) developed in **chapter 3**, where the fluorophore was connected with the ROS-responsive unit through an ether linker. The spectroscopic and *in vitro* studies were carried out thoroughly to understand release of the fluorophore and drug. Spectroscopic studies confirmed the sustained release of the drug. Furthermore, the prodrug **DCI-ROS** exhibited selectivity towards inflammatory sites over normal tissues, which was confirmed from fluorescence microscopic studies in RAW 264.7 cells (with and without LPS pre-treatment). In **chapter 4**, we took the initiative to develop an H_2O_2-responsive theranostic prodrug of an NSAID (diclofenac) with H_2S (**DCF-HS**). The release of fluorophore **DCI-NH$_2$**, drug **DCF**, and H_2S were studied in both an aqueous and cellular medium. Spectroscopic studies indicated the sustained release of fluorophore and drug. Importantly, the effect of released drug **DCF** and H_2S were investigated using western blot analysis. The prodrug **DCF-HS** showed similar anti-inflammatory activity as the parent drug **DCF**, which indicated the release of the active drug

TH-3161_176122050

from the prodrug in the presence of endogenous ROS. In **chapter 5**, we developed a ROS-responsive fluorogenic prodrug (**AM-TCB**) of the anti-cancer drug amonafide along with the delivery of H_2S. We carried out several studies such as spectroscopic, HPLC, and cellular studies to investigate the release of the drug and H_2S and its activity. The results from several studies supported the release of the drug and H_2S in the presence of H_2O_2. Most importantly, our designed prodrug **AM-TCB** showed selectivity towards cancer cells (HeLa) over normal cells (HEK-293). The cytotoxicity of the prodrug **AM-TCB** is similar to free drug amonafide for cancer cells and less toxic towards normal cells as compared to amonafide.

1.16. References

1. D. B. Zorov, M. Juhaszova and S. J. Sollott, *Physiol. Rev.*, 2014, **94**, 909-950.
2. T. Finkel, *Curr. Opin. Cell Biol.*, 2003, **15**, 247-254.
3. S. G. Rhee, *Science*, 2006, **312**, 1882-1883.
4. M. P. Murphy, A. Holmgren, N.-G. Larsson, B. Halliwell, C. J. Chang, B. Kalyanaraman, S. G. Rhee, P. J. Thornalley, L. Partridge and D. Gems, *Cell Metab.*, 2011, **13**, 361-366.
5. D. E. Handy and J. Loscalzo, *Antioxid. Redox Signaling*, 2012, **16**, 1323-1367.
6. T. Fukai and M. Ushio-Fukai, *Antioxid. Redox Signaling*, 2011, **15**, 1583-1606.
7. M. Schieber and N. S. Chandel, *Curr. Biol.*, 2014, **24**, R453-R462.
8. R. Mittler, *Trends Plant Sci.*, 2017, **22**, 11-19.
9. Y. Yang, S. Karakhanova, J. Werner and A. V Bazhin, *Curr. Med. Chem.*, 2013, **20**, 3677-3692.
10. X. Li, P. Fang, J. Mai, E. T. Choi, H. Wang and X.-f. Yang, *J. Hematol. Oncol.*, 2013, **6**, 1-19.
11. J. A. Imlay, *Nat. Rev. Microbiol.*, 2013, **11**, 443-454.
12. V. Vallyathan and X. Shi, *Environ. Health Perspect.*, 1997, **105**, 165-177.
13. L. Tong, C.-C. Chuang, S. Wu and L. Zuo, *Cancer Lett.* , 2015, **367**, 18-25.
14. H. J. Shields, A. Traa and J. M. Van Raamsdonk, *Front. Cell Dev. Biol.*, 2021, **9**, 181.
15. M. Giorgio, M. Trinei, E. Migliaccio and P. G. Pelicci, *Nat. Rev. Mol. Cell Biol.*, 2007, **8**, 722-728.
16. M. T. Lin and M. F. Beal, *Nature*, 2006, **443**, 787-795.
17. G. Saravanakumar, J. Kim and W. J. Kim, *Adv. Sci.*, 2017, **4**, 1600124.

TH-3161_176122050

18. F. Yang, M. Zhu, J. Zhang and H. Zhou, *MedChemComm*, 2018, **9**, 201-211.
19. H. S. Ban and H. Nakamura, *Chem. Rec.*, 2015, **15**, 616-635.
20. G. F. S. Fernandes, W. A. Denny and J. L. Dos Santos, *Eur. J. Med. Chem.*, 2019, **179**, 791-804.
21. A. Bedini, A. Fraternale, R. Crinelli, M. Mari, S. Bartolucci, L. Chiarantini and G. Spadoni, *Chem. Res. Toxicol.*, 2018, **32**, 100-112.
22. X. Wu, X. Li, Z. Li, Y. Yu, Q. You and X. Zhang, *J. Med. Chem.*, 2018, **61**, 11280-11297.
23. A. T. Dharmaraja, *J. Med. Chem.*, 2017, **60**, 3221-3240.
24. M. Gutowski and S. Kowalczyk, *Acta Biochim. Pol.*, 2013, **60**.
25. R. Weinstain, E. N. Savariar, C. N. Felsen and R. Y. Tsien, *J. Am. Chem. Soc.*, 2014, **136**, 874-877.
26. R. Kumar, J. Han, H.-J. Lim, W. X. Ren, J.-Y. Lim, J.-H. Kim and J. S. Kim, *J. Am. Chem. Soc.*, 2014, **136**, 17836-17843.
27. D. Lee, S. Park, S. Bae, D. Jeong, M. Park, C. Kang, W. Yoo, M. A. Samad, Q. Ke and G. Khang, *Sci. Rep.*, 2015, **5**, 16592.
28. N. S. Andersen, J. P. Cadahía, V. Previtali, J. Bondebjerg, C. A. Hansen, A. E. Hansen, T. L. Andresen and M. H. Clausen, *Eur. J. Med. Chem.*, 2018, **156**, 738-746.
29. S. Rajpal, A. Kumar and W. Joe, *PloS One*, 2018, **13**, e0193320.
30. P. Huang, D. Wang, Y. Su, W. Huang, Y. Zhou, D. Cui, X. Zhu and D. Yan, *J. Am. Chem. Soc.*, 2014, **136**, 11748-11756.
31. N. Wang, Y. Wu, J. Bian, X. Qian, H. Lin, H. Sun, Q. You and X. Zhang, *Curr. Cancer Drug Targets*, 2017, **17**, 122-136.
32. Y. Kuang, K. Balakrishnan, V. Gandhi and X. Peng, *J. Am. Chem. Soc.*, 2011, **133**, 19278-19281.
33. W. Chen, Y. Han and X. Peng, *Chem. Eur. J.*, 2014, **20**, 7410-7418.
34. S. Zheng, S. Guo, Q. Zhong, C. Zhang, J. Liu, L. Yang, Q. Zhang and G. Wang, *ACS Med. Chem. Lett.*, 2018, **9**, 149-154.
35. L. T. Geller, M. Barzily-Rokni, T. Danino, O. H. Jonas, N. Shental, D. Nejman, N. Gavert, Y. Zwang, Z. A. Cooper and K. Shee, *Science*, 2017, **357**, 1156-1160.

TH-3161_176122050

36. K. Matsushita, T. Okuda, S. Mori, M. Konno, H. Eguchi, A. Asai, J. Koseki, Y. Iwagami, D. Yamada and H. Akita, *ChemMedChem*, 2019, **14**, 1384-1391.
37. T. Finkel, *Curr. Opin. Cell Biol.*, 2003, **15**, 247-254.
38. R. Brandt and A. S. Keston, *Anal. Biochem.*, 1965, **11**, 6-9.
39. D. S. Yoon, M.-H. Lee and D. S. Cha, *Bio-protocol*, 2018, **8**, e2774-e2774.
40. S. Kenmoku, Y. Urano, H. Kojima and T. Nagano, *J. Am. Chem. Soc.*, 2007, **129**, 7313-7318.
41. L. M. Hyman and K. J. Franz, *Coord. Chem. Rev.*, 2012, **256**, 2333-2356.
42. M. C. Chang, A. Pralle, E. Y. Isacoff and C. J. Chang, *J. Am. Chem. Soc.*, 2004, **126**, 15392-15393.
43. E. W. Miller, A. E. Albers, A. Pralle, E. Y. Isacoff and C. J. Chang, *J. Am. Chem. Soc.*, 2005, **127**, 16652-16659.
44. E. W. Miller, O. Tulyathan, E. Y. Isacoff and C. J. Chang, *Nat. Chem. Biol.*, 2007, **3**, 263-267.
45. B. C. Dickinson and C. J. Chang, *J. Am. Chem. Soc.*, 2008, **130**, 9638-9639.
46. G. Gao, D. Gong, M. Zhang and T. Sun, *Acta Chim. Sin.*, 2016, **74**, 363.
47. F. Xu, H. Li, Q. Yao, J. Fan, J. Wang and X. Peng, *J. Mat. Chem. B*, 2016, **4**, 7363-7367.
48. R. Y. Tsien and M. Poenie, *Trends Biochem. Sci.*, 1986, **11**, 450-455.
49. D. Srikun, E. W. Miller, D. W. Domaille and C. J. Chang, *J. Am. Chem. Soc.*, 2008, **130**, 4596-4597.
50. G. Masanta, C. H. Heo, C. S. Lim, S. K. Bae, B. R. Cho and H. M. Kim, *Chem. Commun.*, 2012, **48**, 3518-3520.
51. K. B. Daniel, A. Agrawal, M. Manchester and S. M. Cohen, *ChemBioChem*, 2013, **14**, 593-598.
52. C. Liu, C. Shao, H. Wu, B. Guo, B. Zhu and X. Zhang, *RSC Adv.*, 2014, **4**, 16055-16061.
53. R. F. Dielschneider, E. S. Henson and S. B. Gibson, *Oxid. Med. Cell. Longevity*, 2017, **2017**.
54. W. Peng, G. Minakaki, M. Nguyen and D. Krainc, *Neurotherapeutics*, 2019, **16**, 611-634.

TH-3161_176122050

55. D. Kim, G. Kim, S.-J. Nam, J. Yin and J. Yoon, *Sci. Rep.*, 2015, **5**, 8488.
56. R. D. Hanna, Y. Naro, A. Deiters and P. E. Floreancig, *J. Am. Chem. Soc.*, 2016, **138**, 13353-13360.
57. J. Liu, J. Ren, X. Bao, W. Gao, C. Wu and Y. Zhao, *Anal. Chem.*, 2016, **88**, 5865-5870.
58. J. Liu, S. Zhou, J. Ren, C. Wu and Y. Zhao, *Analyst*, 2017, **142**, 4522-4528.
59. Y. Shen, X. Zhang, Y. Zhang, Y. Wu, C. Zhang, Y. Chen, J. Jin and H. Li, *Sens. Actuators, B*, 2018, **255**, 42-48.
60. B. Sarkar and P. Paira, *Mini-Rev. Med. Chem.*, 2018, **18**, 969-975.
61. M. H. Lee, J. Y. Kim, J. H. Han, S. Bhuniya, J. L. Sessler, C. Kang and J. S. Kim, *J. Am. Chem. Soc.*, 2012, **134**, 12668-12674.
62. S. Maiti, N. Park, J. H. Han, H. M. Jeon, J. H. Lee, S. Bhuniya, C. Kang and J. S. Kim, *J. Am. Chem. Soc.*, 2013, **135**, 4567-4572.
63. S. Bhuniya, M. H. Lee, H. M. Jeon, J. H. Han, J. H. Lee, N. Park, S. Maiti, C. Kang and J. S. Kim, *Chem. Commun.*, 2013, **49**, 7141-7143.
64. S. Bhuniya, S. Maiti, E. J. Kim, H. Lee, J. L. Sessler, K. S. Hong and J. S. Kim, *Angew. Chem. Int. Ed.*, 2014, **126**, 4558-4563.
65. E.-J. Kim, S. Bhuniya, H. Lee, H. M. Kim, C. Cheong, S. Maiti, K. S. Hong and J. S. Kim, *J. Am. Chem. Soc.*, 2014, **136**, 13888-13894.
66. R. Kumar, J. Han, H.-J. Lim, W. X. Ren, J.-Y. Lim, J.-H. Kim and J. S. Kim, *J. Am. Chem. Soc.*, 2014, **136**, 17836-17843.
67. O. Redy-Keisar, S. Ferber, R. Satchi-Fainaro and D. Shabat, *ChemMedChem*, 2015, **10**, 999-1007.
68. X. Gao, J. Cao, Y. Song, X. Shu, J. Liu, J. Z. Sun, B. Liu and B. Z. Tang, *RSC Adv.*, 2018, **8**, 10975-10979.
69. L.-L. Pan, M. Qin, X.-H. Liu and Y.-Z. Zhu, *Front. Pharmacol.*, 2017, **8**, 686.
70. J. Lewerenz, S. J. Hewett, Y. Huang, M. Lambros, P. W. Gout, P. W. Kalivas, A. Massie, I. Smolders, A. Methner and M. Pergande, *Antioxid. Redox Signaling*, 2013, **18**, 522-555.
71. W.-H. Sun, F. Liu, Y. Chen and Y.-C. Zhu, *Biochem. Biophys. Res. Commun.*, 2012, **421**, 164-169.

TH-3161_176122050

72. Z.-Z. Xie, Y. Liu and J.-S. Bian, *Oxid. Med. Cell. Longevity*, 2016, **2016**.
73. G. Yang, L. Wu, B. Jiang, W. Yang, J. Qi, K. Cao, Q. Meng, A. K. Mustafa, W. Mu and S. Zhang, *Science*, 2008, **322**, 587-590.
74. M. Bhatia, *IUBMB Life*, 2005, **57**, 603-606.
75. D. G. Searcy, J. P. Whitehead and M. J. Maroney, *Arch. Biochem. Biophys.*, 1995, **318**, 251-263.
76. L. Li, M. Whiteman, Y. Y. Guan, K. L. Neo, Y. Cheng, S. W. Lee, Y. Zhao, R. Baskar, C.-H. Tan and P. K. Moore, *Circulation*, 2008, **117**, 2351-2360.
77. J. W. Calvert, S. Jha, S. Gundewar, J. W. Elrod, A. Ramachandran, C. B. Pattillo, C. G. Kevil and D. J. Lefer, *Circ. Res.*, 2009, **105**, 365-374.
78. A. Sivarajah, M. Collino, M. Yasin, E. Benetti, M. Gallicchio, E. Mazzon, S. Cuzzocrea, R. Fantozzi and C. Thiemermann, *Shock*, 2009, **31**, 267-274.
79. F.-S. Quan and G.-J. Lee, *BioMed Res. Int.*, 2021, **2021**.
80. H. Ibrahim, A. Serag and M. A. Farag, *J. Adv. Res.*, 2021, **27**, 137-153.
81. M. D. Hartle and M. D. Pluth, *Chem. Soc. Rev.*, 2016, **45**, 6108-6117.
82. X. Shen, E. A. Peter, S. Bir, R. Wang and C. G. Kevil, *Free Radic. Biol. Med.*, 2012, **52**, 2276-2283.
83. Y.-W. Duan, X.-F. Yang, Y. Zhong, Y. Guo, Z. Li and H. Li, *Anal. Chim. Acta*, 2015, **859**, 59-65.
84. B. Chen, W. Li, C. Lv, M. Zhao, H. Jin, H. Jin, J. Du, L. Zhang and X. Tang, *Analyst*, 2013, **138**, 946-951.
85. K. Wang, H. Peng, N. Ni, C. Dai and B. Wang, *J. Fluoresc.*, 2014, **24**, 1-5.
86. Q. Qiao, M. Zhao, H. Lang, D. Mao, J. Cui and Z. Xu, *RSC Adv.*, 2014, **4**, 25790-25794.
87. C. Liu, B. Peng, S. Li, C.-M. Park, A. R. Whorton and M. Xian, *Org. Lett.*, 2012, **14**, 2184-2187.
88. B. Peng, W. Chen, C. Liu, E. W. Rosser, A. Pacheco, Y. Zhao, H. C. Aguilar and M. Xian, *Chem. Eur. J.*, 2014, **20**, 1010-1016.
89. V. S. Lin, W. Chen, M. Xian and C. J. Chang, *Chem. Soc. Rev.*, 2015, **44**, 4596-4618.
90. S. M de Figueiredo, N. S Binda, J. A Nogueira-Machado, S. A Vieira-Filho and R. B Caligiorne, *Recent Pat. Endocr., Metab. Immune Drug Discovery*, 2015, **9**, 24-39.

TH-3161_176122050

91. X.-X. Zhao, F.-J. Lin, H. Li, H.-B. Li, D.-T. Wu, F. Geng, W. Ma, Y. Wang, B.-H. Miao and R.-Y. Gan, *Front. Nutr.*, 2021, **8**, 669805.
92. X.-X. Zhao, F.-J. Lin, H. Li, H.-B. Li, D.-T. Wu, F. Geng, W. Ma, Y. Wang, B.-H. Miao and R.-Y. Gan, *Front. Nutr.*, 2021, **8**, 669805.
93. K. Miyoshi, Y. Enomoto, E. Fukusaki and S. Shimma, *Anal. Sci.*, 2018, **34**, 997-1001.
94. X. Cao, L. Ding, Z.-z. Xie, Y. Yang, M. Whiteman, P. K. Moore and J.-S. Bian, *Antioxid. Redox Signaling*, 2019, **31**, 1-38.
95. M. D. Pluth, T. S. Bailey, M. D. Hammers, M. D. Hartle, H. A. Henthorn and A. K. Steiger, *Synlett*, 2015, **26**, 2633-2643.
96. N. Shibuya, M. Tanaka, M. Yoshida, Y. Ogasawara, T. Togawa, K. Ishii and H. Kimura, *Antioxid. Redox Signaling*, 2009, **11**, 703-714.
97. C. K. Nicholson and J. W. Calvert, *Pharmacol. Res.*, 2010, **62**, 289-297.
98. D. K. Liu and S. Chang, *Can. J. Chem.*, 1987, **65**, 770-774.
99. D. G. Searcy, *Cell Res.*, 2003, **13**, 229-238.
100. M. Goubern, M. Andriamihaja, T. Nübel, F. Blachier and F. Bouillaud, *FASEB J.*, 2007, **21**, 1699-1706.
101. K. Abe and H. Kimura, *J. Neurosci.*, 1996, **16**, 1066-1071.
102. R. Wang, *FASEB J.*, 2002, **16**, 1792-1798.
103. C. R. Powell, K. M. Dillon and J. B. Matson, *Biochem. Pharmacol.*, 2018, **149**, 110-123.
104. C. R. Powell, K. M. Dillon and J. B. Matson, *Biochem. Pharmacol.*, 2018, **149**, 110-123.
105. E. Magli, E. Perissutti, V. Santagada, G. Caliendo, A. Corvino, G. Esposito, G. Esposito, F. Fiorino, M. Migliaccio and A. Scognamiglio, *Biomolecules*, 2021, **11**, 1899.
106. M. M. Cerda, M. D. Hammers, M. S. Earp, L. N. Zakharov and M. D. Pluth, *Org. Lett.*, 2017, **19**, 2314-2317.
107. S. K. Mahato, D. Bhattacherjee and K. P. Bhabak, *Chem. Commun.*, 2020, **56**, 7769-7772.
108. L. Chang, B. Geng, F. Yu, J. Zhao, H. Jiang, J. Du and C. Tang, *Amino Acids*, 2008, **34**, 573-585.

TH-3161_176122050

109. J. W. Calvert, W. A. Coetzee and D. J. Lefer, *Antioxid. Redox Signaling*, 2010, **12**, 1203-1217.
110. Y. Zhao and M. D. Pluth, *Angew. Chem. Int. Ed.*, 2016, **128**, 14858-14862.
111. Y. Hu, X. Li, Y. Fang, W. Shi, X. Li, W. Chen, M. Xian and H. Ma, *Chem. Sci.*, 2019, **10**, 7690-7694.
112. N. Zhang, P. Hu, Y. Wang, Q. Tang, Q. Zheng, Z. Wang and Y. He, *ACS Sensors*, 2020, **5**, 319-326.
113. M. Yao, Y. Lu, L. Shi, Y. Huang, Q. Zhang, J. Tan, P. Hu, J. Zhang, G. Luo and N. Zhang, *Bioact. Mater.*, 2022, **9**, 168-182.
114. C. Patrono and B. Rocca, *Pharmacol. Res.*, 2009, **59**, 285-289.
115. R. M. Haley and H. A. von Recum, *Expt Biol Med*, 2019, **244**, 433-444.
116. K. M. Knights, A. A. Mangoni and J. O. Miners, *Expert Rev. Clin. Pharmacol.*, 2010, **3**, 769-776.
117. R. N. DuBois, S. B. Abramson, L. Crofford, R. A. Gupta, L. S. Simon, L. B. A. van de Putte and P. E. Lipsky, *FASEB J.*, 1998, **12**, 1063-1073.
118. M. Bäck, L. Yin and E. Ingelsson, *Eur. Heart J.*, 2012, **33**, 1928-1933.
119. C. J. Hawkey, *Best Pract Res Clin Gastroenterol*, 2001, **15**, 801-820.
120. A. M. Qandil, *Int J Mol Sci*, 2012, **13**, 17244-17274.
121. K. Kurahara, T. Matsumoto, M. Iida, K. Honda, T. Yao and M. Fujishima, *Am. J. Gastroenterol.*, 2001, **96**, 473-480.
122. R. W. Blackler, J. P. Motta, A. Manko, M. Workentine, P. Bercik, M. G. Surette and J. L. Wallace, *Br. J. Pharmacol.*, 2015, **172**, 992-1004.
123. L. Li, G. Rossoni, A. Sparatore, L. C. Lee, P. Del Soldato and P. K. Moore, *Free Radic. Biol. Med.*, 2007, **42**, 706-719.
124. M. Chattopadhyay, R. Kodela, N. Nath, Y. M. Dastagirzada, C. A. Velázquez-Martínez, D. Boring and K. Kashfi, *Biochem. Pharmacol.* , 2012, **83**, 715-722.
125. M. V. Chan and J. L. Wallace, *Am. J. Physiol. Gastrointest. Liver Physiol.*, 2013, **305**, G467-G473.

TH-3161_176122050

TH-3161_176122050

Peroxide-responsive boronate ester-containing turn-on fluorogenic probes: impact of the self-immolative linkers on peroxide-triggered sustained drug delivery

TH-3161_176122050

TH-3161_176122050

2.1. Introduction

Reactive oxygen species (ROS), specially hydrogen peroxide (H_2O_2) is an important non-radical oxidant, which is produced in the cells by the metabolism of molecular oxygen.[1] In addition, the overproduction of H_2O_2 (known as oxidative stress) is directly linked to several diseases such as cancer, inflammatory diseases, and neurodegenerative disorders etc. Therefore, it is very important to detect endogenous H_2O_2 under normal as well as pathological conditions.[2-6] Turn-on fluorogenic probes with H_2O_2-responsive groups (e.g. boronate ester or boronic acid) are shown to be an effective, non-invasive, and sensitive tools for monitoring the endogenous level of H_2O_2 under a specific diseased condition.[7] Therefore, several ROS-responsive fluorogenic probes were developed over time (chapter 1). The boronate ester group was connected to the fluorophore for sensing H_2O_2 or drug delivery system using two main strategies, namely- i) direct installation by replacing the -OH group of the fluorophore;[8-11] ii) *via* the ether,[12, 13] carbonate or carbamate[14-19] linkage to couple the self-immolative boronatebenzyl moiety with the -OH or -NH_2 group of the fluorophore (chapter 1). As shown in Scheme 2.1A, the active fluorophore is released in the second strategy upon the reaction with H_2O_2 followed by a self-immolation process *via* quinone methide (QM) intermediate. However, it is released in one-step from the directly linked probes in the presence of H_2O_2. To consider the directly connected or self-immolative boronate ester-containing probes reported till now, there are a few points to be noted: 1) coupling strategies (direct vs. self-immolative) were chosen randomly or without considering their sensitivity to the analyte; 2) there are no comparative data when a new probe with a different coupling strategy was reported; 3) several of the reported probes are not sensitive enough to detect the endogenous level of H_2O_2 in the cellular medium, and therefore H_2O_2 was added externally.[20, 21] However, a proper rationalization is necessary for the sensitivity and reactivity of the probe towards H_2O_2.

2.2. Outline of the chapter

In this chapter, we reported nine probes, where three different fluorophores (coumarin, naphthalimide, and fluorescein) were connected with the H_2O_2-responsive boronate ester unit through three linkers (direct, ether, and carbonate) to comprehend the sensitivity of the linkers in the presence of H_2O_2 (Scheme 2.1B). We observed in the spectroscopic studies that as compared to the ether- or carbonate-linked probes, directly connected boronate ester probes

TH-3161_176122050

2.1, **2.4**, and **2.7** exhibited higher sensitivity towards H_2O_2. Moreover, the cellular viability assay confirmed that all the synthesized probes were non-toxic to HeLa cells upto 25 µM concentration. Due to the blue fluorescence emission of coumarin and the lack of complete solubility of naphthalimide probes in an aqueous medium, further studies were carried out only with fluorescein-based probes (**2.7**-**2.9**).

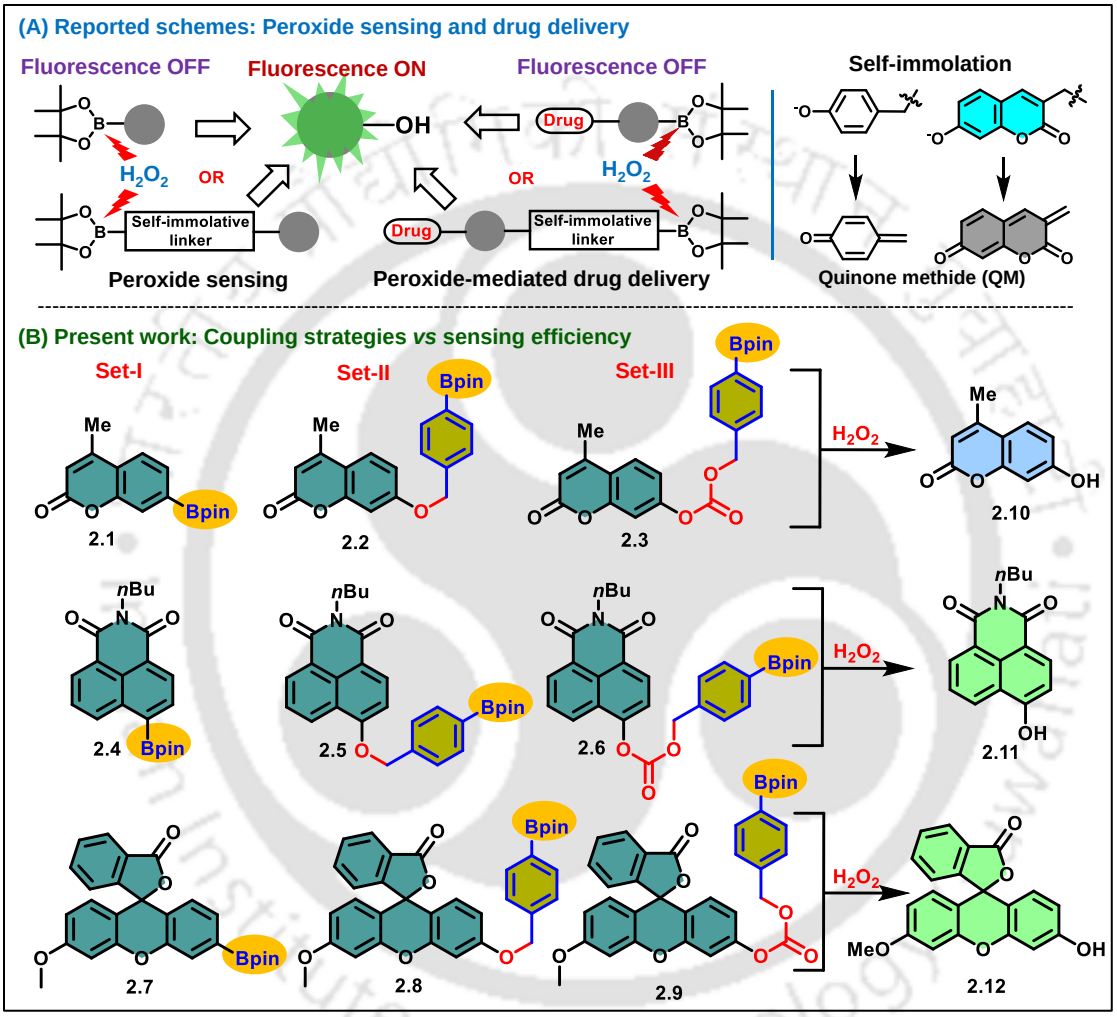

Scheme 2.1. (A) Reported schemes for H_2O_2-sensing and H_2O_2-mediated drug delivery. (B) Chemical structures of the designed turn-on fluorogenic probes and the schematic representation for fluorophore release in the presence of H_2O_2.

The limit of detection (LOD) analysis showed that the directly-linked boronate ester probe **2.7** detected H_2O_2 in nanomolar concentrations whereas ether and carbonate coupled probes **2.8** and **2.9**, respectively detected the micromolar level of H_2O_2. Furthermore, we noticed that all three probes **2.7**-**2.9** were compatible with cellular conditions and they detected the

TH-3161_176122050

endogenous level of H_2O_2. Moreover, a better intense emission response in the green channel was observed for probe **2.7** compared to probes **2.8** and **2.9**, indicating the stronger sensitivity of the directly-linked probe **2.7**. It can be concluded that a directly-coupled boronate ester probe is suitable for detecting very trace amounts of H_2O_2. However, a sustained drug delivery system will be an additional benefit from the self-immolative probes.

2.3. Results and discussion

2.3.1. Design and synthesis of the probes

In the present study, three different sets of turn-on fluorogenic probes were developed considering fluorophores **2.10**-**2.12**. In the first set, boronate ester group was incorporated directly to the aromatic nuclei with the replacement of hydroxyl group (probes **2.1**, **2.4** and **2.7**). The boronate ester group was installed by the Pd-catalyzed transmetalation reaction of triflate/bromide derivative of the fluorophores with bis(pinacolato)diboron under inert conditions. In the second set, the boronate benzyl moiety was installed on the fluorophores *via* ether linkage (probes **2.2**, **2.5** and **2.8**). These probes were synthesized by coupling fluorophore with boronate benzyl bromide in the presence of Cs_2CO_3 or K_2CO_3. Whereas, in the third set, the boronate benzyl alcohol was coupled to the fluorophores *via* carbonate linkage (probes **2.3**, **2.6** and **2.9**). These probes were achieved either by coupling fluorophore with 4-nitrophenyl carbonate adduct of boronate benzyl alcohol or by the conventional coupling using triphosgene. All the final boronate ester-based probes were obtained in reasonably good yields, which were purified and characterized by analytical methods.

2.3.2. Absorption and emission spectroscopic studies

The initial UV-Vis spectroscopic studies were carried out with the directly-linked probes (**2.1**, **2.4** and **2.7**) with and without H_2O_2 to identify the absorption maxima of the intact probes and the released fluorophores. As shown in Figure 2.1 (A-C), a significant red-shift was observed upon their reactions with H_2O_2 and the spectra overlapped well with that of pure fluorophores (**2.10**-**2.12**). For the probe **2.7**, very weak absorption band above 300 nm was probably due to the protection of both hydroxyl groups in fluorescein. Knowing the absorption maxima of all fluorophores **2.10**-**2.12**, the turn-on fluorescence efficacy of the probes **2.1**, **2.4**, and **2.7** were evaluated using fluorescence spectroscopy. As shown in Figure 2.1 (D-F), highly intense emission response was observed for all the probes in the presence

TH-3161_176122050

of H_2O_2 and the emission pattern matched well with that of the respective released fluorophores, indicating the H_2O_2-triggered turn-on fluorescence.

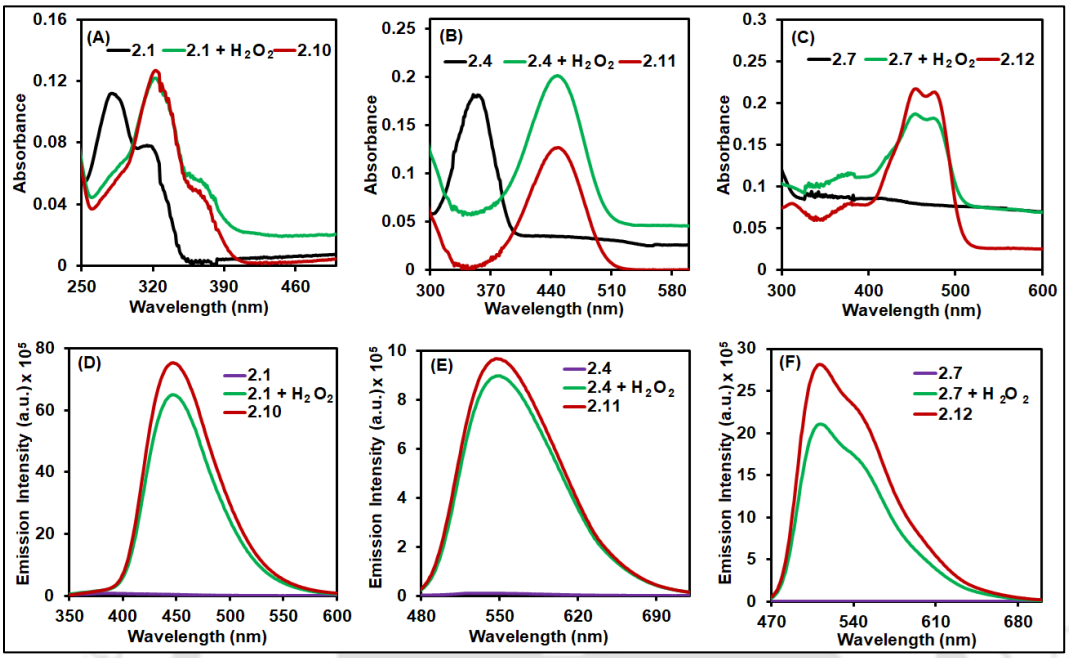

Figure 2.1. Absorption (A-C) and emission (D-F) spectra of directly-linked probes **2.1**, **2.4** and **2.7** (10 µM) in the absence and presence of H_2O_2 (200 µM) along with the spectra of pure released fluorophores (**2.10**-**2.12**, 10 µM) in PBS of pH 7.5. The final spectra of the probes with H_2O_2 were recorded after 90 min.

Similar experiment was carried out for ether (**2.2**, **2.5**, and **2.8**) and carbonate (**2.3**, **2.6**, and **2.9**) linked probes. Similarly, we observed red shifted absorption for all, which were closely matched with the corresponding fluorophores (Figure 2.2A-E). Moreover, turn-on emission was observed for all the probes in the presence of H_2O_2 and the emission pattern was matched well with the standard fluorophore (Figure 2.3). These results indicated that all the probes are capable of releasing fluorophores in the presence of H_2O_2.

TH-3161_176122050

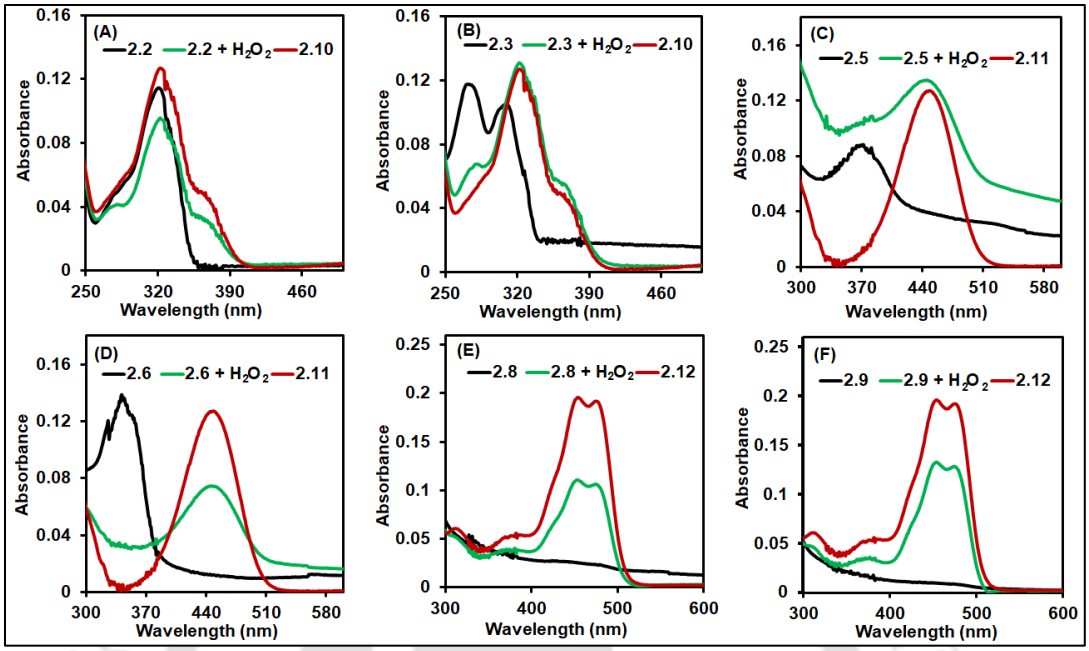

Figure 2.2. Absorption (A-F) spectra of probes **2.2**, **2.3**, **2.5**, **2.6**, **2.8** and **2.9** (10 µM) in the absence and presence of H_2O_2 (200 µM) along with the spectra of pure released fluorophores (**2.10**-**2.12**) in PBS (20 mM, pH 7.5). The final UV-Vis spectra of the probes with H_2O_2 were recorded after 90 min.

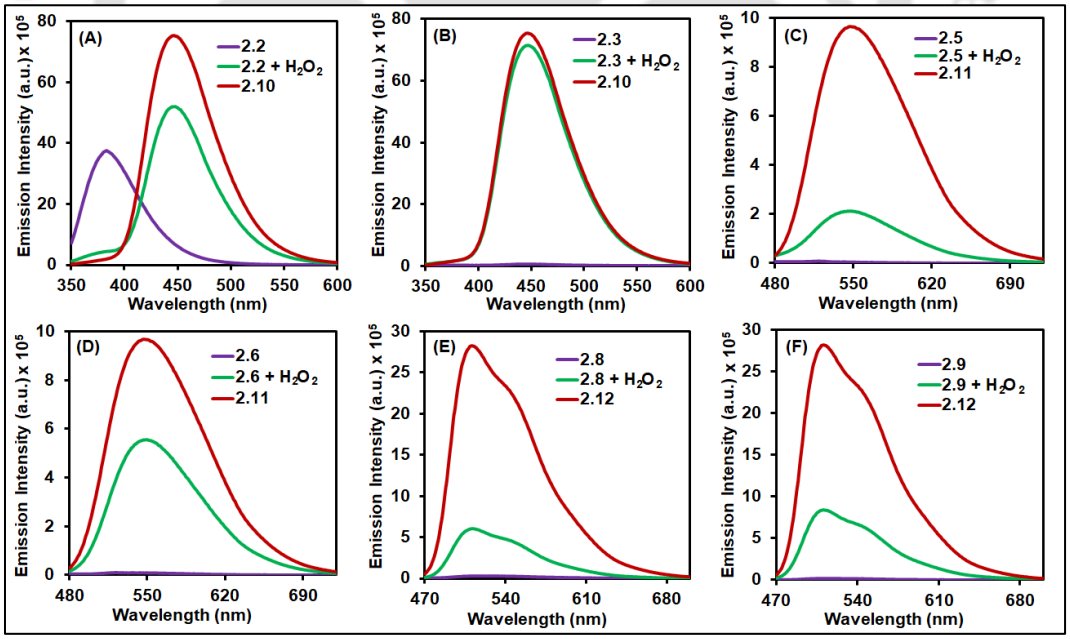

Figure 2.3. Emission (A-F) spectra of probes **2.2**, **2.3**, **2.5**, **2.6**, **2.8** and **2.9** (10 µM) in the absence and presence of H_2O_2 (200 µM) after 90 min along with the spectra of pure released fluorophores (**2.10**-**2.12**) in PBS (20 mM, pH 7.5).

TH-3161_176122050

2.3.3. Kinetic studies using fluorescence spectroscopy

With the preliminary results in hand, we carried out kinetic experiments to understand the relative reactivity of all the boronate ester linked probes in the presence of H_2O_2 upto 90-180 min. As shown in Figure 2.4A, a clear difference in the relative reactivity/sensitivity among the coumarin-based probes (**2.1**, **2.2**, and **2.3**) towards H_2O_2 was observed. A significantly higher reactivity was noted for the directly-linked probe **2.1** and the lowest reactivity was noted for the ether-linked probe **2.2**. While probe **2.1** was highly reactive towards H_2O_2 and the reaction was almost saturated within 30 min, the saturation time was found to be relatively longer for the corresponding self-immolative probes. Interestingly, a similar but more pronounced effect was observed for naphthalimide- and fluorescein-containing probes. For example, the initial saturation time was much longer for the directly-linked probes **2.4** and **2.7** (~50 min) as compared to **2.1** (~30 min). This indicates the higher reactivity of coumarin-based directly-linked boronate ester probes than the corresponding naphthalimide- and fluorescein-based probes. Furthermore, the self-immolative probes corresponding to naphthalimide (**2.5** and **2.6**) and fluorescein (**2.8** and **2.9**) fluorophores were found to be much less reactive than the corresponding directly-linked probes **2.4** and **2.7** (Figures 2.4B-C). Between, two types of self-immolative probes, the reactivity of the ether-linked probes were found to be lower than the carbonate-linked probes in general. Furthermore, it should be noted here that, like coumarin-based probes, typical saturation kinetics was not observed for naphthalimide- and fluorescein-based self-immolative probes till 90 min and therefore, the kinetic experiments were extended upto 180 min to understand their nature of kinetic pattern (Figure 2.4D). Interestingly, while some level of saturation kinetics was observed with relatively higher emission intensity for the carbonate-linked probes (**2.6** and **2.9**), both the ether-linked probes (**2.5** and **2.8**) reflected lower and almost steep increasing intensity pattern without saturation upto 180 min (Figure 2.4D). These results clearly indicate the higher reactivity of directly-linked boronate ester probes than the corresponding self-immolative linker-based probes.

TH-3161_176122050

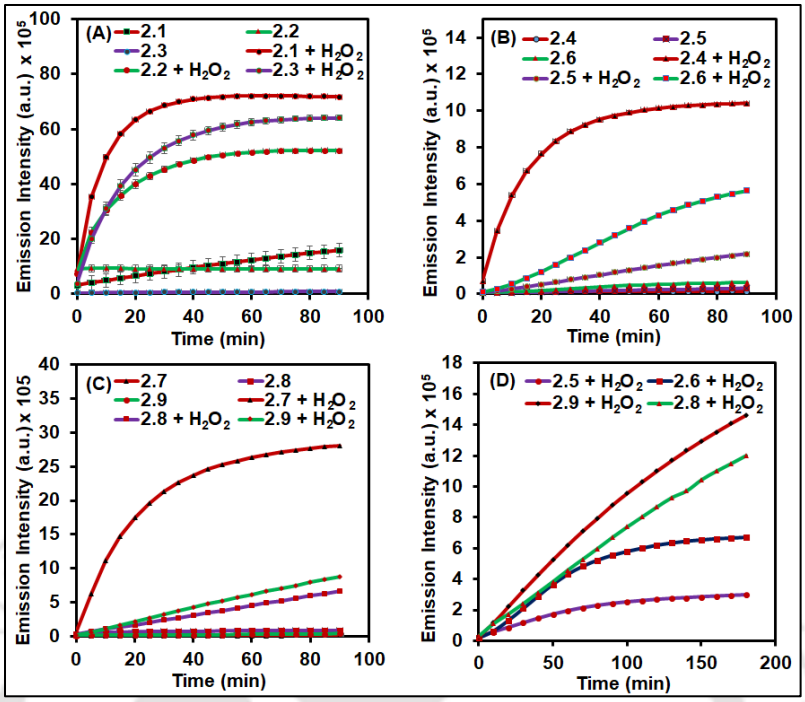

Figure 2.4. Emission spectra of (A) coumarin-, (B) naphthalimide- and (C) fluorescein-based probes (10 μM) with and without H_2O_2 (200 μM) over 90 min in PBS (20 mM) of pH 7.5. (D) Emission spectra of self-immolative probes (**2.5**, **2.6**, **2.8,** and **2.9**) (10 μM) in the presence of H_2O_2 (200 μM) over a longer time (180 min) under identical conditions.

2.3.4. Nature of fluorophore unit on probe efficiency

The fluorophore dependency of the relative rate of fluorescence turn-on from three types of boronate ester-linked probes was evidenced in Figure 2.5. As shown in Figure 2.5A, the difference in relative initial rate of reaction between two different kinds of self-immolative probes was not significant for all three fluorophores and in general, the carbonate-linked probes were slightly more reactive than the corresponding ether-linked probes. However, a significantly higher difference in relative rate is observed between the directly-linked probes and the ether-linked probes towards H_2O_2. Furthermore, this difference was found to be dependent on the nature of fluorophore unit being used. For example, the difference was 14.6-fold, 9.1-fold and 1.7-fold for fluorescein-, naphthalimide- and coumarin-based probes, respectively (Figure 2.5A). The above difference in turn-on response of directly-linked and self-immolative-linked probes form various fluorophores appears to be inversely proportional to the reactivity of directly-linked probes of various fluorophores towards H_2O_2. For example, as the coumarin-based probes react much faster with H_2O_2 than the

TH-3161_176122050

naphthalimide- and fluorescein-based probes, the difference in fluorescence response of directly-linked and self-immolative-linked probes is less pronounced for coumarin-based probes than two other fluorophore-based probes. Overall, the kinetic experiments clearly reveal the better suitability of directly-linked boronate ester probes for sensing traces of H_2O_2. However, the ether- or carbonate-based self-immolative probes might be suitable for H_2O_2-triggered drug delivery applications, often requiring sustained drug release profiles. While both of naphthalimide and fluorescein fluorophores (**2.11** and **2.12**) have almost similar emission ranges (yellow color, naked eye), the turn-on fluorescence emission intensity from the fluorescein-based probes (**2.7**-**2.9**) were higher than that from the naphthalimide-based probes (**2.4**, **2.5**, and **2.6**) under identical condition at a fixed concentration (10 µM) in the presence of H_2O_2 (200 µM). Furthermore, the solubility profiles of naphthalimide-based probes were much narrower than that of fluorescein-based probes. Naphthalimide-based probes were soluble only in THF and not completely soluble in other polar solvents such as DMSO, DMF, ACN and water

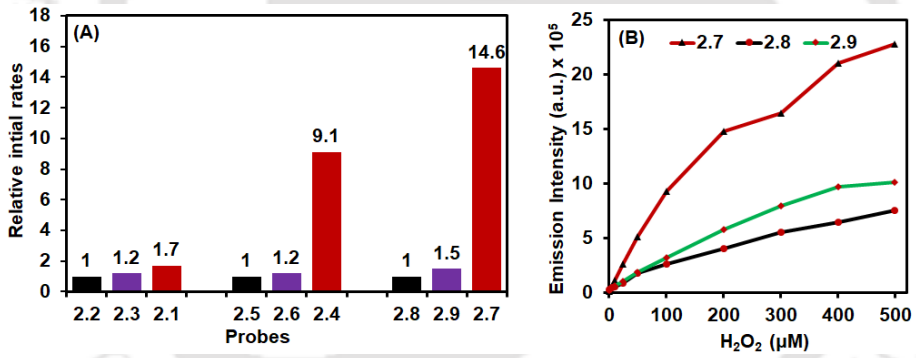

Figure 2.5. (A) Relative initial rates for the turn-on fluorescence of carbonate-linked (green) and directly linked (red) probes w.r.t. ether-linked (black) probes of a particular fluorophore in their reactions with H_2O_2. (B) Emission spectra of fluorescein-based probes (**2.7-2.9**, 10 µM) in the presence of variable concentrations of H_2O_2 (0-500 µM) with a fixed incubation time of 30 min.

However, fluorescein-based probes were soluble in a wider ranges of polar organic solvents including the solvents mentioned above except water. Due to these reasons, fluorescein-based probes (**2.7-2.9**) were chosen for further studies. A significant difference in kinetic pattern of probes **2.7-2.9** (10 µM) with 200 µM H_2O_2 (20-fold) inspired us to understand their behavior with a varied concentration of peroxide (0-500 µM) at a fixed incubation time (30 min). Interestingly, as shown in Figure 2.5B, a clear difference in emission intensity was observed

TH-3161_176122050

at lower concentration and the difference increased gradually with H_2O_2 concentration, supporting our views that directly-linked probe **2.7** is much efficient in sensing H_2O_2 than probes **2.8** and **2.9**.

2.3.5. Sensitivity of the probes

To further understand the relative sensitivity of fluorescein-based probes **2.7-2.9** towards H_2O_2, LOD was calculated as per standard method using fluorescence titration.[22] The emission intensity of the probes (10 µM) was measured in the absence of H_2O_2 and at a lower variable concentration range (2-50 µM) of H_2O_2 (Figure 2.6). Moreover, the standard deviation (σ) of blank run obtained for **2.7**, **2.8**, and **2.9** is 125.435, 814.691, and 432.946, respectively. Interestingly, a significant difference in the sensitivity of probes **2.7-2.9** towards H_2O_2 was observed. For example, while the LOD of directly-linked boronate ester probe **2.7** was 33 nM, the LOD of ether- and carbonate-linked probes (**2.8** and **2.9**) were significantly higher (1.3 and 0.37 µM, respectively), indicating much higher sensitivity of **2.7** than **2.8** and **2.9**.

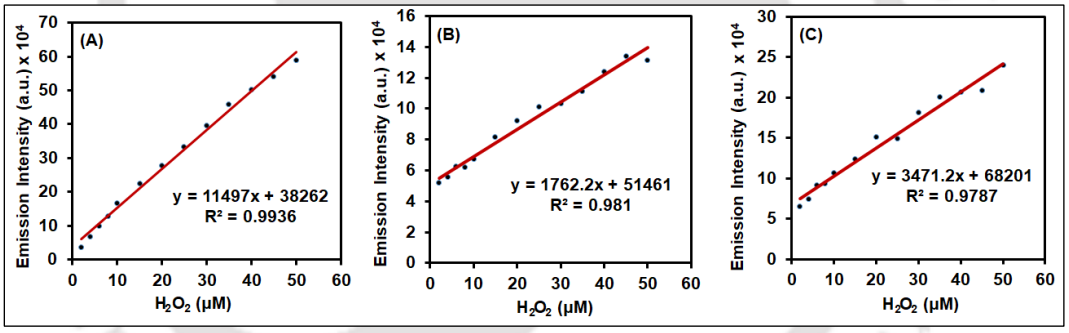

Figure 2.6. Emission (A-C) spectra of probes **2.7**, **2.8** and **2.9** (10 µM) in the presence of H_2O_2 (2 – 50 µM) after 30 min in PBS (20 mM, pH 7.5).

2.3.6. pH responsiveness and selectivity of the probe 2.7 towards H_2O_2

To understand the feasibility of turn-on fluorogenic process and the stability of the probes over a wider range of pH, the emission studies were carried out with variable pH (6.0-10.0) of the medium. Interestingly, a steady increased emission pattern was observed for the probe **2.7** with increasing pH of the medium from 6 to 8 and the emission almost saturates at pH 9. In contrast, steep increase in emission intensity was observed for both the self-immolative probes **2.8** and **2.9** with increasing pH of the medium and eventually that crossed the emission intensity from the probe **2.7** (Figure 2.7A). This is not surprising as increasing pH would facilitate the reaction by partial conversion of H_2O_2 to hydroperoxide ion (HOO^-; *p*Ka of

TH-3161_176122050

H_2O_2: 11.6). Furthermore, the self-immolation process *via* QM intermediate would also be enhanced by the predominant existence of phenoxide ion in the intermediate **2.17** (Figure 2.8D) at higher pH ranges (*p*Ka of phenols: ~10). Additionally, the experiment further evidenced the overall stability of probes **2.7-2.9** in the absence of H_2O_2 over a wide pH range of the medium indicating their compatibility under normal physiological as well as pathological conditions.

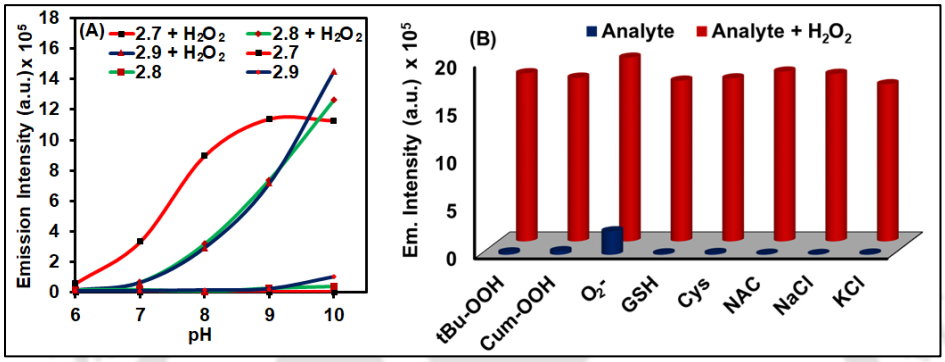

Figure 2.7. (A) Emission spectra of probes **2.7-2.9** (10 μM) in the absence and presence of H_2O_2 (200 μM) at variable pH of the medium; (B) Emission intensity from probe **2.7** (10 μM) in the presence of different analytes (200 μM) and addition of H_2O_2 (200 μM) after 30 min of incubation. The experiment was carried out in PBS (20 mM, pH = 7.5).

Considering the evidences that directly-linked probe **2.7** exhibited significantly higher reactivity towards H_2O_2 than that of the corresponding self-immolative probes **2.8** and **2.9**, the selectivity of the probe towards H_2O_2 was studied. Some of the oxidizing agents, reducing agents and inorganic salts were chosen to see their relative impacts on the selectivity of probe **2.7** towards H_2O_2. The probe (10 μM) was first incubated with various analytes (200 μM) and the emission intensity was measured (red cylinders, Figure 2.7B). To the solution mixture, H_2O_2 (200 μM) was added and the final emission was measured (blue cylinders, Figure 2.7B) following the similar protocol. As shown in Figure 2.7B, a significant enhancement of the emission intensity was observed upon the addition of H_2O_2 in the presence of all the analytes studied herein. We like to mention here that the directly-linked probe was reported by Chang and co-workers in 2010 along with few other directly-linked probes and showed the enhanced selectivity of the probes towards H_2O_2 over other relevant oxidants and radicals.[25]

TH-3161_176122050

2.3.7. Kinetic studies using reverse phase HPLC method and plausible mechanism

Reverse phase HPLC studies were used to evaluate the relative reactivity of the boronate ester groups in probes **2.7** and **2.9** towards H_2O_2 (Figure 2.8A). Fascinatingly, the self-immolative probe **2.8** formed the intermediate phenolic compound **2.17** (L-6, Figure 2.8A), which was relatively durable under HPLC conditions in acetonitrile and water (3:1) mixture with traces of fluorescence (**2.12**) release, while a clean conversion of the directly-linked probe **2.7** to the fluorophore **2.12** was observed in the presence of H_2O_2 with time (L-5, Figure 2.8A). However, by treating the NaOH solution, the intermediate **2.17** could be rapidly transformed into the fluorophore **2.12** (L-8). The ESI-MS analysis also revealed the formation of **2.17** (Figure 2.8B). With the release of fluorophore **2.12** and likely with very little amounts of intermediate, the carbonate-linked probe **2.9** reacted very quickly (L-7, Figure 2.8A). The sample of commercially available H_2O_2 (Merck India) shows a peak at approximately 2.46 min with nearly constant intensity, which is likely the result of the stabilizers used in H_2O_2.

The underlying stepwise mechanistic pathways were proposed portraying the reaction of representative fluorescein-based probes **2.7** and **2.8** towards H_2O_2 in order to better understand possible reasons for the relatively slower reactivity of self-immolative probes over the directly coupled probes (Figure 2.8C and 2.8D). In turn-on fluorescence processes, the feasible reaction pathways for the reaction of the boronate ester group with H_2O_2 are widely used.[26, 27] the directly linked probe **2.7** underwent an initial nucleophilic reaction of hydro peroxide anion at the electrophilic boron-center, followed by a rearrangement and subsequent nucleophilic attack releases the fluorescein fluorophore **2.12** with turn-on fluorescence from the hydroxyl anion (Figure 2.8C). However, the intermediate **2.17** would be generated by an identical procedure in probe **2.8**. It is clear from Figure 2.8D that unlike probe **2.7**, the fluorescence will be turned-on from probe **2.8** once the benzyl group in the intermediate **2.17** self-immolates *via* quinone methide (QM) species (Step 4, Figure 2.8D)[23, 24]

TH-3161_176122050

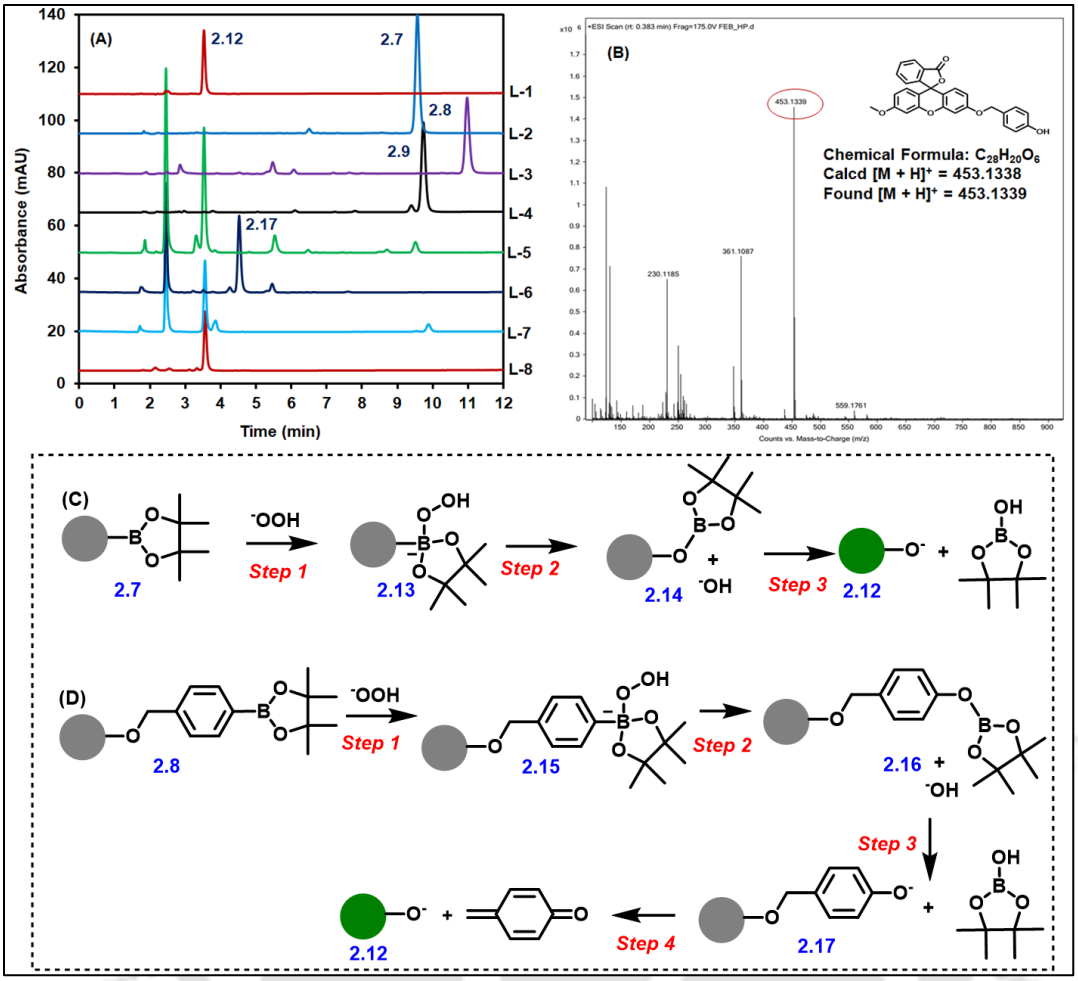

Figure 2.8. (A) HPLC chromatogram of pure probes **2.7-2.9**, released fluorophore (**2.12**) and the reaction mixtures of probes (100 µM) + H_2O_2 (10 mM) after 30 min. L-1: pure **2.12**; L-2 to L-4: pure probes **2.7-2.9**; L-5: **2.7** + H_2O_2; L-6: **2.8** + H_2O_2; L-7: **2.9** + H_2O_2; L-8: **2.8** + H_2O_2 + NaOH (25 mM). The chromatograms L-1 to L-7 were visualized at 254 nm and L-8 was visualized at 454 nm to monitor the released fluorophore **2.12**. Peak at 2.46 min appears from the stabilizers in commercial H_2O_2 sample. (B) ESI-MS spectrum of the intermediate **2.17** in the reaction mixture of probe **2.8** with H_2O_2 during HPLC analysis. ESI-MS (+ve) *m/z* calcd for $C_{28}H_{21}O_6$ $[M + H]^+$: 453.1338; observed: 453.1339. Generalized and most plausible mechanistic pathways for the reactions of fluorescein-based directly-linked probe **2.7** (C) and ether-linked self-immolative probe **2.8** (D) towards H_2O_2 for the release of fluorophore **2.12.**

The clear differences were in the fluorescence turn-on processes for the fluorescein-based probes **2.7**-**2.9** with the naked eye (Figure 2.9A), under UV-Vis light (Figure 2.9B), and

TH-3161_176122050

fluorescence light (Figure 2.9C). These results indicate that the boronate ester cleavage by H_2O_2 is reasonably fast for all of the probes, and the difference between the fluorescence emission responses from directly-linked and self-immolative linker-based probes is generally driven by the comparatively slower rate of self-immolative processes *via* QM intermediate, especially for the ether-linked probes.

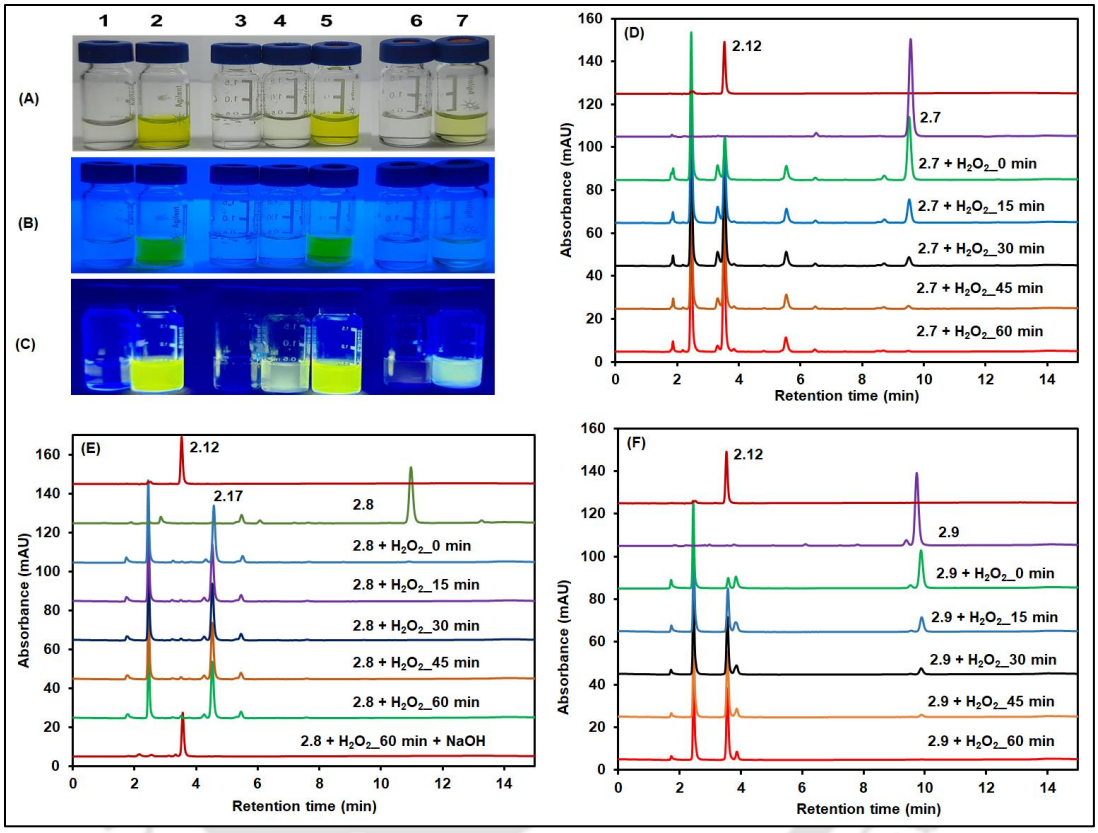

Figure 2.9. (A) Vials under visible light; (B) under UV light (254 nm); (C) under fluorescent light (365 nm); Pure probes **2.7-2.9** (vials 1, 3 and 6); probes **2.7-2.9** + H_2O_2 (vials 2, 4 and 7); probe **2.8** + H_2O_2 + NaOH (vial 5). (D-F) HPLC overlay chromatogram for the reaction of compound **2.7-2.9** with H_2O_2 over 60 min along with the chromatogram of pure probe **2.7-2.9** and the released fluorophore **2.12**. All the chromatograms were extracted at 254 nm. (The peak at 2.46 min with almost fixed intensity appears from the stabilizer in commercial H_2O_2).

The behavior and reactivity of non-fluorogenic peroxide-sensitive methyl salicylate-based metalloproteinase inhibitors as well as the 2,4-dinitrophenyl group-based NIR probes for thiophenol sensing are found to be in contrast to our observation with the significantly higher

TH-3161_176122050

fluorescence-response for the directly-linked boronate ester probes than self-immolative probes.[28, 29] The reaction of **2.7-2.9** with H_2O_2 were analyzed under HPLC condition over 60 min. We observed that the fluorophore **2.12** was released in the presence of H_2O_2 and the intensity increased with time except for **2.8** (Figure 2.9D-F). The fluorophore **2.12** was not released in the presence of H_2O_2, rather the intermediate **2.17** (retention time = 4.52 min) was the predominant species in the reaction mixture with the probe **2.8** (Figure 2.9E). However, the fluorophore **2.12** could be released upon the treatment of base to the reaction mixture that facilitates the self-immolation process.

2.3.8. Toxicity profiles of the probes

To understand the compatibility of the turn-on fluorogenic probes in cellular medium, their toxicity profiles were studied in the same cell line (HeLa) using conventional MTT assay. The toxicity profiles of the probes were evaluated at 5, 10 and 25 μM of probes and incubated for 48 h. Interestingly, all the probes (**2.7-2.9**) were found to be non-toxic upto 25 μM concentrations indicating the feasibility of their applications in cellular medium (Figure 2.10).

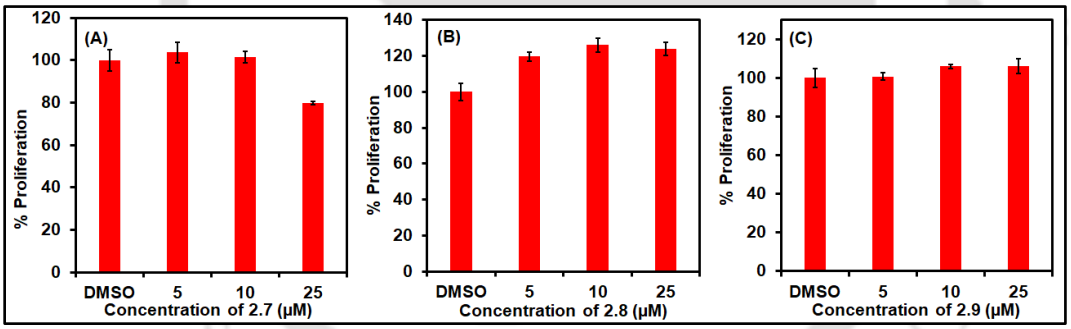

Figure 2.10. Cellular viability of HeLa cells in the presence of probes (**2.7-2.9**) at variable doses (5, 10 and 25 μM). The cells were incubated with the probes for 48 h at 37 °C under humidified incubator in the presence of 5% CO_2 level.

2.3.9 Detection of the endogenous level of H_2O_2 in HeLa cells

To understand the compatibility of the probes in cellular medium for the detection of endogenous level of H_2O_2, the probes (5.0 μM) were treated to human cervical cancer cells (HeLa) and the emission was measured after 60 min (Figure 2.11). Interestingly, a significantly higher emission response under green channel was observed for the probe **2.7** as compared to **2.8** and **2.9**. The emission response was much weaker for the ether-linked

TH-3161_176122050

probe **2.8** under the identical condition, indicating much lesser sensitivity of **2.8** in detecting the endogenous level of H_2O_2 in HeLa cells. To understand the selectivity of the directly-linked probe **2.7** towards the endogenous level of H_2O_2, HeLa cells was pre-treated with *N*-acetyl cysteine (NAC, 2.0 mM) that scavenges the endogenous H_2O_2. Interestingly, no emissive response in the NAC pre-treated cells served as the negative control and also evidenced the lack of any background emission response of the probe **2.7** (Figure 2.11). This also proved the stability of probe **2.7** under cellular environment.

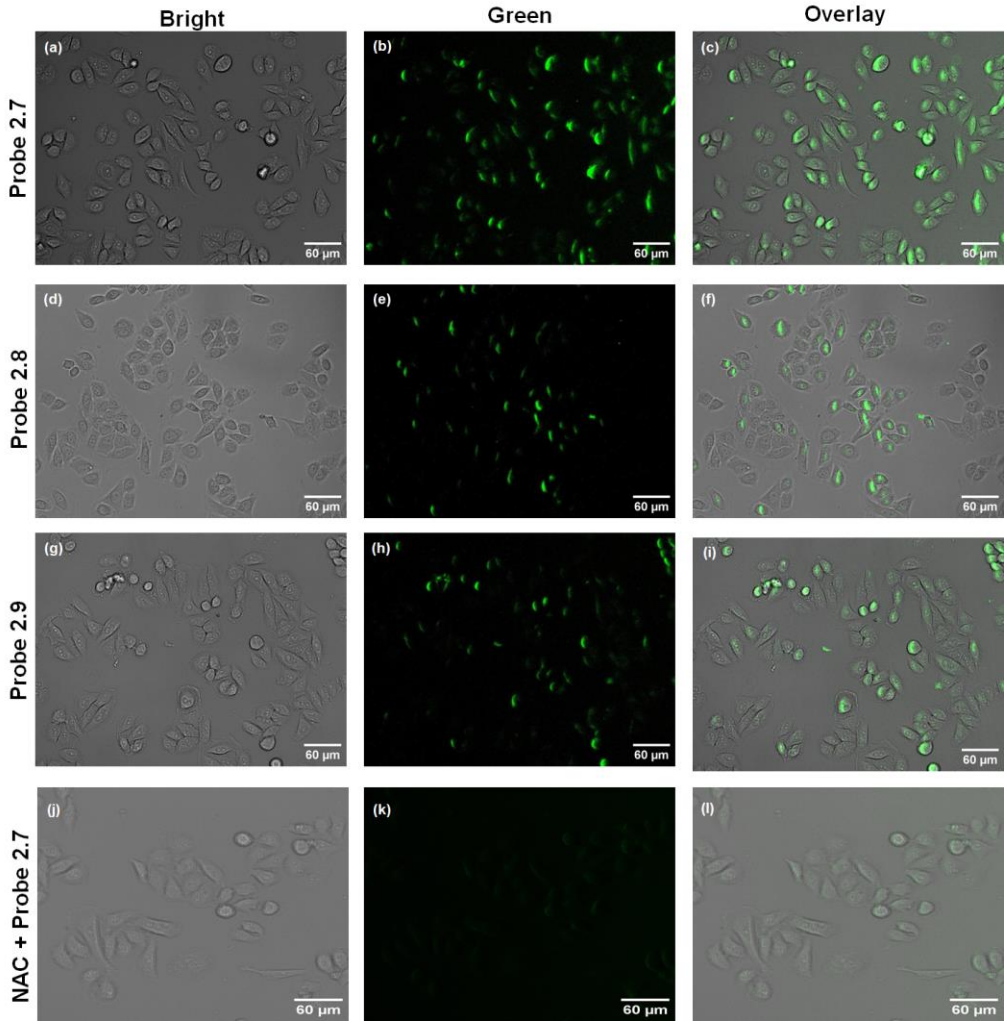

Figure 2.11. (a-i) Fluorescence microscopy images (bright field, green channel, and overlay) of HeLa cells in the presence of fluorescein-based probes **2.7-2.9** for the detection of endogenous level of H_2O_2. (j-l) Fluorescent microscopy images (bright field, green channel and overlay) of HeLa cells pre-treated with NAC (2.0 mM) for 1 h followed by the treatment of probe **2.7**.

TH-3161_176122050

2.4. Conclusions

In summary, we observed that direct coupling of the boronate ester group to the fluorophore unit in peroxide-responsive turn-on fluorogenic probes was strategically superior to the coupling *via* self-immolative linkers in effectively sensing traces of H_2O_2 both in aqueous and cellular medium. Moreover, the turn-on efficiency was also dependent on the nature of fluorophore units used. Considering both linkers and fluorophores, based on several control experiments, fluorescein-based directly-linked probe **2.7** was found to be the best candidate among all the probes studied in the present chapter for its application in sensing H_2O_2 accurately. While directly-coupled boronate ester probes are shown to be suitable for sensing peroxide effectively, the self-immolative linker-based probes may find wider applications in peroxide-triggered drug delivery systems that require a slower, sustained and regulated drug release profile. Despite the availability of many boronate ester-based probes, outcome of this study would certainly be useful as a guideline while designing a new boronate ester-based probe or prodrug for sensing peroxide or utilizing them particularly in ROS-associated pathologies and therapies in future.

2.5. Experimental section

2.5.1. Materials and Methods

All the chemicals and solvents were purchased either from Sigma Aldrich, Merck or from the reputed local suppliers. All the solvents were either distilled or dried following standard methods before using in reactions and chemicals were used without further purification. Thin layer chromatographic (TLC) analyses were carried out on pre-coated silica gel on aluminum sheets and the compounds were visualized by irradiation with UV or fluorescent light and stained by iodine. Organic solvents used for chromatographic separations were distilled before use. The melting point of the synthesized compounds was recorded in a Büchi B540 melting point apparatus and the values are uncorrected. The NMR spectra were recorded with Bruker Ascend^{TM} 400 MHz and 600 MHz NMR Spectrometers. Chemical shifts (^{1}H, and ^{13}C) are cited with respect to Me_4Si as an internal standard. Mass spectra were obtained using an Agilent 6520 Accurate- Mass Quadrupole Time-of-Flight (Q-TOF) LC/MS spectrometer.

TH-3161_176122050

2.5.2. Synthesis of the precursors

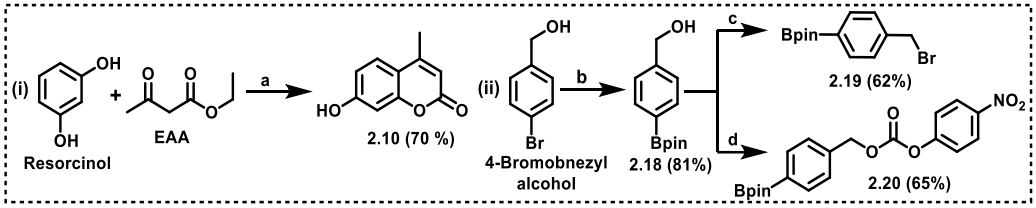

Scheme 2.3. Reagents and conditions: (a) Triflic acid, conc. H_2SO_4, 0 °C – RT, 5 h; (b) B_2pin_2, KOAc, Pd(dppf)Cl_2, dry 1,4-dioxane, 85 °C, 12 h; (c) PBr_3, dry DCM, RT, 5 h; (d) *p*-nitrophenyl chloroformate, Py, dry DCM, 0 °C – RT, 8 h.

Synthesis of compound 2.10[30]

To a stirred solution of resorcinol (2.00 g, 18.16 mmol) in an equimolar mixture of CF_3COOH (2.80 mL, 36.33 mmol) and conc. H_2SO_4 (1.94 mL, 36.33 mmol) was added ethyl acetoacetate (EAA) (2.30 mL, 18.16 mmol) dropwise at ice-cold condition over 1 h. The reaction mixture was stirred at room temperature for another 4 h. Upon completion, cold water was added to the reaction mixture to precipitate the product. The crude precipitate was filtered off and dried at room temperature. The compound was purified by column chromatography using 40% ethyl acetate in pet. ether to afford the pure product **2.10** as a white solid. R_f = 0.5 (30% ethyl acetate in pet. ether). Yield: 2.2 g (70%). ^{1}H NMR (DMSO-d_6, 600 MHz): δ (ppm) = 10.55 (s, 1H), 7.59 (d, J = 8.7 Hz, 1H), 6.80 (dd, J_1 = 8.6 Hz, J_2 = 2.3 Hz, 1H), 6.70 (d, J = 2.2 Hz, 1H), 6.13 (s, 1H), 2.36 (s, 3H). ^{13}C NMR (DMSO-d_6, 150 MHz): δ (ppm) = 161.6, 160.8, 155.2, 154.0, 127.0, 113.3, 112.4, 110.7, 102.5, 18.6.

Synthesis of compound 2.18[31]

Compound **2.18** was synthesized following the reported procedure with a minor modification. To a stirred solution of 4-bromobenzyl alcohol (0.50 g, 2.57 mmol) and bis(pinacolato)diboron (1.02 g, 4.00 mmol) in dry 1,4-dioxane (20 mL) was added Pd(dppf)Cl_2 (0.20 g, 0.27 mmol) and KOAc (0.80 g, 8.02 mmol) sequentially under argon atmosphere at room temperature. The reaction mixture was stirred at 85 ºC for 12 h. Upon completion, the solvent was evaporated under reduced pressure and the mixture was diluted with ethyl acetate (20 mL). The reaction mixture was filtered through a celite pad to remove undesired materials and washed with ethyl acetate (3×20 mL). The combined organic layer was washed sequentially with water and brine solution (3×20 mL) subsequently. Finally, the organic layer was dried over anhydrous sodium sulfate and concentrated under reduced

TH-3161_176122050

pressure to obtain the crude compound. The crude product was purified by silica gel (60-120 mesh) column chromatography using 10% ethyl acetate in pet. ether as a mobile phase to afford the pure product **2.18** as a white solid. R_f = 0.5 (30% ethyl acetate in pet. ether). Yield: 0.50 g (81%). ^{1}H NMR ($CDCl_3$, 400 MHz): δ (ppm) = 7.80 (d, *J* = 7.7 Hz, 2H), 7.36 (d, *J* = 7.5 Hz, 2H), 4.71 (s, 2H), 1.35 (s, 12H). ^{13}C NMR ($CDCl_3$, 100 MHz): δ (ppm) = 144.0, 135.0, 126.0, 83.9, 65.2, 24.9.

Synthesis of compound 2.19[32]

To a stirred solution of compound **2.18** (0.60 g, 2.56 mmol) in anhydrous DCM (8 mL) was added PBr_3 (0.50 mL, 5.12 mmol) dropwise under argon atmosphere at room temperature and the reaction mixture was stirred for 4 h. The progress of the reaction was monitored by TLC analysis. Upon completion, the excess PBr_3 was quenched with water (10 mL) and the reaction mixture was extracted with DCM (3×20 mL). The combined organic layer was washed with brine solution (3×10 mL) and dried over anhydrous sodium sulfate. The organic layer was concentrated under reduced pressure to afford the crude product. The crude compound was purified by Flash chromatography using ethyl acetate and pet. ether as eluents to afford compound **2.19** as a white solid. R_f = 0.5 (5% ethyl acetate in pet. ether). Yield: 0.50 g (62%). ^{1}H NMR ($CDCl_3$, 400 MHz): δ (ppm) = 7.78 (d, *J* = 8.0 Hz, 2H), 7.39 (d, *J* = 8.0 Hz, 2H), 4.49 (s, 2H), 1.34 (s, 12H). ^{13}C NMR ($CDCl_3$, 100 MHz): δ (ppm) = 140.7, 135.2, 128.3, 84.0, 33.3, 24.9.

Synthesis of compound 2.20[33]

To a stirred solution of compound **2.18** (0.20 g, 0.85 mmol) and pyridine (0.2 mL, 2.56 mmol) in anhydrous DCM (8 mL) was added a solution of *p*-nitrophenyl chloroformate (0.20 g, 1.02 mmol) in DCM (2 mL) dropwise at ice-cold condition under argon atmosphere and the reaction mixture was stirred at room temperature for 8 h. Upon completion, the mixture was diluted with DCM (30 mL) and sequentially washed with saturated $NaHCO_3$ solution, water, and brine (3×10 mL). The organic layer was evaporated under reduced pressure to afford the crude product as an amorphous solid. The crude product was further purified by silica gel column chromatography using ethyl acetate and pet. ether as a mobile phase to afford the pure product **2.20** as a white solid. R_f = 0.5 (20% ethyl acetate in pet. ether). Yield: 0.22 g (65%). ^{1}H NMR ($CDCl_3$, 400 MHz): δ (ppm) = 8.27 (d, *J* = 9.2 Hz, 2H), 7.85 (d, *J* = 8.0 Hz, 2H), 7.44 (d, *J* = 8.0 Hz, 2H), 7.38 (d, *J* = 9.2 Hz, 2H), 5.31 (s, 2H), 1.35 (s, 12H). ^{13}C NMR

TH-3161_176122050

($CDCl_3$, 100 MHz): δ (ppm) = 155.5, 152.4, 145.4, 137.0, 135.2, 127.6, 125.3, 121.9, 84.0, 70.9, 24.9.

2.5.3. Synthesis of coumarin-based boronate ester probes

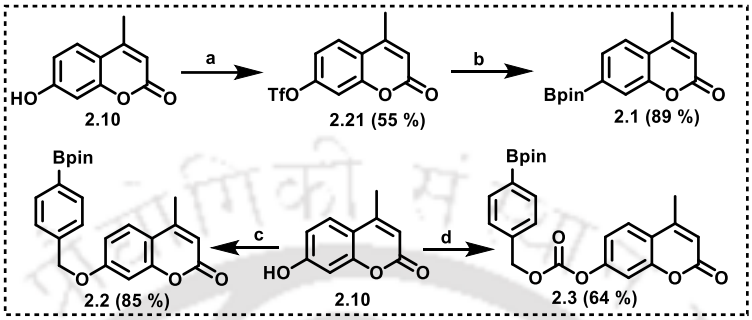

Scheme 2.4. Reagents and conditions: (a) Tf_2O, TEA, dry DCM, 0 ºC – RT, 3 h; (b) B_2pin_2, KOAc, Pd(dppf)Cl_2, dry 1,4-dioxane, 85 ºC, 12 h; (c) **2.19**, K_2CO_3, dry DMF, 0 ºC – RT, 12 h; (d) **2.20**, TEA, dry DCM, 0 ºC – RT, 24 h.

Synthesis of compound 2.21[34]

To a stirred solution of compound **2.10** (0.50 g, 2.83 mmol) and triethylamine (1.6 mL, 11.35 mmol) in dry DCM (10 mL) was added a solution of trifluoromethane sulfonic anhydride (0.56 mL, 3.40 mmol) in dry DCM (2 mL) dropwise at ice-cold condition under argon atmosphere. The reaction was allowed to attain room temperature and stirred for 3 h. Upon completion, the excess trifluoromethane sulfonic anhydride was quenched with water and the mixture was extracted with DCM (50 mL). The combined organic layer was washed with brine and dried over anhydrous sodium sulfate. The solvent was evaporated under reduced pressure to afford the crude residue. The crude product was purified by flash chromatography using 20% ethyl acetate in pet. ether to afford the pure product **2.21** as a white solid. R_f = 0.5 (20% ethyl acetate in pet. ether). Yield: 0.50 g (55%). ^{1}H NMR ($CDCl_3$, 400 MHz): δ (ppm) = 7.70 (d, *J* = 8.7 Hz, 1H), 7.29 (d, *J* = 2.4 Hz, 1H), 7.25 (m, 1H), 6.36 (d, *J* = 1.2 Hz, 1H), 2.47 (d, *J* = 1.2 Hz, 3H). ^{13}C NMR ($CDCl_3$, 100 MHz): δ (ppm) = 159.4, 154.1, 151.1, 150.8, 126.3, 120.3, 120.1, 117.4, 116.7, 116.0, 110.6, 18.8.

Synthesis of compound 2.1[35]

To a stirred solution of compound **2.21** (0.40 g, 1.29 mmol) and bis(pinacolato)diboron (0.60 g, 2.59 mmol) in dry 1,4-dioxane (20 mL) was sequentially added Pd(dppf)Cl_2 (0.10 g, 0.13 mmol) and KOAc (0.40 g, 3.89 mmol) under argon atmosphere at room temperature. The

TH-3161_176122050

reaction mixture was stirred at 85 ºC for 12 h. Upon completion, the solvent was evaporated under reduced pressure and the residue was diluted with ethyl acetate (20 mL). The reaction mixture was filtered through a celite bed to remove undesired materials and washed with ethyl acetate (3×20 mL). The combined organic layer was washed with water and brine (3×20 mL). The organic layer was dried over anhydrous sodium sulfate and concentrated under reduced pressure to afford the crude compound. The crude product was purified by silica gel column chromatography using 20% ethyl acetate in pet. ether to afford the pure product **2.1** as a white solid. R_f = 0.5 (25% ethyl acetate in pet. ether). Yield: 0.40 g (89%); M.P. = 145-147 ºC. ^{1}H NMR ($CDCl_3$, 400 MHz): δ (ppm) = 7.74 (s, 1H), 7.69 (d, *J* = 7.8 Hz, 1H), 7.58 (d, *J* = 7.8 Hz, 1H), 6.33 (d, *J* = 1.1 Hz, 1H), 2.45 (d, *J* = 1.1 Hz, 3H), 1.37 (s, 12H). ^{13}C NMR ($CDCl_3$, 100 MHz): δ (ppm) = 160.8, 152.9, 152.0, 130.0, 123.7, 123.0, 122.0, 116.1, 84.4, 24.9, 18.6. ESI-MS (+ve) *m/z* calcd for $C_{16}H_{20}BO_4$ $[M + H]^+$: 287.1455; observed: 287.1455.

Synthesis of compound 2.2

To a stirred solution of compound **2.10** (0.20 g, 1.13 mmol) in anhydrous DMF (0.5 mL) was added K_2CO_3 (0.10 g, 1.70 mmol) under argon atmosphere at 0 ºC and the mixture was stirred for 1 h. A solution of compound **2.19** (0.20 g, 1.36 mmol) in anhydrous DMF (0.5 mL) was added dropwise to the reaction mixture and stirred at room temperature for 12 h. Upon completion, the reaction mixture was diluted with ethyl acetate (50 mL) and washed with water and brine (3×10 mL). The organic layer was dried over anhydrous sodium sulfate and concentrated under reduced pressure to afford the crude residue. The crude product was purified by flash chromatography using 20% ethyl acetate in pet. ether to afford the pure product **2.2** as a white solid. R_f = 0.5 (20% ethyl acetate in pet. ether). Yield: 0.2 g (85%); M.P. = 192–194 ºC. ^{1}H NMR ($CDCl_3$, 400 MHz): δ (ppm) = 7.84 (d, *J* = 7.9 Hz, 2H), 7.49 (d, *J* = 8.8 Hz, 1H), 7.43 (d, *J* = 7.8 Hz, 2H), 6.93 (dd, J_1 = 8.8 Hz, J_2 = 2.4 Hz, 1H), 6.87 (d, *J* = 2.4 Hz, 1H), 6.14 (s, 1H), 5.15 (s, 2H), 2.39 (s, 3H), 1.35 (s, 12H). ^{13}C NMR ($CDCl_3$, 100 MHz): δ (ppm) = 161.6, 161.2, 155.2, 152.5, 139.0, 135.2, 126.6, 125.6, 113.8, 112.9, 112.1, 102.0, 83.9, 70.4, 24.8, 18.6. ESI-MS (+ve) *m/z* calcd for $C_{23}H_{26}BO_5$ $[M + H]^+$: 393.1873; observed: 393.1880.

TH-3161_176122050

Synthesis of compound 2.3

To a stirred solution of compound **2.10** (0.13 g, 0.75 mmol) and triethylamine (0.2 mL, 1.50 mmol) in anhydrous DCM (5 mL) was added the solution of compound **2.20** (0.20 g, 0.50 mmol) in anhydrous DCM (3 mL) in a dropwise manner at ice-cold condition under argon atmosphere. The reaction mixture was allowed to attain room temperature and stirred for 24 h. Upon completion, the reaction mixture was diluted with DCM (50 mL) and sequentially washed with saturated $NaHCO_3$ solution, water, and brine solution (3×10 mL). The organic layer dried over sodium sulfate and evaporated under reduced pressure to afford the crude product, which was purified by flash chromatography using 10% ethyl acetate in pet. ether to afford the pure product **2.3** as a white solid. R_f = 0.5 (20% ethyl acetate in pet. ether). Yield: 0.11 g (64%). M.P. = 140-141 ºC. ^{1}H NMR ($CDCl_3$, 600 MHz): δ (ppm) = 7.85 (d, *J* = 7.9 Hz, 2H), 7.61 (d, *J* = 8.7 Hz, 1H), 7.45 (d, *J* = 7.9 Hz, 2H), 7.23 (d, *J* = 2.3 Hz, 1H), 7.17 (dd, J_1 = 8.7 Hz, J_2 = 2.3 Hz, 1H), 6.28 (d, *J* = 0.9 Hz, 1H), 5.31 (s, 2H), 2.44 (d, *J* = 1.0 Hz, 3H), 1.36 (s, 12H). ^{13}C NMR ($CDCl_3$, 100 MHz): δ (ppm) = 160.4, 154.1, 153.2, 152.8, 151.9, 137.2, 135.1, 127.6, 125.5, 118.0, 117.3, 114.7, 110.0, 84.0, 70.7, 24.9, 18.7. ESI-MS (+ve) *m/z* calcd for $C_{24}H_{26}BO_7$ $[M + H]^+$: 437.1772; observed: 437.1772.

2.5.4. Synthesis of naphthalimide-based boronate ester probes

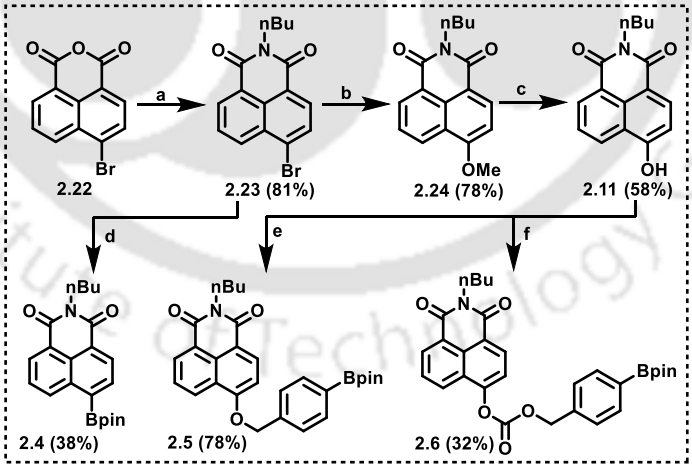

Scheme 2.5. (a) n-Butylamine, EtOH, 80 °C, 6 h; (b) NaOMe, $CuSO_4.5H_2O$, dry MeOH, 70 °C, 12 h; (c) 57% HI, 130 °C, 12 h; (d) B_2pin_2, KOAc, $Pd(dppf)Cl_2$, dry 1,4-dioxane, 85 ºC, 12 h; (e) **2.19**, K_2CO_3, dry ACN, 0 ºC - RT, 12 h; (f) triphosgene, Py, **2.18**, dry DCM, TEA, -70 ºC - 0 ºC - RT, 16 h.

TH-3161_176122050

Synthesis of compound 2.23[36]

To a stirred solution of compound **2.22** (2.00 g, 7.22 mmol) in ethanol (60 mL) was added n-n-butylamine (0.64 g, 8.66 mmol) dropwise at room temperature. The reaction mixture was refluxed for 6 h. The progress of the reaction was monitored by TLC analysis. Upon completion of the reaction, the crude mixture was diluted with cold water (100 mL) and filtered off. The residue was washed with cold water, and cold ethanol sequentially and dried under vacuum to afford product **2.23** as a brown solid. R_f = 0.6 (5% ethyl acetate in pet. ether). Yield: 2.0 g (81%). ^{1}H NMR ($CDCl_3$, 600 MHz): δ (ppm) = 9.60 (dd, J_1 = 7.3 Hz, J_2 = 1.2 Hz, 1H), 8.49 (dd, J_1 = 8.5 Hz, J_2 = 1.2 Hz, 1H), 8.35 (d, J = 7.8 Hz, 1H), 7.98 (d, J = 7.8 Hz, 1H), 7.80 (dd, J_1 = 8.5 Hz, J_2 = 7.3 Hz, , 1H), 4.19-4.13 (m, 2H), 1.75-1.67 (m, 2H), 1.49-1.42 (m, 2H), 0.99 (t, J = 7.4 Hz, 3H). ^{13}C NMR ($CDCl_3$, 150 MHz): δ (ppm) = 163.6, 163.5, 133.2, 132.0, 131.2, 131.1, 130.6, 130.2, 128.9, 128.1, 123.1, 122.3, 40.5, 30.2, 20.5, 13.9.

Synthesis of compound 2.24[37]

Compound **2.24** was synthesized following the reported procedure with minor modifications. To a mixture of compound **2.23** (1.50 g, 4.51 mmol), NaOMe (2.00 g, 36.12 mmol), and $CuSO_4.5H_2O$ (0.20 g, 0.90 mmol) was added dry MeOH (45 mL) under argon atmosphere at room temperature. The reaction mixture was stirred at 70 °C for 12 h. Upon completion of the reaction, the solvent was evaporated under reduced pressure and diluted with 1N HCl to obtain the greenish-yellow precipitate. The crude product was filtered off, washed with water and dried under the vacuum to afford compound **2.24** as a greenish-yellow solid. R_f = 0.4 (10% ethyl acetate in pet. ether). Yield: 1.00 g (78%). ^{1}H NMR ($CDCl_3$, 400 MHz): δ (ppm) = 8.59 (dd, J_1 = 7.3 Hz, J_2 = 1.5 Hz, 1H), 8.54 (dd, J_1 = 8.7 Hz, J_2 = 1.8 Hz, 2H), 7.69 (d, J = 7.8 Hz, 1H), 7.03 (d, J = 8.3 Hz, 1H), 4.21-4.14 (m, 2H), 4.13 (s, 3H), 1.77-1.64 (m, 2H), 1.49-1.42 (m, 2H), 0.98 (t, J = 7.4 Hz, 3H). ^{13}C NMR (150 MHz, $CDCl_3$): δ (ppm) = 164.7, 164.1, 160.9, 133.5, 131.6, 129.5, 128.7, 126.0, 123.6, 122.5, 115.3, 105.3, 56.3, 40.2, 30.4, 20.5, 14.0.

Synthesis of compound 2.11[37]

The compound **2.11** was synthesized according to the reported literature with minor modifications. The mixture of compound **2.24** (1.30 g, 4.58 mmol) and 57% HI (11.70 g,

TH-3161_176122050

91.60 mmol) was stirred at 130 °C for 12 h. The progress of the reaction was monitored by TLC analysis. Upon completion of the reaction, it was cooled down to room temperature and neutralized with 5N NaOH. The obtained precipitate was filtered off, washed with water, and dried under the vacuum to afford the crude compound, which was further purified by silica gel column chromatography using 10% methanol in dichloromethane to afford the pure product **2.11** as a yellow solid. R_f = 0.5 (40% ethyl acetate in pet. ether). Yield: 0.70 g (58%). ^{1}H NMR (DMSO-d_6, 600 MHz): δ (ppm) = 11.89 (s, 1H), 8.52 (d, *J* = 8.3 Hz, 1H), 8.46 (d, *J* = 7.2 Hz, 1H), 8.35 (d, *J* = 8.1 Hz, 1H), 7.76 (t, *J* = 7.8 Hz, 1H), 7.15 (d, *J* = 8.2 Hz, 1H), 4.01 (t, *J* = 7.5 Hz, 2H), 1.56-1.61 (m, 2H), 1.31-1.37 (m, 2H), 0.92 (t, *J* = 7.4 Hz, 3H). ^{13}C NMR (DMSO-d_6, 150 MHz): δ (ppm) = 164.1, 163.5, 160.7, 134.0, 131.6, 129.6, 129.4, 126.1, 122.8, 122.3, 113.0, 110.4, 39.5, 30.2, 20.3, 14.2.

Synthesis of compound 2.4

To a mixture of bis(pinacolato)diboron (0.60 g, 2.25 mmol) and compound **2.23** (0.25 g, 0.75 mmol) in dry 1,4-dioxane (20 mL) was added Pd(dppf)Cl_2 (55 mg, 0.07 mmol) and KOAc (0.18 g, 2.25 mmol) under argon atmosphere at room temperature. The reaction mixture was stirred at 90 ºC overnight and upon completion, the solvent was evaporated under the reduced pressure. The residue was diluted with ethyl acetate (20 mL) and the precipitate was filtered through a celite pad and washed with ethyl acetate (3×20 mL). The combined organic layer was washed with water and brine (3×20 mL) and dried over anhydrous sodium sulfate. The solvent was evaporated under reduced pressure to afford the crude product, which was purified by flash chromatography using 10% ethyl acetate in the pet. ether to afford the pure product **2.4** as a white solid. R_f = 0.5 (10% ethyl acetate in pet. ether). Yield: 0.11g (38%); M.P. = 115-117 ºC. ^{1}H NMR ($CDCl_3$, 400 MHz): δ (ppm) = 9.11 (dd, J_1 = 8.5 Hz, J_2 = 1.0 Hz, 1H), 8.60 (dd, J_1 = 7.2 Hz, J_2 = 1.0 Hz, 1H), 8.56 (d, *J* = 7.3 Hz, 1H), 8.29 (d, *J* = 7.3 Hz, 1H), 7.78 (dd, J_1 = 8.4 Hz, J_2 = 7.3 Hz, , 1H), 4.21-4.15 (m, 2H), 1.78-1.68 (m, 2H), 1.52-1.39 (m, 2H), 1.45 (s, 12H), 0.98 (t, *J* = 7.4 Hz, 3H). ^{13}C NMR ($CDCl_3$, 100 MHz): δ (ppm) = 164.4, 164.4, 135.8, 135.3, 134.9, 130.8, 129.7, 127.8, 127.0, 124.8, 122.5, 84.6, 40.3, 30.2, 25.0, 20.4, 13.9. ESI-MS (+ve) *m/z* calcd for $C_{22}H_{27}BNO_4$ $[M + H]^+$: 380.2030; observed: 380.2030.

TH-3161_176122050

Synthesis of compound 2.5[38]

To a mixture of compound **2.11** (30 mg, 0.11 mmol) and compound **2.19** (40 mg, 0.13 mmol) in anhydrous acetonitrile (2 mL) was added anhydrous K_2CO_3 (23 mg, 0.17 mmol) under argon atmosphere at 0 ºC. After 30 min, the reaction mixture was allowed to attain room temperature and stirred overnight. Upon completion of the reaction, the solvent was evaporated under reduced pressure and the residue was diluted with ethyl acetate (50 mL). The mixture was washed with water and brine and the organic layer was dried over anhydrous sodium sulfate and evaporated under reduced pressure. The crude residue was purified by flash chromatography using 20% ethyl acetate in pet. ether to afford the pure product **2.5** as a bright green solid. R_f = 0.5 (20% ethyl acetate in pet. ether). Yield: 43 mg (78%); M.P. = 166-168 ºC. ^{1}H NMR ($CDCl_3$, 600 MHz): δ (ppm) = 8.62-8.64 (m, 2H), 8.52 (dd, J_1 = 8.2 Hz, J_2 = 1.5 Hz, 1H), 7.89 (d, J = 7.9 Hz, 2H), 7.71-7.74 (m, 1H), 7.52 (d, J = 7.8 Hz, 2H), 7.09 (dd, J_1 = 8.3 Hz, J_2 = 1.0 Hz, 1H), 5.39 (s, 2H), 4.19 (t, J = 7.6 Hz, 2H), 1.70-1.75 (m, 2H), 1.43-1.50 (m, 2H), 1.36 (s, 12H), 0.97 (t, J = 7.4 Hz, 3H). ^{13}C NMR ($CDCl_3$, 150 MHz): δ (ppm) = 164.5, 164.0, 159.7, 138.5, 135.3, 133.3, 131.6, 129.4, 128.7, 126.7, 126.0, 123.6, 122.5, 115.4, 106.5, 84.0, 70.8, 40.1, 30.3, 24.9, 20.4, 13.9. ESI-MS (+ve) *m/z* calcd for $C_{29}H_{33}BNO_5$ $[M + H]^+$: 486.2452; observed: 486.2483.

Synthesis of compound 2.6

To a stirred solution of triphosgene (126 mg, 0.42 mmol) in anhydrous DCM (2 mL) was added pyridine (0.07 mL, 0.85 mmol) dropwise at ice-cold condition under argon atmosphere. The reaction mixture was stirred at room temperature for 30 min and then kept at -70 ºC. To this solution, the compound **2.18** (0.20 g, 0.85 mmol) in dry DCM (2 mL) was added dropwise at that condition. The progress of the reaction was monitored by TLC analysis. Upon the complete consumption of compound **2.18** completely, the mixture was added dropwise into the solution of compound **2.11** (114 mg, 0.42 mmol) and triethylamine (0.06 mL, 0.42 mmol) in anhydrous DCM (5 mL) at -70 ºC. Slowly the reaction mixture was warmed to room temperature and stirred at the same temperature. The progress of the reaction was monitored by TLC analysis. Upon completion of the reaction, the excess triphosgene was quenched with water, and the crude product was extracted by DCM (3×20 mL). The combined organic layer was washed with brine (2×10 mL) and dried over anhydrous sodium sulfate. The solvent was evaporated under reduced pressure to afford the crude residue, which

TH-3161_176122050

was purified by flash chromatography using 15% ethyl acetate in the pet. ether to afford the pure product **2.6** as a white solid. R_f = 0.5 (20% ethyl acetate in pet. ether). Yield: 60 mg (32%); M.P. = 131-132 ºC. ^{1}H NMR ($CDCl_3$, 400 MHz): δ (ppm) = 8.59-8.64 (m, 2H), 8.32 (dd, J_1 = 8.4 Hz, J_2 = 1.0 Hz, 1H), 7.87 (d, J = 8.0 Hz, 2H), 7.77 (dd, J_1 = 8 Hz, J_2 = 7.4 Hz, 1H), 7.67 (d, J = 8.1 Hz, 1H), 7.47 (d, J = 8.0 Hz, 2H), 5.37 (s, 2H), 4.18 (t, J = 8.0 Hz, 2H), 1.69-1.75 (m, 2H), 1.40-1.49 (m, 2H), 1.36 (s, 12H), 0.98 (t, J = 7.4 Hz, 3H). ^{13}C NMR ($CDCl_3$, 150 MHz): δ (ppm) = 164.0, 163.4, 152.5, 151.4, 137.1, 135.2, 131.8, 131.7, 129.3, 127.7, 127.6, 127.4, 124.8, 122.9, 120.6, 118.6, 84.0, 71.0, 40.3, 30.2, 24.9, 20.4, 13.9. ESI-MS (+ve) *m/z* calcd for $C_{30}H_{33}BNO_7$ $[M + H]^+$: 530.2350; observed: 530.2360.

2.5.5. Synthesis of fluorescein-based boronate ester probes

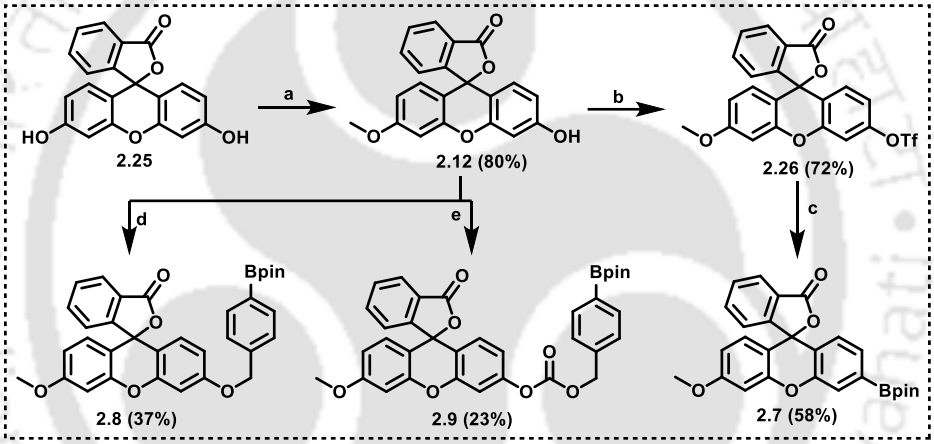

Scheme 2.6: (a) (i) MeI, K_2CO_3, dry DMF, RT, 24 h; (ii) 10% aq. NaOH, MeOH, RT, 6h; (b) phenyl triflimide, DIPEA, dry DMF 0 ºC-RT, 3 h; (c) B_2pin_2, KOAc, $Pd(dppf)Cl_2$, dry 1,4-dioxane, 85 ºC, 12 h; (d) **2.19**, Ag_2O, dry toluene, 0 ºC-RT, 5 h; (e) **2.20**, TEA, dry DCM, 0 ºC-RT, 48 h.

Synthesis of compound 2.12[39]

To a mixture of compound **2.25** (2.50 g, 7.50 mmol) and K_2CO_3 (3.10 g, 22.5 mmol) was added dry DMF (20 mL) and stirred at room temperature under an argon atmosphere. After 30 min, MeI (4.20 g, 30.00 mmol) was added dropwise and the reaction mixture was stirred at the same temperature. The progress of the reaction was monitored by TLC analysis. Upon completion of the reaction, 100 mL of ice-cold water was added to obtain the precipitate. The crude product was filtered off, washed with cold water, and dried under air to afford the yellow solid with a quantitative yield. A suspension of this intermediate in MeOH (50 mL)

TH-3161_176122050

was added to 10% aqueous NaOH (30 mL) and stirred at room temperature for 6 h. Upon completion of the reaction, the solvent was evaporated under reduced pressure and diluted with 100 mL of water. The reaction mixture was acidified to pH = 5.0 using 4N HCl dropwise at 0 °C to obtain the precipitate. The crude product was filtered off, washed with water, and dried under air to afford compound **2.12** as a yellow solid. R_f = 0.5 (60% ethyl acetate in pet. ether). Yield: 2.10 g (80%). ^{1}H NMR (DMSO-d_6, 600 MHz): δ (ppm) = 10.24 (s, 1H), 8.01 (d, *J* = 7.7 Hz, 1H), 7.80 (t, *J* = 7.5 Hz, 1H), 7.73 (t, *J* = 7.5 Hz, 1H), 7.27 (d, *J* = 7.7 Hz, 1H), 6.94 (d, *J* = 2.5 Hz, 1H), 6.73-6.68 (m, 2H), 6.65 (d, *J* = 8.8 Hz, 1H), 6.58 (s, 2H), 3.81 (s, 3H), 1.35 (s, 12H). ^{13}C NMR (DMSO-d_6, 150 MHz): δ (ppm) = 169.2, 161.5, 160.0, 152.9, 152.3, 152.2, 136.2, 130.6, 129.6, 129.4, 126.5, 125.1, 124.5, 113.3, 112.4, 111.4, 109.9, 102.7, 101.2, 83.2, 56.1.

Synthesis of compound 2.26

To a stirred solution of compound **2.12** (0.60 g, 1.73 mmol) and phenyl triflimide (2.47 g, 6.92 mmol) in dry DMF (10 mL) was added DIPEA (1.12 g, 8.66 mmol) dropwise at 0 °C under argon atmosphere and the reaction mixture was kept for stirring at room temperature. The progress of the reaction was monitored by TLC analysis. Upon completion of the reaction, the mixture was diluted with ethyl acetate (50 mL) and washed sequentially with water (5×10 mL), and brine (2×10 mL). The organic layer was dried over anhydrous sodium sulfate and evaporated under reduced pressure to afford the crude product, which was purified by flash chromatography using 20% ethyl acetate in the pet. ether to afford the pure product **2.26** as a white solid. R_f = 0.5 (20% ethyl acetate in pet. ether). Yield: 0.60 g (72%). ^{1}H NMR ($CDCl_3$, 400 MHz): δ (ppm) = 8.09-8.02 (m, 1H), 7.75-7.62 (m, 2H), 7.25 (d, *J* = 2.4 Hz, 1H), 7.21-7.15 (m, 1H), 6.96 (dd, J_1 = 8.8, J_2 = 2.4 Hz, 1H), 6.90 (d, *J* = 8.8 Hz, 1H), 6.81 (d, *J* = 2.4 Hz, 1H), 6.75-6.63 (m, 2H), 3.85 (s, 3H). ^{13}C NMR ($CDCl_3$, 150 MHz): δ (ppm) = 169.2, 161.8, 152.7, 152.2, 152.0, 150.1, 135.5, 130.3, 130.2, 129.7, 129.1, 126.4, 125.5, 124.0, 123.7, 119.9, 119.9, 117.7, 116.8, 112.5, 110.6, 101.0, 81.8, 55.8.

Synthesis of compound 2.7[40]

To a solution of bis(pinacolato)diboron (0.53 g, 2.09 mmol), compound **2.26** (0.50 g, 1.04 mmol), and KOAc (0.20 g, 3.12 mmol) in anhydrous 1, 4-dioxane (20 mL) were added Pd(dppf)Cl_2 (70 mg, 0.10 mmol) under argon atmosphere at room temperature. The reaction

TH-3161_176122050

mixture was stirred at 85 ºC for 12 h. Upon completion, the solvent was evaporated under reduced pressure and the residue was diluted with ethyl acetate (20 mL). The mixture was filtered through a celite pad and washed with ethyl acetate (3×20 mL). The combined organic layer was washed sequentially with water and brine (3×20 mL). The organic layer was dried over anhydrous sodium sulfate. The solvent was evaporated under reduced pressure to afford the crude product, which was purified by flash chromatography using 17% ethyl acetate in the pet. ether to afford the pure product **2.7** as a white solid. R_f = 0.5 (20% ethyl acetate in pet. ether). Yield: 0.38 g (58%); M.P. = 166-168 ºC. ^{1}H NMR ($CDCl_3$, 600 MHz): δ (ppm) = 8.03 (d, *J* = 7.4 Hz, 1H), 7.74(s, 1H), 7.60-7.66 (m, 2H), 7.43 (dd, J_1 = 7.8 Hz, J_2 = 0.7 Hz, 1H), 7.12 (d, *J* = 7.5 Hz, 1H), 6.81 (d, *J* = 7.8 Hz, 1H), 6.77 (d, *J* = 2.5 Hz, 1H), 6.72 (d, *J* = 8.8 Hz, 1H), 6.62 (dd, J_1 = 8.8 Hz, J_2 = 2.5 Hz, 1H), 3.84 (s, 3H), 1.35 (s, 12H). ^{13}C NMR ($CDCl_3$, 150 MHz): δ (ppm) = 169.5, 161.4, 153.5, 152.4, 150.7, 135.1, 129.7, 129.4, 129.0, 127.2, 126.2, 125.1, 123.8, 123.5, 121.5, 111.7, 110.9, ,100.9, 84.2, 82.7, 55.6, 24.9. ESI-MS (+ve) *m/z* calcd. for $C_{27}H_{26}BO_6$ $[M+H]^+$: 457.1822; observed: 457.1841.

Synthesis of compound 2.8[41]

The compound was prepared following the reported method with modifications. To a stirred solution of compound **2.12** (0.20 g, 0.57 mmol) and compound **2.19** (0.20 g, 0.69 mmol) in anhydrous toluene (10 mL) was added silver oxide (0.20 g, 0.86 mmol) under an inert atmosphere at room temperature, and the reaction mixture was refluxed. The progress of the reaction was monitored by TLC analysis. Upon completion, the solvent was evaporated under reduced pressure and the residue was diluted with DCM (20 mL). The mixture was filtered through a celite pad and washed with DCM (3×10 mL). The combined organic layer was dried over anhydrous sodium sulfate and the solvent was evaporated to afford the crude product. The crude product was purified by flash chromatography using 20% ethyl acetate in pet. ether to afford the pure product **2.8** as a yellow solid. R_f = 0.5 (20% ethyl acetate in pet. ether). Yield: 0.12 g (37%); M.P. = 98-100 ºC. ^{1}H NMR ($CDCl_3$, 600 MHz): δ (ppm) = 8.02 (d, *J* = 7.6 Hz, 1H), 7.83 (d, *J* = 7.8 Hz, 2H), 7.66 (t, *J* = 7.2 Hz, 1H), 7.61 (t, *J* = 7.3 Hz, 1H), 7.43 (d, *J* = 7.7 Hz, 2H), 7.15 (d, *J* = 7.5 Hz, 1H), 6.82 (s, 1H), 6.76 (d, *J* = 2.2 Hz, 1H), 6.66-6.70 (m, 3H), 6.60 (dd, J_1 = 8.7 Hz, J_2 = 2.4 Hz, 1H), 5.12 (s, 2H), 3.83 (s, 3H), 1.34 (s, 12H). ^{13}C NMR ($CDCl_3$, 150 MHz): δ (ppm) = 169.4, 161.3, 160.3, 153.2, 152.5, 152.4, 139.4, 135.1, 135.0, 129.7, 129.2, 129.1, 126.5, 126.5, 125.0, 124.0, 112.3, 111.7, 111.5, 111.2,

TH-3161_176122050

101.9, 100.8, 83.9, 83.2, 70.1, 55.6, 24.9. ESI-MS (+ve) *m/z* calcd for $C_{34}H_{32}BO_7$ $[M + H]^+$: 563.2241; observed: 563.2275.

Synthesis of compound 2.9

To a stirred solution of compound **2.12** (0.20 g, 0.34 mmol) and triethylamine (0.14 mL, 1.04 mmol) in anhydrous DCM (8 mL) at 0 ºC under argon atmosphere was dropwise added a solution of compound **2.20** (0.35 g, 0.86 mmol) in anhydrous DCM (2 mL). The mixture was then allowed to attain room temperature and stirred for 48 h. The progress of the reaction was monitored by TLC analysis. Upon completion, the reaction mixture was diluted with DCM (50 mL) and washed with water followed by a saturated $NaHCO_3$ solution. The organic layer was washed with brine (3×10 mL) and dried over anhydrous sodium sulfate. The solvent was evaporated under reduced pressure to afford the crude residue, which was purified by flash chromatography using 30% ethyl acetate in the pet. ether to afford the pure product **2.9** as an off-white solid. R_f = 0.5 (30% ethyl acetate in pet. ether). Yield: 80 mg (23%); M.P. = 100-102 ºC. ^{1}H NMR ($CDCl_3$, 600 MHz): δ (ppm) = 8.03 (d, *J* = 7.6 Hz, 1H), 7.84 (d, *J* = 7.9 Hz, 2H), 7.68 (t, *J* = 7.1 Hz, 1H), 7.63 (t, *J* = 7.3 Hz, 1H), 7.44 (d, *J* = 7.9 Hz, 2H), 7.16-7.17 (m, 2H), 6.88 (dd, J_1 = 8.7 Hz, J_2 = 2.3 Hz, 1H), 6.81 (d, *J* = 8.7 Hz, 1H), 6.78 (d, *J* = 2.4 Hz, 1H), 6.70 (d, *J* = 8.8 Hz, 1H), 6.63 (dd, J_1 = 8.8 Hz, J_2 = 2.5 Hz, 1H), 5.29 (s, 2H), 3.84 (s, 3H), 1.35 (s, 12H). ^{13}C NMR ($CDCl_3$, 150 MHz): δ (ppm) = 169.3, 161.5, 153.0, 152.2, 152.1, 151.8, 137.4, 135.2, 135.1, 129.9, 129.2, 129.0, 127.6, 126.4, 125.1, 124.0, 117.0, 116.9, 112.0, 110.8, 109.8, 100.8, 84.0, 82.4, 75.0, 70.5, 55.6, 24.9. ESI-MS (+ve) *m/z* calcd for $C_{35}H_{32}BO_9$ $[M+H]^+$: 607.2139; observed: 607.2187.

2.5.6. UV-Visible and fluorescence spectroscopic studies

All the stock solution of probes and the released fluorophores were prepared in spectroscopy grade DMSO (note: 20% THF was added with DMSO for the naphthalimide-based probes **2.4**, **2.5** and **2.6** to dissolve them completely), and the stock solution of H_2O_2 was prepared in mili-Q water. All the spectroscopic studies were performed under physiological conditions (PBS, 20 mM, pH = 7.5). Buffers with higher pH (9 and 10) were prepared by adding 1N NaOH solution to the buffer. Samples for absorption and emission spectroscopic measurements were carried out in quartz cuvettes (1.0 mL). UV-Vis spectroscopic analyses were performed on a Lambda 45 UV-Vis spectrophotometer and fluorescence emission spectra were recorded on a Fluoromax-4 spectrophotometer (FluoroMax-4-Horiba). For

TH-3161_176122050

coumarin-based probes, λ_{ex} = 322 nm and λ_{em} = 447 nm with slit width = 3/3 nm, for naphthalimide-based probes, λ_{ex} = 442 nm and λ_{em} = 550 nm with slit width = 5/5 nm and for fluorescein-based probes, λ_{ex} = 454 nm and λ_{em} = 511 nm with slit width = 3/3 nm were used in the fluorescence emission spectroscopic studies. The selectivity of the directly-linked probe **2.7** (10 μM) towards H_2O_2 (200 μM) was carried out over different analytes such as *t*-Bu-OOH), Cum-OOH, KO_2, GSH, Cys, NAC, NaCl, and KCl. The probe was initially incubated for 30 min with the analytes (200 μM) and the emission intensity was measured. An equal amount of H_2O_2 (200 μM) was added to the resulting solution and the emission was measured after incubation for 30 min.

2.5.7. Determination of LOD

LOD of all the fluorescein-based probes **2.7**, **2.8**, and **2.9** were determined using fluorescence titration. The detection limit was calculated using the equation, LOD = 3σ/K, where σ is the standard deviation of blank measurements (without H_2O_2) and K is the slope of emission intensity versus H_2O_2 concentration. To get the standard deviation of the blank measurements, the emission intensity of all the probes (10 μM) was measured 10 times in the absence of H_2O_2. For the determination of slopes, the emission spectra were measured at different concentrations of H_2O_2 (2-50 μM) after incubating each reaction mixture for 30 min.

2.5.8. Analysis of the reaction kinetics using the reverse phase HPLC method

Purity of the synthesized compounds was analyzed by analytical high-performance liquid chromatography (HPLC), Agilent 1220 infinity II LC system using a reverse phase C_{18} column (Luna®, 250 × 4.6 mm, 5 μm). HPLC grade acetonitrile and water (Finar Ltd) were used as mobile phase and the absorbance profile of compounds were detected by PDA detector at wavelengths of 254 and 454 nm (as applicable). The stock solutions of the samples were prepared in acetonitrile and were injected into the HPLC system using the in-built autosampler at a flow rate of 1.0 mL/min using acetonitrile/water system as a mobile phase for 15 min (0-10 min: 80%-97% of acetonitrile in water; 10-15 min: 97-80% of acetonitrile in water. Concentrations of the pure probes and the released fluorophore are 100 μM and in the reaction mixture, 100 equivalents of H_2O_2 (10 mM) were added. The reactions of probes with H_2O_2 were carried out in HPLC grade acetonitrile and water system (3:1) at room temperature and the samples were injected into the system at different time intervals to monitor the progress of the reaction.

TH-3161_176122050

2.5.9. Detection of the endogenous level of H_2O_2 in HeLa cells by cellular imaging

HeLa cells were cultured in high glucose Dulbecco's modified Eagle's medium (DMEM) supplemented with 10% fetal bovine serum (FBS) and 1% penicillin/streptomycin at 37 °C under a 5% CO_2 atmosphere. Cells were then plated (0.5×10^4 cells/plate) in 35 mm cell culture petri dishes containing 2.0 mL of DMEM and incubated at 37 ºC under 5% CO_2 for 24 h. The confluent cells were washed with DPBS and finally incubated with the fluorescein-based probes (**2.7-2.9)** (5.0 μM) at 37 ºC under 5% CO_2 for 1 h. After washing with DPBS (5 times), cellular morphology was carefully observed and imaged in a Bio-Rad ZOE^{TM} fluorescent cell imager under a bright field and suitable fluorescent-colored filters. Additionally, the control experiments were designed and performed with the pre-treatment of NAC (2.0 mM, 1 h) to the HeLa cells to affirm the quenching of endogenous ROS level. The cells were washed with DPBS and treated further with the fluorogenic probes and incubated for 1 h. Finally, the treated cells were washed with DPBS (5 times) and imaged in a Bio-Rad ZOE^{TM} fluorescent cell imager to understand the reactivity of hydrogen peroxide with fluorescent probes. Further, to confirm the sensitivity of the boronate-based probes towards hydrogen peroxide, exogenous H_2O_2 (200 μM) was added to the cells and incubated at 37 ºC under 5% CO_2 for 1 h. The cells were washed with DPBS and probes (**2.7**-**2.9**) (5.0 μM) were added and incubated as discussed above. Finally, after sequential washing with DPBS, treated cells were imaged under Bio-Rad ZOE^{TM} fluorescent cell imager.

2.5.10. Cell culture and cellular viability studies

Human cervical cancer cell line (HeLa) was obtained from the National Centre for Cell Science (NCCS), Pune, India. HeLa cells were cultured in DMEM medium (Gibco) supplemented with 10% (v/v) FBS (Gibco) and 1% Pen-Strep (Gibco). Cells were cultured as a monolayer in a humidified incubator at 37 °C in the presence of 5% CO_2 level. The fluorescein-based probes (**2.7-2.9**) were screened for their anti-proliferative activities using the conventional MTT assay. All the test compounds were dissolved in DMSO (HiMedia). HeLa cells were seeded in 96-well culture plates at a density of 1×10^4 cells /100 μl/well and treated with the freshly prepared test compounds (5, 10, and 25 μM) for 0 h (control) and 48 h (experimental). At the end of the treatment period, 10 μL of 5.0 mg/mL of MTT was added to the plate (control) and incubated for 4 h. Following the 4 h incubation, the culture media from the plate was removed and the purple formazan crystals were dissolved using 100 μL

TH-3161_176122050

of DMSO (HiMedia) and the absorbance at 570 nm was measured using a microplate reader (Thermo Scientific™ Multiskan™ GO microplate reader). In the experimental set, a similar MTT treatment protocol was followed only after 48 h. The mean ΔOD values were calculated by the subtraction of mean OD values of 0 h plate (control) from the mean OD values of identical wells at 48 h plate (experimental) and the percentage proliferation was calculated keeping the mean ΔOD of untreated control as 100%.

2.6. References

1. H. Sies, *Redox Biol.*, 2017, **11**, 613-619.
2. H. Ohshima, M. Tatemichi and T. Sawa, *Arch. Biochem. Biophys.*, 2003, **417**, 3-11.
3. A. Shah and K. Channon, *Heart*, 2004, **90**, 486-487.
4. H. Sies, *Am. J. Med.*, 1991, **91**, S31-S38.
5. K. J. Barnham, C. L. Masters and A. I. Bush, *Nat. Rev. Drug Discov*, 2004, **3**, 205-214.
6. K. P. Bhabak and G. Mugesh, *Acc. Chem. Res.*, 2010, **43**, 1408-1419.
7. J. Liang and B. Liu, *Bioeng. Transl. Med.*, 2016, **1**, 239-251.
8. S. Kenmoku, Y. Urano, H. Kojima and T. Nagano, *J. Am. Chem. Soc.*, 2007, **129**, 7313-7318.
9. M. C. Chang, A. Pralle, E. Y. Isacoff and C. J. Chang, *J. Am. Chem. Soc.*, 2004, **126**, 15392-15393.
10. E. W. Miller, A. E. Albers, A. Pralle, E. Y. Isacoff and C. J. Chang, *J. Am. Chem. Soc.*, 2005, **127**, 16652-16659.
11. E. W. Miller, O. Tulyathan, E. Y. Isacoff and C. J. Chang, *Nat. Chem. Biol.*, 2007, **3**, 263-267.
12. J. Liu, J. Ren, X. Bao, W. Gao, C. Wu and Y. Zhao, *Anal. Chem.*, 2016, **88**, 5865-5870.
13. J. Liu, S. Zhou, J. Ren, C. Wu and Y. Zhao, *Analyst*, 2017, **142**, 4522-4528.
14. W. Chen, Y. Han and X. Peng, *Chem. Eur. J.*, 2014, **20**, 7410-7418.
15. K. Matsushita, T. Okuda, S. Mori, M. Konno, H. Eguchi, A. Asai, J. Koseki, Y. Iwagami, D. Yamada and H. Akita, *ChemMedChem*, 2019, **14**, 1384-1391.
16. C. Skarbek, S. Serra, H. Maslah, E. Rascol and R. Labruère, *Bioorg. Chem.*, 2019, **91**, 103158.

TH-3161_176122050

17. G. Masanta, C. H. Heo, C. S. Lim, S. K. Bae, B. R. Cho and H. M. Kim, *Chem. Commun.*, 2012, **48**, 3518-3520.
18. G. Gao, D. Gong, M. Zhang and T. Sun, *Acta Chim. Sin.*, 2016, **74**, 363.
19. F. Xu, H. Li, Q. Yao, J. Fan, J. Wang and X. Peng, *J. Mat. Chem. B*, 2016, **4**, 7363-7367.
20. H. Xiao, P. Li, X. Hu, X. Shi, W. Zhang and B. Tang, *Chem. Sci.*, 2016, **7**, 6153-6159.
21. J. Xu, Y. Zhang, H. Yu, X. Gao and S. Shao, *Anal. Chem.*, 2016, **88**, 1455-1461.
22. J. Xu, Y. Zhang, H. Yu, X. Gao and S. Shao, *Anal. Chem.*, 2016, **88**, 1455-1461.
23. K. B. Daniel, A. Agrawal, M. Manchester and S. M. Cohen, *ChemBioChem*, 2013, **14**, 593-598.
24. C. Chung, D. Srikun, C. S. Lim, C. J. Chang and B. R. Cho, *Chem. Commun.* , 2011, **47**, 9618-9620.
25. B. C. Dickinson, C. Huynh and C. J. Chang, *J. Am. Chem. Soc.*, 2010, **132**, 5906-5915.
26. M. S. Purdey, H. J. McLennan, M. L. Sutton-McDowall, D. W. Drumm, X. Zhang, P. K. Capon, S. Heng, J. G. Thompson and A. D. Abell, *Sens. Actuators, B*, 2018, **262**, 750-757.
27. S. Mori, K. Morihiro, T. Okuda, Y. Kasahara and S. Obika, *Chem. Sci.*, 2018, **9**, 1112-1118.
28. J. L. M. Jourden, K. B. Daniel and S. M. Cohen, *Chem. Commun.* , 2011, **47**, 7968-7970.
29. S. Feng and G. Zhang, *Talanta*, 2021, **224**, 121785.
30. D. Ganeshapillai, L. L. Woo, M. P. Thomas, A. Purohit and B. V. Potter, *ACS Omega*, 2018, **3**, 10748-10772.
31. F. Guibbal, V. Meneyrol, I. Ait-Arsa, N. Diotel, J. Patché, B. Veeren, S. b. Bénard, F. Gimié, J. Yong-Sang and I. Khantalin, *ACS Med. Chem. Lett.*, 2019, **10**, 743-748.
32. G. Zeng, R. Zhang, W. Xuan, W. Wang and F.-S. Liang, *ACS Chem. Biol.*, 2015, **10**, 1404-1410.
33. C. Skarbek, S. Serra, H. Maslah, E. Rascol and R. Labruère, *Bioorg. Chem.*, 2019, **91**, 103158.

TH-3161_176122050

34. S. Srivastava, D. Bimal, K. Bohra, B. Singh, P. Ponnan, R. Jain, M. Varma-Basil, J. Maity, M. Thirumal and A. K. Prasad, *Eur. J. Med. Chem.*, 2018, **150**, 268-281.

35. A. Mukhopadhyay, V. K. Maka and J. N. Moorthy, *Phys. Chem. Chem. Phys.*, 2017, **19**, 4758-4767.

36. Y. Xu, H. Zhang, K. Shen, S. Mao, X. Shi and H. Wu, *Appl. Organomet. Chem.*, 2018, **32**, e3902.

37. X. Hou, Q. Yu, F. Zeng, J. Ye and S. Wu, *J. Mater. Chem. B*, 2015, **3**, 1042-1048.

38. C. Liu, C. Shao, H. Wu, B. Guo, B. Zhu and X. Zhang, *RSC Adv.*, 2014, **4**, 16055-16061.

39. B. UmuráKaya, *Chem. Commun.*, 2019, **55**, 4937-4940.

40. B. C. Dickinson, C. Huynh and C. J. Chang, *J. Am. Chem. Soc.*, 2010, **132**, 5906-5915.

41. K. N. More, T.-H. Lim, S.-Y. Kim, J. Kang, K.-S. Inn and D.-J. Chang, *Dyes Pigm.*, 2018, **151**, 245-253.

TH-3161_176122050

TH-3161_176122050

Peroxide-responsive prodrug of non-steroidal anti-inflammatory drug diclofenac: sustained drug release with turn-on near-infrared fluorescence

TH-3161_176122050

TH-3161_176122050

3.1. Introduction

NSAIDs are the most prescribed medicines in clinical practices. These are widely used for the treatment of inflammatory diseases such as rheumatoid arthritis (RA), migraine, gout, dentistry, and acute and chronic inflammation.[1] While the expression of COX-1 is constitutive and associated to the gastric mucosal protection and the COX-2 isoform is induced at inflammatory sites, which promotes inflammation and pain.[2] However, most marketed NSAIDs are non-selective COX inhibitors and exhibit several side-effects, specifically gastrointestinal (GI) damage.[3] In addition, regular uptake of NSAIDs for a longer period causes gastric or intestinal ulcers by damaging the gastroduodenal mucosa.[3] Therefore, several prodrugs of NSAIDs have been developed to reduce the side-effects of conventional NSAIDs as discussed in chapter 1.[4-6] However, these prodrugs are non-fluorogenic and generally release the modified NSAIDs instead of the active drugs. In comparison to the non-fluorogenic prodrugs, the strategies with stimuli-responsive turn-on fluorogenic prodrugs have extra advantages for very convenient and non-invasive real-time monitoring of the drug release. It is suitable for both *in vitro* and *in vivo* applications.[7-12] Due to the increased levels of H_2O_2 in cancer cells as compared to normal cells, the H_2O_2-responsive non-fluorogenic and fluorogenic prodrugs of anti-cancer drugs have been developed throughout the last decade by coupling the active drugs with aryl boronic acid or ester moiety for the targeted drug delivery (chapter 1).[13-20] Since inflammatory sites are overexpressed with COX-2 and the inflamed tissues are associated with an elevated level of ROS (H_2O_2), the development of H_2O_2-triggered sustained drug release could be extremely helpful for the targeted delivery of NSAIDs for anti-inflammatory therapy with minimal side-effects. As observed in chapter 2, prodrugs with sustained drug delivery can be developed by coupling the fluorophore with boronate ester unit *via* an ether linker. Therefore, a novel prodrug can be developed for the sustained delivery of NSAID by connecting the fluorophore with the boronate ester *via* ether linker. It may allow for selective distributions into the inflammatory sites and a prolonged half-life of the drug. When we were about to submit the article for the development of ROS-responsive fluorogenic prodrug of NSAID (diclofenac) in 2021, Peng and co-workers reported a fluorogenic naphthalimide adduct of ibuprofen **IBLN** for the treatment of breast cancer by inhibiting COX-2 (Figure 3.1).[21] The fluorogenic naphthalimide unit assisted in tracking cellular absorption and localization. However, the active drug was not released from

TH-3161_176122050

the prodrug due to lack of triggering unit. In later 2021, Kim and co-workers developed the hydrogen polysulfide (H_2S_n)-triggered mitochondria-targeting theranostic prodrug of NSAID (**TA1**) for the targeted delivery of indomethacin (Figure 3.1).[22] The spectroscopic results indicated that the active drug was released with turn-on fluorescence in the presence of H_2S_n. The anti-inflammatory prodrug **TA1** downregulated prostaglandin E2 (PGE2) and COX-2 levels in the blood serum of inflammation-induced mice models (C57Bl/6 male mice).

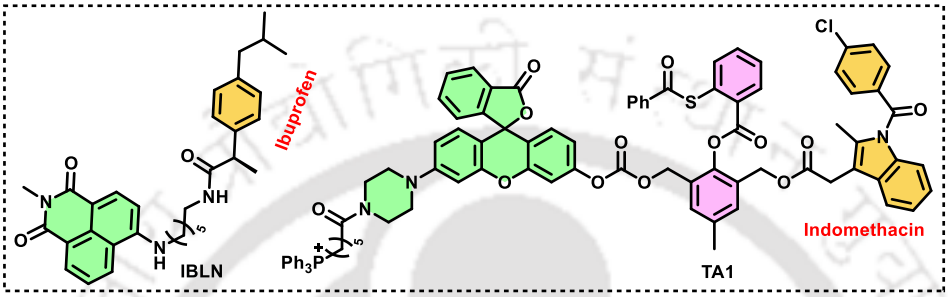

Figure 3.1. Chemical structures of the recently reported fluorogenic prodrugs of NSAIDs.

However, the NSAID (indomethacin) was released from the prodrug quite rapidly, and it is more COX-1 selective than COX-2. In addition, green emissive fluorophore was used for monitoring the drug release, which has less tissue penetrating power and has more interferences with biomolecules.[10, 23]

3.2. Outline of the chapter

Herein, we developed H_2O_2-responsive turn-on fluorogenic prodrug of NSAID (**DCI-ROS)**, for a prolonged release of diclofenac (**DCF**) and near-infrared (NIR) fluorophore concurrently (Figure 3.2). Among around 40 different NSAIDs, **DCF** and ibuprofen are widely used worldwide.[24, 25] Interestingly, unlike ibuprofen, **DCF** is more selective towards COX-2, making it a better candidate for anti-inflammatory responses.[10, 23] Since **DCF** has a shorter plasma half-life, multiple self-immolative linkers were incorporated into the prodrug for a sustained release strategy to prolong the plasma half-life of the drug. The larger stokes shift, minimal interference from biomolecules, and higher tissue penetrating power of the dicyanoisophorone-based red-emissive NIR fluorophore **DCI-OH** were also taken into consideration.[26, 27] In addition, **DCI-Con**, a negative control prodrug was also synthesized without any H_2O_2-triggering unit to understand the role of boronate ester moiety in activating the drug release. The prodrug was synthesized by following the multi-step organic synthesis strategy. The purification and characterization were performed using analytical techniques.

TH-3161_176122050

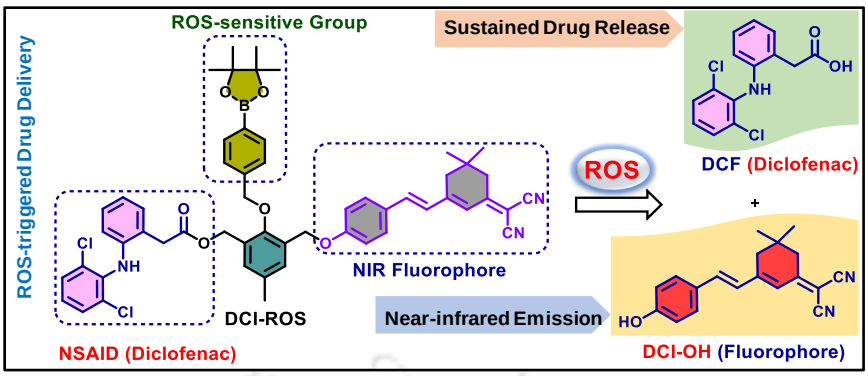

Figure 3.2. Schematic representation of our rationally designed ROS-responsive prodrug of diclofenac (**DCI-ROS**).

Inflammation-induced elevated ROS at the site of inflammation would cleave the boronate ester moiety in **DCI-ROS** facilitating the self-immolative process for the active drug release with simultaneous turn-on NIR fluorescence. Spectroscopic studies, HPLC, and ESI-MS analyses confirmed the feasibility of drug release process in aqueous medium. Moreover, the prodrug was found to be non-toxic in cancer cells MDA-MB-231 and macrophage cells RAW 264.7 and exhibited turn-on red emission in the presence of endogenous ROS. Anti-inflammatory activity of the prodrug was validated further with the inhibition of COX-2 expression in the inflammation-induced macrophage cells (RAW 264.7).

3.3. Results and Discussion

3.3.1. Synthesis of the prodrugs DCI-ROS and DCI-Con

The boronate benzyl bromide unit (**3.3**) was synthesized from 4-bromotoluene (**3.1**) following the reported procedure involving Suzuki coupling followed by selective mono-bromination in the presence of *N*-bromosuccinimide in two steps with a satisfactory yield (Scheme 3.1A).[28, 29] Following the reported procedure, the dicyanoisophorone-based NIR fluorophore **DCI-OH** was synthesized from isophorone (**3.4**) in two steps *via* Knoevenagel and Aldol condensation processes (Scheme 3.1B).[30] The final prodrug (**DCI-ROS**) was synthesized *via* a multi-step organic synthesis, beginning with the alcoholic precursor based on *p*-cresol (**3.6**) (Scheme 3.1C). The benzylic hydroxyl groups of compound **3.6** was protected selectively using *tert*-butyldimethylsilyl chloride (TBDMSCl) to get an intermediate (**3.7**) with a reasonably good yield. Compound **3.8** was synthesized by combining the phenolic hydroxyl group of compound **3.7** with compound **3.3**. Subsequent

TH-3161_176122050

deprotection of the silyl protecting groups in **3.8** using *p*-toluenesulfonic acid afforded compound **3.10**.[31] Furthermore, bromination of benzylic hydroxyl groups in **3.10** was carried out using phosphorus tribromide with the formation of compound **3.12**, which was mono-esterified selectively with **DCF** leading to the formation of compound **3.14**. To get the designed prodrug **DCI-ROS**, the nucleophilic substitution reaction was performed in compound **3.14** with **DCI-OH** (Scheme 3.1C).

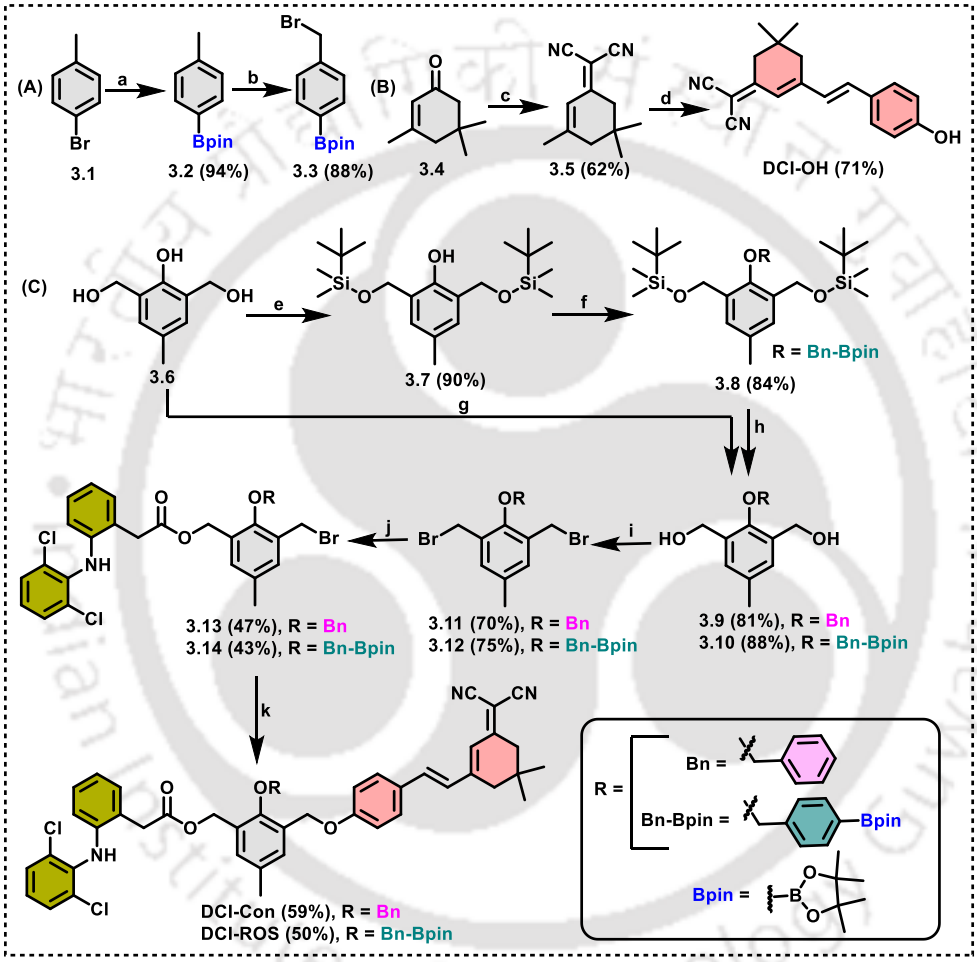

Scheme 3.1. Synthetic schemes of (A) boronate ester precursor **3.3**, (B) NIR fluorophore **DCI-OH**, and (C) prodrugs **DCI-Con** and **DCI-ROS**. Reagents and conditions: (a) 2-Isopropoxy-4,4,5,5-tetramethyl-1,3,2-dioxaborolane, *n*-BuLi, dry THF, -78 °C, 2 h; (b) NBS, AIBN, dry ACN, reflux, 3 h; (c) Malononitrile, piperidine, glacial AcOH, EtOH, reflux, 12 h; (d) 4-hydroxy benzaldehyde, piperidine, dry ACN, reflux, 6 h; (e) TBDMSCl, imidazole, dry DMF, 0 °C – RT, 2 h; (f) **3.3**, K_2CO_3, dry DMF, 0 °C – RT, 12 h; (g) Benzyl bromide, K_2CO_3, dry DMF, 0 °C – RT, 12 h; (h) *p*-TsOH, MeOH, RT, 12 h; (i) PBr_3, dry DCM, RT, 5 h; (j) Diclofenac, DIPEA, dry ACN, 0 °C – RT, 12 h; (k) **DCI-OH**, K_2CO_3, acetone, 55 °C, 4 h.

TH-3161_176122050

The control prodrug **DCI-Con** without the H_2O_2-sensitive boronate ester moiety was also synthesized starting from the precursor **3.6**. Here, a direct selective O-benzylation at the phenolic hydroxyl group in **3.6** yielded the intermediate **3.9**, which was brominated subsequently forming compound **3.11**. Similarly, selective mono-esterification of compound **3.11** with **DCF** yielded compound **3.13**, which was reacted further with **DCI-OH** leading to the formation of the control prodrug **DCI-Con** at reasonably good yield. Both the final prodrugs were purified and characterized before carried out the spectroscopic and cellular studies. Before performing the spectroscopic studies, reverse-phase analytical HPLC was used to determine the purity of the prodrug **DCI-ROS** and the control prodrug **DCI-Con**. The HPLC chromatogram indicated that both prodrugs were more than 99% pure.

3.3.2. UV-Vis and fluorescence spectroscopic studies

The initial absorption spectra of the designed prodrug **DCI-ROS** (50 μM) with and without H_2O_2 (1000 μM) indicated the significant spectral change of the prodrug **DCI-ROS** in the presence of H_2O_2 (after 14 h) and the spectrum matched well with that of **DCI-OH** and **DCF** (Figure 3.3A). The results indicate a feasible reaction of **DCI-ROS** with H_2O_2 releasing both the active drug **DCF** and NIR fluorophore **DCI-OH**. Subsequently, the emission spectrum of the reaction of **DCI-ROS** (10 μM) in the presence of H_2O_2 (200 μM) was measured (λ_{ex} = 550 nm). Interestingly, the emission pattern (λ_{em} (max) = 670 nm) resembled well with that of pure **DCI-OH**, indicating the turn-on fluorescence from **DCI-ROS** (Figure 3.3B). The emission intensity of **DCI-ROS** in the presence of H_2O_2 is 8-times higher than the emission intensity of **DCI-ROS** in the absence of H_2O_2. However, similar reactions with the control prodrug **DCI-Con** with H_2O_2 did not change the absorption and emission spectral profiles (Figures 3.3C and D). These initial observations indicated the reaction of the boronate ester group of **DCI-ROS** with H_2O_2 and the subsequent occurrence of self-immolative processes for the release of the fluorophore **DCI-OH** and the active drug **DCF** from the prodrug **DCI-ROS**. With the evidence of the turn-on fluorogenic process, the kinetics of the turn-on emissive drug release process was studied with **DCI-ROS** (10 μM) in the presence of H_2O_2 (200 μM) over the time (0-18 h). It is interesting to note that the emission intensity gradually increased over time upto 10 h and slowly saturated afterward upto 18 h (Figure 3.3E). However, the emission intensity of the pure **DCI-ROS** in the absence of H_2O_2 was negligibly

TH-3161_176122050

small and did not increase upto 18 h, indicating significant stability of the prodrug over time (Figure3.3E).

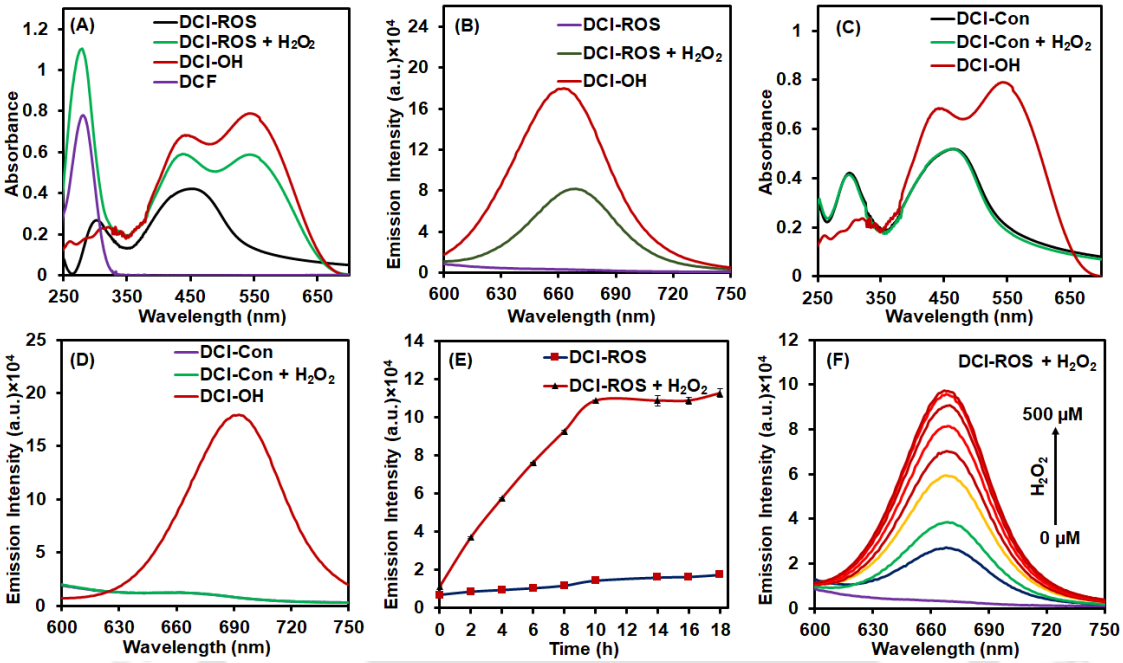

Figure 3.3. (A) Absorption spectra of **DCI-ROS** (50 µM) with and without H_2O_2 (1000 µM) along with spectra of pure released fluorophore **DCI-OH** (50 µM) and **DCF** (50 µM). (B) Emission spectra of prodrug **DCI-ROS** (10 µM) with and without H_2O_2 (200 µM) along with the emission spectrum of pure **DCI-OH** (10 µM). The incubation time = 14 h. (C) Absorption spectra of prodrug **DCI-Con** (50 µM) in the absence and presence of H_2O_2 (1 mM) (D) Emission spectra of prodrug **DCI-Con** (10 µM) in the absence and presence of H_2O_2 (200 µM) (E) Emission spectra of **DCI-ROS** (10 µM) in the absence and presence of H_2O_2 (200 µM) with variable time (0-18 h). (F) Emission spectra of **DCI-ROS** (10 µM) with variable concentration of H_2O_2 (0-500 µM) with a fixed incubation time of 14 h. The experiments were carried out in phosphate buffered saline (PBS) (20 mM, pH 7.5, with 50% DMSO v/v). λ_{ex} = 550 nm.

Considering the prodrug responsiveness towards H_2O_2, the release of the drug and the fluorophore from **DCI-ROS** (10 µM) was studied with the variable concentration of H_2O_2 (0-500 µM). As shown in Figure 3.3F, the emission intensity increased gradually with the increasing concentration of H_2O_2 under a fixed incubation time (14 h) and showed saturation behavior from 300 µM concentration onwards. This observation could have high significance for the applicability of this prodrug to the biological system. Considering the relatively higher

TH-3161_176122050

level of ROS in inflamed cells/tissues, a higher amount of NSAID and fluorophore would be released in the inflammatory sites.

3.3.3. Analyte selectivity and the pH dependency

Although boronate ester-based prodrugs are frequently utilized due to their high level of sensitivity and selectivity towards H_2O_2 over other analytes, the analyte selectivity analysis was carried out with **DCI-ROS** with several biologically relevant analytes. As shown in Figure 3.4A, the prodrug was found to be very selective towards H_2O_2 over other oxidants such as cumene hydroperoxide (Cum-OOH), *tert*-butyl hydroperoxide (*t*-Bu-OOH), potassium superoxide (KO_2), peroxynitrite ($ONOO^-$), and sodium hypochlorite (NaOCl); thiol-based nucleophilic reducing agents such as glutathione (GSH), L-cysteine (Cys), and *N*-acetyl cysteine (NAC). These results indicated that the prodrug had extremely high selectivity towards H_2O_2 with minimal interferences from other bio-analytes. Moreover, the stability and feasibility of the fluorogenic drug release from **DCI-ROS** at variable pH was studied by measuring the emission from **DCI-ROS** (10 μM) in the presence or absence of H_2O_2 (200 μM) over a variable pH (5-11) of the medium. The emission intensity from **DCI-ROS** increased significantly upon increasing the pH from 7 onwards in the presence of H_2O_2, however, a very negligible increase was observed in the absence of H_2O_2 (Figure 3.4B).

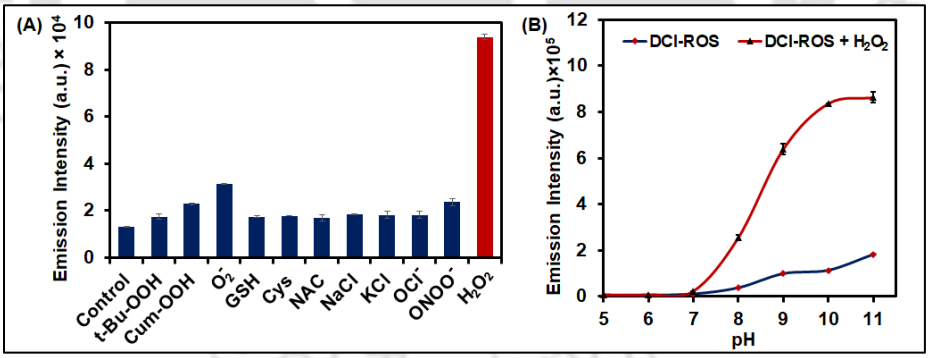

Figure 3.4. (A) Emission response of **DCI-ROS** (10 μM) in the presence of biologically relevant analytes (200 μM) after incubating for 14 h. (B) The emission intensity of **DCI-ROS** (10 μM) in the presence/absence of H_2O_2 (200 μM) with variable pH of the medium (pH: 5-11).

It is noted that the emission intensity at the NIR region is expected to be enhanced at higher pH levels (≤7) as the phenolic –OH group of **DCI-OH** becomes deprotonated, leading to the extended conjugation. Furthermore, at the increased pH, the analyte H_2O_2 may undergoes

TH-3161_176122050

through deprotonation to produce the highly nucleophilic and reactive hydroperoxide ($^{-}$OOH) anion having much higher reactivity towards **DCI-ROS**.

3.3.4. Reaction kinetics for the drug release using HPLC

The release profile of the drug **DCF** and fluorophore **DCI-OH** from **DCI-ROS** was further monitored using the reverse phase HPLC method. In a 60:40 ACN/water mixture, **DCI-ROS** (100 µM) was incubated with H_2O_2 (2 mM), and the composition of the reaction mixture was analyzed using reverse phase HPLC over 0-10 h. Before analyzing the reaction mixture, the retention times of the pure **DCI-ROS** (19.6 min), **DCF** (2.1 min), and **DCI-OH** (5.3 min) were optimized under similar conditions. The peak of the prodrug **DCI-ROS** at 19.6 min almost vanished upon the reaction with H_2O_2, and new peaks at 2.1 min and 5.3 min appeared that precisely coincided with the retention times of pure **DCF** and **DCI-OH**, respectively (Figure 3.5A and 3.5B). This observation clearly illustrated that the drug and fluorophore are released from the prodrug **DCI-ROS** upon the reaction with H_2O_2. Interestingly, two additional peaks were observed at 12.3 and 7.8 min during the formation of **DCI-OH** and **DCF** in the reaction mixture (Figure 3.5A). Although they vanished over time as the reaction progressed, it was possible to attribute these peaks for intermediates **3.15** and **3.16** (Figure 3.5A and 3.5B).

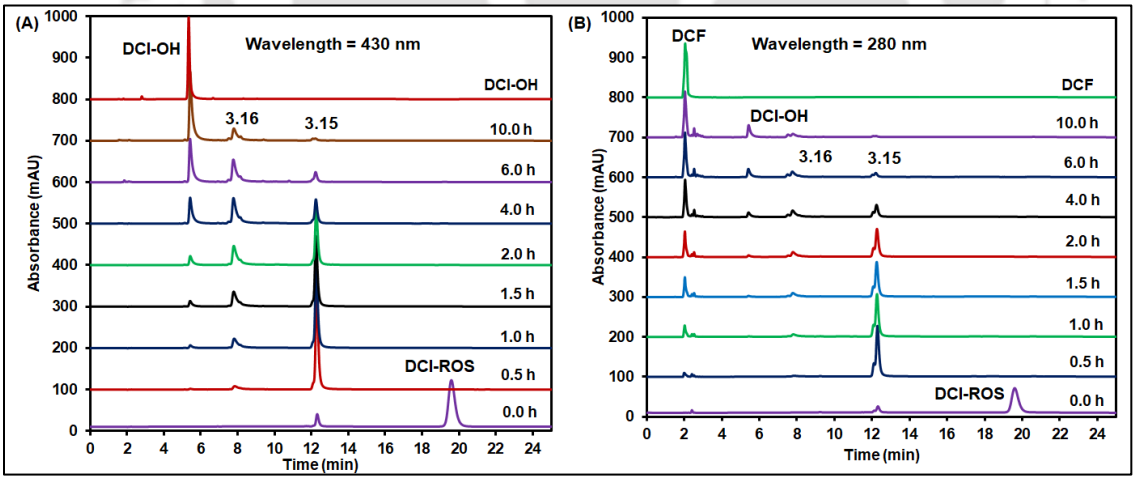

Figure 3.5. HPLC overlay chromatogram for the reaction of **DCI-ROS** (100 µM) with H_2O_2 (2 mM) over 10 h along with the chromatogram of released active drug **DCF** and fluorophore **DCI-OH** (100 µM). All the chromatograms were extracted at 430 nm (A) and 280 nm (B).

TH-3161_176122050

The composition of the reaction mixture was analyzed after 4 h of incubation using ESI-MS analysis to identify the intermediates **3.15** and **3.16**. ESI-MS results further supported the presence of intermediates **3.15** and **3.16** in the reaction mixture. (Figure 3.6).

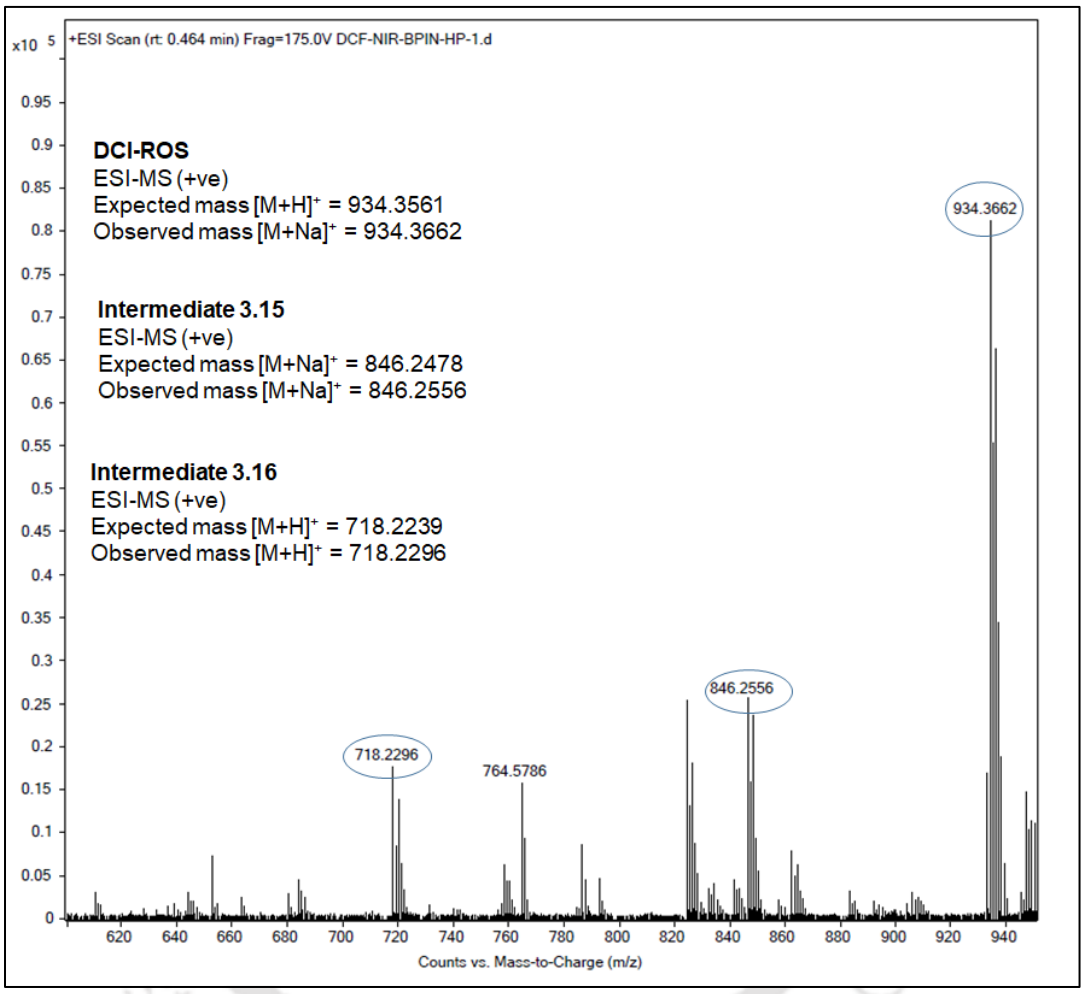

Figure 3.6. ESI-MS spectrum of the reaction mixture of **DCI-ROS** with H_2O_2 showing the presence of intermediates **3.15** and **3.16**. ESI-MS (+ve) *m/z* calcd for $C_{49}H_{43}Cl_2N_3O_5$ $[M + Na]^+$: 846.2478; obs. 846.2556 (intermediate **3.15**), for $C_{42}H_{37}Cl_2N_3O_4$ $[M + H]^+$: 718.2239; obs. 718.2296 (intermediate **3.16**) and for $C_{55}H_{54}BCl_2N_3O_6$ $[M + H]^+$: 934.3561; Obs. 934.3662 (prodrug **DCI-ROS**).

3.3.5. Plausible mechanistic pathway

The obtained results from the kinetics experiments (HPLC) can be summarized as shown in Figure 3.7A. The prodrug **DCI-ROS** reacted rapidly with H_2O_2 and almost disappeared during the first 30 min with the exclusive formation of intermediates **3.15** and **3.16** as well

TH-3161_176122050

as the released products. With the gradual disappearance of intermediates **3.15** and **3.16**, the drug **DCF** and fluorophore **DCI-OH** were gradually released over time. Furthermore, the control prodrug **DCI-Con** was incubated with H_2O_2 following a similar condition as **DCI-ROS**, and the reaction mixture was analyzed using reverse-phase HPLC after 10 h. However, the prodrug **DCI-Con** was still present even after 10 h with no release of **DCF** or **DCI-OH**, indicating the significance of the boronate ester moiety for the drug release. (Figure 3.7B). Based on the results from spectroscopic studies, HPLC, and ESI-MS analyses, a plausible mechanism was proposed for the H_2O_2-triggered fluorogenic drug release process, as shown in Figure 3.7C. Due to the high reactivity of the boronate ester group in **DCI-ROS** with H_2O_2, **DCI-ROS** disappeared rapidly during the HPLC kinetics, and intermediate **3.15** was produced. Moreover, the intensity of intermediate **3.15** decreased whereas intermediate **3.16** appeared through the first self-immolative process with the formation of quinone methide (QM) species. This QM intermediate is further converted into 4-hydroxybenzyl alcohol in the presence of H_2O. The final release of the active drug **DCF** and the fluorophore **DCI-OH** along with the precursor **3.6** were took place by the slower self-immolation processes (2^{nd} and 3^{rd}) of the intermediate **3.16**.

TH-3161_176122050

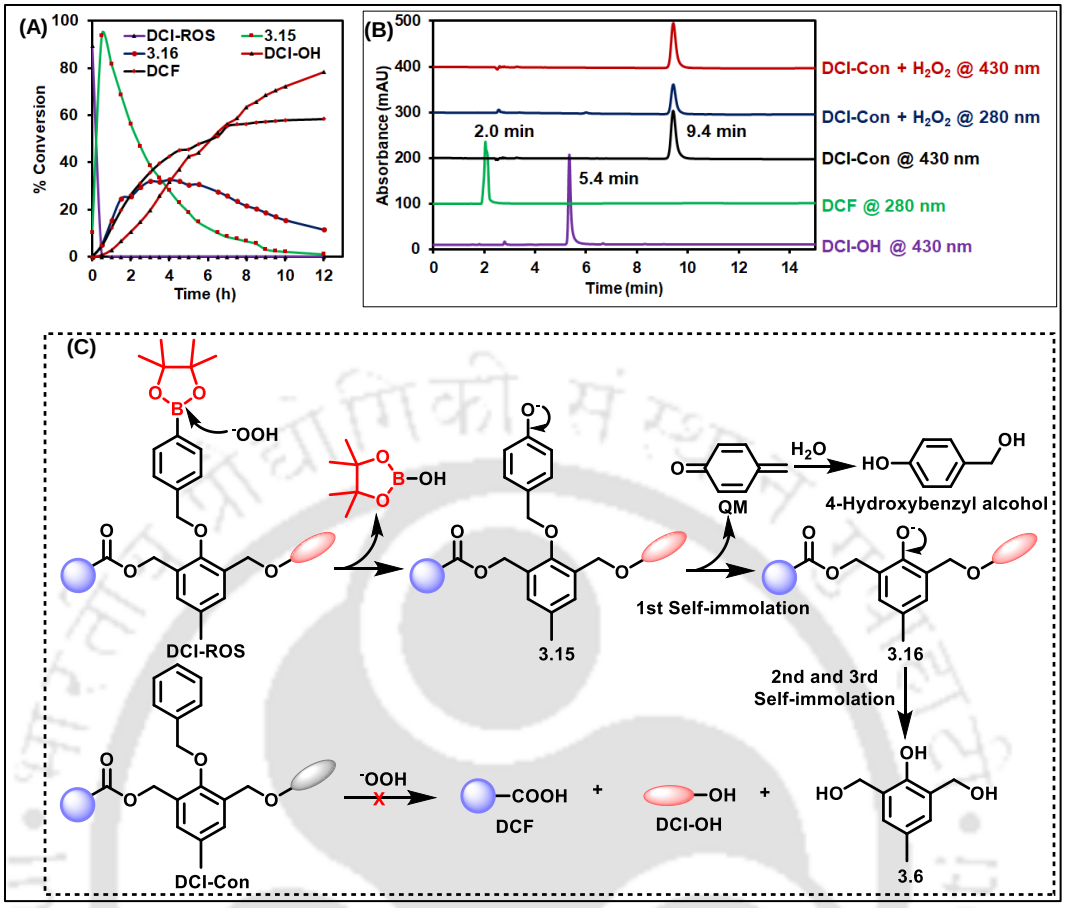

Figure 3.7. (A) Relative peak areas of various components present in the reaction mixture of **DCI-ROS** (100 μM) + H_2O_2 (2 mM) over 10 h were monitored for the percentage conversion. While the peak area of **DCF** was measured at 280 nm, the peaks area of **DCI-ROS**, **3.15**, **3.16,** and **DCI-OH** were measured at 430 nm. (B) A complete HPLC overlay chromatogram for the reaction of **DCI-Con** (100 μM) with and without H_2O_2 (2 mM), along with released drug **DCF** (100 μM, 280 nm), and fluorophore **DCI-OH** (100 μM, 430 nm). All the chromatograms were extracted at 280 and 430 nm wavelengths. Incubation time: 10 h. (C) Proposed mechanistic insights for the reaction of **DCI-ROS** with H_2O_2 for the fluorogenic drug release. The control prodrug **DCI-Con** does not react with H_2O_2 for the drug release.

Here, it should be mentioned that the occurrence of the following self-immolative processes in intermediates **3.15** and **3.16**, respectively, made it possible to achieve the sustained drug release from **DCI-ROS**. These results supported our earlier observations that ether-linked boronate ester groups are appropriate for prolonged drug release, whereas the direct boronate ester linkers are appropriate for analyte sensing applications (chapter 2).[15] Contrary to the prolonged release of a fluorogenic drug from **DCI-ROS** in the presence of H_2O_2, the

TH-3161_176122050

corresponding benzyl-substituted prodrug **DCI-Con** was unable to release the drug or the fluorophore because of the absence of ROS-responsive boronate ester group.

3.3.6. Cell viability and fluorescence microscopic studies of DCI-ROS

With the confirmation of ROS-induced release of the NIR fluorophore **DCI-OH** and the active drug **DCF** from the prodrug **DCI-ROS** in the aqueous medium, feasibility of the process was investigated next in the cellular medium. In order to understand the compatibility of the prodrug in cellular medium a representative breast cancer cell line (MDA-MB-231) and the murine macrophage cell line (RAW 264.7) were chosen. It should be noted that the cancer cells MDA-MB-231 contain higher levels of intracellular ROS[32, 33] and higher expression levels of the inflammatory enzyme COX-2.[34, 35] Using the standard MTT assay, the cellular toxicity profile of **DCI-ROS** was investigated in both the cell lines. Cellular viability was determined after 48 h of treatment with **DCI-ROS** and pure **DCF** at various dosages (0, 10, 25, 50, and 100 μM). Interestingly, the prodrug **DCI-ROS** and the active drug **DCF** were found to be non-toxic towards both the cell lines upto 100 μM concentrations (Figure 3.8A and 3.8B), indicating the biocompatible nature of the synthesized prodrug **DCI-ROS**.

Knowing that the prodrug was non-toxic in the MDA-MB-231 or RAW 264.7 cell lines, the endogenous ROS-induced release of the fluorophore **DCI-OH** from the prodrug **DCI-ROS** was studied in the MDA-MB-231 cell line (Figure 3.8C). The MDA-MB-231 cells were incubated with the prodrug **DCI-ROS** (50 μM) for 5 h and the cellular images were collected using fluorescence microscope. Interestingly, significant emission response under red channel was observed indicating the endogenous ROS-triggered fluorescence emission from the prodrug. Moreover, a ROS scavenger (NAC) was used further to confirm the role of endogenous H_2O_2 in the fluorogenic drug release.

TH-3161_176122050

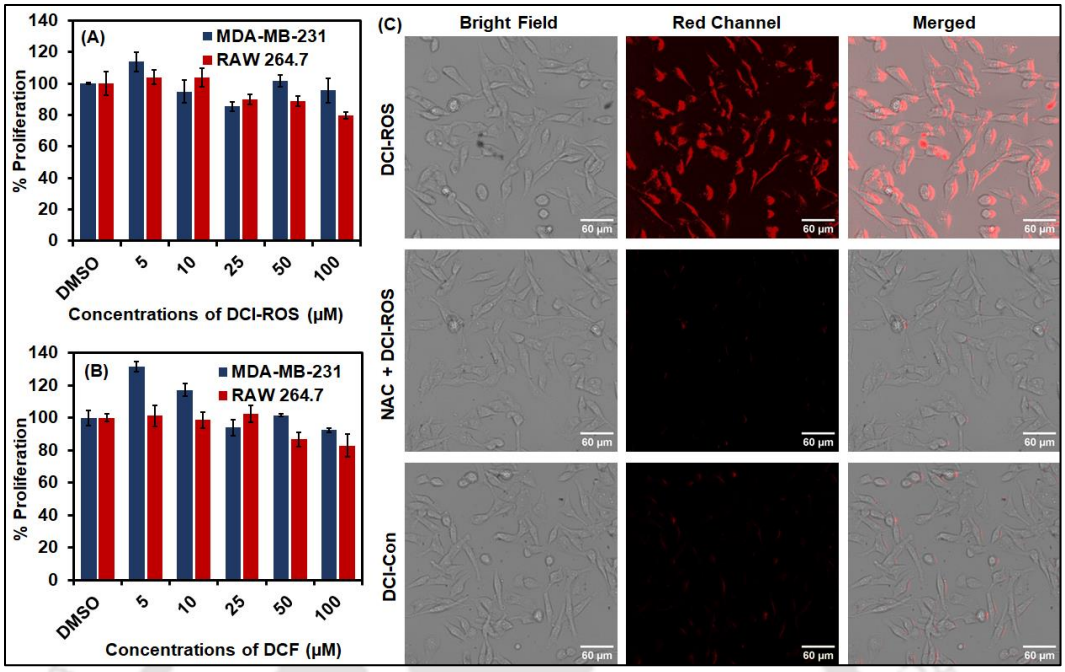

Figure 3.8. Cellular viability of MDA-MB-231 and RAW 264.7 cells in the presence of (A) **DCI-ROS** and (B) **DCF**. The cells were incubated with the compounds for 48 h. (C) Fluorescence microscopy images (bright field, red channel, and merged) of MDA-MB-231 cells in the presence of **DCI-ROS** or **DCI-Con** (50 μM) for the endogenous ROS-triggered fluorogenic drug release. The cells were pre-treated with NAC (2 mM) for 1 h to quench the endogenous ROS. Scale bar: 60 μm.

To ensure that the endogenous ROS levels get quenched by NAC, the cells were pre-treated with NAC (2.0 mM) before being treated with **DCI-ROS**. Interestingly, the lower emissive response in the presence of NAC indicated the major role of endogenous H_2O_2 in the fluorogenic drug release from the **DCI-ROS**. Furthermore, the control prodrug **DCI-Con** (50 μM) showed no emission after being incubated in MDA-MB-231 cells under the identical condition. This result supported the significance of the H_2O_2-reactive boronate ester group in the prodrug **DCI-ROS** for the drug delivery (Figure 3.8C).

Upon confirmation of endogenous H_2O_2-induced **DCI-OH** release from **DCI-ROS** occurring in breast cancer cells, the release of **DCI-OH** and **DCF** from the **DCI-ROS** were investigated in inflammation-induced macrophage cells. To understand the endogenous H_2O_2-triggered fluorophore release from the prodrug **DCI-ROS**, RAW 264.7 cells were treated with **DCI-ROS** (50 μM) and incubated for 5 h (Figure 3.9A). The fluorescence emission under the red channel indicated the release of the fluorophore **DCI-OH** due to endogenous H_2O_2. In

TH-3161_176122050

addition, cells were pre-treated with ROS-inducer lipopolysaccharide (LPS) (50 µg/mL, 14 h) to induce the inflammation (overexpression of COX-2), thereafter, the cells were treated with **DCI-ROS** (50 µM). The LPS pre-treated RAW 264.7 cells showed significant enhancement in red emission as compared to those without LPS, indicating the LPS-induced ROS production, which results in higher fluorophore release from inflamed cells. (Figure 3.9B). This result indicates that more amount of drug would be released from the prodrug in the inflammatory sites over normal tissues.

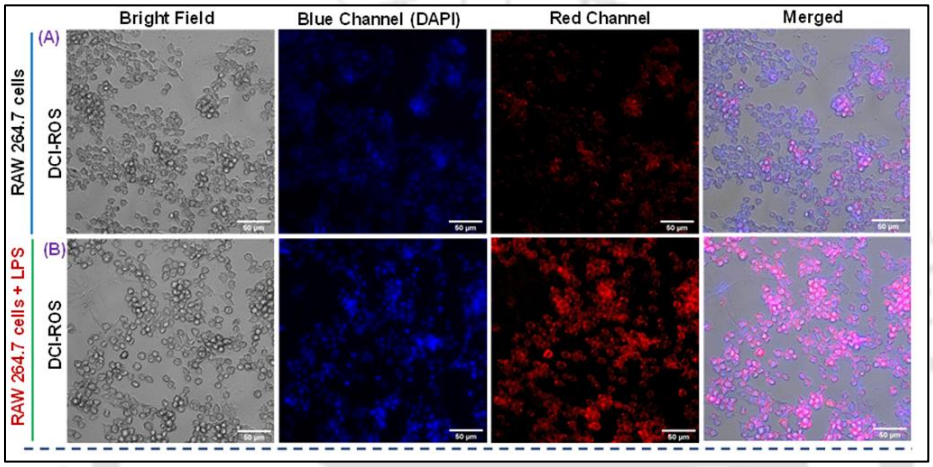

Figure 3.9. Fluorescence microscopy images (bright field, blue channel, red channel, and merged) of RAW 264.7 cells in the presence of **DCI-ROS** (50 µM) for (A) endogenous ROS-triggered and (B) LPS-induced ROS-triggered fluorogenic drug release. RAW 264.7 cells were pre-incubated with LPS (50 µg mL^{-1}) for 14 h to elevate the ROS level. DAPI (blue channel) was used for the nuclear staining of cells. Scale bar: 50 µm.

3.3.7. Anti-inflammatory activity of the DCI-ROS

The anti-inflammatory activity of the released drug **DCF** from the prodrug **DCI-ROS** was investigated in the macrophage cell line (RAW 264.7) using western blot analysis. The prodrug activation was enhanced by the increased intracellular ROS levels caused by the inflammation that was produced by pre-treating the cells with LPS (50 g/mL) for 14 h. The expression level of COX-2 was dramatically increased in the presence of LPS (Figure 3.10A). Upon the addition of **DCI-ROS** (50 and 100 µM) to the LPS-pretreated cells, the COX-2 level was measured after an incubation period of 24 h. A considerable down-regulation was observed in the presence of **DCI-ROS** dose-dependently. To verify the anti-inflammatory effect of the released **DCF** from prodrug **DCI-ROS**, a similar experiment was also conducted

TH-3161_176122050

on pure **DCF** (Figure 3.10B). Significantly, down-regulation of COX-2 was observed in the presence of pure **DCF**. These observations reveal the H_2O_2-triggered release of **DCF** from the prodrug **DCI-ROS** and its subsequent anti-inflammatory activity in the cellular medium.

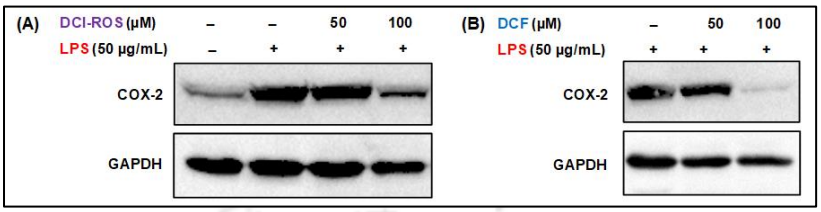

Figure 3.10. Anti-inflammatory activity of the prodrug **DCI-ROS** as well as the **DCF** in RAW 264.7 cells. Western blot analysis for COX-2 protein expression level in RAW 264.7 cells and the effect of (A) **DCI-ROS** (50 and 100 μM) and (B) pure **DCF** in the LPS (50 μg/mL) pre-treated cells. GAPDH was used as a housekeeping gene.

3.4. Conclusions

In summary, we described herein the design and synthesis of the H_2O_2-responsive turn-on fluorogenic prodrug **DCI-ROS** of diclofenac (**DCF**) with NIR fluorescence. Rapid reactivity of the boronate ester moiety in **DCI-ROS** with H_2O_2 activates the prodrug and sequential self-immolative processes control the drug release profile with simultaneous turn-on NIR fluorescence both in the aqueous and cellular medium. Turn-on fluorogenic process for the endogenous H_2O_2-induced activation of the non-toxic **DCI-ROS** in cancer cells and the inhibition of COX-2 level (anti-inflammatory activity) in the inflammation-induced macrophage cells validated the feasibility of fluorogenic drug release in the cellular medium. Therefore, the inflammatory stimuli H_2O_2-responsive controlled release of **DCF** with NIR fluorogenic emission from **DCI-ROS** would certainly be useful for the selective delivery of anti-inflammatory drugs with feasible non-invasive monitoring for the treatment of inflammatory diseases in the future.

3.5. Experimental section

3.5.1. Materials and methods

All the reagents were purchased either from Sigma Aldrich or from reputed local suppliers and used without further purification unless otherwise stated. Thin layer chromatographic (TLC) analyses were carried out on pre-coated silica gel on aluminum sheets and the compounds were visualized by irradiation with UV or fluorescent light. Organic solvents used for chromatographic separations were distilled before use. The melting point of the

TH-3161_176122050

synthesized compounds was recorded in a Büchi B540 melting point apparatus and the values are uncorrected. The NMR spectra (^{1}H and ^{13}C) were recorded on Bruker (400, 500, or 600 MHz) NMR spectrometers, and the chemical shifts are cited with respect to TMS (Me_4Si) as an internal standard. UV-Vis spectroscopic analyses were performed on a Lambda 45 UV-Vis spectrophotometer (PerkinElmer) and fluorescence emission spectra were recorded on a Fluoromax-4 spectrophotometer (FluoroMax-4 -Horiba). Mass spectra were obtained using an Agilent 6520 Accurate-Mass Quadrupole Time-of-Flight (Q-TOF) LC/MS spectrometer.

3.5.2. Synthesis of prodrugs DCI-ROS and DCI-Con

Synthesis of compound 3.2[28]

Compound **3.2** was synthesized following the reported procedure with a minor modification.[28] To a stirred solution of 4-bromotoluene (3.00 g, 17.54 mmol) in dry THF (80 mL) was added *n*-butyllithium solution (2.0 M in cyclohexane, 10.52 mL, 21.04 mmol) dropwise at -78 ºC under inert condition. After stirring for 30 min at the same condition, 2-isopropoxy-4,4,5,5-tetramethyl-1,3,2-dioxaborolane (4.23 g, 4.65 mL, 22.77 mmol) was added dropwise and the reaction was stirred at -78 °C for 2 h. The progress of the reaction was monitored by TLC analysis. Upon completion, the reaction was quenched with saturated NH_4Cl solution (20 mL) and water (10 mL) and the solution was allowed to attain room temperature. The biphasic mixture was extracted with pet. ether (3×50 mL). The combined organic layer was washed with brine solution (3×20 mL), dried over anhydrous sodium sulfate, and concentrated under reduced pressure to obtain the crude compound. The crude product was purified by flash chromatography using 100% pet. ether as a mobile phase to afford the pure product **3.2** as a white solid. R_f = 0.8 (100% pet. ether); Yield: 3.60 g (94%). ^{1}H NMR ($CDCl_3$, 600 MHz): δ (ppm) = 7.70 (d, J = 7.7 Hz, 2H), 7.18 (d, J = 7.6 Hz, 2H), 2.36 (s, 2H), 1.34 (s, 12H). ^{13}C NMR ($CDCl_3$, 150 MHz): δ (ppm) = 141.5, 134.9, 128.7, 83.8, 25.0, 21.9.

Synthesis of compound 3.3[36]

Compound **3.3** was synthesized following the reported procedure with a minor modification.[36] A mixture of compound **3.2** (2.20 g, 10.08 mmol), NBS (2.15 g, 12.10 mmol), and AIBN (0.16 g, 1.00 mmol) in dry acetonitrile (110 mL) was refluxed under inert condition for 3 h. The progress of the reaction was monitored by TLC analysis. Upon completion, the solvent was evaporated under reduced pressure. The reaction mixture was diluted with water

TH-3161_176122050

(30 mL) and the crude product was extracted with ethyl acetate (3×30 mL). The combined organic layer was washed with brine solution (3×20 mL) and dried over anhydrous sodium sulfate. The organic layer was concentrated under reduced pressure to afford the crude product, which was further purified by flash chromatography using ethyl acetate and pet. ether as eluents to afford compound **3.3** as a white solid. R_f = 0.6 (5% ethyl acetate in pet. ether); Yield: 2.60 g (88%). ^{1}H NMR ($CDCl_3$, 400 MHz): δ (ppm) = 7.78 (d, *J* = 8.0 Hz, 2H), 7.39 (d, *J* = 8.0 Hz, 2H), 4.49 (s, 2H), 1.34 (s, 12H). ^{13}C NMR ($CDCl_3$, 100 MHz): δ (ppm) = 140.8, 135.4, 128.5, 84.1, 33.5, 25.0.

Synthesis of compound 3.5[30]

Compound **3.5** was synthesized following the reported procedure with a minor modification.[30] To a stirred solution of isophorone **3.4** (3.00 g, 21.69 mmol) and malononitrile (2.16 g, 32.55 mmol) in dry ethanol (30 mL) was added piperidine (0.42 mL, 4.35 mmol) under inert atmosphere. Subsequently, glacial acetic acid (75 µL) was added to the reaction mixture and refluxed for 12 h. The progress of the reaction was monitored by TLC analysis. Upon completion of the reaction, the reaction mixture was cooled to room temperature, and the solvent was removed under reduced pressure. The crude product was purified by 60-120 mesh silica gel column chromatography using 30% DCM in pet. ether as the eluent to afford the pure product **3.5** as a white solid. R_f = 0.5 (50% DCM in pet. ether), Yield: 2.30 g (62%). ^{1}H NMR ($CDCl_3$, 600 MHz): δ (ppm) = 6.62 (s, 1H), 2.51 (s, 2H), 2.17 (s, 2H), 2.03 (s, 3H), 1.01 (s, 6H). ^{13}C NMR (DMSO-d_6, 150 MHz): δ (ppm) = 170.5, 159.9, 120.7, 113.3, 112.5, 78.3, 45.8, 42.7, 32.5, 27.9, 25.4.

Synthesis of DCI-OH[30]

The fluorophore **DCI-OH** was synthesized following the reported procedure with a minor modification.[30] To a stirred solution of 4-hydroxybenzaldehyde (0.53 g, 4.35 mmol) and compound **3.5** (0.90 g, 4.83 mmol) in dry acetonitrile (20 mL) was added piperidine (100 µL, 0.96 mmol) under inert atmosphere and the mixture was refluxed for 6 h. The progress of the reaction was monitored by TLC analysis. Upon completion, the solvent was evaporated under reduced pressure. The crude product was purified by neutral alumina column chromatography using 2% MeOH in DCM as eluent to afford the pure product **DCI-OH** as a reddish solid. R_f = 0.2 (100% DCM), Yield: 0.90 g (71%). ^{1}H NMR (DMSO-d_6, 600 MHz): δ (ppm) = 10.00 (s, 1H), 7.56 (d, *J* = 8.6 Hz, 2H), 7.22 (d, *J* = 7.8 Hz, 2H), 6.80 (m, 3H), 2.60

TH-3161_176122050

(s, 2H), 2.53 (s, 2H), 1.01 (s, 6H). ^{13}C NMR (DMSO-d_6, 150 MHz): δ (ppm) = 170.1, 159.3, 156.7, 138.3, 129.9, 127.1, 126.2, 121.4, 115.9, 114.1, 113.3, 74.8, 42.3, 38.2, 31.7, 27.4.

Synthesis of compound 3.7[31]

To a mixture of compound **3.6** (4.00 g, 23.78 mmol), TBDMSCl (8.70 g, 57.72 mmol) and imidazole (4.00 g, 58.76 mmol) was added dry DMF (10 mL) at 0 ºC under inert atmosphere. The reaction mixture was stirred at room temperature for 4 h. The progress of the reaction was monitored by TLC analysis. After completion of the reaction, the mixture was diluted with 150 mL of pet. ether and washed with water (5×20 mL) and saturated brine solution (2×20 mL). The organic layer was dried over anhydrous sodium sulfate and evaporated under reduced pressure to afford the crude product. The crude compound was purified by flash chromatography using 100% pet. ether to afford the pure product **3.7** as a colorless oil. R_f = 0.5 (100% pet. ether), Yield: 8.50 g (90%). ^{1}H NMR ($CDCl_3$, 600 MHz): δ (ppm) = 8.02 (s, 1H), 6.90 (s, 2H), 4.82 (s, 4H), 2.25 (s, 3H), 0.94 (s, 18H), 0.12 (s, 12H). ^{13}C NMR ($CDCl_3$, 150 MHz): δ (ppm) = 151.0, 128.4, 126.3, 125.9, 63.1, 26.0, 20.8, 18.5, -5.3.

Synthesis of compound 3.8[31]

The solution of compound **3.7** (5.00 g, 12.60 mmol) and K_2CO_3 (2.61 g, 18.90 mmol) in dry DMF (7 mL) was stirred at 0 ºC under an inert atmosphere. After 10 min, the solution of compound **3.3** (3.74 g, 12.60 mmol) in dry DMF (8 mL) was added to the solution in a dropwise manner. The reaction mixture was stirred at room temperature for 12 h. The progress of the reaction was monitored by the TLC study. Upon completion of the reaction, the reaction mixture was diluted with ethyl acetate (150 mL) and sequentially washed with water (3×10 mL) and brine (2×10 mL). The organic phase was dried over anhydrous sodium sulfate and evaporated under reduced pressure to afford the crude compound. The crude product was purified by flash chromatography using 100% pet. ether to afford the pure product as a colorless liquid. R_f = 0.5 (5% EtOAc in pet. ether), Yield: 6.5 g (84%). ^{1}H NMR ($CDCl_3$, 400 MHz): δ (ppm) = 7.83 (d, J = 8.5 Hz, 2H), 7.42 (d, J =7.7 Hz, 2H), 7.17 (s, 2H), 4.88 (s, 2H), 4.70 (s, 4H), 2.34 (s, 3H), 1.35 (s, 12 H), 0.91 (s, 18H), 0.06 (s, 12 H). ^{13}C NMR ($CDCl_3$, 100 MHz): δ (ppm) = 151.3, 140.9, 135.2, 133.9, 133.8, 128.0, 127.1, 83.9, 76.3, 60.5, 26.1, 25.0, 21.3, 18.6, -5.1.

Synthesis of compound 3.9[31]

TH-3161_176122050

The solution of compound **3.6** (2.00 g, 11.89 mmol) and K_2CO_3 (2.46 g, 17.84 mmol) in dry DMF (5 mL) was stirred at 0 ºC under an inert atmosphere. After 10 min, the benzyl bromide (2.42 g, 14.27 mmol) was added to the solution in a dropwise manner. The reaction mixture was stirred at room temperature for 12 h. The progress of the reaction was monitored by the TLC study. Upon completion of the reaction, the reaction mixture was diluted with ethyl acetate (100 mL) and sequentially washed with water (3×20 mL) and brine (2×20 mL). The organic phase was dried over anhydrous sodium sulfate and evaporated under reduced pressure to afford the crude compound. The crude product was purified by flash chromatography using 40% ethyl acetate in pet. ether to afford the pure product as a white solid. R_f = 0.5 (40% EtOAc in pet. ether), Yield: 2.50 g (81%). ^{1}H NMR ($CDCl_3$, 600 MHz) δ (ppm) = 7.45 (d, *J* = 7.1 Hz, 2H), 7.41 (t, *J* = 7.2 Hz, 2H), 7.37 (d, *J* = 7.1 Hz, 1H), 7.16 (s, 2H), 4.95 (s, 2H), 4.68 (d, *J* = 5.5 Hz, 4H), 2.33 (s, 3H), 1.97 (m, 2H). ^{13}C NMR ($CDCl_3$, 150 MHz): δ (ppm) = 152.8, 137.0, 134.6, 134.0, 129.8, 128.9, 128.6, 128.3, 77.0, 61.3, 21.0.

Synthesis of compound 3.10[31]

To a stirred solution of compound **3.8** (2.00 g, 3.26 mmol) in distilled MeOH (20 mL) was added *p*-TsOH (0.15 g, 0.82 mmol) under an inert atmosphere. The reaction mixture was stirred at room temperature overnight. Upon completion of the reaction, the solvent was evaporated under reduced pressure and diluted with water (20 mL). The crude compound was extracted with EtOAc (3×30 mL). The combined organic phase was washed with brine (2×10 mL), and dried over anhydrous sodium sulfate. The solvent was evaporated under reduced pressure to afford the crude compound, which was purified by flash chromatography using 50% EtOAc in pet. ether to afford the pure product **3.10** as a white solid. R_f= 0.5 (40% EtOAc in pet. ether), Yield: 1.10 g (88%). ^{1}H NMR ($CDCl_3$, 600 MHz): δ (ppm) = 7.83 (d, *J* = 7.8 Hz, 2H), 7.41 (d, *J* = 7.7 Hz, 2H), 7.14 (s, 2H), 4.92 (s, 2H), 4.64 (s, 4H), 2.31 (s, 3H), 1.35 (s, 12H). ^{13}C NMR ($CDCl_3$, 150 MHz) δ (ppm) = 152.6, 140.0, 135.3, 134.6, 133.9, 129.7, 127.3, 84.0, 76.9, 61.0, 25.0, 21.0.

Synthesis of compound 3.11[37]

To a stirred solution of compound **3.9** (2.00 g, 7.76 mmol) in dry DCM (40 mL) was added PBr_3 (3.70 mL, 38.80 mmol) in a dropwise manner at 0 ºC under inert condition and the mixture was stirred at room temperature for 12 h. The progress of the reaction was monitored by TLC analysis. Upon completion, the reaction was quenched with water at 0 ºC and the

TH-3161_176122050

crude product was extracted with DCM (3×30 mL). The combined organic phase was washed with brine (3×30 mL) and dried over anhydrous sodium sulfate. The solvent was evaporated under reduced pressure to obtain the crude compound, which was purified by flash chromatography using 5% EtOAc in pet. ether to afford the pure product **3.11** as a white solid. R_f = 0.5 (5% EtOAc in pet. ether), Yield: 2.00 g (70%). ^{1}H NMR ($CDCl_3$, 500 MHz): δ (ppm) = 7.54 (d, *J* = 6.9 Hz, 2H), 7.43 (t, *J* = 7.3 Hz, 2H), 7.38 (t, *J* = 7.3 Hz, 1H), 7.20 (s, 2H), 5.16 (s, 2H), 4.52 (s, 4H), 2.32 (s, 3H). ^{13}C NMR ($CDCl_3$, 125 MHz): δ (ppm) = 153.2, 137.0, 135.0, 133.0, 132.0, 128.8, 128.5, 128.2, 77.4, 76.3, 28.1, 20.8.

Synthesis of compound 3.12[37]

To a stirred solution of compound **3.10** (2.00 g, 5.20 mmol) in dry DCM (40 mL) was added PBr_3 (2.50 mL, 26.00 mmol) in a dropwise manner at 0 ºC under inert condition and the reaction mixture was stirred at room temperature for 5 h. The progress of the reaction was monitored by TLC analysis. Upon completion, the reaction was quenched with water at 0 ºC and the crude product was extracted with DCM (3×30 mL). The combined organic phase was washed with brine (3×30 mL), and dried over anhydrous sodium sulfate. The solvent was evaporated under reduced pressure to obtain the crude compound. The crude product was purified by flash chromatography using 5% EtOAc in pet. ether to afford the pure product **3.12** as a white solid. R_f = 0.5 (5% EtOAc in pet. ether), Yield: 2.00 g (75%). ^{1}H NMR ($CDCl_3$, 600 MHz) δ (ppm) = 7.87 (d, *J* = 7.8 Hz, 2H), 7.53 (d, *J* = 7.8 Hz, 2H), 7.20 (s, 2H), 5.18 (s, 2H), 4.50 (s, 2H), 2.32 (s, 3H), 1.36 (s, 12H). ^{13}C NMR ($CDCl_3$, 150 MHz) δ (ppm) = 153.1, 140.0, 135.3, 135.0, 133.0, 131.9, 127.1, 84.0, 76.1 28.1, 25.0, 20.8; ESI-MS *m/z* calcd. for $C_{22}H_{31}BBr_2NO_3$ $[M+NH_4]^+$ = 528.0743, observed. 528.0745.

Synthesis of compound 3.13

To a stirred solution of compound **3.11** (0.90 g, 2.45 mmol) in dry acetonitrile (40 mL) was added the solution of diclofenac (0.72 g, 2.45 mmol) and DIPEA (1.27 mL, 7.33 mmol) in dry acetonitrile (10 mL) at ice-cold condition under argon atmosphere. The reaction mixture was stirred at room temperature overnight. Upon completion of the reaction, the solvent was evaporated under reduced pressure and diluted with DCM (50 mL). The reaction mixture was washed sequentially with water (3×10 mL) and brine (2×20 mL). The combined organic phase was dried over anhydrous sodium sulfate and the solvent was evaporated under reduced pressure to afford the crude compound. The compound was purified by flash chromatography

TH-3161_176122050

using 8% EtOAc in pet. ether as the eluent to afford the pure product **3.13** as a white solid. R_f = 0.4 (5% EtOAc in pet. ether), Yield: 0.70 g (47%). ^{1}H NMR ($CDCl_3$, 600 MHz): δ (ppm) = 7.41 (t, *J* = 7.6 Hz, 2H), 7.35 (t, *J* = 7.3 Hz, 2H), 7.31 (d, *J* = 8.1 Hz, 2H), 7.21 (m, 2H), 7.12 -7.06 (m, 2H), 6.95 (t, *J* =8.1 Hz, 3H), 6.91 (t, *J* = 7.4 Hz, 1H), 6.79 (s, 1H), 6.53 (d, *J* = 8.0 Hz, 1H), 5.21 (d, *J* = 3.2 Hz, 2H), 4.98 (s, 2H), 4.51 (s, 2H), 3.83 (s, 2H), 2.26 (s, 3H). ^{13}C NMR ($CDCl_3$, 150 MHz): δ (ppm) = 172.2, 153.5, 142.8, 137.9, 136.8, 134.7, 132.7, 132.0, 131.6, 131.0, 129.6, 129.4, 128.9, 128.7, 128.4, 128.2, 128.0, 124.3, 124.1, 122.2, 118.5, 76.8, 62.4, 38.7, 28.1, 20.8.

Synthesis of compound 3.14

To a stirred solution of compound **3.12** (0.65 g, 1.27 mmol) in dry acetonitrile (10 mL) was added a solution of diclofenac (0.38 g, 1.27 mmol) and DIPEA (0.6 mL, 3.82 mmol) in dry acetonitrile (5 mL) dropwise at 0 ºC under argon atmosphere. The reaction mixture was stirred at room temperature overnight. Upon completion of the reaction, the solvent was evaporated under reduced pressure and diluted with DCM (50 mL). The reaction mixture was then washed with water (3×10 mL) and brine (2×10 mL). The combined organic phase was dried over anhydrous sodium sulfate and the solvent was evaporated under reduced pressure to afford the crude compound, which was purified by silica gel column chromatography using 5% EtOAc in pet. ether as the eluent to afford the pure product **3.14** as a white solid. R_f = 0.5 (10% EtOAc in pet. ether), Yield: 0.40 g (43%). ^{1}H NMR ($CDCl_3$, 600 MHz) δ (ppm) = 7.81 (d, *J* = 7.6 Hz, 2H), 7.41 (d, *J* = 7.7 Hz, 2H), 7.31 (d, *J* = 8.1 Hz, 2H), 7.19 (d, *J* = 9.8 Hz, 2H), 7.09 (t, *J* = 7.7 Hz, 1H), 7.07 (s, 1H), 6.96 (t, *J* = 8.1 Hz, 1H), 6.92 (t, *J* = 7.4 Hz, 1H), 6.78 (s, 1H), 6.53 (d, *J* = 8.0 Hz, 1H), 5.21 (s, 2H), 4.99 (s, 2H), 4.48 (s, 2H), 3.83 (s, 2H), 2.26 (s, 3H), 1.35 (s, 12H). ^{13}C NMR ($CDCl_3$, 150 MHz) δ (ppm) = 172.0, 153.6 142.8, 139.9, 137.9, 135.2, 134.7, 132.7, 132.0, 131.6, 131.0, 129.6, 129.4, 128.9, 128.2, 127.0, 124.3, 124.1, 122.3, 118.5, 83.9, 76.7, 62.4, 38.8, 28.1, 25.0, 20.8; ESI-MS *m/z* calcd. for $C_{36}H_{39}BBrCl_2LiNO_6$ $[M+Li+H_2O]^+$ = 748.1591, observed = 748.1608.

Synthesis of DCI-Con

The mixture of compound **3.13** (0.50 g, 0.83 mmol), **DCI-OH** (0.29 g, 1.00 mmol), and K_2CO_3 (0.17 g, 1.25 mmol) in acetone (2 mL) was stirred at 55 ºC for 4 h. Progress of the reaction was monitored by TLC analysis. Upon completion of the reaction, the solvent was evaporated under reduced pressure, diluted with EtOAc (30 mL), and washed with water

TH-3161_176122050

(3×10 mL). The organic phase was washed with brine (2×10 mL) and dried over anhydrous sodium sulfate. The solvent was evaporated under reduced pressure to obtain the crude compound, which was further purified by flash chromatography with 100% DCM to obtain the pure product **DCI-Con** as red solid. R_f = 0.5 (15% EtOAc in pet. ether), Yield: 0.40 g (59%). M.P. = 73-75 ºC. ^{1}H NMR ($CDCl_3$, 600 MHz): δ (ppm) = 7.44 (d, *J* = 8.6 Hz, 2H), 7.32 (d, *J* =8.1 Hz, 2H), 7.28 (d, *J* = 8.1 Hz, 6H), 7.21 (d, *J* = 7.2 Hz, 1H), 7.14 (s, 1H), 7.10 (t, *J* = 7.6 Hz, 1H), 7.02 (d, *J* = 16.0 Hz, 1H), 6.98 (t, *J* = 8.1 Hz, 1H), 6.95-6.91(m, 3H), 6.88 (t, *J* = 14.5 Hz, 1H), 6.81 (s, 2H), 6.54 (d, *J* = 8.0 Hz, 2H), 5.25 (s, 2H), 5.01 (s, 2H), 4.88 (s. 2H), 3.85 (s, 2H), 2.59 (s, 2H), 2.46 (s, 2H), 2.29 (s, 3H), 1.08 (s, 6H). ^{13}C NMR ($CDCl_3$, 125 MHz): δ (ppm) = 172.2, 169.4, 160.1, 154.4, 153.7, 142.8, 137.9, 136.9, 136.8, 134.5, 131.6, 131.2, 131.0, 129.9, 129.6, 129.4, 129.1, 128.9, 128.7, 128.4, 128.2, 128.1, 127.3, 124.3, 124.1, 122.9, 122.2, 118.5, 115.4, 77.9, 77.8, 65.5, 62.5, 43.1, 39.4, 38.8, 32.2, 28.2, 20.9. ESI-MS *m/z* calcd. for $C_{49}H_{47}Cl_2N_4O_4$ $[M+NH_4]^+$ = 825.2974, observed = 825.2856.

Synthesis of compound DCI-ROS

The mixture of compound **3.14** (0.28 g, 0.39 mmol), **DCI-OH** (0.09 g, 0.31 mmol), and K_2CO_3 (0.05 g, 0.39 mmol) was dissolved in acetone (2 mL) under an inert atmosphere and stirred at 55 ºC for 4 h. Progress of the reaction was monitored by TLC analysis. Upon completion of the reaction, the solvent was evaporated under reduced pressure and diluted with EtOAc (50 mL), and washed with water (3×10 mL). The combined organic phase was washed with brine (2×10 mL) and dried over anhydrous sodium sulfate. The solvent was evaporated under reduced pressure to obtain the crude compound, which was further purified by flash chromatography with 25% EtOAc in pet. ether to obtain the pure product **DCI-ROS** as red solid. R_f = 0.5 (20% EtOAc in pet. ether), Yield: 0.14 g (50%). M.P. = 92-94 ºC. ^{1}H NMR ($CDCl_3$, 600 MHz): δ (ppm) = 7.74 (d, *J* = 7.8 Hz, 2H), 7.43 (d, *J* =8.6 Hz, 2H), 7.32 (d, *J* =8.1 Hz, 2H), 7.28 (d, *J* = 7.7 Hz, 2H), 7.20 (d, *J* = 7.5 Hz, 1H), 7.13 (s, 1H), 7.10 (t, *J* = 7.6 Hz, 1H), 7.01 (d, *J* = 16.0 Hz, 1H), 6.97 (t, *J* = 8.1 Hz, 1H), 6.95-6.85 (m, 4H), 6.80 (s, 2H), 6.54(d, *J* = 8.0 Hz, 1H), (5.26 (s, 2H), 4.97 (s, 2H), 4.88 (s. 2H), 3.85 (s, 2H), 2.60 (s, 2H), 2.46 (s, 2H), 2.28 (s, 3H), 1.34 (s, 12 H), 1.08 (s, 6H). ^{13}C NMR ($CDCl_3$, 150 MHz): δ (ppm) = 172.1, 169.4, 160.2, 154.5, 153.7, 142.8, 139.9, 137.9, 137.0, 135.2, 134.6, 131.6, 131.2, 131.0, 129.9, 129.6, 129.4, 129.1, 129.0, 128.8, 128.2, 127.3, 127.2, 124.4, 124.1,

TH-3161_176122050

122.9, 122.3, 118.5, 115.4, 113.9, 113.1, 84.0, 77.9, 77.6, 65.4, 62.5, 43.1, 39.4, 38.8, 32.2, 28.2, 25.0, 20.9. ESI-MS *m/z* calcd. for $C_{55}H_{54}BCl_2LiN_3O_6$ $[M+Li]^+$ = 940.3642, observed = 940.3642.

3.5.3. UV-Vis and fluorescence spectroscopic studies

All the stock solutions of prodrugs and the released fluorophore were prepared in spectroscopy grade DMSO and the stock solution of H_2O_2 was prepared in Milli-Q water. The pronounced absorption band at 550 nm and the emission in the NIR range (λ_{em} = 670 nm) of **DCI-OH** was observed in PBS buffer (20 mM, pH 7.5) in the presence of 50% DMSO.[38] Therefore, the absorption and emission spectra of the released fluorophore **DCI-OH** were collected in PBS with the added DMSO just before the measurements. Samples for absorption and emission spectroscopic measurements were carried out in quartz cuvettes (1.0 mL). The fluorescence emission spectroscopic studies used excitation wavelength (λ_{ex}) = 550 nm and emission range (λ_{em}) = 670-750 nm with slit width = 10/10 nm.

3.5.4. Analyte selectivity and pH variation studies

Analyte selectivity of the prodrug **DCI-ROS** (10 μM) was studied by measuring the emission intensity of the released fluorophore **DCI-OH** upon the incubation of the prodrug **DCI-ROS** (10 μM) with different bio-analytes (200 μM) in phosphate buffer saline (PBS) (20 mM, pH 7.5) with 50% DMSO after incubating for 14 h. For the pH variation study, the emission intensity from **DCI-ROS** (10 μM) was measured in the presence or absence of H_2O_2 (200 μM) with variable pH of the medium (pH: 5-11) in PBS (50% DMSO v/v, 14 h). Control reactions with the prodrug in the absence of H_2O_2 were studied under the identical reaction condition to understand the stability of the prodrugs at different pH ranges.

3.5.5. Measurements of reaction kinetics by HPLC analysis

The purity of the synthesized prodrugs **DCI-ROS** and **DCI-Con** along with **DCF** and the released fluorophore **DCI-OH** were analyzed using analytical high-performance liquid chromatography (HPLC) Agilent 1220 infinity II LC system using a reverse-phase C_{18} column (Luna®, 150 × 4.6 mm, 5 μm). HPLC grade acetonitrile and water (Finar Ltd) were used as mobile phase and the absorbance profile of compounds was detected by PDA detector at wavelengths of 230, 254, 280, and 430 nm (as applicable). The samples were prepared in acetonitrile and were injected into the HPLC system using the in-built autosampler at a flow

TH-3161_176122050

rate of 1.0 mL/min using acetonitrile/water system as a mobile phase for 25 min (0-7 min: 75%-99% acetonitrile in water; 7-15 min: 99% acetonitrile in water; 15-20 min: 99%-75% acetonitrile in water; 20-25 min: 75% acetonitrile in water). The reaction of **DCI-ROS** (100 µM) or **DCI-Con** (100 µM) with H_2O_2 (2 mM) and sodium bicarbonate (500 µM) was prepared in acetonitrile/water system (60:40). The peaks due to the analytes, prodrugs, reaction intermediates and the released drug and fluorophore were analyzed/identified at different wavelengths (230, 280 and 430 nm) as applicable at various time intervals.

3.5.6. Cell culture

The triple-negative breast cancer (TNBC) cells (MDA-MB-231) and a macrophage-like, Abelson leukemia virus-transformed cell line (derived from BALB/c mice) (RAW 264.7) were obtained from the National Centre for Cell Science (NCCS), Pune, India. The cells were cultured in DMEM medium (Gibco) supplemented with 10% (v/v) FBS (Gibco) and 1% Pen-Strep (Gibco). Cells were cultured as a monolayer in a humidified incubator at 37 °C in the presence of a 5% CO_2 level.

3.5.7. Cell viability assay

The synthesized prodrug **DCI-ROS** and the drug **DCF** were screened for their anti-proliferative activities using the conventional MTT assay. MDA-MB- 231 cells and RAW 264.7 cells were seeded separately in 96-well culture plates at a density of 2×10^4 cells /100 µL/well and 1×10^4 cells /100 µL/well, respectively. Cells were treated with the freshly prepared test compounds **DCI-ROS** and **DCF** (10, 25, 50, and 100 µM) for 0 h (control) and 48 h (experimental), respectively. At the end of the treatment period, 10 µL of 5.0 mg/mL of MTT was added to the plate (control) and incubated for 4 h. Following the 4 h incubation, the reagent from the plate was removed and the purple formazan crystals were dissolved using 100 µL of DMSO (Avra Synthesis Pvt Ltd) and the absorbance at 570 nm was measured using a microplate reader (Thermo Scientific™ Multiskan™ GO microplate reader). In the experimental set, a similar MTT treatment protocol was followed only after 48 h. The mean ΔOD values were calculated by the subtraction of mean OD values of 0 h plate (control) from the mean OD values of identical wells at 48 h plate (experimental) and the percentage proliferation was calculated keeping the mean ΔOD of untreated control as 100%.

3.5.8. Fluorescence microscopic studies

TH-3161_176122050

MDA-MB-231 cells and RAW 264.7 cells were separately cultured in high glucose Dulbecco's modified Eagle's medium (DMEM) supplemented with 10% fetal bovine serum (FBS) and 1% penicillin/streptomycin at 37 °C in the incubator under 5% CO_2 atmosphere. MDA-MB-231 cells (3.0×10^4 cells/plate) and RAW 264.7 cells (2.0×10^4 cells/plate) were then plated in 35 mm cell culture Petri dishes containing 2.0 mL of DMEM and incubated at 37 °C under 5% CO_2 for 24 h. The confluent cells (MDA-MB-231, RAW 264.7) were washed with DPBS and finally incubated with **DCI-ROS** (50.0 μM) at 37 °C under 5% CO_2 for 5 h. After washing with DPBS (3 times), cellular morphology was carefully observed and imaged in a Bio-Rad ZOE^{TM} fluorescent cell imager under a bright field and red fluorescent emission filter. A negative control experiment was performed upon the pre-treatment of cells with *N*-acetyl cysteine (NAC, 2 mM) for 2 h to quench the endogenous ROS. After the pre-treatment, cells were washed with DPBS (3 times) and finally, the cells were incubated with **DCI-ROS** (50.0 μM) at 37 °C under 5% CO_2 for 5 h. The treated cells were finally washed with DPBS (3 times) and imaged in a Bio-Rad ZOE^{TM} fluorescent cell imager under a bright field and red fluorescent emission filter.

3.5.9. Western blot analysis

To estimate the COX-2 expression upon the release of the **DCF** from the prodrug **DCI-ROS**, an immunoblotting experiment was performed. RAW 264.7 cells (5×10^5 cells per 10 mL) were plated in a 60 mm cell culture dish and cultured in high glucose Dulbecco's modified Eagle's medium (DMEM) supplemented with 10% fetal bovine serum (FBS) and 1% penicillin/streptomycin at 37 °C in the incubator under 5% CO_2 atmosphere. The overexpression of COX-2 level in RAW 264.7 cells was induced upon the pre-treatment with LPS (50 μg/mL, 14 h). After the treatment, cells were washed with DPBS (3 times) and further treated with compound **DCI-ROS** and **DCF** (50.0 and 100.0 μM) and incubated for 24 h under a 5% CO_2 atmosphere. After completion of the treatment, cells were washed with cold PBS (1X) and the protein extraction was performed. The whole cell protein was extracted using RIPA cell lysis buffer (150 mM of NaCl, 1% (v/v) NP-40, 0.5% sodium deoxycholate, 0.1% SDS, 25 mM of Tris, 10 mg/mL of PMSF). An equal volume of protein was loaded and separated on 12% sodium dodecyl sulfate (SDS)–polyacrylamide gel by electrophoresis and transferred to a nitrocellulose membrane. Protein transfer was confirmed by Ponceau-S (HiMedia) staining. The blots were blocked with 5% non-fat dry milk in 1X

TH-3161_176122050

TBST buffer for 1 h at room temperature. Finally, the primary antibody (1:5000) specific for COX-2 (Cell Signalling, D5H5) and GAPDH (Cell Signalling, 14C10) were incubated overnight at 4 °C. Following the primary antibody incubation, the blots were washed with TBST (1X) buffer and incubated with HRP-conjugated secondary antibodies (Abcam) for 1 h and developed with an ECL Detect Kit (Bio-Rad) and imaged using ChemiDoc™ XRS System (Bio-Rad). The housekeeping gene GAPDH was used as a loading control.

3.6. References

1. M. F. Singgih, H. Achmad, B. I. Sukmana, A. B. Carmelita, A. P. Putra, S. Ramadhany and A. P. Putri, *Syst. Rev. Pharm.*, 2020, **11**, 293-298.
2. R. N. DuBois, S. B. Abramson, L. Crofford, R. A. Gupta, L. S. Simon, L. B. A. van de Putte and P. E. Lipsky, *FASEB J.*, 1998, **12**, 1063-1073.
3. A. M. Qandil, *Int. J. Mol. Sci.*, 2012, **13**, 17244-17274.
4. L. Li, G. Rossoni, A. Sparatore, L. C. Lee, P. Del Soldato and P. K. Moore, *Free Radic. Biol. Med.*, 2007, **42**, 706-719.
5. M. Chattopadhyay, R. Kodela, N. Nath, Y. M. Dastagirzada, C. A. Velázquez-Martínez, D. Boring and K. Kashfi, *Biochem. Pharmacol.* , 2012, **83**, 715-722.
6. M. V. Chan and J. L. Wallace, *Am. J. Physiol. Gastrointest. Liver Physiol.*, 2013, **305**, G467-G473.
7. Z. Liu, B. Zhang, S. Xia, L. Fang and S. Gou, *Eur. J. Med. Chem.*, 2021, **212**, 112997.
8. S. Dreve, I. Kacso, I. Bratu and E. Indrea, *J. Phys. Conf. Ser.*, 2009, **182**, 012065.
9. Y. Ma, J. Zhou, Z. Miao, H. Qian and Z. Zha, *ACS Appl. Bio Mater.*, 2019, **2**, 848-855.
10. H. Al-Lawati, Z. Binkhathlan and A. Lavasanifar, *Eur. J. Pharm. Biopharm.*, 2019, **142**, 179-194.
11. S. Thakur, B. Riyaz, A. Patil, A. Kaur, B. Kapoor and V. Mishra, *Biomed. Pharmacother*, 2018, **106**, 1011-1023.
12. D. Wu, A. C. Sedgwick, T. Gunnlaugsson, E. U. Akkaya, J. Yoon and T. D. James, *Chem. Soc. Rev.*, 2017, **46**, 7105-7123.
13. A. E. Albers, V. S. Okreglak and C. J. Chang, *J. Am. Chem. Soc.*, 2006, **128**, 9640-9641.

TH-3161_176122050

14. M. C. Y. Chang, A. Pralle, E. Y. Isacoff and C. J. Chang, *J. Am. Chem. Soc.*, 2004, **126**, 15392-15393.
15. A. Sufian, D. Bhattacherjee, T. Mishra and K. P. Bhabak, *Dyes Pigm.*, 2021, **191**, 109363.
16. E.-J. Kim, S. Bhuniya, H. Lee, H. M. Kim, C. Cheong, S. Maiti, K. S. Hong and J. S. Kim, *J. Am. Chem. Soc.*, 2014, **136**, 13888-13894.
17. W. Chen, Y. Cheng and B. Wang, *Angew Chem. Int. Ed.*, 2012, **51**, 5293-5295.
18. J. Peiró Cadahía, V. Previtali, N. S. Troelsen and M. H. Clausen, *MedChemComm*, 2019, **10**, 1531-1549.
19. E.-J. Kim, S. Bhuniya, H. Lee, H. M. Kim, C. Cheong, S. Maiti, K. S. Hong and J. S. Kim, *J. Am. Chem. Soc.*, 2014, **136**, 13888-13894.
20. R. Kumar, J. Han, H.-J. Lim, W. X. Ren, J.-Y. Lim, J.-H. Kim and J. S. Kim, *J. Am. Chem. Soc.*, 2014, **136**, 17836-17843.
21. W. Xia, S. Zhang, Y. Li, J. Fan, B. Liu, L. Wang and X. Peng, *Dyes Pigm.*, 2021, **190**, 109326.
22. W. Y. Kim, M. Won, S. Koo, X. Zhang and J. S. Kim, *Nano-Micro Lett.*, 2021, **13**, 168.
23. J. A. Mitchell, P. Akarasereenont, C. Thiemermann, R. J. Flower and J. R. Vane, *Proc. Natl. Acad. Sci. USA*, 1993, **90**, 11693-11697.
24. R. M. Haley and H. A. von Recum, *Expt. Biol. Med.*, 2019, **244**, 433-444.
25. W. Badri, K. Miladi, Q. A. Nazari, H. Greige-Gerges, H. Fessi and A. Elaissari, *Int. J. Pharm.*, 2016, **515**, 757-773.
26. L. Yuan, W. Lin, S. Zhao, W. Gao, B. Chen, L. He and S. Zhu, *J. Am. Chem. Soc.*, 2012, **134**, 13510-13523.
27. X. Liang, L. Zhang, B. Shi, H. Chang, D. Qiao, T. Shen, W. Zhao, Z. Yin and L. Shang, *Talanta*, 2020, **220**, 121433.
28. D. C. Ebner, J. T. Bagdanoff, E. M. Ferreira, R. M. McFadden, D. D. Caspi, R. M. Trend and B. M. Stoltz, *Chem. Eur. J.*, 2009, **15**, 12978-12992.
29. W. Zhai, B. M. Chapin, A. Yoshizawa, H.-C. Wang, S. A. Hodge, T. D. James, E. V. Anslyn and J. S. Fossey, *Org. Chem. Front.*, 2016, **3**, 918-928.

TH-3161_176122050

30. M. Yang, J. Fan, W. Sun, J. Du, S. Long, K. Shao and X. Peng, *Chem. Commun.*, 2019, **55**, 8583-8586.
31. S. Wu, S. Y. Tan, C. Y. Ang, Z. Luo and Y. Zhao, *Chem. Commun.*, 2016, **52**, 3508-3511.
32. B. Perillo, M. Di Donato, A. Pezone, E. Di Zazzo, P. Giovannelli, G. Galasso, G. Castoria and A. Migliaccio, *Exp. Mol. Med.*, 2020, **52**, 192-203.
33. P. Wang, J. Geng, J. Gao, H. Zhao, J. Li, Y. Shi, B. Yang, C. Xiao, Y. Linghu, X. Sun, X. Chen, L. Hong, F. Qin, X. Li, J.-S. Yu, H. You, Z. Yuan, D. Zhou, R. L. Johnson and L. Chen, *Nat. Commun.*, 2019, **10**, 755.
34. B. Krishnamachary, I. Stasinopoulos, S. Kakkad, M.-F. Penet, D. Jacob, F. Wildes, Y. Mironchik, A. P. Pathak, M. Solaiyappan and Z. M. Bhujwalla, *Oncotarget*, 2017, **8**.
35. T. L. Larkins, M. Nowell, S. Singh and G. L. Sanford, *BMC Cancer*, 2006, **6**, 181.
36. W. Zhai, B. M. Chapin, A. Yoshizawa, H.-C. Wang, S. A. Hodge, T. D. James, E. V. Anslyn and J. S. Fossey, *Org. Chem. Front.*, 2016, **3**, 918-928.
37. A. Kastrati and C. G. Bochet, *J. Org. Chem.*, 2019, **84**, 7776-7785.
38. K. Wang, C.-X. Zhao, T.-H. Leng, C.-Y. Wang, Y.-X. Lu, Y.-J. Shen and W.-H. Zhu, *Dyes Pigm.*, 2018, **151**, 194-201.

TH-3161_176122050

Peroxide-activatable turn-on fluorogenic prodrug of diclofenac: adjuvant drug delivery with hydrogen sulfide

TH-3161_176122050

TH-3161_176122050

4.1. Introduction

Examples of the literature reported ROS-responsive prodrugs of non-steroidal anti-inflammatory drugs are described in chapter 3. The prodrug **DCI-ROS** was designed in overcoming the limitations of diclofenac (NSAID) by making it anti-inflammatory site-selective and to improve the bioavailability by releasing the drug in a sustainable manner. However, the side-effects (GI damage, renal and ulcer) of non-selective COX inhibitors could be overcome by delivering the H_2S along with the NSAID (diclofenac). The importance of H_2S with NSAID delivery was described in chapter 1, and observed that GI damage is reduced significantly by the co-delivery of H_2S with NSAID. However, in most of the reports, modified NSAIDs were delivered instead of the active drugs due to the absence of triggering units in the hybrids. In addition, all the prodrugs were non-fluorogenic in nature and therefore, it was not feasible to monitor the release of the drug and H_2S in living cells. Therefore, the peroxide-responsive turn-on fluorogenic prodrug strategies exhibit more advantages over the non-stimuli-responsive and non-fluorogenic prodrugs. The peroxide-triggered prodrug strategy by coupling aryl boronic acid/ester moiety with the prodrug is the most widely used strategy for the targeted delivery over other stimuli-responsive prodrug strategies.[1-6] Owing to the higher level of ROS in inflammatory sites over normal tissues,[7] peroxide-responsive drug delivery systems could be more advantageous for the delivery of anti-inflammatory drugs (NSAIDs) selectively to inflammatory sites with minimized side-effects and higher anti-inflammatory properties. Among all the non-selective COX inhibitors (except the coxib family), diclofenac is more selective towards COX-2 over COX-1. However, it has several limitations, including a short half-life, GI toxicity, ulcer, etc.[8] Owing to the shorter plasma half-life of diclofenac (**DCF**), the sustained release strategy can be adopted in the prodrug using self-immolative linkers. Moreover, use of an NIR fluorophore would be advantageous for the minimum interferences/photo-damages from bio-molecules.[9, 10] Herein, we report for the first time that partially COX-2 selective NSAIDs can be delivered more selectively into the inflammatory sites over normal tissues in a sustained manner using inflammation marker (ROS) as a trigger. The drug release profile could also be conveniently monitored in real-time using the non-invasive turn-on fluorescence technique. Moreover, the produced H_2S from the prodrug may reduce the side-effects of **DCF** and enhance the anti-inflammatory activity.

TH-3161_176122050

4.2. Outline of the chapter

Herein, a peroxide-triggered turn-on fluorogenic prodrug **DCF-HS** was developed for a sustained and simultaneous release of both diclofenac (**DCF**) and H_2S. A convenient monitoring of the drug release profiles could be achieved by following the turn-on fluorogenic response from the NIR fluorophore **DCI-NH$_2$** (Figure 4.1). The fluorophore in the prodrug **DCF-HS** was connected *via* thiocarbamate linker as a source of COS, which further metabolize into H_2S in the presence of carbonic anhydrase (CA) enzyme. A negative control prodrug **DCF-Con** was also designed by connecting the fluorophore *via* a carbamate linker. Upon the activation by ROS, the prodrug would release the drug **DCF** and the fluorophore **DCI-NH$_2$**, however, without any COS/H_2S.

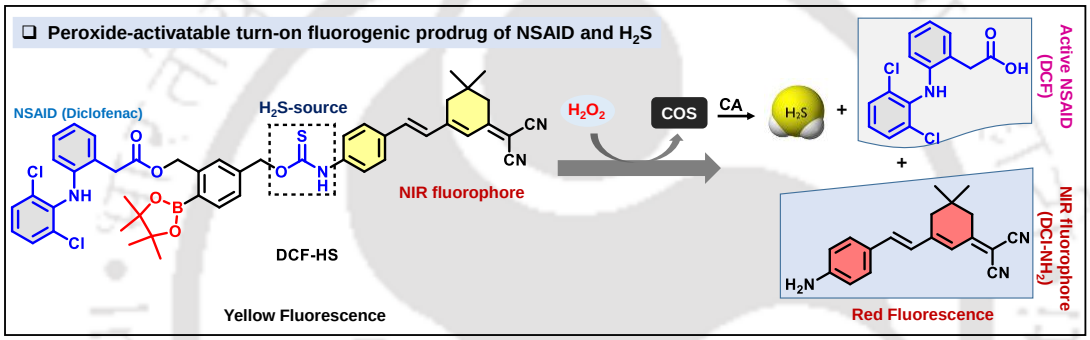

Figure 4.1. Schematic representation of the rationally designed peroxide-responsive prodrug of diclofenac and H_2S (**DCF-HS**).

Upon the synthesis of prodrugs **DCF-HS** and **DCF-Con**, they were purified and characterized by the spectroscopic and cellular studies. Spectroscopic studies (UV-Vis and fluorescence) with **DCF-HS** in the presence of H_2O_2 indicated the release of fluorophore **DCI-NH$_2$** along with the sustained release of the drug **DCF** under the physiological condition (Figure 4.2E). In addition, the prodrug **DCF-HS** was found to be selective towards H_2O_2 over other relevant bio-analytes. Furthermore, the release of fluorophore **DCI-NH$_2$** and drug **DCF** was confirmed using reverse phase HPLC method. Upon confirming the release of the fluorophore and drug from the prodrug **DCF-HS** in the aqueous medium, the fluorescence turn-on process was investigated in cellular media. Interestingly, the prodrug **DCF-HS** was found to be non-toxic in cancer cells (HeLa), normal cells (HEK-293), and macrophage cells (RAW 264.7) upto 100 µM concentration, indicating the biocompatibility of the prodrug (Figure 4.6A). As the prodrug was non-toxic, the release of the NIR fluorophore **DCI-NH$_2$** was confirmed in HeLa cells with red emission in the presence of endogenous ROS (Figure

TH-3161_176122050

4.6B). The release of H_2S from the prodrug **DCF-HS** was investigated in HeLa cells using H_2S-selective probe **WSP2**. Interestingly, the blue emission of umbelliferone from the probe **WSP2** indicated the release of H_2S from the prodrug **DCF-HS**. The anti-inflammatory activity of the **DCF-HS** and the parent drug **DCF** was investigated in the macrophage cells using western blot analysis. Interestingly, the results indicated that **DCF-HS** inhibited COX-2 in a dose dependent manner as the parent drug **DCF**, which indicated the release of active drug from the prodrug **DCF-HS** in the presence of endogenous ROS.

4.3. Results and Discussion

4.3.1. Synthesis of the prodrugs DCF-HS and DCF-Con

The designed prodrug **DCF-HS** and a control prodrug **DCF-Con** were synthesized following the multistep organic synthesis (Scheme 4.1). First, the **DCI-NCS** was synthesized starting from compound **4.1**. The condensation of **4.1** with malononitrile in the presence of piperidine produced compound **4.2**, which was further condensed with 4-nitrobenzaldehyde to obtain compound **4.3** with a good yield. The NIR fluorophore **DCI-NH_2** was synthesized from compound **4.3** by reducing with tin(II) chloride and HCl. The fluorophore **DCI-NH_2** was further converted into **DCI-NCS** in the presence of carbon disulfide and trimethylamine, followed by the addition of *p*-toluene sulfonyl chloride (Scheme 4.1A). In another component, the boronate ester group was installed on the phenyl ring of compound **4.4** (compound **4.5**) following the Suzuki-Miyaura coupling reaction in the presence of $Pd(PPh_3)_2Cl_2$ catalyst (Scheme 4.1B). Compound **4.5** was subsequently reacted with NBS in the presence of AIBN radical initiator to afford compound **4.6**, which was further reacted with DIBAL-H to reduce the ester moiety selectively to obtain compound **4.7** with moderate yield. The coupling of compound **4.7** at the bromomethyl group with the drug diclofenac (**DCF**) led to the synthesis of compound **4.8**. While, the coupling of compound **4.8** with **DCI-NH_2** in the presence of triphosgene led to the synthesis of carbamate-based prodrug **DCF-Con**, the coupling of compound **4.8** with **DCI-NCS** led to the formation of the thiocarbamate-based prodrug **DCF-HS** (Scheme 4.1B). All the synthesized intermediates and prodrugs were purified and characterized by analytical methods.

TH-3161_176122050

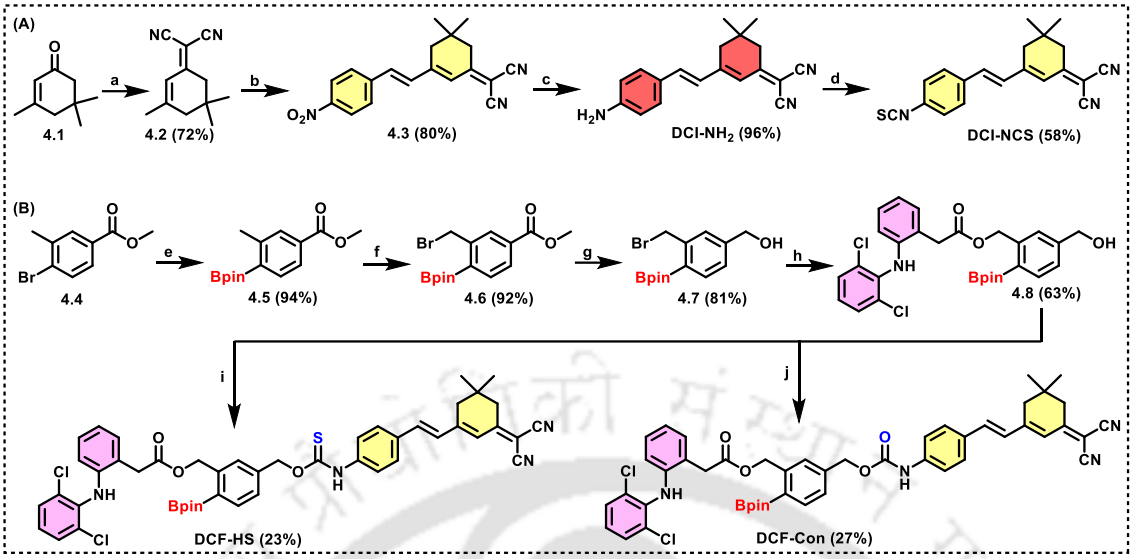

Scheme 4.1. Synthetic schemes to the prodrugs **DCF-HS** and **DCF-Con**. Reagents and conditions. (a) Malononitrile, piperidine, glacial AcOH, dry EtOH, 80 °C, 12 h. (b) 4-nitrobenzaldehyde, piperidine, dry ACN, 60 °C, 6 h. (c) $SnCl_2.2H_2O$, conc. HCl, EtOH, 80 °C, 2 h. (d) (i) CS_2, TEA, dry THF, 0 °C – RT, 18 h; (ii) *p*-TsCl, RT, 2 h. (e) B_2pin_2, KOAc, $Pd(PPh_3)_2Cl_2$, dry 1,4-dioxane, 90 °C, 5 h. (f) NBS, AIBN, dry ACN, 90 °C, 3 h. (g) DIBAL-H (1 M in toluene), dry toluene, 0 °C – RT, 6 h. (h) Diclofenac, DIPEA, dry ACN, 0 °C – RT, 24 h. (i) **DCI-NCS**, DBU, dry THF, 0 °C – RT, 3 h. (j) **DCI-NH$_2$**, triphosgene, D-MAP, DIPEA, dry DCM, 0 °C – RT, 24 h.

4.3.2. Absorption and emission spectroscopic studies

After synthesizing the designed prodrugs (**DCF-HS** and **DCF-Con**), the initial absorption and emission spectroscopic studies were carried out to investigate the release of the fluorophore **DCI-NH$_2$** and the active drug **DCF** in the presence of H_2O_2. The prodrug **DCF-HS** (10 µM) was incubated with H_2O_2 (400 µM) for 10 h in PBS/DMSO (1:1, v/v) and the absorbance was measured using UV-Vis spectroscopy. A significant red-shift was observed with H_2O_2, which was well resembled with the pattern of pure NIR fluorophore **DCI-NH$_2$** (10 µM) (Figure 4.2A). This observation indicated the release of fluorophore in the presence of H_2O_2. In addition, the prodrug **DCF-HS** (5 µM) was incubated with H_2O_2 (200 µM) for 10 h in PBS/DMSO (1:1, v/v) and the emission spectrum was measured using fluorescence spectroscopy. A significant red-shift was observed with H_2O_2, which exactly matched with the emission spectrum of the NIR fluorophore **DCI-NH$_2$** (5 µM) (Figure 4.2B). The emission intensity of **DCF-HS** in the presence of H_2O_2 is 4-times higher than the emission intesnsity

TH-3161_176122050

of **DCF-HS** in the absence of H_2O_2. Similarly, the absorption and emission spectra were measured for the control prodrug **DCF-Con** under identical conditions as **DCF-HS**. As expected, a red-shift was observed in the presence of H_2O_2, indicating the release of fluorophore (Figure 4.2C and 4.2D). These outcomes confirmed the release of the fluorophore **DCI-NH2** from the prodrugs **DCF-HS** and **DCF-Con** in the presence of H_2O_2.

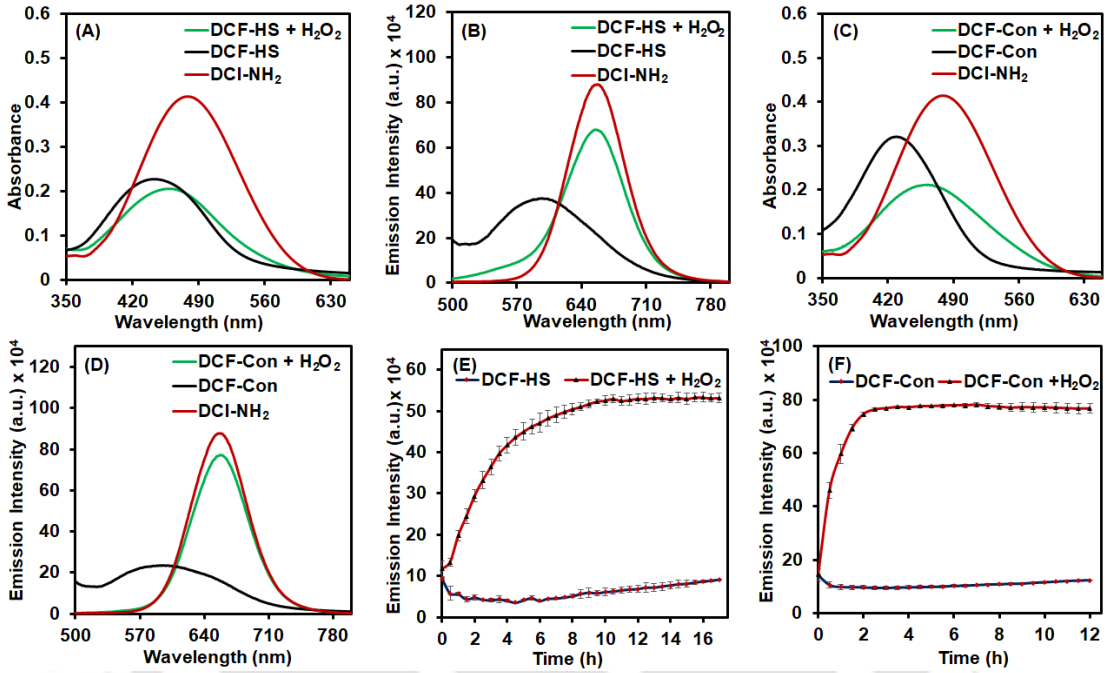

Figure 4.2. (A) The absorption spectrum of **DCF-HS** (10 μM) with and without H_2O_2 (400 μM) along with the spectrum of pure fluorophore **DCI-NH2** (10 μM). (B) The emission spectrum of prodrug **DCF-HS** (5 μM) with and without H_2O_2 (200 μM) along with the emission spectrum of pure **DCI-NH2** (10 μM). The absorption and emission spectra of **DCF-HS** + H_2O_2 were recorded after 10 h. (C) Absorption spectra of probe **DCF-Con** (10 μM) in the absence and presence of H_2O_2 (400 μM). (D) Emission spectra of probe **DCF-Con** (5 μM) in the absence and presence of H_2O_2 (200 μM). (E) Emission spectra of **DCF-HS** (5 μM) in the absence and presence of H_2O_2 (200 μM) with variable time (0-17 h). (F) Emission spectra of **DCF-Con** (5 μM) with variable time (0-12 h) with or without a fixed concentration of H_2O_2 (200 μM). The experiments were carried out in PBS (20 mM, pH 7.4, with 50% DMSO v/v), λ_{ex} = 472 nm.

Upon confirmation of the release of fluorophore and drug from the prodrug, the kinetics of the fluorophore release was carried out for both the prodrugs (5 μM) in the absence and

TH-3161_176122050

presence of H_2O_2 (200 μM) using fluorescence spectroscopy. As shown in Figure 4.2E, the emission intensity from **DCF-HS** increased gradually over the time upto 10 h then a saturation pattern was observed upto 17 h. This observation indicated that the prodrug **DCF-HS** is capable of releasing the fluorophore in a sustained manner in the presence of H_2O_2. Additionally, a very negligible emission was observed from **DCF-HS** in the absence of H_2O_2 upto 17 h, which indicated good stability of the prodrug in the aqueous medium (Figure 4.2E). Similarly, the kinetics of fluorophore release from the control prodrug **DCF-Con** was carried out under the similar condition with variable time (0-12 h). Contrastingly, the saturation pattern was attained within 2 h, indicating relatively faster self-immolative process in the prodrug **DCF-Con** as compared to **DCF-HS** for the release of fluorophore in the presence of H_2O_2 (Figure 4.2F). As the main objective of the present work is associated with the adjuvant delivery of both the drug (**DCF**) and H_2S with the turn-on fluorescence, further detailed studies are mostly carried out with the main prodrug **DCF-HS**.

4.3.3. Analyte selectivity and pH dependency

It is well-known that the boronate ester-based probes are mostly used in the drug delivery systems owing to their high level of sensitivity and selectivity towards H_2O_2 over other bio-analytes. However, to validate it further, the analyte selectivity study was carried out with **DCF-HS** (5 μM) with several biologically relevant analytes (200 μM) such as H_2O_2, cumene hydroperoxide (Cum-OOH), *tert*-butyl hydroperoxide (*t*Bu-OOH), potassium superoxide (KO_2), peroxynitrite ($ONOO^-$), sodium hypochlorite (NaOCl), glutathione (GSH), L-cysteine (Cys), glycine (Gly), alanine (Ala), sodium chloride (NaCl) and sodium iodide (NaI). The prodrug was incubated with these analytes for a 10 h and the emission response was measured using fluorescence spectroscopy. Very high emission profile in the presence of H_2O_2 indicated very high selectivity of the prodrug towards H_2O_2 and very little interferences from other bio-analytes except O_2^- and $ONOO^-$ (Figure 4.3A).

To understand the effect of pH on the reactivity and stability of the prodrug, the emission intensity of **DCI-NH$_2$** from **DCF-HS** (5 μM) was monitored in the presence or absence of H_2O_2 (200 μM) over a varying pH (4-10) of the medium. As shown in Figure 4.3B, a significant increase in emission intensity was observed for **DCF-HS** in the presence of H_2O_2 upto pH 8 with a subsequent saturation pattern. However, a slight decrease in the emission intensity at a higher pH (10) could be due to the base-induced quenching of the released

TH-3161_176122050

fluorophore **DCI-NH$_2$**. Interestingly, a very negligible emission intensity from the prodrug in the absence of H_2O_2 over the entire range of pH (4-10) indicates the overall stability of the prodrug **DCF-HS** in acidic, neutral and basic conditions. The increase in emission intensity from the prodrug with the increasing pH of the medium in the presence of H_2O_2 could be due to the enhanced reactivity of the highly nucleophilic and reactive hydroperoxide ($^-$OOH) anion in the alkaline medium. Moreover, the feasibility of self-immolation process is also enhanced at a higher pH of the medium.

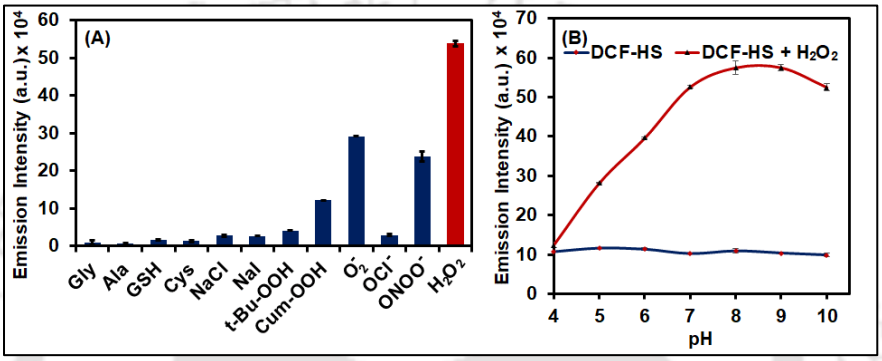

Figure 4.3. (A) Emission response of **DCF-HS** (5 μM) in the presence of biologically relevant analytes (200 μM) after incubating for 10 h. (B) The emission intensity of **DCF-HS** (5 μM) in the presence/absence of H_2O_2 (200 μM) with variable pH of the medium (pH: 4-10).

4.3.4. Sensitivity of DCF-HS towards H_2O_2

Upon confirming the analyte selectivity of the prodrug **DCF-HS**, the emission intensity from **DCF-HS** (5 μM) was measured in the presence of a variable concentration of H_2O_2 (0-500 μM) with a fixed incubation time (10 h). The emission spectrum was red-shifted in the presence of H_2O_2 and the intensity gradually increased upto a concentration of 200 μM, and a saturation pattern was observed thereafter upto 500 μM (Figure 4.4A and 4.4B). For utilizing this prodrug in the diseased conditions, this result would be quite important as the endogenous level of ROS is much higher in the inflamed cells than that in the normal cells. Additionally, the limit of detection (LOD) was calculated for the prodrug **DCF-HS** to understand its sensitivity towards H_2O_2 as per the standard method.[11] The emission intensity of **DCF-HS** (5 μM) was measured in the absence of H_2O_2 and at a lower variable concentration range (2-20 μM) of H_2O_2 (Figure 4.4C). Interestingly, LOD was found to be 1.2 μM for **DCF-HS**, indicating very high sensitivity of the prodrug towards H_2O_2.

TH-3161_176122050

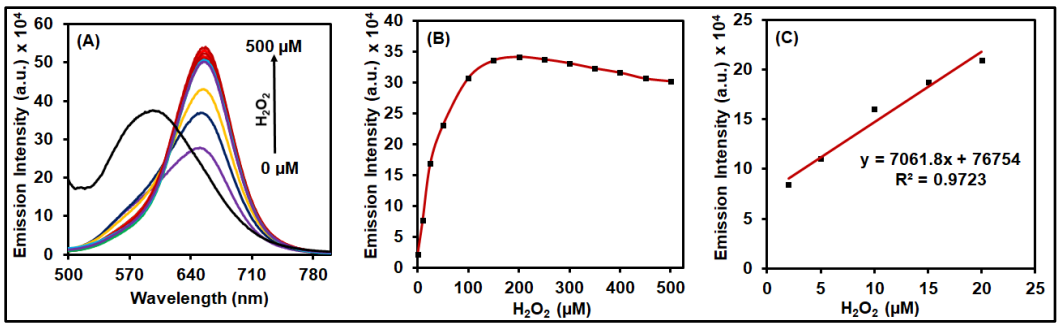

Figure 4.4. (A) Emission spectra of **DCF-HS** (5 µM) with variable concentration of H_2O_2 (0-500 µM) with a fixed incubation time of 10 h. (B) Emission spectra of **DCF-HS** (5 µM) at 670 nm with variable concentration of H_2O_2. (C) Emission spectra of **DCF-HS** (5 µM) with variable concentration of H_2O_2 (0-20 µM) with fixed incubation time of 10 h for calculating the LOD of **DCF-HS** towards H_2O_2.

4.3.5. Reaction kinetics for the drug release using HPLC

Upon confirming the release of the fluorophore **DCI-NH$_2$** from the prodrug **DCF-HS** using the UV-Vis and fluorescence spectroscopic studies, the release profile of the drug **DCF** and the fluorophore **DCI-NH$_2$** from **DCF-HS** was studied using the reverse phase HPLC method. In a 60:40 ACN/water mixture, **DCF-HS** (50 µM) was incubated with H_2O_2 (2 mM) in the presence of $NaHCO_3$ (200 µM), and the composition of the reaction mixture was analyzed using reverse phase HPLC after 2 h and 24 h. Before analyzing the reaction mixture, the retention time of the pure **DCF-HS** (19.1 min), **DCF** (6.3 min), and **DCI-NH$_2$** (5.6 min) were optimized. Considering the different absorption maxima of **DCF** (~280 nm) and **DCI-NH$_2$** (~400 nm), the chromatograms were extracted at 280 and 400 nm to monitor their release profiles. Interestingly, upon the reaction with H_2O_2, the peak of the prodrug **DCF-HS** at 19.1 min almost disappeared and new peaks at 5.6 min and 6.3 min appeared that matched precisely with the retention time of pure **DCI-NH$_2$** and **DCF**, respectively (Figure 4.5A). Additionally, three different peaks at 14.2 min, 7.6 min, and 7.3 min appeared during the progress of the reaction and disappeared finally during the release of **DCI-NH$_2$** and **DCF** from the prodrug **DCF-HS**.

This observation clearly illustrated that the fluorophore **DCI-NH$_2$** and **DCF** were released from the prodrug **DCF-HS** upon the reaction with H_2O_2. Monitoring the kinetics upto 48 h indicated that the intermediate **4.9** (14.2 min) was generated initially within 2 h upon the disappearance of the prodrug **DCF-HS** (Figure 4.5B). With time, the intermediate **4.9** was

TH-3161_176122050

converted to another intermediate **4.10** (7.6 min) and released the drug **DCF** concomitantly. As shown in Figure 4.5B, the release of drug **DCF** and the appearance of intermediate **4.10** reached a maximum after 8 h. Next, the intermediate **4.11** (7.3 min) appeared with the disappearance of intermediate **4.10** over time and released the fluorophore **DCI-NH$_2$**

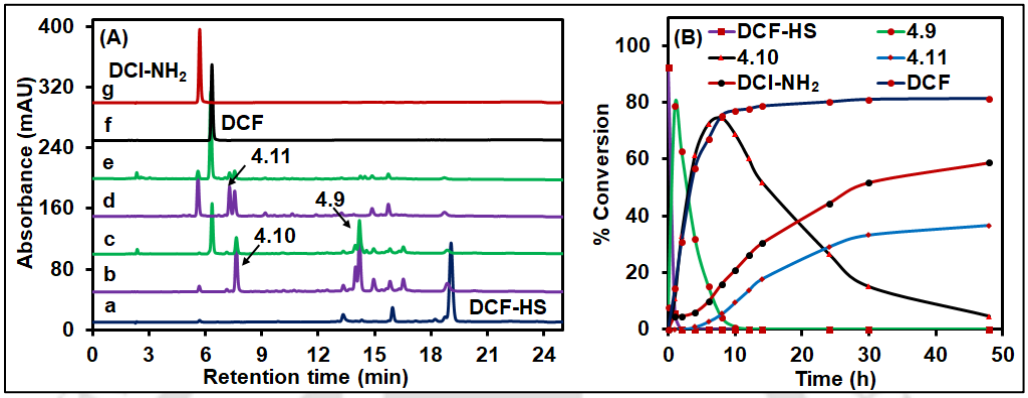

Figure 4.5. (A) HPLC chromatogram of pure (a) **DCF-HS**,(b) **DCF-HS** (50 μM) + H_2O_2 (2 mM) (t = 2 h, 400 nm), (c) **DCF-HS** (50 μM) + H_2O_2 (2 mM) (t = 2 h, 280 nm), (d) **DCF-HS** (50 μM) + H_2O_2 (2 mM) (t = 24 h, 400 nm), (e) **DCF-HS** (50 μM) + H_2O_2 (2 mM) (t = 24 h, 280 nm),(f) pure **DCF** (50 μM), and (g) pure **DCI-NH$_2$** (50 μM). Lanes (a, b, d, and g) were visualized at 400 nm and lanes (c, e, and f) were visualized at 280 nm. Reaction was carried out in ACN/water (3:2) and $NaHCO_3$ (200 μM). (B) Relative peak areas of various components present in the reaction mixture of **DCF-HS** (50 μM) + H_2O_2 (2 mM) over 48 h were monitored for the % conversion upon measuring the peak area of all the components (**DCF-HS**, **4.9**, **4.10**, **4.11**, and **DCI-NH$_2$**) at 400 nm and **DCF** at 280 nm.

4.3.6. Anti-proliferative activity and the fluorescence microscopic studies

With the confirmation of ROS-induced release of the NIR fluorophore **DCI-NH$_2$** and the NSAID (**DCF**) from the probe **DCF-HS** in the aqueous medium, feasibility of the release was investigated next in the cellular medium. In order to understand the compatibility of the prodrug in cellular medium, a representative cervical cancer cell line (HeLa), a nonmalignant cell line (HEK-293), and a macrophage cell line (RAW 264.7) were chosen. It should be noted that the cancer cells contain higher levels of intracellular ROS[12, 13] and higher expression levels of the inflammatory enzyme COX-2.[14, 15] Using the standard MTT assay, the cellular viability of HeLa, HEK-293, and RAW 264.7 cells were investigated in the presence of **DCF-HS** and **DCF-Con** (0, 10, 25, 50, and 100 μM) with an incubation of 48 h. Interestingly, the prodrugs **DCF-HS** and **DCF-Con** were found to be non-toxic in all three

TH-3161_176122050

cell lines upto 100 µM concentrations (Figure 4.6A), indicating the biocompatibility of the synthesized prodrugs **DCF-HS** and **DCF-Con**.

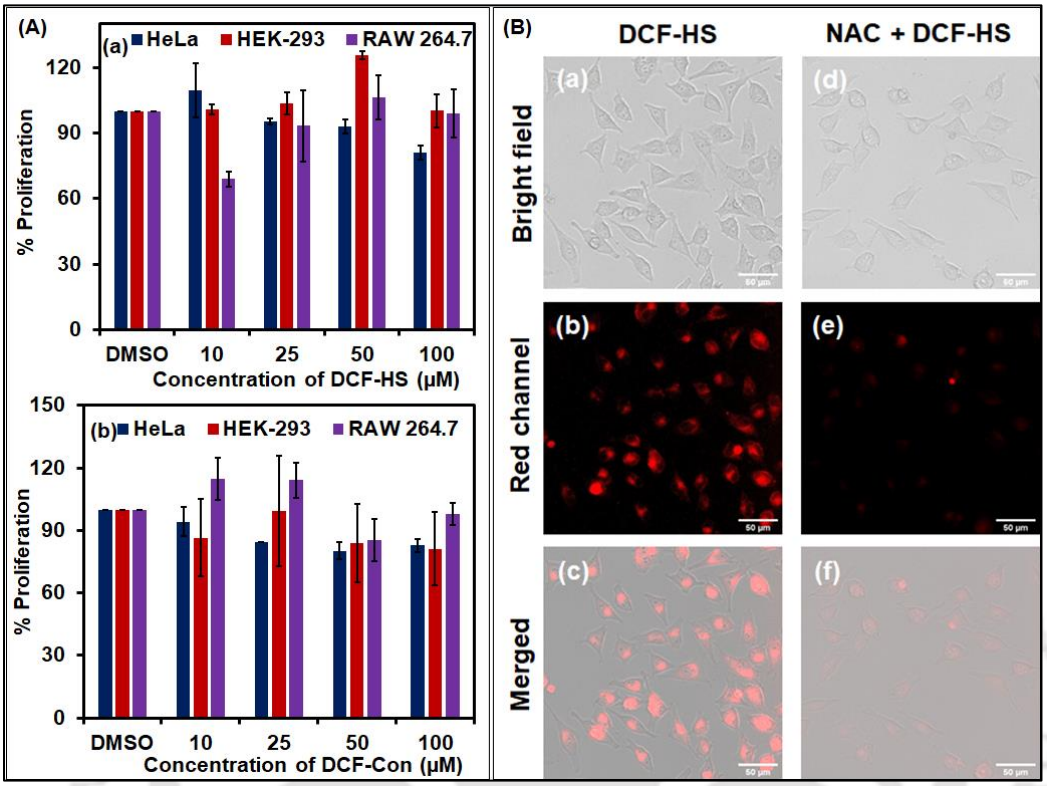

Figure 4.6. (A) Cellular viability of HeLa, HEK-293, and RAW 264.7 cells in the presence of (a) **DCF-HS**, and (b) **DCF-Con**. The cells were incubated with the compounds for 48 h. (B) Fluorescence microscopy images (bright field, red channel, and merged) of HeLa cells in the presence of **DCF-HS** (100 µM) for the endogenous ROS-triggered fluorogenic drug release (a-c). The cells were pre-treated with NAC (2 mM) for 1 h to quench the endogenous ROS followed by the treatment of **DCF-HS** (100 µM) (d-f). Scale bar: 50 µm.

Since the prodrug **DCF-HS** was found to be non-toxic in the HeLa, HEK-293, and RAW 264.7 cell lines, the endogenous ROS-responsive release of the fluorophore **DCI-NH$_2$** from the prodrug **DCF-HS** was studied in the HeLa cells (Figure 4.6B). The HeLa cells were incubated with the pure prodrug **DCF-HS** (100 µM) for 5 h and the cellular images were collected using fluorescence microscope. Interestingly, significant emission response under red channel was observed, indicating the endogenous ROS-triggered release of the NIR fluorophore **DCI-NH$_2$** from the prodrug **DCF-HS**. Moreover, a ROS scavenger NAC was used to confirm the role of endogenous H_2O_2 in the fluorogenic drug release. The endogenous

TH-3161_176122050

ROS was quenched by pre-treating the cells with NAC (2 mM) before the treatment of **DCF-HS** (100 μM). Interestingly, the lower emissive response in the presence of NAC indicated the primary role of the endogenous H_2O_2 in the fluorogenic drug release from the **DCF-HS** (Figure 4.6B).

4.3.7. Fluorescence microscopic studies for detecting the released H_2S

The adjuvant release of H_2S from the prodrug **DCF-HS** (100 μM) was next investigated in the cellular medium using an H_2S-selective turn-on fluorogenic probe **WSP2** (5 μM) (Figure 4.7). To understand the endogenous H_2S-triggered residual fluorescence in the HeLa cells, the cells were incubated with **WSP2** (5 μM) for 1 h and fluorescent microscopic images were collected (Figure 4.7A). Very weak emissive response under the blue channel was indicative of very low level of endogenous H_2S in HeLa cells. Interestingly, the co-treatment of **WSP2** (5 μM) and the prodrug **DCF-HS** (100 μM) in HeLa cells led to a higher emission under the blue channel indicating the release of H_2S from the prodrug. Moreover, the emission under the red channel indicated the release of NIR fluorophore **DCI-NH$_2$** from the prodrug **DCF-HS** (Figure 4.7B). In contrast, the co-treatment of **WSP2** and the control prodrug **DCF-Con** led to the negligible blue emission and a significant red emission. These observations clearly indicate the ROS-triggered release of NIR fluorophore **DCI-NH$_2$** from both the prodrugs and the release of H_2S only from the prodrug **DCF-HS** (Figure 4.7B). It should be noted here that, unlike the prodrug **DCF-Con**, the reaction of prodrug **DCF-HS** with the endogenous ROS would release carbonyl sulfide (COS) along with the NIR fluorophore (**DCI-NH$_2$**) and drug (**DCF**). The final release of H_2S from COS would be enzymatically catalyzed by the endogenous carbonic anhydrase (CA). Therefore, the intense blue emission due to the release of umbelliferone was observed in HeLa cells upon the co-treatment of **DCF-HS** and **WSP2**. Furthermore, involvement of the endogenous ROS for the fluorogenic response was validated by the pre-treatment of cells with the ROS-quencher NAC (2 mM) and the inhibitor (propargyl glycine, PAG, 20 μM) of the endogenous H_2S producing enzyme cystathionine-γ-lyase followed by the treatment of prodrug **DCF-HS** (100 μM) (Figure 4.7B). The negligible blue and red emission clearly indicated the effective scavenging of ROS and the inhibition of the key H_2S biosynthesis process. The mechanism of H_2S release from the prodrug **DCF-HS** and detection of it using H_2S-selective probe **WSP2** is shown in Figure 4.7C.

TH-3161_176122050

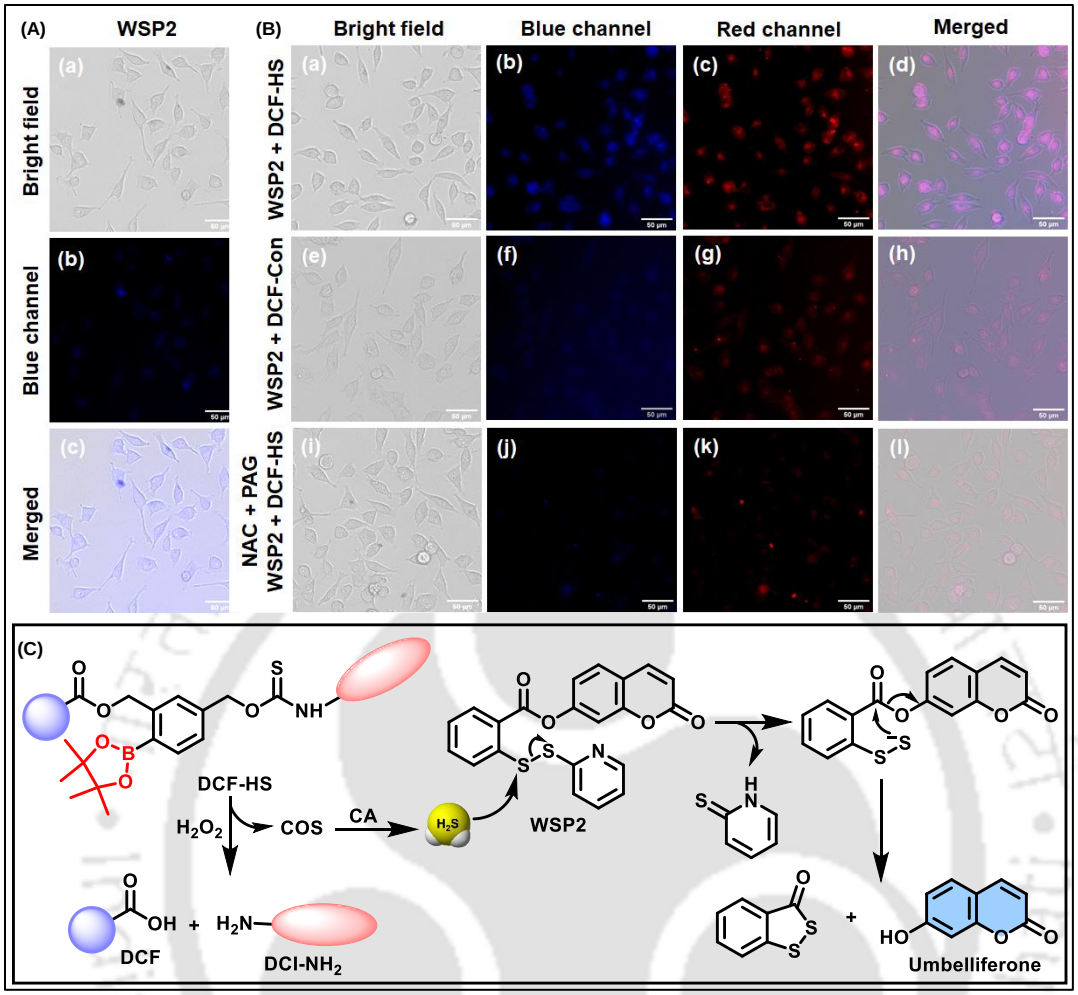

Figure 4.7. (A) Fluorescence microscopy images (bright field, blue channel, and merged) of HeLa cells for the detection of endogenous H_2S using the H_2S-selective turn-on fluorogenic probe **WSP2** (5 μM), (B) Fluorescence microscopy images (bright field, blue channel, red channel, and merged) of HeLa cells for the detection of released H_2S from **DCF-HS** and **DCF-Con** (100 μM) using the H_2S-selective turn-on fluorogenic probe **WSP2** (5 μM). Scale bar: 50 μm. (C) Schematic representation for the detection of released H_2S from **DCF-HS** using H_2S-selective turn-on fluorogenic probe **WSP2**.

4.3.8. Mechanistic insights

The composition of the reaction mixture was analyzed using ESI-MS analysis after 2 h and 24 h of incubation in order to identify the intermediates **4.9**, **4.10**, and **4.11**. It is indeed interesting to note that the ESI-MS results further supported the presence of intermediates **4.9**, **4.10**, and **4.11** in the reaction mixture (Annexure V, A5.21-23).

TH-3161_176122050

Therefore, a plausible reaction mechanism is proposed for the H_2O_2-triggered release of **DCF** and **DCI-NH$_2$** from the **DCF-HS** and the subsequent release of H_2S in the presence of CA enzyme (Scheme 4.2). The prodrug **DCF-HS** initially interacted with H_2O_2 and instantly changed into the first intermediate, **4.9**. Through a self-immolation process (1,6 – elimination), intermediate **4.10** and drug **DCF** are generated from intermediate **4.9** in the second step. Finally, fluorophore **DCI-NH$_2$** and COS are released from the intermediate **4.10** in two ways; in Path a, the intermediate **4.11** is generated from **4.10** followed by the release of the fluorophore **DCI-NH$_2$** and COS, whereas in Path b, the fluorophore **DCI-NH$_2$** and COS are released from intermediate **4.10** through concerted pathway without forming the intermediate **4.11**. The conversion of **4.11** to **DCI-NH$_2$**, also referred to as a rate-determining step, is the step that moves slowest. The released COS further transformed into H_2S in the presence of CA enzyme.

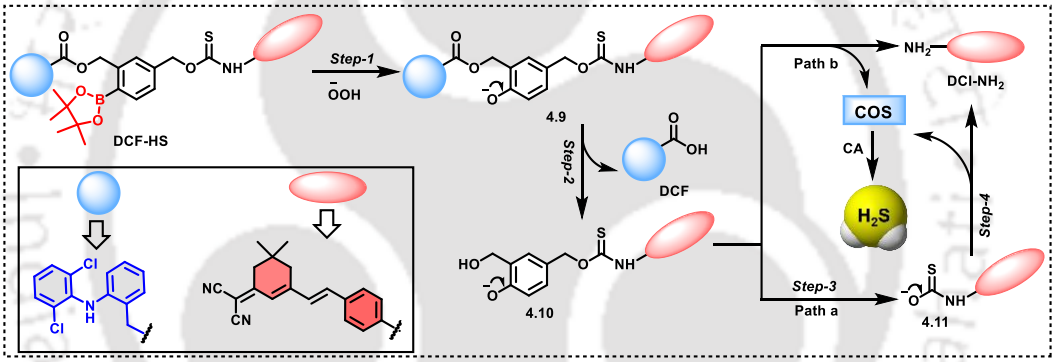

Scheme 4.2. Proposed mechanism for the feasibility of H_2O_2-triggered fluorogenic release of the active drug (**DCF**), NIR fluorophore (**DCI-NH$_2$**), and H_2S from the prodrug **DCF-HS**.

4.3.9. Anti-inflammatory activity

The anti-inflammatory activity of the released drug (**DCF**) from the prodrug **DCF-HS** was investigated in the macrophage cell line (RAW 264.7) using western blot analysis. The cells were pre-treated with lipopolysaccharides (LPS, 45 µg/mL, 14 h) for increasing the intracellular ROS, which directly induce the expression of COX-2. The expression level of COX-2 was dramatically increased in the presence of LPS (Figure 4.8A). The level of COX-2 was measured after the treatment of LPS-pretreated cells with **DCF-HS** (50 and 100 µM) followed by the incubation for 48 h. A dose-dependent down-regulation of COX-2 expression level was observed in the presence of **DCF-HS**. To verify the anti-inflammatory effect of the released **DCF** from the prodrug **DCF-HS**, a similar experiment was also carried out with

TH-3161_176122050

pure **DCF** (Figure 4.8B). A considerable down-regulation of COX-2 was observed in the presence of pure **DCF**. These observations reveal the H_2O_2-triggered release of **DCF** from the prodrug **DCF-HS** and its subsequent anti-inflammatory activity in the cellular medium.

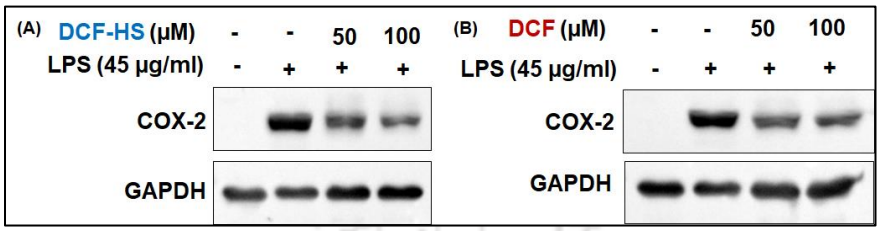

Figure 4.8. Anti-inflammatory activity of the prodrug **DCF-HS** as well as the **DCF** in RAW 264.7 cells. Western blot analysis for the expression level of COX-2 in RAW 264.7 cells and the effect of (A) **DCF-HS** (50 and 100 μM) and (B) pure **DCF** in the LPS (50 μg/mL) pre-treated cells. GAPDH was used as a housekeeping gene.

4.4. Conclusions

In summary, we describe herein the design and synthesis of peroxide-responsive turn-on fluorogenic prodrug **DCF-HS** for the adjuvant delivery of diclofenac (**DCF**) and H_2S with the turn-on NIR fluorescence. The involvement of self-immolative processes in the prodrugs induce sustained delivery of the drug as well as fluorophore both in the aqueous and cellular medium. Our designed prodrug **DCF-HS** was found to be non-toxic in the cellular medium and the prodrug was capable of releasing the active drug (**DCF**), fluorophore (**DCI-NH$_2$**), and H_2S in the cellular media using the endogenous stimuli. Moreover, the anti-inflammatory activity of the released active drug (**DCF**) from the prodrug **DCF-HS** was confirmed by studying the inhibition of COX-2 level in the inflammation-induced macrophage cells (RAW 264.7). Therefore, H_2O_2-responsive sustained release of **DCF** with NIR fluorogenic emission from **DCF-HS** would certainly be useful for the selective delivery of the anti-inflammatory drug to the inflammatory sites and the adjuvant release of H_2S would help in reducing the side-effects of anti-inflammatory drugs.

4.5. Experimental Section

4.5.1. Materials and methods

All the reagents were purchased either from Sigma Aldrich or from reputed local suppliers and used without further purification unless otherwise stated. Thin layer chromatographic (TLC) analyses were carried out on pre-coated silica gel on aluminum sheets and the

TH-3161_176122050

compounds were visualized by irradiation with UV or fluorescent light. Organic solvents used for chromatographic separations were distilled before use. The melting point of the synthesized compounds was recorded in a Büchi B540 melting point apparatus and the values are uncorrected. The NMR spectra (^{1}H and ^{13}C) were recorded on Bruker (400, 500, or 600 MHz) NMR spectrometers, and the chemical shifts are cited with respect to TMS (Me_4Si) as an internal standard. UV-Vis spectroscopic analyses were performed on a Lambda 45 UV-Vis spectrophotometer (Agilent) and fluorescence emission spectra were recorded on a Fluoromax-4 spectrophotometer (FluoroMax-4 -Horiba). Mass spectra were obtained using an Agilent 6520 Accurate-Mass Quadrupole Time-of-Flight (Q-TOF) LC/MS spectrometer.

4.5.2. Synthesis of prodrugs DCF-HS and DCF-Con

Synthesis compound 4.2[16]

To a stirred solution of malononitrile (8.60 g, 130.20 mmol) in dry ethanol (120 mL) was added piperidine (1.70 mL, 17.35 mmol) under inert at room temperature. After 10 min, the compound **4.1** (12 g, 86.76 mmol) and glacial AcOH (0.30 mL) were subsequently added dropwise at 50 °C and the reaction mixture was refluxed for 12 h. The progress of the reaction was monitored by TLC analysis. Upon completion of the reaction, the solvent was evaporated under reduced pressure, and the crude compound was further purified by silica gel (60-120 mesh) column chromatography using 30% DCM in pet. ether as a mobile phase to afford the pure product **4.2** as a white solid. R_f = 0.5 (30% DCM in pet. ether); Yield: 11.60 g (72%). ^{1}H NMR (600 MHz, $CDCl_3$) δ (ppm) = 6.62 (s, 1H), 2.51 (s, 2H), 2.18 (s, 2H), 2.03 (s, 3H), 1.01 (s, 6H); ^{13}C NMR (150 MHz, $CDCl_3$) δ (ppm) = 170.5, 159.9, 120.7, 113.3, 112.5, 78.3, 45.8, 42.7, 32.5, 27.9, 25.4.

Synthesis of compound 4.3[17]

To a stirred solution of 4-nitrobenzaldehyde (5.00 g, 33.00 mmol) and compound **4.2** (7.00 g, 39.60 mmol) in dry ACN (100 mL) was added piperidine (0.60 mL, 6.60 mmol) under inert at room temperature and the reaction mixture was heated at 60 °C for 6 h. The progress of the reaction was monitored by TLC analysis. Upon completion of the reaction, the solvent was evaporated under reduced pressure, and the crude compound was further purified by silica gel (100-200 mesh) column chromatography using 50% DCM in pet. ether as a mobile phase to afford the pure product **4.3** as a yellow solid. R_f = 0.5 (50% DCM in pet. ether); Yield: 8.50 g (80%). ^{1}H NMR (600 MHz, $CDCl_3$) δ (ppm) = 8.28 – 8.21 (m, 2H), 7.65 (d, *J*

TH-3161_176122050

= 8.4 Hz, 2H), 7.09 (q, *J* = 16.2 Hz, 2H), 6.94 (s, 1H), 2.63 (s, 2H), 2.49 (s, 2H), 1.10 (s, 6H). ^{13}C NMR (150 MHz, $CDCl_3$) δ (ppm) = 168.9, 152.3, 148.0, 141.98, 133.9, 133.3, 128.1, 125.8, 124.5, 113.1, 112.4, 80.9, 43.1, 39.3, 32.2, 28.1.

Synthesis of DCI-NH$_2$[17]

The free fluorophore **DCI-NH$_2$** was synthesized following the reported procedure with minor modifications.[17] To a suspension of compound **4.3** (3.00 g, 9.39 mmol) in distilled EtOH (8 mL) was added the solution of $SnCl_2.2H_2O$ (10.60 g, 46.96 mmol) in conc. HCl (8 mL) dropwise at room temperature and the reaction mixture was heated at 80 °C for 2 h. The progress of the reaction was monitored by TLC analysis. Upon completion of the reaction, the solvent evaporated and 150 mL of water was added to get the precipitate, which was further filtered off and washed with water (5 × 20 mL). The residue was dissolved in EtOAc (150 mL) and washed sequentially with saturated $NaHCO_3$ (3 × 20 mL) and water (3 × 20 mL) until the white precipitate disappeared. The organic layer was further washed with brine (2 × 20 mL) and dried over anhydrous Na_2SO_4. The crude compound was obtained by evaporating the solvent under reduced pressure, which was further purified by neutral alumina column chromatography using 80% DCM in pet. ether as a mobile phase to afford pure product **DCI-NH$_2$** as a red solid. R_f = 0.3 (50% DCM in pet. ether); Yield: 2.6 g (96%). ^{1}H NMR (600 MHz, $CDCl_3$) δ (ppm) = 7.34 (d, *J* = 8.1 Hz, 2H), 6.99 (d, *J* = 15.9 Hz, 1H), 6.81 (d, *J* = 16.0 Hz, 1H), 6.76 (s, 1H), 6.67 (d, *J* = 8.1 Hz, 2H), 3.98 (s, 2H), 2.58 (s, 2H), 2.45 (s, 2H), 1.07 (s, 6H). ^{13}C NMR (150 MHz, $CDCl_3$) δ (ppm) = 169.5, 155.1, 148.6, 137.9, 129.6, 126.2, 125.4, 122.1, 115.2, 114.1, 113.3, 43.2, 39.4, 32.1, 28.2.

Synthesis of DCI-NCS

To a stirred solution of compound **DCI-NH$_2$** (3.00 g, 10.35 mmol) in dry THF (30 mL) was added TEA (10.47 g, 103.66 mmol) dropwise at 0 °C under an inert atmosphere. After 30 min, carbonyl sulfide (15.78 g, 207.34 mmol) was added to the reaction mixture at 0 °C, and the reaction mixture was stirred at room temperature. The progress of the reaction was monitored by TLC analysis. Upon consumption of compound **DCI-NH$_2$**, *p*-toluene sulfonyl chloride was added at room temperature and stirred for another 2 h. upon completion of the reaction, the solvent was evaporated under reduced pressure, which was diluted with water (30 mL), and the crude compound was extracted by EtOAc (3 × 30 mL). The combined organic layer was further washed with brine (2 × 20 mL) and dried over anhydrous sodium

TH-3161_176122050

sulfate. The organic layer was evaporated under reduced pressure to obtain the crude compound, which was further purified by silica gel (230-400 mesh) column chromatography using 30% DCM in pet. ether as a mobile phase to afford the pure product **DCI-NCS** as a yellow solid. R_f = 0.5 (40% DCM in pet. ether); Yield: 2.00 g (58%). ^{1}H NMR (600 MHz, $CDCl_3$) δ (ppm) = 7.49 (d, *J* = 8.2 Hz, 2H), 7.24 (d, *J* = 8.3 Hz, 2H), 7.00 (d, *J* = 16.1 Hz, 1H), 6.96 (d, *J* = 16.1 Hz, 1H), 6.86 (s, 1H), 2.61 (s, 2H), 2.46 (s, 2H), 1.09 (s, 6H). ^{13}C NMR (150 MHz, $CDCl_3$) δ (ppm) = 169.1, 153.2, 136.9, 135.2, 134.8, 132.3, 130.3, 128.7, 126.5, 124.4, 113.4, 112.7, 79.5, 43.1, 39.3, 32.2, 28.1.

Synthesis of compound 4.5[18]

To a mixture of compound **4.4** (4.0 g, 17.46 mmol), B_2pin_2 (5.3 g, 20.96 mmol), $Pd(PPh_3)_2Cl_2$ (250 mg, 2 mol%), and KOAc (5.1 g, 52.40 mmol) was added dry 1,4-dioxane (100 mL) under inert at room temperature. The reaction mixture was stirred at 90 °C for 6 h. The progress of the reaction was monitored by TLC analysis. Upon completion, the reaction mixture was cooled down to room temperature, and the solvent was evaporated under reduced pressure. The obtained crude mixture was diluted with ethyl acetate (50 mL), which was filtered off through a celite pad and washed with ethyl acetate (5 × 20 mL). The combined organic layer was further washed with brine (2 × 20 mL), and dried over anhydrous sodium sulfate. The organic layer was evaporated under reduced pressure to obtain the crude compound, which was further purified by silica gel (230-400 mesh) column chromatography using 2% ethyl acetate in pet. ether as a mobile phase to afford the pure product **4.5** as a white solid. R_f = 0.5 (4% ethyl acetate in pet. ether); Yield: 4.5 g (94%). ^{1}H NMR (600 MHz, $CDCl_3$) δ (ppm) = 7.84 – 7.81 (m, 1H), 7.81 – 7.78 (m, 2H), 3.91 (s, 3H), 2.57 (s, 3H), 1.35 (s, 12H). ^{13}C NMR (150 MHz, $CDCl_3$) δ (ppm) = 167.5, 145.0, 135.9, 131.9, 130.6, 125.7, 83.9, 52.2, 25.0, 22.2. ESI-MS *m/z* calcd. for $C_{15}H_{22}BO_4$ $[M + H]^+$ = 277.1611, observed = 277.1609.

Synthesis of compound 4.6[18]

To a mixture of compound **4.5** (4.0 g, 14.48 mmol), NBS (3.1 g, 17.38 mmol), and AIBN (240 mg, 1.44 mmol) was added dry ACN (40 mL) under inert and the reaction mixture was heated at 90 °C for 3 h. The progress of the reaction was monitored by TLC analysis. Upon completion of the reaction, the solvent was evaporated under reduced pressure, which was diluted with water (30 mL), and the crude compound was extracted by EtOAc (3×30 mL).

TH-3161_176122050

The combined organic layer was further washed with brine (2 × 20 mL) and dried over anhydrous sodium sulfate. The organic layer was evaporated under reduced pressure to obtain the crude compound, which was further purified by silica gel (100-200 mesh) column chromatography using 5% ethyl acetate in pet. ether as a mobile phase to afford the pure product **4.6** as a white solid. R_f = 0.5 (5% ethyl acetate in pet. ether); Yield: 4.80 g (92%). ^{1}H NMR (600 MHz, $CDCl_3$) δ (ppm) = 8.04 (d, *J* = 1.6 Hz, 1H), 7.92 (dd, J_1 = 7.8, J_2 = 1.6 Hz, 1H), 7.88 (d, *J* = 7.7 Hz, 1H), 4.92 (s, 2H), 3.93 (s, 3H), 1.39 (s, 12H). ^{13}C NMR (150 MHz, $CDCl_3$) δ (ppm) = 166.71, 144.7, 136.6, 132.6, 130.9, 128.4, 84.4, 52.4, 33.2, 25.0. ESI-MS *m/z* calcd. for $C_{15}H_{21}BBrO_4$ $[M + H]^+$ = 355.0716, observed = 355.0713.

Synthesis of compound 4.7

To a stirred solution of compound **4.6** (4.0 g, 11.24 mmol) in dry toluene (60 mL) was added DIBAL-H (1M in toluene) dropwise at 0 °C under an inert atmosphere. Slowly the reaction mixture was kept at room temperature and stirred for 6 h. The progress of the reaction was monitored by TLC analysis. Upon completion, 1 M HCl (30 mL) was added slowly at ice-cold conditions to quench the reaction mixture. Further, the solvent was evaporated and extracted by ethyl acetate (3 × 30 mL). The combined organic layer was further washed with brine (2 × 20 mL), and dried over anhydrous sodium sulfate. The organic layer was evaporated under reduced pressure to obtain the crude compound, which was further purified by silica gel (230-400 mesh) column chromatography using 20% ethyl acetate in pet. ether as a mobile phase to afford the pure product **4.7** as a white solid. R_f = 0.5 (20% ethyl acetate in pet. ether); Yield: 3.00 g (81%). ^{1}H NMR (600 MHz, $CDCl_3$) δ (ppm) = 7.81 (d, *J* = 7.5 Hz, 1H), 7.39 (s, 1H), 7.28 (d, *J* = 7.7 Hz, 1H), 4.92 (s, 2H), 4.70 (s, 2H), 1.37 (s, 12H). ^{13}C NMR (151 MHz, $CDCl_3$) δ (ppm) = 144.8, 144.3, 136.9, 128.4, 125.9, 84.0, 64.9, 33.9, 24.9. ESI-MS *m/z* calcd. for $C_{14}H_{24}BBrNO_3$ $[M + NH_4]^+$ = 344.1033; observed = 344.1026.

Synthesis of compound 4.8[19]

To a stirred solution of compound **4.7** (2.4 g, 7.32 mmol) in dry ACN (20 mL) was added the solution of diclofenac (1.7 g, 5.86 mmol) and DIPEA (3.8 mL, 22.00 mmol) in ACN (10 mL) dropwise at 0 °C under inert atmosphere. Slowly the reaction mixture was warmed to room temperature and stirred for 24 h. The progress of the reaction mixture was monitored by TLC analysis. Upon completion, the solvent was evaporated and diluted with DCM (100 mL). The

TH-3161_176122050

solution was washed with water (3 × 20 mL) and saturated with $NaHCO_3$ (3 × 20 mL) solution alternatively to remove the unwanted left-over diclofenac. Furthermore, the organic layer was washed with brine (2 × 20 mL) and dried over anhydrous sodium sulfate. The organic layer was evaporated under reduced pressure to obtain the crude compound, which was further purified by silica gel (100-200 mesh) column chromatography using 100% DCM as a mobile phase to afford the pure product **4.8** as a white solid. R_f = 0.5 (100% DCM); Yield: 2.0 g (63%). ^{1}H NMR (600 MHz, $CDCl_3$) δ (ppm) = 7.84 (d, *J* = 7.6 Hz, 1H), 7.32 (s, 1H), 7.31 – 7.28 (m, 2H), 7.25 – 7.22 (m, 2H), 7.12 (td, *J* = 7.7, 1.6 Hz, 1H), 6.97 (d, *J* = 8.1 Hz, 1H), 6.96 – 6.93 (m, 2H), 6.54 (d, *J* = 8.0 Hz, 1H), 5.46 (s, 2H), 4.64 – 4.60 (m, 2H), 3.86 (s, 2H), 1.29 (s, 12H). ^{13}C NMR (151 MHz, $CDCl_3$) δ (ppm) = 172.13, 144.16, 142.97, 142.09, 137.96, 136.73, 131.10, 129.67, 128.94, 128.06, 126.74, 125.81, 124.59, 124.10, 122.08, 118.36, 83.94, 67.00, 65.06, 38.88, 24.91. ESI-MS *m/z* calcd. for $C_{28}H_{31}BCl_2NO_5$ $[M + H]^+$ = 542.1672, observed = 542.1673.

Synthesis of DCF-HS

To a stirred solution of compound **4.8** (0.40 g, 0.74 mmol) in dry THF (4 mL) was added DBU (0.13 mL, 0.88 mmol) dropwise at 0 °C under an argon atmosphere. Upon stirring the reaction mixture at the same temperature for 30 min, the solution of **DCI-NCS** (0.29 g, 0.81 mmol) in dry THF (4 mL) was added dropwise at the ice-cold condition and the reaction mixture was warmed to room temperature slowly. The progress of the reaction was monitored by TLC analysis. Upon completion of the reaction, the solvent was evaporated under reduced pressure, which was further purified by silica gel (230-400 mesh) column chromatography using 10% ethyl acetate in pet. ether as a mobile phase to afford the pure product **DCF-HS** as a yellow solid. R_f = 0.5 (30% ethyl acetate in pet. ether); Yield: 0.20 g (23%). M.P. = 81-83 °C. ^{1}H NMR (400 MHz, $CDCl_3$) δ (ppm) = 8.48 (s, 1H), 7.87 (d, *J* = 7.6 Hz, 1H), 7.44 (d, *J* = 6.6 Hz, 2H), 7.37 – 7.27 (m, 5H), 7.21 (d, *J* = 7.5 Hz, 2H), 7.12 (td, *J* = 7.7, 1.6 Hz, 1H), 6.94 (qd, *J* = 9.9, 9.0, 3.8 Hz, 5H), 6.83 (s, 1H), 6.53 (d, *J* = 8.0 Hz, 1H), 5.52 (s, 2H), 5.48 (s, 2H), 3.84 (s, 2H), 2.59 (s, 2H), 2.44 (s, 2H), 1.30 (s, 12H), 1.07 (s, 6H). ^{13}C NMR (150 MHz, $CDCl_3$) δ (ppm) = 172.1, 153.8, 142.9, 142.4, 137.9, 136.7, 136.0, 131.0, 129.6, 129.1, 128.9, 128.2, 127.1, 124.5, 124.1, 123.7, 122.2, 118.4, 84.1, 78.8, 66.7, 43.1, 39.3, 38.8, 32.1, 28.1, 24.9. ESI-MS *m/z* calcd. for $C_{48}H_{47}BCl_2N_4NaO_4S$ $[M + Na]^+$ = 895.2635, observed = 895.2614.

TH-3161_176122050

Synthesis of DCF-Con

To a stirred solution of **DCI-NH$_2$** (0.20 g, 0.69 mmol), triphosgene (0.10 g, 0.34 mmol), and DMAP (10 mg, cat.) in dry DCM (8 mL) was added the solution of DIPEA (0.27 g, 2.07 mmol) in dry DCM (2 mL) dropwise at 0 °C under argon atmosphere. The reaction mixture was kept at room temperature after 30 min and stirred at room temperature. The progress of the reaction mixture was monitored by TLC analysis. Upon consumption of the **DCI-NH$_2$**, the reaction mixture was cooled down to 0 °C and a solution of compound **4.8** (0.19 g, 0.34 mmol) in dry DCM (4 mL) was added dropwise at the same temperature under inert. Furthermore, the reaction mixture was stirred at room temperature for 18 h, and the progress of the reaction was monitored by TLC analysis. Upon completion, the solvent was evaporated under reduced pressure, which was further purified by silica gel (230-400 mesh) flash chromatography using 25% ethyl acetate in pet. ether as a mobile phase to afford the pure product **DCF-Con** as a yellow solid. R_f = 0.5 (30% ethyl acetate in pet. ether); Yield: 0.08 g (27%). M.P. = 90 - 92 °C. ^{1}H NMR (600 MHz, $CDCl_3$) δ (ppm) = 7.86 (d, *J* = 7.6 Hz, 1H), 7.45 (d, *J* = 8.2 Hz, 2H), 7.42 (d, *J* = 8.6 Hz, 2H), 7.33 (d, *J* = 7.9 Hz, 1H), 7.31 (d, *J* = 7.8 Hz, 2H), 7.28 (s, 1H), 7.23 (d, *J* = 7.5 Hz, 1H), 7.11 (t, *J* = 7.7 Hz, 1H), 7.01 (d, *J* = 16.0 Hz, 1H), 6.96 (d, *J* = 8.2 Hz, 1H), 6.95 – 6.92 (m, 2H), 6.90 (d, *J* = 16.0 Hz, 1H), 6.83 (d, *J* = 19.3 Hz, 2H), 6.54 (d, *J* = 8.0 Hz, 1H), 5.47 (s, 2H), 5.14 (s, 2H), 3.86 (s, 2H), 2.59 (s, 2H), 2.46 (s, 2H), 1.29 (s, 12H), 1.07 (s, 6H). ^{13}C NMR (150 MHz, $CDCl_3$) δ (ppm) = 172.1, 169.4, 154.2, 152.9, 142.9, 142.3, 139.3, 138.9, 137.9, 136.8, 136.6, 131.1, 129.6, 128.9, 128.7, 128.1, 128.1, 127.9, 127.1, 124.6, 124.1, 123.3, 122.1, 118.4, 112.9, 84.1, 78.3, 66.9, 66.8, 43.1, 39.3, 38.8, 32.2, 28.2, 24.9. ESI-MS *m/z* calcd. for $C_{48}H_{48}BCl_2N_4O_6$ $[M + H]^+$ = 857.3044, observed = 857.3035.

4.5.3. UV-Visible and fluorescence spectroscopic studies

All the stock solution of prodrugs (**DCF-HS** and **DCF-Con**) and the released fluorophore **DCI-NH$_2$** and active drug **DCF** were prepared in spectroscopy grade DMSO; the stock solution of H_2O_2 was prepared in milli-Q water. All the spectroscopic studies were performed under physiological conditions (PBS, 20 mM, pH = 7.4). Buffers with higher pH (9 and 10) were prepared by adding 1N NaOH solution to the buffer and lower pH (4 and 5) by adding 1N HCl. Samples for absorption and emission spectroscopic measurements were carried out in quartz cuvettes (1.0 ml). UV-Vis spectroscopic analyses were performed on a Lambda 45

TH-3161_176122050

UV-Vis spectrophotometer (Agilent) and fluorescence emission spectra were recorded on a Fluoromax-4 spectrophotometer (FluoroMax-4 -Horiba). For prodrugs **DCF-HS** and **DCF-Con**, λ_{ex} = 472 nm and λ_{em} = 490-800 nm with slit width = 5/5 nm were used in the fluorescence emission spectroscopic studies. The selectivity of the prodrug **DCF-HS** (5 µM) towards H_2O_2 (200 µM) was carried out over different analytes such as *t*-Bu-OOH, Cum-OOH, GSH, Cys, Gly, Ala, NaCl and NaI prepared in milli-Q water. KO_2 was used as a source of O_2^- and $ONOO^-$ prepared from H_2O_2 prior to use for the experiment.[20] The prodrug **DCF-HS** (5 µM) was initially incubated for 10 h with the analytes (200 µM) and the emission intensity was measured. All the experiments were carried out in PBS (20 mM, with 50% DMSO v/v, pH = 7.4).

4.5.4. Determination of limit of detection (LOD) of the prodrug

LOD of the prodrug **DCF-HS** was determined using fluorescence titration. The detection limit was calculated using the equation, LOD = 3σ/K, where σ is the standard deviation of blank measurements (without H_2O_2) and K is the slope of emission intensity versus H_2O_2 concentration. To get the standard deviation of the blank measurements, the emission intensity of the **DCF-HS** (5 µM) was measured 10 times in the absence of H_2O_2 and obtained 2886.139. For the determination of slopes (K), the emission spectra were measured at different concentrations of H_2O_2 (2-20 µM) after incubating the reaction mixture for 10 h and found 7061.8. The experiment was carried out in PBS (20 mM, with 50% DMSO v/v, pH = 7.4), λ_{ex} = 472 nm and λ_{em} = 490-800 nm with slit width = 5/5 nm.

4.5.5. Analysis of reaction kinetics using reverse phase HPLC method

Purity of the synthesized compounds was analyzed by analytical high-performance liquid chromatography (HPLC), Agilent 1220 infinity II LC system using a reverse phase C_{18} column (Luna®, 250 × 4.6 mm, 5 µm). HPLC grade acetonitrile and Millipore water was used as mobile phase and HPLC chromatogram of the prodrug **DCF-HS**, free drug diclofenac (**DCF**) and fluorophore **DCI-NH$_2$** were detected by PDA detector at 254, 280, 400 nm (as applicable). A stock solution of prodrug **DCF-HS** in DMSO and H_2O_2 in water was prepared immediately prior to use. The samples were injected using a flow rate of 1.0 ml/min with a linear gradient (35-1% v/v) H_2O/ACN (0–12 min), followed by 1% v/v, H_2O/ACN (12-20 min), finally, (1-35% v/v) H_2O/ACN (20-25 min) and 0.1% of TFA was used in water. Concentrations of the pure prodrug **DCF-HS** and the released drug **DCF** are 50 µM and in

TH-3161_176122050

the reaction mixture, 40 equivalents of H_2O_2 (2 mM) and 4 equivalents of $NaHCO_3$ (200 µM) were added. The reactions of the prodrug with H_2O_2 were carried out in PBS (20 mM, pH = 7.4) at room temperature and the samples were injected into the system at different time intervals to monitor the progress of the reaction.

4.5.6. Cell culture

The Human cervical cancer cells (HeLa), Human Embryonic Kidney cells (HEK-293) and a macrophage-like, Abelson leukemia virus-transformed cell line (derived from BALB/c mice) (RAW 264.7) were obtained from the National Centre for Cell Science (NCCS), Pune, India. The cells were cultured in DMEM medium (Gibco) supplemented with 10% (v/v) FBS (Gibco) and 1% Pen-Strep (Gibco). Cells were cultured as a monolayer in a humidified incubator at 37 ºC in the presence of 5% CO_2 level.

4.5.7. Cell viability assay

The synthesized prodrugs were screened for their anti-proliferative activities using the conventional MTT assay in HeLa, HEK-293, and RAW 264.7 cell lines. These cells were seeded in 96-well culture plates at a density of 1×10^4, 2×10^4, and 1×10^4 cells/100 µL per well, respectively and treated with the freshly prepared test compounds **DCF-HS** (10, 25, 50, and 100 µM) and **DCF-Con** (10, 25, 50, and 100 µM) for 0 h (control) and 48 h (experimental), respectively. At the end of the treatment period, 100 µL of 5 mg/mL of MTT was added to the plate (control) and incubated for 4 h. Following the 4 h incubation, the reagent from the plate was removed and the purple formazan crystals were dissolved using 100 µL of DMSO (Avra Synthesis Pvt Ltd) and the absorbance at 570 nm was measured using a microplate reader (Thermo Scientific™ Multiskan™ GO microplate reader). In the experimental set, a similar MTT treatment protocol was followed only after 48 h. The mean ΔOD values were calculated by the subtraction of mean OD values of 0 h plate (control) from the mean OD values of identical wells at 48 h plate (experimental) and the percentage proliferation was calculated keeping the mean ΔOD of untreated control as 100%.

4.5.8. Fluorescence microscopic studies

HeLa cells were cultured in high glucose DMEM medium supplemented with 10% (v/v) fetal bovine serum (FBS) and 1% penicillin/streptomycin at 37 °C under 5% CO_2 atmosphere. Cells were then plated (1.5×10^6 cells per plate) in 35 mm cell culture Petri dishes containing

TH-3161_176122050

2 mL of DMEM and incubated at 37 °C under 5% CO_2 for 24 h. The confluent cells were washed with DPBS and finally incubated with **DCF-HS** (100 µM) for 1 h. After washing the cells with DPBS (3 times), cellular morphology was carefully observed and imaged using Bio-Rad ZOE^{TM} fluorescent cell imager under a bright field and red channel. A negative control experiment was performed upon the pre-treatment of cells with *N*-acetyl cysteine (NAC, 2 mM) for 1.5 h to quench the endogenous ROS. The cells were washed with DPBS (3 times) and treated with **DCF-HS** (100 µM).

For the detection of the release of H_2S from **DCF-HS** (100 µM), the HeLa cells were grown like the above condition and the cells were treated with **WSP2** (5 µM) for 1 h and cells were imaged under bright field and blue channel after washing to understand the endogenous level of H_2S. For studying the released H_2S from **DCF-HS** or **DCF-Con**, the cells were treated with **WSP2** (5 µM) for 1 h and the cells were washed with DPBS (3 times) and treated with **DCF-HS** or **DCF-Con** (100 µM) for 1 h. The cells were washed finally with DPBS and imaged under bright field, blue, and red channels.

4.5.9. Western blot analysis

In order to estimate the COX-2 expression upon the release of the NSAID (**DCF**) from the probe **DCF-HS**, immunoblotting experiment was performed. RAW 264.7 cells (3×10^5 cells per 5 mL) were plated in 60 mm cell culture dish and cultured in high glucose Dulbecco's modified Eagle's medium (DMEM) supplemented with 10% fetal bovine serum (FBS) and 1% penicillin/streptomycin at 37 °C in the incubator under 5% CO_2 atmosphere. The overexpression of COX-2 level in RAW 264.7 cells was induced upon the pre-treatment of LPS (45 µg/mL, 14 h). After the treatment, cells were washed with DPBS (3 times) and further treated with compounds **DCF** and **DCF-HS** (50.0 and 100.0 µM), respectively and incubated for 48 h under 5% CO_2 atmosphere. After completion of the treatment, cells were washed with cold PBS (1X) and the protein extraction was performed. The whole cell protein was extracted using RIPA cell lysis buffer (150 mM of NaCl, 1% (v/v) NP-40, 0.5% sodium deoxycholate, 0.1% SDS, 25 mM of Tris, 10 mg/mL of PMSF). Equal volume of protein was loaded and separated on 12% sodium dodecyl sulfate (SDS)–polyacrylamide gel by electrophoresis and transferred to a nitrocellulose membrane. Protein transfer was confirmed by Ponceau-S (HiMedia) staining. The blots were blocked with 5% non-fat dry milk in 1X TBST buffer for 1 h at room temperature. Finally, the primary antibody (1:5000) specific for

TH-3161_176122050

COX-2 (Cell Signaling, D5H5) and GAPDH (Cell Signaling, 14C10) were incubated overnight at 4 °C. Following the primary antibody incubation, the blots were washed with TBST (1X) buffer and incubated with HRP-conjugated secondary antibodies (Abcam) for 1 h and developed with an ECL Detect Kit (Bio-Rad) and imaged using ChemiDoc™XRS System (Bio-Rad). The house-keeping gene GAPDH was used as a loading control.

4.6. References

1. A. E. Albers, V. S. Okreglak and C. J. Chang, *J. Am. Chem. Soc.*, 2006, **128**, 9640-9641.
2. M. C. Y. Chang, A. Pralle, E. Y. Isacoff and C. J. Chang, *J. Am. Chem. Soc.*, 2004, **126**, 15392-15393.
3. A. Sufian, D. Bhattacherjee, T. Mishra and K. P. Bhabak, *Dyes Pigm.*, 2021, **191**, 109363.
4. E.-J. Kim, S. Bhuniya, H. Lee, H. M. Kim, C. Cheong, S. Maiti, K. S. Hong and J. S. Kim, *J. Am. Chem. Soc.*, 2014, **136**, 13888-13894.
5. W. Chen, Y. Cheng and B. Wang, *Angew. Chem. Int. Ed.*, 2012, **51**, 5293-5295.
6. J. Peiró Cadahía, V. Previtali, N. S. Troelsen and M. H. Clausen, *MedChemComm*, 2019, **10**, 1531-1549.
7. S. Rizwan, P. ReddySekhar and B. MalikAsrar, *Antioxid. Redox Signaling*, 2014.
8. A. M. Qandil, *Int. J. Mol. Sci.*, 2012, **13**, 17244-17274.
9. L. Yuan, W. Lin, S. Zhao, W. Gao, B. Chen, L. He and S. Zhu, *J. Am. Chem. Soc.*, 2012, **134**, 13510-13523.
10. X. Liang, L. Zhang, B. Shi, H. Chang, D. Qiao, T. Shen, W. Zhao, Z. Yin and L. Shang, *Talanta*, 2020, **220**, 121433.
11. A. Sufian, D. Bhattacherjee, T. Mishra and K. P. Bhabak, *Dyes Pigm.*, 2021, **191**, 109363.
12. B. Perillo, M. Di Donato, A. Pezone, E. Di Zazzo, P. Giovannelli, G. Galasso, G. Castoria and A. Migliaccio, *Exp. Mol. Med.*, 2020, **52**, 192-203.
13. P. Wang, J. Geng, J. Gao, H. Zhao, J. Li, Y. Shi, B. Yang, C. Xiao, Y. Linghu, X. Sun, X. Chen, L. Hong, F. Qin, X. Li, J.-S. Yu, H. You, Z. Yuan, D. Zhou, R. L. Johnson and L. Chen, *Nat. Commun.*, 2019, **10**, 755.

TH-3161_176122050

14. B. Krishnamachary, I. Stasinopoulos, S. Kakkad, M.-F. Penet, D. Jacob, F. Wildes, Y. Mironchik, A. P. Pathak, M. Solaiyappan and Z. M. Bhujwalla, *Oncotarget*, 2017, **8**.
15. T. L. Larkins, M. Nowell, S. Singh and G. L. Sanford, *BMC Cancer*, 2006, **6**, 181.
16. M. Yang, J. Fan, W. Sun, J. Du, S. Long, K. Shao and X. Peng, *Chem. Commun.*, 2019, **55**, 8583-8586.
17. F. Liu, Z. Wang, T. Zhu, W. Wang, B. Nie, J. Li, Y. Zhang, J. Luo and L. Kong, *Talanta*, 2019, **191**, 126-132.
18. M. Imanishi, Y. Tomishima, S. Itou, H. Hamashima, Y. Nakajima, K. Washizuka, M. Sakurai, S. Matsui, E. Imamura and K. Ueshima, *J. Med. Chem.*, 2008, **51**, 1925-1944.
19. A. Sufian, D. Bhattacherjee, P. Barman, A. Srivastava, R. P. Thummer and K. P. Bhabak, *Chem. Commun.*, 2022, **58**, 7833-7836.
20. K. P. Bhabak and G. Mugesh, *Chem. Eur. J.*, 2010, **16**, 1175-1185.

TH-3161_176122050

TH-3161_176122050

Peroxide-responsive turn-on fluorogenic prodrug of the anti-cancer drug amonafide: adjuvant drug delivery with hydrogen sulfide

TH-3161_176122050

TH-3161_176122050

5.1. Introduction

Examples of the literature reported ROS-responsive turn-on fluorogenic prodrugs of various anti-cancer drugs are discussed in chapter 1. Although those prodrugs were suitable for monitoring the drug release in living cells, they failed to overcome the side-effects of the corresponding active drugs significantly. It is to be noted that H_2S has multiple biological functions such as antioxidants, anti-inflammatory, and vasodilatory, which were discussed in chapter 1. Considering the beneficial biological functions of H_2S, the side-effects of anti-cancer drugs could be overcome by delivering H_2S along with the conventional anti-cancer drug. Therefore, prodrugs of anti-cancer drugs with the co-delivery of H_2S would be important in the field of prodrug development. In 2022, Lukesh III and co-workers developed a novel doxorubicin hybrid prodrug (**5.1**) that responded to the high levels of ROS in uncaging of doxorubicin with the concomitant delivery of H_2S (Figure 5.1).[1] Interestingly, the cardioprotective effect of H_2S was helpful in ameliorating the cardiovascular side-effect of doxorubicin. However, the fluorescence turn-on property was not observed in **5.1**, which is a very important tool for monitoring the drug release in a real-time. Therefore, developing a ROS-responsive turn-on fluorogenic hybrid prodrug for the delivery of anti-cancer drug and H_2S will be an innovative and attractive drug delivery system. To address this issue, amonafide (a potent anti-cancer drug) is a perfect choice, which is utilized as a self-reporting fluorogenic drug. Moreover, the fluorescence ON-OFF process can be tuned by masking the aromatic amino group of amonafide. In addition, amonafide is a novel synthetic naphthalimide derivative known as a neoplastic agent and acts as a DNA intercalator.[2] Amonafide inhibits topoisomerase II (TOPO-II) catalysis rather than the formation of TOPO-II-DNA cleavable complexes, resulting in less DNA damage than the classical TOPO-II drugs.[3] However, the drug has a free amino group in the 3-position of the naphthalimide ring that undergoes acetylation to form a toxic metabolite (*N*-acetyl metabolite) by *N*-acetyl transferase 2 (NAT2) in humans, causing unwanted side-effects and reducing the bioavailability.[4] Therefore, a prodrug of amonafide where free amino group will be masked with a protecting group is crucial in overcoming the unwanted toxicity and side-effects of the drug. To address this issue, in 2018, Xiao and co-workers developed the first prodrug of amonafide where it was delivered from fructose-coated nanodiamonds. The prodrug ND-Polymer-AMF showed lower IC_{50} (7.19 μM for MCF-7 and 4.92 μM for MDA-MB-231)

TH-3161_176122050

than free amonafide (11.23 μM for MCF-7 and 13.98 μM for MDA-MB-231).[5] However, there was no indication of drug release and fluorescence turn-on property, which is important for monitoring the drug release profile in real-time. . In 2021, Ge *et al.* reported hydrogen sulfide-responsive lysosome-targeted prodrug of amonafide **PNF** (Figure 5.1).[6] The prodrug was designed as hydrophobic by masking the amine by azide group to overcome the limited cellular accumulation of free amonafide. Interestingly, launching the azide group improved the lipophilicity and biocompatibility of **PNF**. Importantly, prodrug **PNF** shows more significant potential than free drug amonafide to inhibit the proliferation of drug-resistant cancer cells.

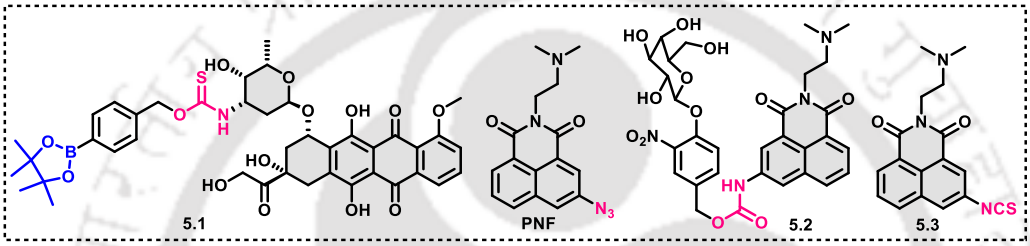

Figure 5.1. Chemical structures of reported hybrid prodrugs of anti-cancer drugs and H_2S.

Recently in 2022, Scanlan and co-workers have reported an enzyme-triggered theranostic prodrug of amonafide (**5.2**), where the drug was released in the presence of glycosidase, which is elevated in cancer cells (Figure 5.1).[7] Importantly, this prodrug preserved the strong cytotoxicity of free amonafide. However, considering the importance of the adjuvant delivery of the drug and H_2S in minimizing the side-effects of the drug, in the early year of 2023, Bhabak and co-workers reported a cysteine-triggered prodrug (**5.3**) of amonafide (Figure 5.1).[8] Cysteine, an overexpressed biothiol in cancer cells, triggered the release of both the drug and H_2S concomitantly. Since ROS is overexpressed in cancer cells as compared to normal cells, the ROS-responsive turn-on fluorogenic prodrug strategies will be suitable to overcome the limitations of free amonafide.

5.2. Outline of the chapter

Herein, we describe the development a ROS-responsive turn-on fluorogenic hybrid prodrug of amonafide (**AM-TCB**), capable of releasing both the active drug amonafide and H_2S (Scheme 5.1). While the release of amonafide takes place upon the prodrug activation by ROS, the release of H_2S is effected by the hydrolysis of carbonyl sulfide (COS) by the enzyme carbonic anhydrase (CA).

TH-3161_176122050

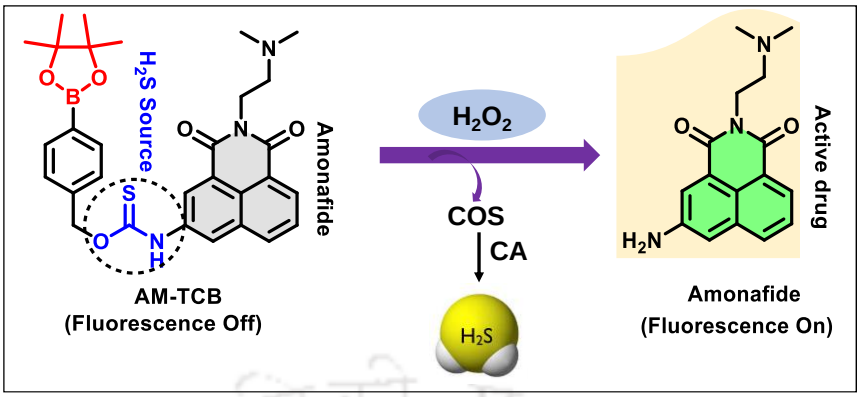

Scheme 5.1. Schematic representation of peroxide-responsive turn-on fluorogenic prodrug for the co-delivery of amonafide and H_2S.

In addition, a control prodrug (**AM-CB**) was also synthesized, which would react with H_2O_2 and release the active drug amonafide but without H_2S. Upon synthesizing the designed prodrugs, purification and characterization were performed using analytical methods. Spectroscopic studies confirmed the release of the active drug amonafide from the prodrug **AM-TCB** in the presence of H_2O_2 (Figure 5.2). Moreover, the prodrug **AM-TCB** showed selectivity towards H_2O_2 over other bio-analytes and exhibited stability over a wide range of pH (Figure 5.3). Furthermore, the release of H_2S was confirmed using UV-Vis (MB assay) as well as fluorescence spectroscopy (**WSP2** assay) and observed controlled H_2S delivery over time (Figure 5.4). Mechanistic insight into drug release from the prodrug **AM-TCB** was discussed from HPLC studies and ESI-MS analysis (Figure 5.5). Upon confirming the drug and H_2S release from the prodrug **AM-TCB** in an aqueous medium, further, it was investigated in a cellular medium (HeLa cells). Interestingly, the release of the active drug from the prodrug **AM-TCB** was confirmed in the presence of endogenous ROS from the green emission of amonafide and the release of H_2S was confirmed using the H_2S-selective turn-on fluorogenic probe **WSP2** following the blue emission of the released umbelliferone (Figure 5.6). The anti-proliferative activity was carried out to investigate the cytotoxicity of the prodrug **AM-TCB** towards cancer cell lines (HeLa and MDA-MB-231) and in a representative normal cell line (HEK-293). While the the prodrug showed almost similar anti-cancer activity in cancer cell lines as the parent drug, it exhibited cytoprotective effects on normal cells due to the co-delivery of H_2S (Figure 5.6). This result indicated that the prodrug could be helpful in reducing the side-effects of amonafide for the treatment of cancer.

TH-3161_176122050

5.3. Results and Discussion

5.3.1. Synthesis of the prodrugs AM-TCB and AM-CB

The prodrugs **AM-TCB** and **AM-CB** in the present study were synthesized from the readily available precursor 1,8-naphthalic anhydride **5.4** with multi-step organic synthesis as shown in Scheme 5.2. The nitration of 1,8-naphthalic anhydride (**5.4**) with the nitrating mixture produced 3-nitro-1,8-naphthalic anhydride (**5.5**), which upon the reduction with stannous chloride dihydrate afforded 3-amino-1,8-naphthalic anhydride (**5.6**).[9] The anti-cancer drug amonafide was prepared subsequently by the condensation of the anhydride **5.6** with *N,N*-dimethylethylenediamine using the reported method.[4] The isothiocyanate derivative **5.7** was prepared from amonafide using carbon disulfide and *p*-tosyl chloride in the presence of triethylamine. The coupling of amonafide and the isothiocyanate **5.7** with the boronate ester containing benzyl alcohol (**5.8**) led to the synthesis of final prodrugs **AM-CB** and **AM-TCB**, respectively at good yields (Scheme 5.2A).The boronate ester **5.9** was synthesized from 4-bromobenzyl alcohol (**5.8**) following the literature method at a good yield (Scheme 5.2B).[10] All the intermediates and the final prodrugs were purified (as applicable) and characterized by analytical methods.

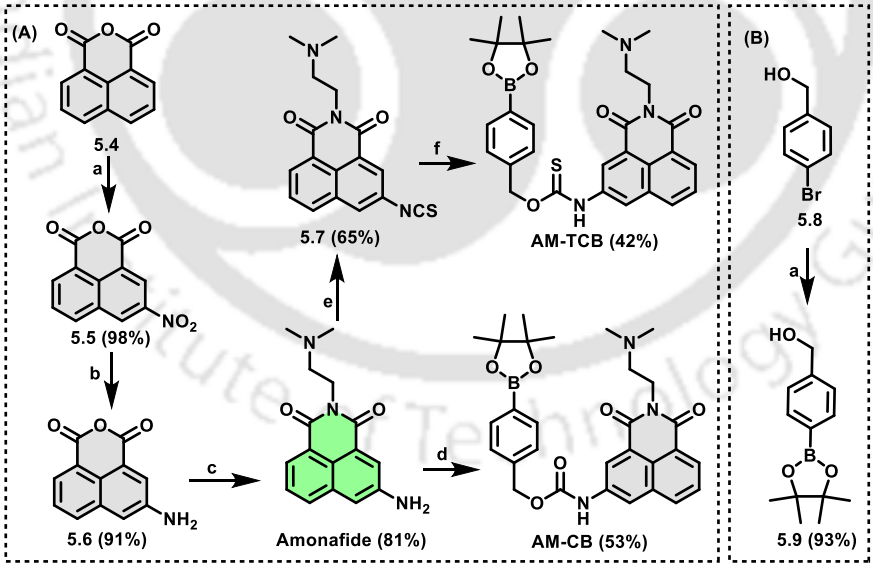

Scheme 5.2. Synthetic schemes to (A) prodrugs **AM-TCB** and **AM-CB**. Reagents and conditions: (A) (a) Conc. HNO_3, conc. H_2SO_4, 0 °C – RT, 2 h; (b) $SnCl_2.2H_2O$, conc. HCl, EtOH, reflux, 3 h; (c) *N,N*-dimethylethylenediamine, EtOH, reflux, 3 h; (d) **5.9**, triphosgene, DMAP, DIPEA, dry DCM, 0 °C – RT, 23 h; (e) CS_2, triethylamine, *p*-TsCl, dry DMF, 0 °C –

TH-3161_176122050

RT, 6 h; (f) **5.9**, DBU, dry THF, 0 °C, 4 h. (B) (a) B_2Pin_2, KOAc, $Pd(dppf)Cl_2$, dry 1,4-dioxane, 85 °C, 12 h.

5.3.2. Absorption and emission spectroscopic studies

The boronate ester-containing prodrugs **AM-TCB** and **AM-CB** were studied for their reactivities towards ROS (H_2O_2) using UV-Vis and fluorescence spectroscopic studies. As shown in Figure 5.2A, the absorption spectrum of pure prodrug **AM-TCB** (5 μM) exhibited the absorption maxima at around 350 nm with a weak hump at 390 nm (Figure 5.2A). A slightly red-shifted and more intense hump (at 405 nm) was observed in the absorption spectrum of the reaction mixture of **AM-TCB** (5 μM) and H_2O_2 (200 μM). Interestingly, the absorption pattern of the reaction mixture matched well with that of pure amonafide (Figure 5.2A). A similar pattern of spectral changes was also observed for the reaction of **AM-CB** (5 μM) with H_2O_2 (200 μM) (Figure 5.2B). The emission intensity of **AM-TCB** in the presence of H_2O_2 is 6-times higher than the emission intensity of **AM-TCB** in the absence of H_2O_2. Considering the absorption band of amonafide at around 405 nm, the prodrugs were excited at that wavelength for monitoring their reactions with H_2O_2 using fluorescence spectrophotometry. While a very weak emission spectrum was observed for the pure **AM-TCB** (5 μM), an intense emission spectrum with an emission maximum at around 575 nm was observed for the reaction mixture of **AM-TCB** (5 μM) with H_2O_2 (200 μM), which resembled well with the emission spectrum of the pure amonafide (Figure 5.2C). A similar emission profile was observed for the reaction of **AM-CB** (5 μM) with H_2O_2 (200 μM) (Figure 5.2D). These initial results indicated the feasible reactions of the boronate ester-based prodrugs with H_2O_2 and the release of the active drug amonafide. With the evidence of the turn-on fluorogenic processes, the kinetics of the drug release process was studied with **AM-TCB** (5 μM) over time (0-240 min) in the presence of H_2O_2 (200 μM) (Figure 5.2E). Interestingly, the emission intensity gradually increased over the time upto 90 min and exhibited a saturation pattern thereafter upto 240 min. However, the emission intensity of the pure prodrug **AM-TCB** (5 μM) in the absence of H_2O_2 was found to be negligibly small and did not increase much over the time (240 min), indicating the stability of the prodrug under the physiological condition (Figure 5.2E). The dependency of the drug release process from **AM-TCB** (5 μM) on the concentration of H_2O_2 was studied next by monitoring the emission response with the varying concentration of H_2O_2 (0-500 μM) with a fixed incubation time

TH-3161_176122050

(90 min) (Figure 5.2F). The emission intensity increased gradually with the increasing concentration of H_2O_2 with a typical saturated emission pattern over the concentration of 200 µM (Figure 5.2F). This observation would have high significance for the applicability of this prodrug for the pathological condition. Considering the relatively higher level of ROS in cancer cells than the normal cells, a higher amount of drug amonafide would be released selectively in the cancer cells.

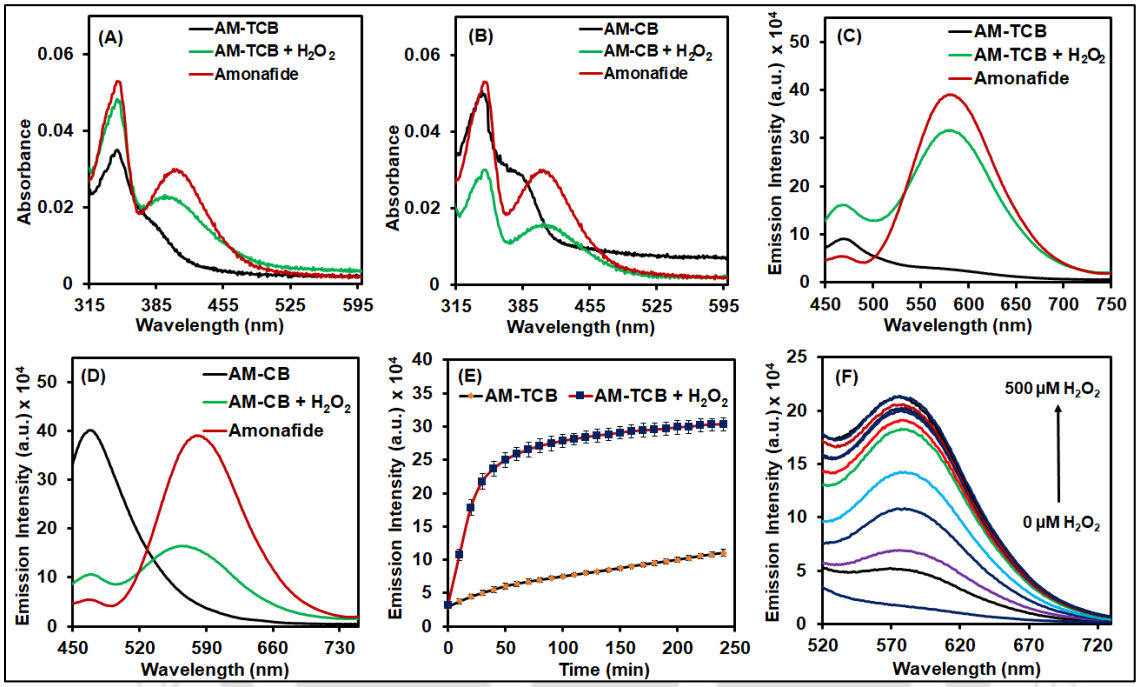

Figure 5.2. Absorption spectra of (A) **AM-TCB** (5 µM) and (B) **AM-CB** (5 µM) in the presence and absence of H_2O_2 (200 µM). Emission spectra of (C) **AM-TCB** (5 µM) and (D) **AM-CB** (5 µM) in the presence and absence of H_2O_2 (200 µM); Pure sample of the free drug amonafide was also analyzed under the identical experimental conditions. (E) Emission spectra of **AM-TCB** (5 µM) in the absence and presence of H_2O_2 (200 µM) with variable time (0-240 min). (F) Emission spectra of **AM-TCB** (5 µM) with variable concentration of H_2O_2 (0-500 µM) with a fixed incubation time of 90 min. The experiment were carried out in phosphate buffered saline (20 mM) of pH 7.4; Excitation wavelength (λ_{ex}) = 405 nm.

5.3.3. Analyte selectivity and pH dependency

With the basic spectroscopic and kinetic results for the prodrug **AM-TCB**, we proceeded to identify the best bio-analyte for the triggered fluorogenic processes. Some of the common oxidants such as H_2O_2, *tert*-butyl hydroperoxide (*t*-Bu-OOH), cumene hydroperoxide (Cum-OOH), potassium superoxide (KO_2), sodium oxychloride (NaOCl), peroxynitrite ($ONOO^-$),

TH-3161_176122050

reducing agents such as reduced glutathione (GSH), L-cysteine (Cys), representative amino acids such as glycine (Gly) and L-alanine (Ala), and inorganic salts such as sodium chloride (NaCl), sodium iodide (NaI) were chosen to see their relative reactivities towards **AM-TCB** as compared to H_2O_2. The turn-on fluorescence emission intensity was measured after the reaction of **AM-TCB** (5 µM) with different bio-analytes (200 µM) after an incubation of 90 min (Figure 5.3A). Interestingly, the highest emission intensity was observed in the presence of H_2O_2, although a few oxidants such as KO_2, NaOCl, and $ONOO^-$ exhibited some emission responses. The emission response was nominal in the presence of other analytes, indicating the highest selectivity of **AM-TCB** towards H_2O_2. With this result in hand, the sensitivity of **AM-TCB** towards H_2O_2 was studied by determining its limit of detection (LOD) as per the standard method using fluorescence spectroscopy.[10, 11] Interestingly, the LOD of **AM-TCB** was found to be as low as 1.0 µM, indicating its high sensitivity towards H_2O_2 (Figure 5.3B). To understand the compatibility of the ROS-triggered activation of **AM-TCB** and its stability at various pH of the medium, the fluorescence emission from **AM-TCB** (5 µM) was monitored with varying pH (4.0–10.0) in both the presence and absence of H_2O_2 (200 µM).

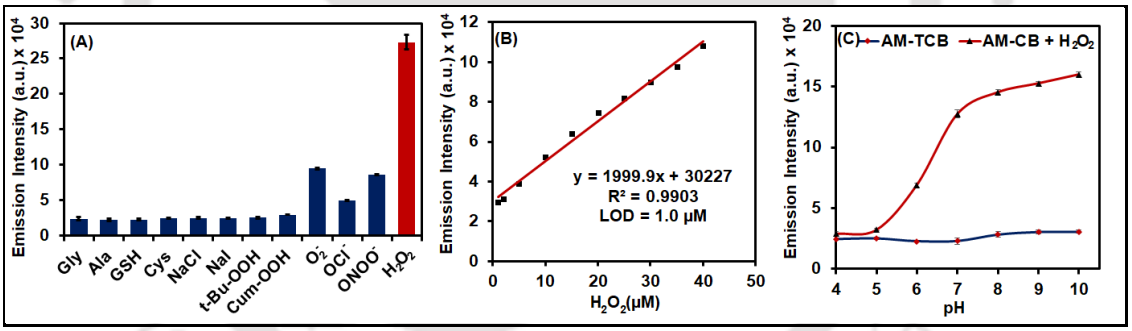

Figure 5.3. (A) Emission response of **AM-TCB** (5 µM) in the presence of different analytes (200 µM) in phosphate-buffered saline (20 mM, pH 7.4) after incubating for 90 min. (B) LOD calculation: emission response of **AM-TCB** (5 µM) with variable concentration of H_2O_2 (0-40 µM) with fixed incubation time of 90 min. (C) Emission intensity of **AM-TCB** (5 µM) in the presence/absence of H_2O_2 (200 µM) with variable pH of the medium (pH: 4-10) after incubating for 90 min. Excitation wavelength (λ_{ex}) = 405 nm.

As shown in Figure 5.3C, very weak emission was observed from **AM-TCB** in the absence of any H_2O_2 over the complete pH range, indicating very good stability of the prodrug over the entire pH range. However, the scenario was different in the presence of H_2O_2. For example, while a very weak emissive response was observed at the lower pH range (4-5),

TH-3161_176122050

emission intensity increased significantly over the pH 6-7 and almost saturated thereafter till pH 10. This indicates the compatibility of the prodrug under physiological and pathophysiological conditions.

5.3.4. H_2S release: absorption and emission studies

After confirming the release of active drug amonafide by the turn-on fluorogenic response from both **AM-TCB** and **AM-CB** in the presence of H_2O_2, feasibility of the release of H_2S from **AM-TCB** was studied by the well-known methylene blue (**MB**) assay. The release of H_2S from the prodrug can be confirmed by the formation of MB dye that exhibits a characteristic absorption band at 670 nm. It is quite evident that, unlike the carbamate-based prodrug **AM-CB**, the release of H_2S could be possible from **AM-TCB** having a thiocarbamate group. However, the H_2O_2-mediated activation of the prodrug **AM-TCB** would release the active drug amonafide along with carbonyl sulfide (COS), which needs a subsequent activation by the enzyme carbonic anhydrase (CA) for the final release of H_2S.[12] Therefore, the MB assay for the determination of the H_2S release profile from **AM-TCB** was performed in the presence of both H_2O_2 and CA. Interestingly, the absorption spectrum observed for **AM-TCB** in the presence of H_2O_2 and CA resembled with that of pure **MB** spectrum (Figure 5.4A). Similarly, as expected, no noticeable formation of **MB** was detected from the carbamate-based prodrug **AM-CB** in the presence of H_2O_2 and CA (Figure 5.4A). In addition, feasibility of the H_2S release from the **AM-TCB** was studied over time (0-4 h) in the presence of H_2O_2 and CA. Interestingly, a sustained release of H_2S from **AM-TCB** was observed over 4 h; however, H_2S was not released from **AM-CB** under similar conditions (Figure 5.4B). The released H_2S from **AM-TCB** was estimated next using the calibration curve generated using Na_2S in the MB assay. As shown in Figure 5.4B, prodrug **AM-TCB** (50 μM) was able to release H_2S in a sustained manner with a maximum of more than 10 μM of H_2S after around 2 h in the presence of H_2O_2 (100 μM) and CA (50 μg/mL). Although the loss of some amount of the generated H_2S cannot be ignored as the estimation method was not carried out under completely inert conditions. Therefore, these results confirm the efficient release of H_2S from **AM-TCB** in a sustained manner over time, which could be helpful in reducing the anti-cancer drug-induced inflammations.

The release of H_2S from **AM-TCB** was further confirmed using the reported nucleophilic substitution-cyclization-based umbelliferone-containing turn-on fluorogenic probe **WSP2**.[13]

TH-3161_176122050

The reaction of **AM-TCB** (20 µM) with H_2O_2 (100 µM) and CA (50 µg/mL) for the generation of H_2S was carried out in the presence of **WSP2** (5 µM) for 2 h. The emission response for the release of free umbelliferone was measured at 448 nm. Interestingly, emission intensity increased significantly at 448 nm, which overlapped with that of free umbelliferone, indicating the release of H_2S from **AM-TCB** in the presence of H_2O_2 and CA (Figure 5.4C). Very negligible emission at 448 nm was observed from **AM-TCB** without H_2O_2 and CA. Moreover, no such enhanced emission from prodrug **AM-CB** under the identical condition supporting the importance of the thiocarbamate linker as a COS-based H_2S donor. As shown in Figure 5.4D, COS is released from the prodrug **AM-TCB** in the presence H_2O_2, which further converts into H_2S in the presence enzyme CA. The H_2S-selective sensor **WSP2** detects the release of H_2S from the prodrug **AM-TCB** and releases the umbelliferone.

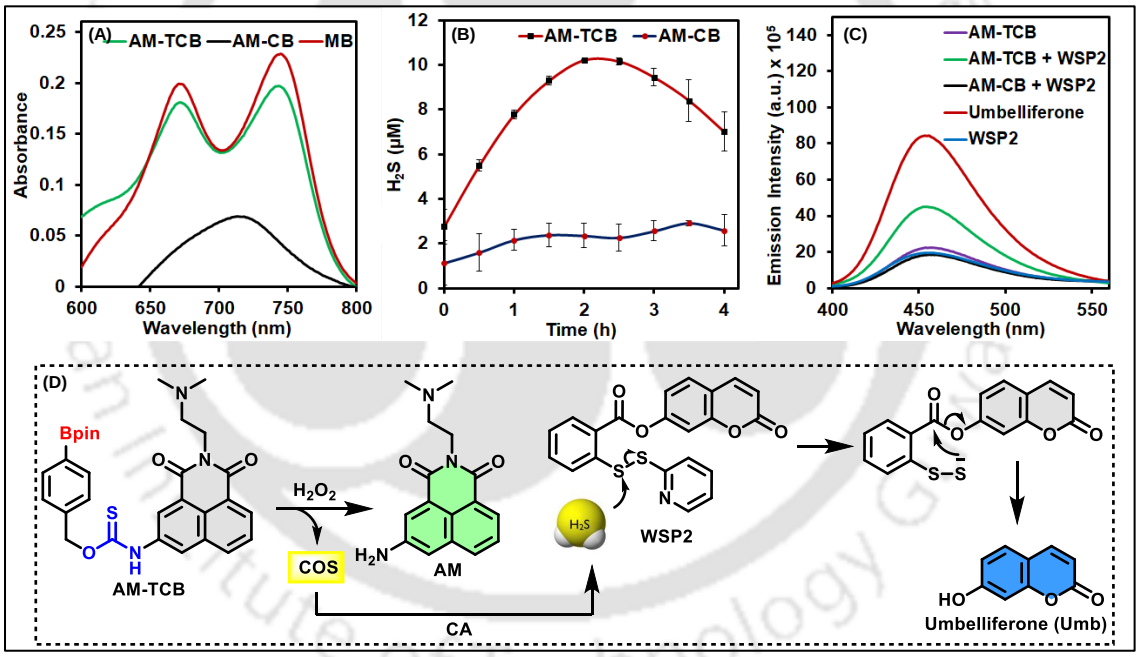

Figure 5.4. (A) Absorption spectra of the MB solution upon introducing **AM-TCB** and **AM-CB** (50 µM) in the presence of H_2O_2 (100 µM) and CA (50 µg/mL); incubation time = 2 h. (B) MB assay depicting the feasibility of time-dependent release of H_2S from **AM-TCB** and **AM-CB** (50 µM) in the presence of H_2O_2 (100 µM) and CA (50 µg/mL) over 4 h. (B) Emission spectra of **WSP2** probe (5 µM) in the presence of prodrug **AM-TCB** and **AM-CB** (20 µM). Pure samples of the released fluorophore umbelliferone, **WSP2**, and **AM-TCB** without H_2O_2 and CA were also analyzed under the identical experimental conditions. (D) Schematic

TH-3161_176122050

representation for the detection of released H_2S from **AM-TCB** using H_2S-selective turn-on fluorogenic probe **WSP2**.

5.3.5. Reaction kinetics and mechanistic insight

After confirming the release of both the fluorogenic drug amonafide and H_2S from the prodrug **AM-TCB**, the drug uncaging process was monitored using the reverse-phase HPLC method. The kinetics was monitored to identify the possible intermediates and the product distributions upon the reaction of **AM-TCB** with H_2O_2. The reaction of **AM-TCB** (20 μM) with H_2O_2 (800 μM) was carried out in PBS (20 mM, pH = 7.4) and the composition of the reaction mixture was analyzed after 2 h. The retention time of pure samples of **AM-TCB** (11.3 min), and amonafide (6.4 min) was optimized before the analysis of the reaction mixtures (Figure 5.5A). Interestingly, the peak of the prodrug **AM-TCB** at 11.3 min almost disappeared upon its reaction with H_2O_2 and a new peak at 6.4 min appeared that exactly matched the retention time of pure amonafide (Figure 5.5A). This observation indicated the ROS-responsive self-immolative release of the active drug amonafide from **AM-TCB**. In addition to the peak of amonafide, two additional peaks were also observed in the reaction mixture at 10.6 and 9.8 min that could be ascribed to the possible intermediates **5.10** and **5.11**, respectively. Monitoring the kinetics upto 4 h indicated that the intermediate **5.10** was generated initially upon the disappearance of the prodrug **AM-TCB**. Over time, the intermediate **5.10** was converted to **5.11**, which was persistent along with the final product amonafide (Figure 5.5B). To identify the intermediates **5.10** and **5.11**, the composition of the reaction mixture after 2 h was analyzed by ESI-MS analysis, which confirmed the presence of **5.10** in the reaction mixture. In 2017, Pluth and co-workers analyzed the kinetics of H_2S release from the ROS-responsive thiocarbamate-based probes and showed that two intermediates can form during the release of H_2S and fluorophore in the presence H_2O_2.[14] Interestingly, two intermediates were observed in HPLC study during drug release from the prodrug **AM-TCB** in the presence of H_2O_2.

Therefore, a plausible reaction mechanism is proposed for the H_2O_2-triggered release of amonafide from the **AM-TCB** and the subsequent CA-responsive release of H_2S (Figure 5.5C). The prodrug **AM-TCB** initially interacted with H_2O_2 and instantly changed into the first intermediate, **5.10**. There can be two possible pathways for the release of drug amonafide and H_2S from the intermediate **5.10**. In path a, through a self-immolation process (1,6-

TH-3161_176122050

elimination), intermediate **5.11** gets generated from intermediate **5.10** and finally, amonafide and COS are generated from intermediate **5.11**, whereas in path b, drug amonafide and COS are released from intermediate **5.10** through the concerted pathway (Figure 5.5C). The released COS is further transformed into H_2S in the presence of CA and hydrolysis of quinonemethide (**QM**) generates the 4-hydroxybenzyl alcohol (**5.12**).

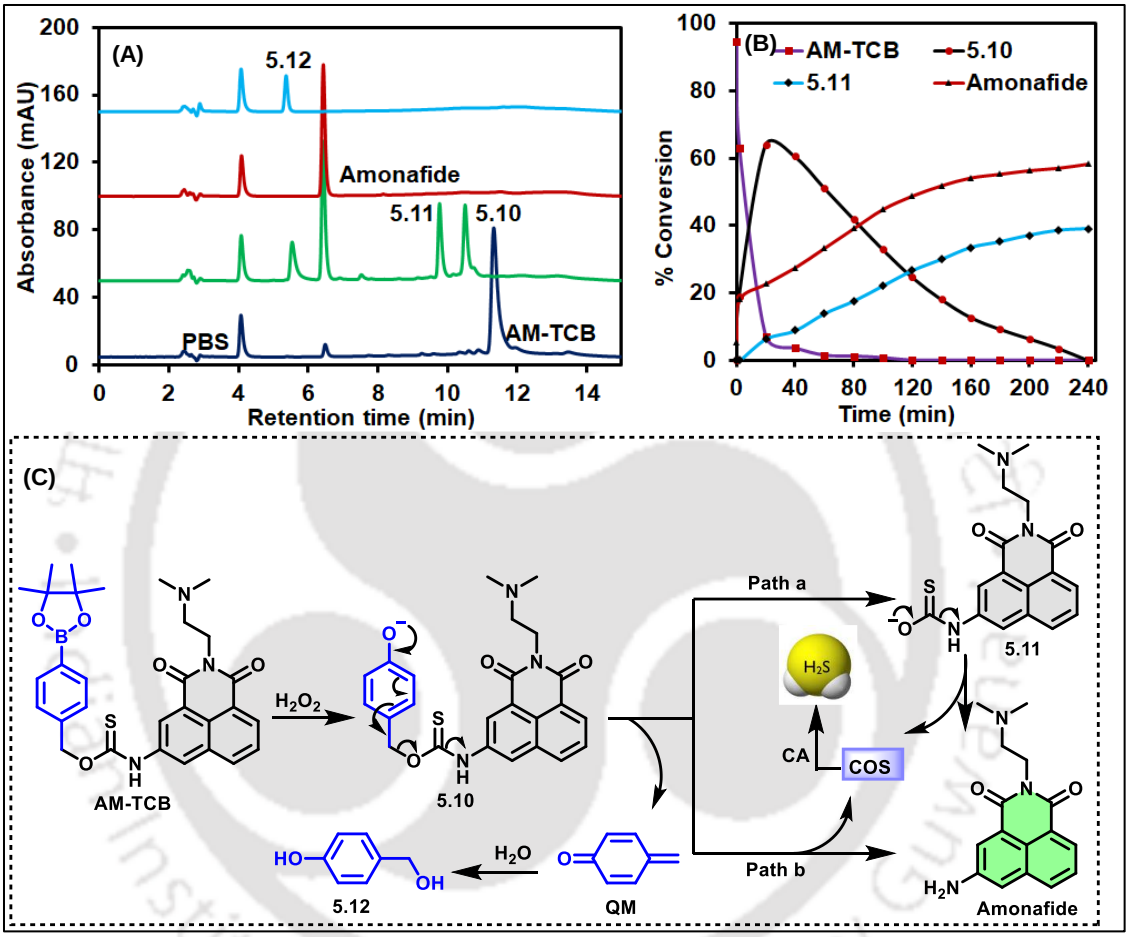

Figure 5.5. (A) HPLC chromatogram of pure **AM-TCB** (a), **AM-TCB** (20 μM) + H_2O_2 (800 μM) (b), amonafide (c), and **5.12** (d). Lanes (a-d) were visualized at 254 nm. Reaction was carried out in PBS (20 mM, pH = 7.4) and analyzed after 2 h. (B) Relative peak areas of various components present in the reaction mixture of **AM-TCB** (20 μM) + H_2O_2 (800 μM) over 4 h were monitored for the % conversion upon measuring the peak area of all the compounds (**AM-TCB**, **5.10**, **5.11**, amonafide) at 254 nm. (C) Proposed mechanism for the feasibility of H_2O_2-triggered fluorogenic drug release from the **AM-TCB**.

TH-3161_176122050

5.3.6. Anti-cancer activity and fluorescence microscopic studies

In order to investigate the relative anti-cancer activity of the prodrug (**AM-TCB**) and the active drug amonafide, their dose-dependent (0, 5, 10, and 25 µM) anti-proliferative activities were studied in cancer cell lines (HeLa and MDA-MB-231) and a normal cell line (HEK-293) using the conventional MTT assay. The prodrug **AM-TCB** showed almost similar anti-proliferative activity as the parent drug amonafide upto 5 µM and exhibited lesser toxicity than amonafide upto 25 µM in both the cancer cell lines (Figure 5.6A and B). The relatively lower anti-proliferative activity of **AM-TCB** than the active drug amonafide could be due to (a) the gradual release of amonafide from the prodrug **AM-TCB** in the presence of endogenous ROS and (b) the cytoprotective activity of the released H_2S. Interestingly, the active drug amonafide showed potent cytotoxicity in a normal cell line (HEK-293) dose-dependently, whereas prodrug **AM-TCB** exhibited significantly lower toxicity (Figure 5.6C). The significant difference in cytotoxicity between the prodrug **AM-TCB** and the active drug amonafide in normal cells could be due to the cytoprotective effects of H_2S in minimizing the side-effects of amonafide.

Furthermore, the fluorescence microscopic studies were carried out in HeLa cells to investigate the release of the active drug from the prodrug **AM-TCB** (25 µM) (Figure 5.6D). A significant green emission was observed when cells were treated with prodrug **AM-TCB**, indicating the release of the active drug amonafide in the presence of endogenous ROS. However, very negligible green emission was observed when cells were pretreated with ROS-scavengers such as *N*-acetyl cysteine (NAC, 2 mM) followed by prodrug **AM-TCB** (25 µM) treatment. This result further supported the selectivity of the prodrug **AM-TCB** towards ROS. The adjuvant release of H_2S from the prodrug **AM-TCB** (25 µM) was next investigated in the cellular medium using an H_2S-selective turn-un fluorogenic probe **WSP2** (5 µM) (Figure 5.6E). While the treatment of **WSP2** in HeLa cells led to the negligible blue emission, the co-treatment of **WSP2** and **AM-TCB** led to intense blue emission due to the release of umbelliferone from the **WSP2** in the presence of released H_2S from the prodrug **AM-TCB** (Figure 5.6E). Moreover, very weak blue emission was observed upon the pre-treatment of intracellular ROS quencher NAC and DL-propargyl glycine (PAG) inhibitor of cystathionine-γ-lyase for H_2S generation. This observation clearly indicated the release of H_2S from the prodrug **AM-TCB**

TH-3161_176122050

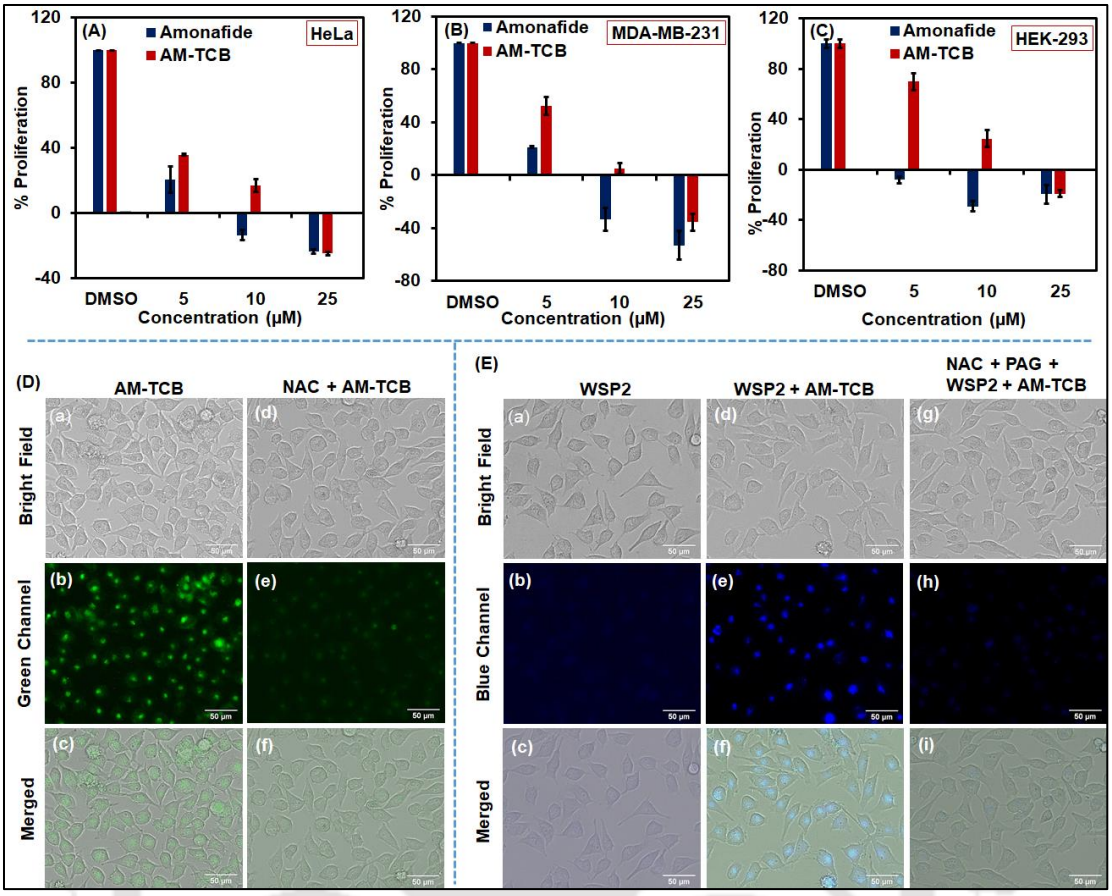

Figure 5.6. The dose-dependent anti-proliferative activity of amonafide and **AM-TCB** in (A) HeLa (B) MDA-MB-231 and (C) HEK-293 cells after an incubation of 48 h. (D) Fluorescence microscopy images (bright field, green channel, and merged) of HeLa cells in the presence of **AM-TCB** (25 μM) for the endogenous ROS-triggered fluorogenic drug release (a-c). The cells were pre-treated with NAC (2 mM) to quench the endogenous ROS followed by the treatment of **AM-TCB** (25 μM) (d-f). (E) Fluorescence microscopy images (bright field, blue channel, and merged) of HeLa cells for the detection of released H_2S from **AM-TCB** (25 μM) using the H_2S-selective turn-on fluorogenic probe **WSP2** (5 μM). Scale bar: 50 μm.

5.4. Conclusions

In summary, we describe herein the design and synthesis of the H_2O_2-responsive turn-on fluorogenic prodrug (**AM-TCB**) of the anti-cancer drug amonafide along with the gasotransmitter H_2S. The adjuvant delivery of the active drug amonafide and H_2S were confirmed in the aqueous as well as cellular medium. Rapid reactivity of the boronate ester moiety in **AM-TCB** with H_2O_2 activates the prodrug and self-immolative processes control the drug release profile along with H_2S with turn-on fluorescence both in the aqueous and

TH-3161_176122050

cellular medium. Interestingly, the significantly lower cytotoxicity of the prodrug **AM-TCB** than the active drug amonafide in normal cells supports the cytoprotective effects of the released H_2S and selectivity of the prodrug **AM-TCB** towards cancer cells over normal cells, which would help in ameliorating the amonafide-induced side-effects during anti-cancer treatments.

5.5. Experimental section

5.5.1. Materials and methods

All the chemicals and solvents were purchased either from Sigma Aldrich, Merck, or reputed local suppliers. All the solvents were either distilled or dried following the standard method before using in reactions and chemicals were used without further purification. Thin layer chromatographic (TLC) analyses were carried out on pre-coated silica gel on aluminum sheets and the compounds were visualized by irradiation with UV or fluorescent light and stained by iodine. Organic solvents used for the chromatographic separations were distilled before use. The melting point of the synthesized compounds was recorded in a Büchi B540 melting point apparatus and the values are uncorrected. The NMR spectra were recorded with a Bruker Ascend^{TM} 400 MHz, 500 MHz, and 600 MHz NMR sectrometers. Chemical shifts are cited with respect to Me_4Si as an internal standard. Mass spectra were obtained using an Agilent 6520 Accurate- Mass Quadrupole Time-of-Flight (Q-TOF) LC/MS spectrometer.

5.5.2. Synthesis of the prodrugs AM-TCB and AM-CB

Synthesis of compound 5.5[15]

To a stirred solution of compound **5.4** (5.00 g, 25.20 mmol) in conc. H_2SO_4 (10 mL) was added to the mixture of conc HNO_3 (1.20 mL) and conc. H_2SO_4 (5 mL) dropwise at ice-cold conditions. After 30 min, the reaction mixture was stirred at room temperature for another 90 min to complete the reaction. The progress of the reaction was monitored by TLC analysis. Upon completion of the reaction, cold water (200 mL) was added slowly to obtain the precipitate and filtered off to get the crude product, which was washed with water several times to remove the unwanted materials and dried under the vacuum to obtain compound **5.5** as a greenish-yellow solid with a quantitive yield. The crude compound was used in the next step without purification. R_f = 0.3 (30% ethyl acetate in pet ether). ^{1}H NMR (600 MHz, DMSO-d_6): δ (ppm) = 9.54 (t, J = 2.9 Hz, 1H), 8.94 (t, J = 2.5 Hz, 1H), 8.84 (dd, J_1 = 8.4, J_2

TH-3161_176122050

= 3.0 Hz, 1H), 8.73 – 8.69 (m, 1H), 8.12 – 8.06 (m, 1H). ^{13}C NMR (150 MHz, DMSO-d_6): δ (ppm) = 160.3, 160.0, 146.3, 137.7, 135.9, 132.2, 131.3, 131.1, 129.9, 124.7, 121.8, 120.3.

Synthesis of compound 5.6[9]

To a stirred solution of compound **5.5** (5.00 g, 20.50 mmol) in absolute ethanol (10 mL) was added $SnCl_2.2H_2O$ (23.00 g, 102.50 mmol) in conc. HCl (17.5 mL) dropwise at room temperature. The reaction mixture was stirred at 80 °C for 3 h to complete the reaction. The progress of the reaction was monitored by TLC analysis. Upon completion of the reaction, it was cooled to room temperature followed by the precipitate being filtered off and washed with water several times to remove unwanted materials. Finally, the crude product was dried under the vacuum to obtain compound **5.6** as a yellow solid with a quantitive yield. The crude compound was used in the next step without purification. R_f = 0.3 (50% ethyl acetate in pet ether). ^{1}H NMR (600 MHz, DMSO-d_6): δ (ppm) = 8.19 (d, *J* = 8.3 Hz, 1H), 8.14 (d, *J* = 7.2 Hz, 1H), 8.03 (d, *J* = 2.3 Hz, 1H), 7.69 (t, *J* = 7.8 Hz, 1H), 7.53 (d, *J* = 2.4 Hz, 1H), 5.82 (s, 2H). ^{13}C NMR (150 MHz, DMSO-d_6): δ (ppm) = 161.3, 161.2, 133.7, 133.4, 128.5, 127.9, 124.2, 124.1, 119.9, 119.0.

Synthesis of amonafide[16]

To a stirred solution of compound **5.6** (2.00 g, 9.36 mmol) in distilled ethanol (30 mL) was added *N*,*N*-dimethylethylenediamine (1.54 mL, 14.04 mmol) at room temperature and refluxed for 3 h. The progress of the reaction was monitored by TLC analysis. Upon completion, the solvent was evaporated under reduced pressure. The crude product was further purified by column chromatography using aluminum oxide (basic) as a stationary phase and 2% methanol in DCM as eluents to afford amonafide as a yellow solid. R_f = 0.3 (2% methanol in DCM); Yield: 2.15 g (81%). ^{1}H NMR (600 MHz, $CDCl_3$): δ (ppm) = 8.30 (dd, J_1 = 7.3 Hz, J_2 = 1.3 Hz, 1H), 7.99 (t, *J* = 2.0 Hz, 1H), 7.91 (d, *J* = 8.1 Hz, 1H), 7.59 (t, *J* = 7.8 Hz, 1H), 7.26 (d, *J* = 4.3 Hz, 1H), 4.31 (t, *J* = 7.1 Hz, 2H), 4.18 (s, 2H), 2.65 (t, *J* = 7.1 Hz, 2H), 2.36 (s, 6H). ^{13}C NMR (150 MHz, $CDCl_3$): δ (ppm) = 164.7, 164.4, 145.4, 133.5, 131.9, 127.6, 127.3, 123.7, 122.7, 122.6, 122.1, 114.1, 57.1, 45.9, 38.3.

Synthesis of compound 5.7

To a stirred solution of amonafide (0.50 g, 1.76 mmol) in dry DMF (4 mL) was added triethylamine (2.45 mL, 17.64 mmol) dropwise at 0 °C. After 30 min, carbon disulfide (1.65

TH-3161_176122050

mL, 35.27 mmol) was added dropwise at 0 °C and the reaction mixture was stirred at room temperature for 5 h. The progress of the reaction was monitored by TLC analysis. Upon consumption of the amonafide completely, *p*-toluenesulfonyl chloride (0.50 g, 2.62 mmol) was added at room temperature and stirred for 30 min. Upon completion of the reaction, excess carbon disulfide and triethylamine were removed under reduced pressure, and the crude product was further purified by 230-400 mesh silica gel column chromatography using ethyl acetate as the eluent to afford the pure product **5.7** as a yellow solid. R_f = 0.4 (80% EtOAc in pet. ether); Yield: (0.37 g, 65%). ^{1}H NMR (500 MHz, $CDCl_3$): δ (ppm) = 8.58 (d, *J* = 7.3 Hz, 1H), 8.40 (d, *J* = 1.9 Hz, 1H), 8.13 (d, *J* = 8.3 Hz, 1H), 7.98 (d, *J* = 2.1 Hz, 1H), 7.79 (t, *J* = 7.8 Hz, 1H), 4.32 (t, *J* = 6.9 Hz, 2H), 2.65 (t, *J* = 6.9 Hz, 2H), 2.34 (s, 6H). ^{13}C NMR (150 MHz, $CDCl_3$): δ (ppm) = 163.8, 163.2, 139.3, 133.3, 132.3, 131.7, 131.0, 128.8, 128.8, 128.4, 126.6, 124.7, 123.0, 57.1, 45.9, 38.5. ESI-MS *m/z* calcd. for $C_{17}H_{16}N_3O_2S$ $[M+H]^+$ = 326.0963, obs. 326.0979.

Synthesis of compound 5.9[17]

The mixture of compound **5.8** (2.00 g, 10.69 mmol) and bis(pinacolato)diboron (4.00 g, 16.04 mmol), Pd(dppf)Cl_2 (0.78 g, 1.06 mmol) and KOAc (3.10 g, 32.08 mmol) was dissolved in dry 1,4-dioxane (100 mL) under argon atmosphere at room temperature. The reaction mixture was stirred at 85 ºC for 12 h. The progress of the reaction was monitored by TLC analysis. Upon completion, the solvent was evaporated under reduced pressure and the mixture was diluted with ethyl acetate (50 ml). The reaction mixture was filtered through a celite pad to remove the undesired materials and washed with ethyl acetate (5×20 ml). The combined organic layer was washed sequentially with water and brine solution (3×20 ml). Finally, the organic layer was dried over anhydrous sodium sulfate and concentrated under reduced pressure to obtain the crude compound. The crude product was purified by silica gel (230-400 mesh) column chromatography using 20% ethyl acetate in pet. ether as a mobile phase to afford the pure product **5.9** as a white solid. R_f = 0.5 (20% ethyl acetate in pet. ether); Yield: 2.30 g (93%). ^{1}H NMR ($CDCl_3$, 400 MHz) δ (ppm): 7.80 (d, *J* = 7.9 Hz, 2H), 7.36 (d, *J* = 7.7 Hz, 2H), 4.71 (s, 2H), 1.35 (s, 12H). ^{13}C NMR (150 MHz, $CDCl_3$) δ (ppm): 144.1, 135.2, 126.2, 83.9, 65.4, 25.0.

TH-3161_176122050

Synthesis of AM-CB

To a stirred solution of amonafide (0.20 g, 0.70 mmol), triphosgene (0.10 g, 0.35 mmol), and DMAP (5.0 mg, 0.07 mmol) in dry DCM (20 mL) was added DIPEA (0.37 mL, 2.10 mmol) dropwise at 0 °C under argon atmosphere and the reaction mixture was stirred at room temperature. After 3 h, the solution of compound **5.9** (0.25 g, 1.05 mmol) in dry DCM (5 mL) was added dropwise at 0 °C and the reaction mixture was stirred at room temperature for 20 h. The progress of the reaction was monitored by TLC analysis. Upon completion, the solvent was evaporated under reduced pressure. The crude product was purified by neutral alumina column chromatography using 20% MeOH in EtOAc as eluent to afford the pure product **AM-CB** as a yellow solid. R_f = 0.4 (100% EtOAc); Yield: (0.19 g, 53%). M.P. = 213-215 °C. ^{1}H NMR (600 MHz, $CDCl_3$): δ (ppm) = 8.55 (s, 1H), 8.33 (d, *J* = 7.2 Hz, 1H), 8.24 (s, 1H), 8.24 (s, 1H), 7.92 (s, 1H), 7.88 (d, *J* = 7.2 Hz, 1 H), 7.86 (d, *J* = 7.6 Hz, 2H) 7.63 (t, *J* = 7.7 Hz, 1H), 7.49 (d, *J* = 7.6 Hz, 2H), 5.27 (s, 2H), 4.35 (t, *J* = 6.2 Hz, 2H), 2.80 (t, *J* = 6.2 Hz, 2H), 2.40 (s, 6H), 1.35 (s, 12H). ^{13}C NMR (150 MHz, $CDCl_3$): δ (ppm) = 164.4, 163.8, 153.5, 139.0, 137.1, 135.2, 132.5, 129.5, 127.7, 127.5, 124.2, 123.2, 122.7, 122.3, 119.5, 84.1, 67.3, 57.8, 45.9, 37.9, 25.0. ESI-MS *m/z* calcd. for $C_{30}H_{35}BN_3O_6$ $[M+H]^+$ = 544.2619, obs. 544.2631.

Synthesis of AM-TCB

To a stirred solution of compound **5.9** (0.10 g, 0.42 mmol) and **5.7** (0.14 g, 0.42 mmol) in a dry THF (4 mL) was added DBU (0.08 mL, 0.51 mmol) in dry THF (2 mL) dropwise at 0 °C under argon atmosphere. The progress of the reaction was monitored by TLC analysis. Upon completion of the reaction, the solvent was evaporated under reduced pressure. The crude compound was further purified by 230-400 mesh silica gel column chromatography using ethyl acetate as the eluent to afford the pure product **AM-TCB** as a yellow solid. R_f = 0.3 (100% EtOAc); Yield: (0.10 g, 42%). M.P. = 110-112 °C. ^{1}H NMR (400 MHz, $CDCl_3$): δ (ppm) = 10.12 (s, 1H), 8.61 (s, 1H), 8.39 (d, *J* = 7.2 Hz, 1H), 8.12 (s, 1H), 7.93-7.78 (m, 3H), 7.63 (t, *J* = 7.8 Hz, 1H), 7.48 (d, *J* = 7.3 Hz, 2H), 5.61 (s, 2H), 4.32 (t, *J* = 6.1 Hz, 2H), 2.79 (s, 2H), 2.39 (s, 6H), 1.36 (s, 12H). ^{13}C NMR (150 MHz, $CDCl_3$): δ (ppm) = 164.1, 163.5, 138.3, 135.2, 133.7, 131.8, 130.3, 129.4, 128.9, 127.8, 127.6, 126.2, 125.5, 125.2, 123.6, 122.3, 84.1, 57.8, 45.9, 38.0, 29.8, 25.0. ESI-MS *m/z* calcd. for $C_{30}H_{35}BN_3O_5S$ $[M+H]^+$ = 560.2390, obs. 560.2403.

TH-3161_176122050

5.5.3. UV-Visible and fluorescence spectroscopic studies

All the stock solution of probes and the released fluorophores were prepared in spectroscopy grade DMSO (note: 20% THF was added with DMSO for the **AM-CB** prodrug to dissolve it completely) and the stock solution of H_2O_2 was prepared in mili-Q water. All the spectroscopic studies were performed under physiological conditions (PBS, 20 mM, pH = 7.4). PBS with higher pH (9 and 10) were prepared by adding 1N NaOH solution to the buffer and lower pH (4 and 5) by adding 1N HCl. Samples for absorption and emission spectroscopic measurements were carried out in quartz cuvettes (1.0 ml). UV-Vis spectroscopic analyses were performed on a Lambda 45 UV-Vis spectrophotometer (Agilent) and fluorescence emission spectra were recorded on a Fluoromax-4 spectrophotometer (FluoroMax-4-Horiba). For prodrugs **AM-TCB** and **AM-CB**, λ_{ex} = 405 nm and λ_{em} = 430-750 nm with slit width = 10/10 nm were used in the fluorescence emission spectroscopic studies. The selectivity of the prodrug **AM-TCB** (5 μM) towards H_2O_2 (200 μM) was carried out over different analytes such as *t*-Bu-OOH, Cum-OOH, GSH, Cys, Gly, Ala, NaCl, and NaI prepared in milli-Q water. KO_2 was used as a source of O_2^- and $ONOO^-$ was prepared from H_2O_2 prior to its use in the experiment.[18] The probe was initially incubated for 90 min with the analytes (200 μM) and the emission intensity was measured. All the experiments were carried out in PBS (20 mM, pH = 7.4).

5.5.4. Determination of LOD of the prodrug

LOD of the prodrug **AM-TCB** was determined using fluorescence titration. The detection limit was calculated using the equation, LOD = 3σ/K, where σ is the standard deviation of blank measurements (without H_2O_2) and K is the slope of emission intensity versus H_2O_2 concentration. To get the standard deviation of the blank measurements, the emission intensity of the **AM-TCB** (5 μM) was measured 10 times in the absence of H_2O_2 and found to be 700.8. For the determination of slope (K), the emission spectra were measured at different concentrations of H_2O_2 (1-40 μM) after incubating the reaction mixture for 90 min and found to be 1999.9.

5.5.5. Analysis of reaction kinetics using reverse phase HPLC method

Purity of the synthesized compounds was analyzed by analytical high-performance liquid chromatography (HPLC), Agilent 1220 infinity II LC system using a reverse phase C_{18} column (Luna®, 250 × 4.6 mm, 5 μm). HPLC grade Methanol and millipore water was used

TH-3161_176122050

as mobile phase and HPLC chromatogram of the prodrug **AM-TCB** and free drug amonafide were detected by PDA detector at 254, 280, 405 nm (as applicable). To a solution of prodrug **AM-TCB** (20 μM) in PBS (20 mM, pH = 7.4) was added H_2O_2 (800 μM) at room temperature and the reaction mixture was injected into the system at different time intervals to monitor the progress of the reaction. The samples were injected using a flow rate of 1.0 ml/min with a linear gradient (70–30% v/v) H_2O/MeOH (0–7 min), followed by isocratic 30% v/v H_2O/MeOH (7–10 min), finally, (30–70% v/v) H_2O/MeOH (10–15 min) and 0.05% of TFA was used in water.

5.5.6. Measurement of H_2S release from AM-TCB (MB assay)[19, 20]

A 10 mM stock solution of **AM-TCB** (or **AM-CB**) was prepared in DMSO immediately prior to use. H_2O_2 (10 mM) was prepared in PBS (20 mM, pH = 7.4). Carbonic anhydrase (CA) was prepared at 10 mg/mL in PBS buffer (pH = 7.4). Methylene blue cocktail was prepared as follows: $FeCl_3$ (20 mM, 1.2 M HCl), $Zn(OAc)_2$ (100 mM in dd water), and *N*,*N*-dimethyl-*p*-phenylene diamine (20 mM, 7.2 M HCl).

To a 10 mL vial containing 4960 μL of freshly prepared PBS (pH 7.4) was added stock solutions of carbonic anhydrase (25 μL), H_2O_2 (5 μL), and **AM-TCB** (or **AM-CB**) (10 μL). The resulting mixture was then stirred at 37 °C, and at various time points (0.0 h, 0.5 h, 1.0 h, 1.5 h, 2.0 h, 2.5 h, 3.0 h, 3.5 h, 4.0 h), a 500 μL aliquot was removed and added to the MB solution (200 μL $FeCl_3$ and 200 μL *N*,*N*-dimethyl-*p*-phenylene diamine, 100 μL $Zn(OAc)_2$). After incubating for 15 min in the dark, absorbance were recorded at 670 nm. The H_2S concentration of each sample was calculated against a calibration curve, which was obtained using the known concentrations of $Na_2S.9H_2O$ solution under identical conditions.

5.5.7. Detection of the released H_2S using the turn-on fluorogenic probe WSP2[13]

To a solution of **AM-TCB** or **AM-CB** (20 μM) in PBS (20 mM, pH = 7.4) were added H_2O_2 (100 μM), CA (50 μg/mL), and **WSP2** (5 μM) and incubated for 2 h at 37 °C. The emission intensity was measured at 350-650 nm (λ_{ex} = 322 nm, slit = 3/3 nm). The emission intensity of pure samples **WSP2** and umbelliferone were measured under similar conditions.

5.5.8. Cell culture

The triple-negative breast cancer (TNBC) cells (MDA-MB-231), Human cervical cancer cells (HeLa), and Human Embryonic Kidney cells (HEK-293) were obtained from the National Centre for Cell Science (NCCS), Pune, India. The cells were cultured in DMEM

TH-3161_176122050

medium (Gibco) supplemented with 10% (v/v) FBS (Gibco) and 1% Pen-Strep (Gibco). Cells were cultured as a monolayer in a humidified incubator at 37 ºC in the presence of 5% CO_2 level.

5.5.9. Cell viability assay

The synthesized prodrugs were screened for their anti-proliferative activities using the conventional MTT assay in MDA-MB-231, HeLa, and HEK-293 cell lines. MDA-MB-231, HeLa, and HEK-293 cells were seeded in 96-well culture plates at a density of 2×10^4, 1×10^4, and 2×10^4 cells/100 µL per well, respectively and treated with the freshly prepared test compounds amonafide (5, 10, and 25 µM), **AM-TCB** (5, 10, and 25 µM), and **AM-CB** (5, 10, and 25 µM) for 0 h (control) and 48 h (experimental), respectively. At the end of the treatment period, 100 µL of 5 mg/mL of MTT was added to the plate (control) and incubated for 4 h. Following the 4 h incubation, the reagent from the plate was removed and the purple formazan crystals were dissolved using 100 µL of DMSO (Avra Synthesis Pvt Ltd) and the absorbance at 570 nm was measured using a microplate reader (Thermo Scientific™ Multiskan™ GO microplate reader). In the experimental set, a similar MTT treatment protocol was followed only after 48 h. The mean ΔOD values were calculated by the subtraction of mean OD values of 0 h plate (control) from the mean OD values of identical wells at 48 h plate (experimental) and the percentage proliferation was calculated keeping the mean ΔOD of untreated control as 100%.

5.5.10. Fluorescence microscopic studies

HeLa cells were cultured in high glucose DMEM medium supplemented with 10% (v/v) fetal bovine serum (FBS) and 1% penicillin/streptomycin at 37 °C under a 5% CO_2 atmosphere. Cells were then plated (1.5×10^6 cells per plate) in 35 mm cell culture Petri dishes containing 2 mL of DMEM and incubated at 37 °C under 5% CO_2 for 24 h. The confluent cells were washed with DPBS and finally incubated with **AM-TCB** (25 µM) for 5 h. After washing the cells with DPBS (3 times), cellular morphology was carefully observed and imaged using Bio-Rad ZOE™ fluorescent cell imager under a bright field and green channel. A negative control experiment was performed upon the pre-treatment of cells with NAC (2 mM) for 1h and 30 min to quench the endogenous ROS. The cells were washed with DPBS (3 times) and treated with **AM-TCB** (25 µM).

TH-3161_176122050

For the detection of the release of H_2S from **AM-TCB**, the HeLa cells were grown like the above condition, and the cells were treated with **WSP2** (5 μM) for 1 h and cells were imaged under a blue channel after washing to understand the detection of H_2S. For studying the released H_2S from **AM-TCB**, the cells were treated with **WSP2** (5 μM) for 1 h and the cells were washed with DPBS (3 times) and treated with **AM-TCB** (25 μM) for 5 h. The cells were washed finally with DPBS and imaged under bright field, blue, and green channels. The contribution of the endogenous ROS and H_2S towards the triggered H_2S release process, the negative control experiment was carried out by the pre-incubation of cells with NAC (2 mM) and PAG (20 μM) for 1 h and 30 min. The cells were washed and treated with **AM-TCB** (25 μM) + **WSP2** (5 μM) and incubated for 5 h. The cells were washed finally with DPBS (3 times) and imaged under bright field, blue, and green channels.

5.6. References

1. Q. Hu, R. D. Yammani, H. Brown-Harding, D. R. Soto-Pantoja, L. B. Poole and J. C. Lukesh III, *Redox Biol.*, 2022, **53**, 102338.
2. S. L. Allen, J. E. Kolitz, A. S. Lundberg, J. M. Bennett, R. L. Capizzi and D. R. Budman, *Leuk. Res.*, 2010, **34**, 487-491.
3. S. L. Allen and A. S. Lundberg, *Expert Opin. Invest. Drugs*, 2011, **20**, 995-1003.
4. L. Cui, Y. Zhong, W. Zhu, Y. Xu and X. Qian, *Chem. Commun.* , 2010, **46**, 7121-7123.
5. J. Zhao, M. Lu, H. Lai, H. Lu, J. Lalevée, C. Barner-Kowollik, M. H. Stenzel and P. Xiao, *Biomacromolecules*, 2018, **19**, 481-489.
6. C. Ge, X. Di, S. Han, M. Wang, X. Qian, Z. Su, H.-K. Liu and Y. Qian, *Chem. Commun.*, 2021, **57**, 1931-1934.
7. E. Calatrava-Pérez, L. A. Marchetti, G. J. McManus, D. M. Lynch, R. B. Elmes, D. C. Williams, T. Gunnlaugsson and E. M. Scanlan, *Chem. Eur. J.*, 2022, **28**, e202103858.
8. S. K. Mahato, P. Barman, M. Badirujjaman and K. P. Bhabak, *Chem. Commun.*, 2023.
9. K. A. MacGregor, M. J. Robertson, K. A. Young, L. von Kleist, W. Stahlschmidt, A. Whiting, N. Chau, P. J. Robinson, V. Haucke and A. McCluskey, *J. Med. Chem.*, 2014, **57**, 131-143.

TH-3161_176122050

10. A. Sufian, D. Bhattacherjee, T. Mishra and K. P. Bhabak, *Dyes Pigm.*, 2021, **191**, 109363.
11. A. Sufian, D. Bhattacherjee, P. Barman, A. Srivastava, R. P. Thummer and K. P. Bhabak, *Chem. Commun.*, 2022, **58**, 7833-7836.
12. Y. Zhao, S. G. Bolton and M. D. Pluth, *Org. Lett.*, 2017, **19**, 2278-2281.
13. S. K. Mahato, D. Bhattacherjee, P. Barman and K. P. Bhabak, *J. Mater. Chem. B*, 2022, **10**, 2183-2193.
14. Y. Zhao, H. A. Henthorn and M. D. Pluth, *J. Am. Chem. Soc.*, 2017, **139**, 16365-16376.
15. Q. Wang, G. Li, Z. Liu, X. Tan, Z. Ding, J. Ma, L. Li, D. Li, J. Han and B. Wang, *Eur. J. Inorg. Chem.*, 2018, **2018**, 4442-4451.
16. L. Cui, Y. Zhong, W. Zhu, Y. Xu and X. Qian, *Chem. Commun.*, 2010, **46**, 7121-7123.
17. D. C. Ebner, J. T. Bagdanoff, E. M. Ferreira, R. M. McFadden, D. D. Caspi, R. M. Trend and B. M. Stoltz, *Chem. Eur. J.*, 2009, **15**, 12978-12992.
18. K. P. Bhabak and G. Mugesh, *Chem. Eur. J.*, 2010, **16**, 1175-1185.
19. Q. Hu, R. D. Yammani, H. Brown-Harding, D. R. Soto-Pantoja, L. B. Poole and J. C. Lukesh III, *Redox Biol.*, 2022, **53**, 102338.
20. Y. Hu, X. Li, Y. Fang, W. Shi, X. Li, W. Chen, M. Xian and H. Ma, *Chem. Sci.*, 2019, **10**, 7690-7694.

TH-3161_176122050

Thesis Summary and Future Perspectives

The present thesis entitled "***Development of ROS-responsive Turn-on Fluorogenic Prodrugs for the Delivery of Anti-inflammatory and Anti-cancer Drugs along with Hydrogen Sulfide***" describes the development of turn-on fluorogenic prodrugs of anti-inflammatory and anti-cancer drugs, which are activated in the presence of ROS such as H_2O_2 with the concomitant delivery of H_2S. Our designed prodrugs are non-fluorogenic or weakly fluorescent in the absence of ROS and exhibit strong fluorescence properties in the presence of ROS.

The level of ROS is higher in cancer and inflammatory diseases; therefore, it is very important to estimate the level of intracellular ROS in normal as well as pathological conditions. Since fluorescent molecules are well-adapted tools for estimating the concentration of intracellular ROS; therefore, researchers have developed ROS-responsive fluorogenic probes to investigate the concentration of intracellular ROS in normal as well as diseased cells (**chapter 1**). As a ROS-responsive moiety, boronate ester or boronic acid was connected to the fluorophore *via* different linkers such as direct, ether, carbonate, carbamate, and so on for developing such probes. However, a proper rationalization is missing for developing ROS-responsive probes or prodrugs for understanding the reactivity and sensitivity of the probes towards H_2O_2. Since marketed anti-cancer and anti-inflammatory drugs have several genuine side-effects; therefore, developing ROS-responsive fluorogenic prodrugs are very important, which may reduce the side-effects of conventional drugs and help to monitor the drug release in living cells. Although few ROS-responsive non-fluorogenic anti-inflammatory prodrugs were developed for the treatment of inflammatory diseases (**chapter 1**). However, ROS-responsive fluorogenic anti-inflammatory prodrugs for non-steroidal anti-inflammatory drugs (NSAIDs) are yet to be developed. NSAIDs are most widely used for the treatment of inflammatory diseases and prolonged use of NSAIDs leads to several side-effects such as gastrointestinal (GI) damage and stomach ulcer. H_2S has several pharmacological properties such as antioxidant, anti-inflammatory, cytoprotective, vasodilatory, and so on. Therefore, researchers have developed NSAID-H_2S conjugate, where a controlled H_2S donor (ADT-OH) was connected to the NSAIDs to reduce their side effects (GI toxicity, renal, and ulcer) and to improve the anti-inflammatory properties of corresponding drugs. However, those are non-fluorogenic and incompatible with activating

TH-3161_176122050

the prodrug due to the absence of any triggering unit. Several prolonged H_2S donors such as hydrolysis-based, thiol-triggered, and ROS-responsive probes (non-fluorogenic, fluorogenic) have developed over time to investigate the biological importance of H_2S. Interestingly, it showed cytoprotective and other pharmacological properties. It is to be noted that ROS-responsive fluorogenic prodrugs of anti-cancer drugs have developed over time to reduce the side-effects of conventional drugs. However, adjuvant drug delivery with H_2S is very rare. Therefore, it is important to develop ROS-responsive fluorogenic prodrugs of anti-inflammatory and anti-cancer drugs in such a way that H_2S would be released along with it in the presence of H_2O_2.

In search of understanding the importance of fluorophores and different linkers for the development of ROS-responsive probes/prodrugs, we designed total nine probes using three different fluorophores (coumarin, naphthalimide, and fluorescein unit) connected with boronate ester with three different linkers (direct, ether, and carbonate) as shown in **chapter 2**. According to the spectroscopic studies in aqueous medium, directly-coupled boronate ester probes are more sensitive than linker-based probes towards H_2O_2, whereas self-immolative probes are capable of releasing the fluorophore in a sustainable manner. Fluorescence microscopic studies also further confirmed the higher sensitivity of the directly-coupled probe than self-immolative-based probes. These results inspired us to develop ROS-responsive linker-based turn-on fluorogenic prodrugs for the delivery of the drug in a sustainable manner. .

In **chapter 3**, we developed a peroxide-responsive fluorogenic prodrug **DCI-ROS** of NSAID (diclofenac), where the drug will be released sustainably with turn-on NIR fluorescence in the presence of H_2O_2. We synthesized the designed prodrug **DCI-ROS** using a multi-step organic synthetic strategy. The spectroscopic studies indicated that the drug was released from the prodrug sustainably in the presence of H_2O_2. Moreover, fluorescence microscopic studies in MDA-MB-231 cells confirmed the release of the fluorophore in the presence of endogenous ROS. The cellular studies in inflammation-induced macrophage cells RAW 264.7 indicated that our prodrug **DCI-ROS** is more selective towards inflammatory sites over normal tissues. Finally, western blot analysis confirmed the release of the active drug from the prodrug in the presence of endogenous ROS by inhibiting COX-2 as the parent drug diclofenac.

TH-3161_176122050

Next, in **chapter 4**, we have developed a peroxide-responsive turn-on fluorogenic prodrug **DCF-HS** of diclofenac along with the delivery of H_2S. In this chapter, we synthesized the prodrug **DCF-HS** using a multi-step organic synthetic strategy. Several spectroscopic, HPLC, and cellular studies were carried out to investigate the release of the drug and H_2S from the prodrug and its activity. Spectroscopic and HPLC studies confirmed the release of the fluorophore and drug in a sustainable manner. Moreover, cellular studies confirmed the release of fluorophore and H_2S. In addition, the anti-inflammatory effect was observed from western blot analysis where prodrug **DCF-HS** inhibited the COX-2 as the parent drug diclofenac, indicating the release of the drug in the presence of intracellular ROS. The released H_2S may show the cytoprotective effect, which will reduce the side-effects of diclofenac.

Amonafide is a very potent fluorogenic anti-cancer drug. However, it has several side-effects; most importantly, a toxic *N*-acetyl metabolite is formed by reacting its free amino group with the *N*-acetyl transferase 2 (NAT2) enzyme, which reduces the bioavailability and increases the side-effects of the drug. Therefore, in **chapter 5**, we have developed a ROS-responsive fluorogenic prodrug **AM-TCB** of anti-cancer drug amonafide along with the delivery of H_2S. We synthesized the prodrug **AM-TCB** and carried out the several studies such as spectroscopic, HPLC and cellular studies to investigate the release of the drug and H_2S and its activity. The results from several studies supported the release of the drug and H_2S in the presence of H_2O_2. The anti-proliferative activity was carried out to investigate the cytotoxicity of the prodrug **AM-TCB** towards cancer cell lines (HeLa and MDA-MB-231) and in a representative normal cell line (HEK-293). While the prodrug showed almost similar anti-cancer activity in cancer cells as the parent drug amonafide and exhibited cytoprotective effects on normal cells due to the co-delivery of H_2S.

In summary, we developed peroxide-responsive fluorogenic prodrugs of anti-inflammatory and anti-cancer drugs along with the delivery of H_2S. These prodrugs are suitable to monitor the drug release in living cells. Moreover, they may reduce the side-effects and improve the bioavailability of conventional drugs. The release of the drug and H_2S were confirmed by spectroscopic, HPLC, and cellular studies. Moreover, the activity of the released drug and H_2S from the prodrug was investigated by *in vitro* studies. In addition, some more aspects

TH-3161_176122050

might be considered as future perspectives of the present thesis to the innovative and attractive prodrugs forward up to their applications.

1. To understand their activity in animal models, further *in vivo* studies can be carried out for all the developed prodrugs (**DCI-ROS**, **DCF-HS**, and **AM-TCB**).
2. We observed solubility issues for **DCI-ROS** and **DCF-HS** in aqueous as well as cellular media. Therefore, the water-soluble fluorophore or hydrophilic unit can be connected to the prodrug to overcome the solubility issues prior to designing a second generation of these prodrugs.
3. Organelle-targeting ROS-responsive turn-on fluorogenic prodrugs for anti-cancer and anti-inflammatory drugs along with H_2S can be developed further.
4. Finally, ROS-responsive prodrugs along with H_2S delivery for the treatment of other diseases such as thyroid, Alzheimer, diabetes, and neurodegenerative diseases can be developed to reduce the side-effects and improve the bioavailability of the corresponding drugs.

TH-3161_176122050

List of publications and conferences

Thesis Publications

1. **Sufian, A.**; Barman, P.; Badirujjaman, Md.; Bhabak, K. P.* Stimuli-activatable hybrid prodrug for the self-immolative delivery of non-steroidal anti-inflammatory drug diclofenac and hydrogen sulfide with turn-on near-infrared fluorescence. (manuscript under preparation).

2. **Sufian, A.**; Barman, P.; Badirujjaman, Md.; Bhabak, K. P.* Dual-stimuli-activatable hybrid prodrug for the self-immolative delivery of an anti-cancer drug and hydrogen sulfide with turn-on fluorescence. *Chem. Eur. J.* (manuscript under minor revision).

3. **Sufian, A.**; Bhattacherjee, D.; Barman, P.; Srivastava, A.; Thummer, R. P.; Bhabak, K. P.* Stimuli-responsive prodrug of non-steroidal anti-inflammatory drug diclofenac: self-immolative drug release with turn-on near-infrared fluorescence. *Chem. Commun*., **2022**, *58*, 7833-7836.

4. **Sufian, A**.; Bhattacherjee, D.; Mishra, T.; Bhabak, K. P.* Peroxide-responsive boronate ester-coupled turn-on fluorogenic probes: Direct linkers supersede selfimmolative linkers for sensing peroxides. *Dyes Pigm.*, **2021**, *191*, 109363.

Other Publications

1. Banerjee, K.; Bhattacherjee, D.; Mahato, S. K.; **Sufian, A.**, Bhabak, K. P.* Benzimidazole-and imidazole-Fused selenazolium and selenazinium selenocyanates: ionic organoselenium compounds with efficient peroxide scavenging activities. *Inorganic Chemistry*, **2021**, 60, *17*, 12984–12999.

2. Bhattacherjee, D.; **Sufian, A.**; Mahato, S. K.; Begum, S.; Banerjee, K.; De, S.; Srivastava, H. K.* Bhabak, K. P.* Trisulfides over disulfides: highly selective synthetic strategies, anti-proliferative activities and sustained H_2S release profiles. *Chem. Commun.*, **2019**, *55*, 13534-13537.

Conferences

1. **Sufian, A.**; Bhabak, K. P. Stimuli-responsive Prodrug of Diclofenac: Sustained Drug Release with Turn-on Near-infrared Fluorescence. Participated as an oral

TH-3161_176122050

presenter at **Emerging Trends in Chemical Sciences** (**ETCS- 2023**) held during March 02 – 04, 2023, at the North-Eastern Hill University, Shillong, India.

2. **Sufian, A.**; Bhabak, K. P. Hydrogen Peroxide-responsive Turn-on Fluoregenic Probes: Direct Linkers Supersede Self-immolative Linkers for Sensing H_2O_2. Participated as poster presenter at **Frontiers in Chemical Sciences** (**FICS, 2022**) held during December 02-04, 2022, at the Indian Institute of Technology Guwahati, India.

3. **Sufian, A.**; Bhabak, K. P. Hydrogen Peroxide-responsive Turn-on Fluoregenic Probes: Direct Linkers Supersede Self-immolative Linkers for Sensing H_2O_2. Participated as a poster presenter at **North-East Research Conclave** (**NERC**) held during May 20-22, 2022, at the Indian Institute of Technology Guwahati, India.

4. **Sufian, A.**; Bhabak, K. P. Hydrogen Peroxide-responsive Turn-on Fluoregenic Probes: Direct Linkers Supersede Self-immolative Linkers for Sensing H_2O_2. Participated as a poster presenter at **28th National Symposium in Chemistry** (**CRSI-NSC-28**) held during March 25-27, 2022, at the Indian Institute of Technology Guwahati, India.

5. **Sufian, A.**; Bhabak, K. P. Hydrogen Peroxide-responsive Turn-on Fluoregenic Probes: Direct Linkers Supersede Self-immolative Linkers for Sensing H_2O_2. Participated as an oral presenter at **Research Conclave (RIC-2022)**, held during January 20 – 23, 2022, at the Indian Institute of Technology Guwahati, India.

TH-3161_176122050

Supplementary data of chapter 2

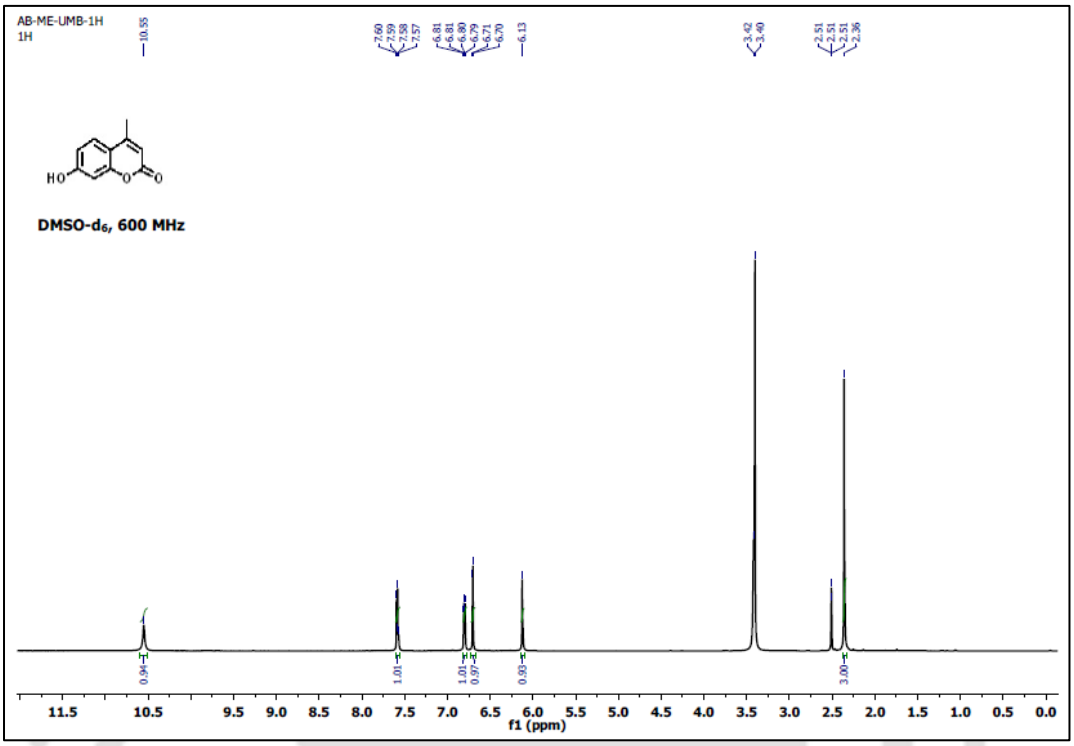

Figure A3.1: ^{1}H NMR spectrum (DMSO-d_6, 600 MHz) of compound **2.10**.

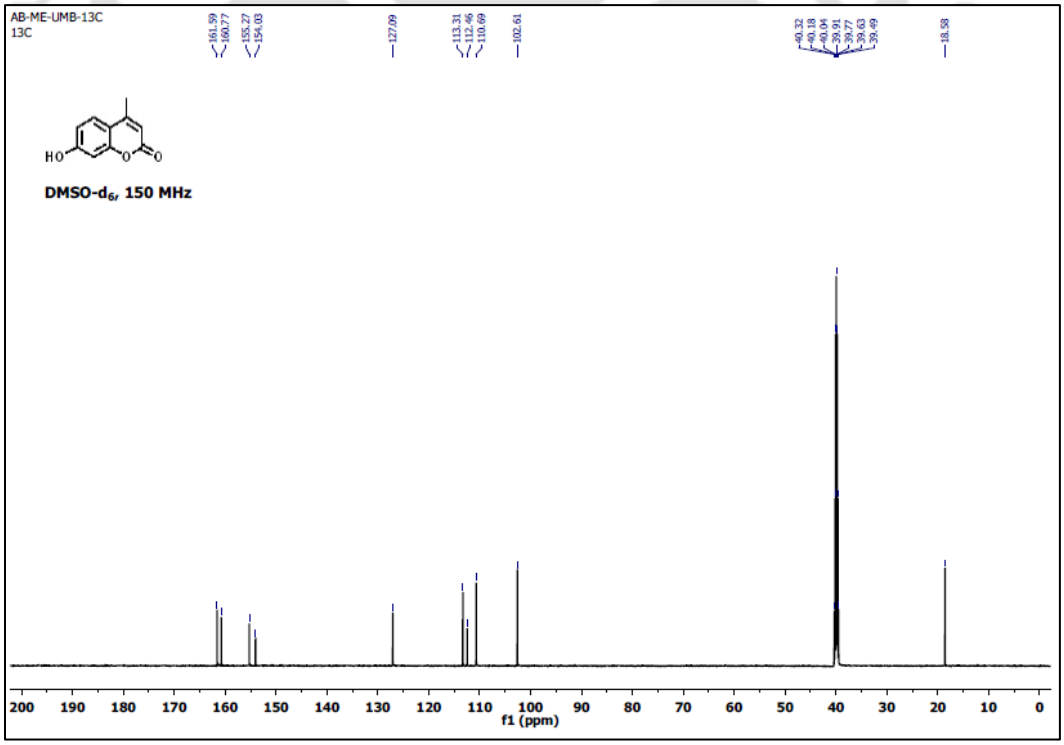

Figure A3.2: ^{13}C NMR spectrum (DMSO-d_6, 150 MHz) of compound **2.10**.

TH-3161_176122050

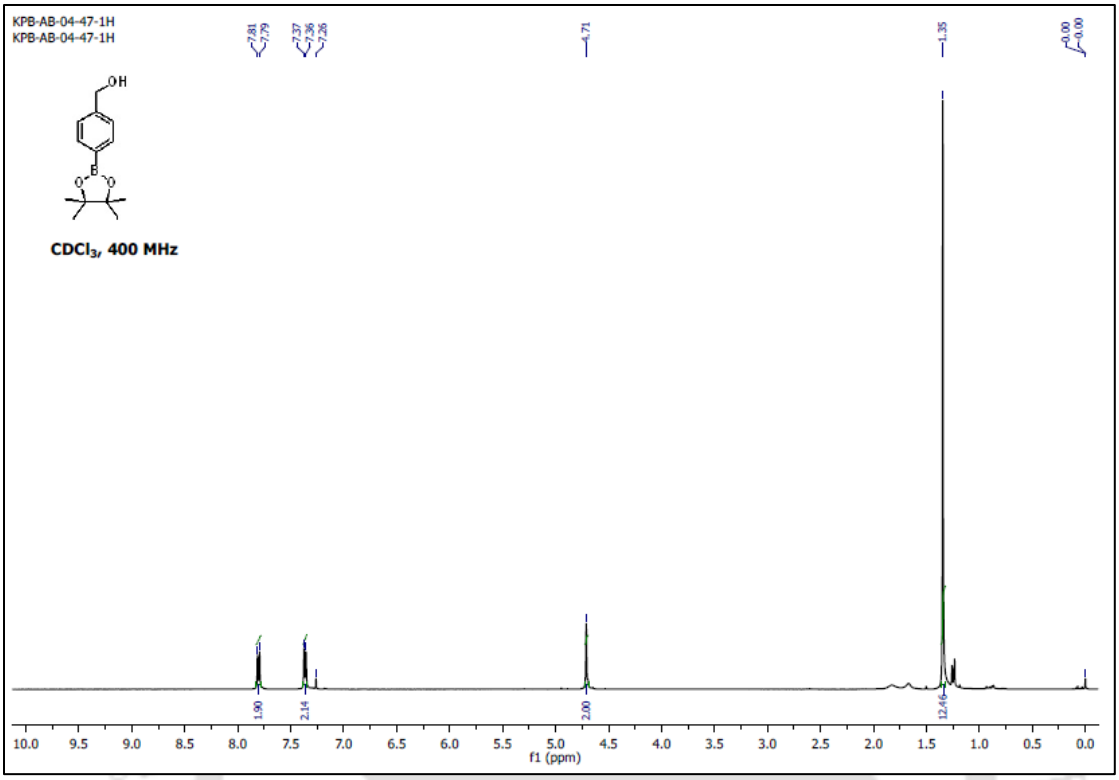

Figure A3.3: ^{1}H NMR spectrum ($CDCl_3$, 400 MHz) of compound **2.18**.

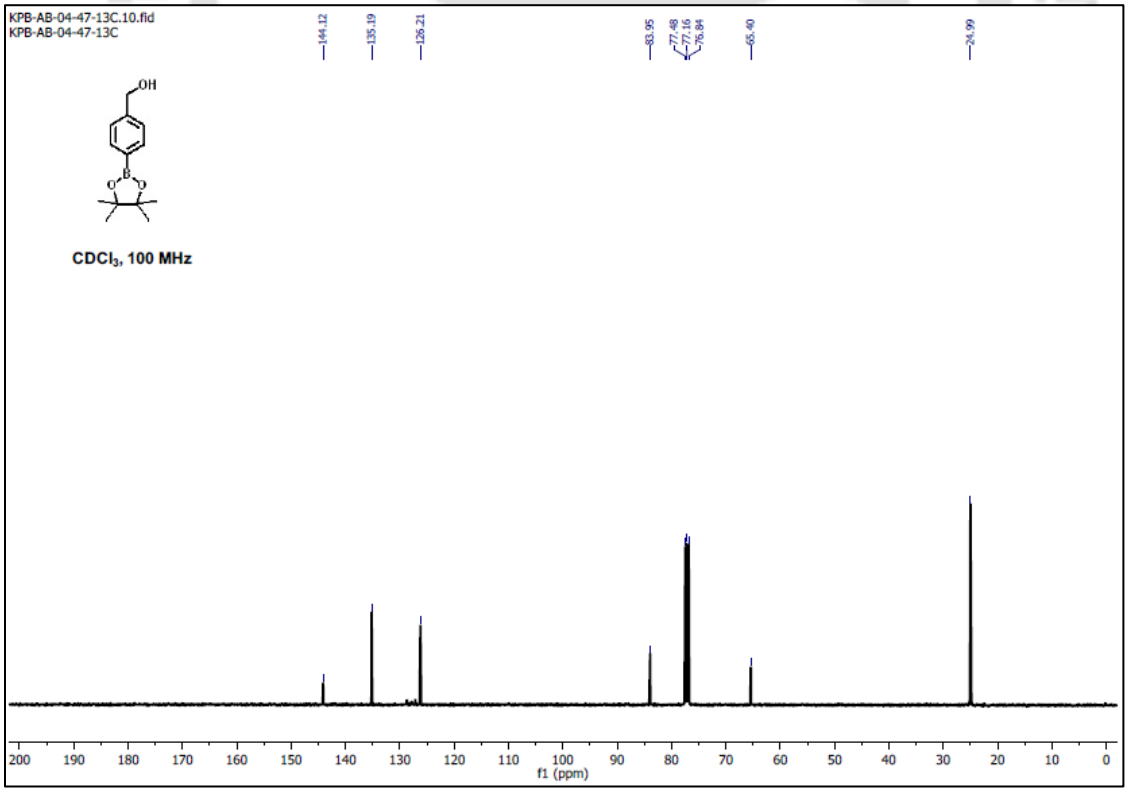

Figure A3.4: ^{13}C NMR spectrum ($CDCl_3$, 100 MHz) of compound **2.18**.

TH-3161_176122050

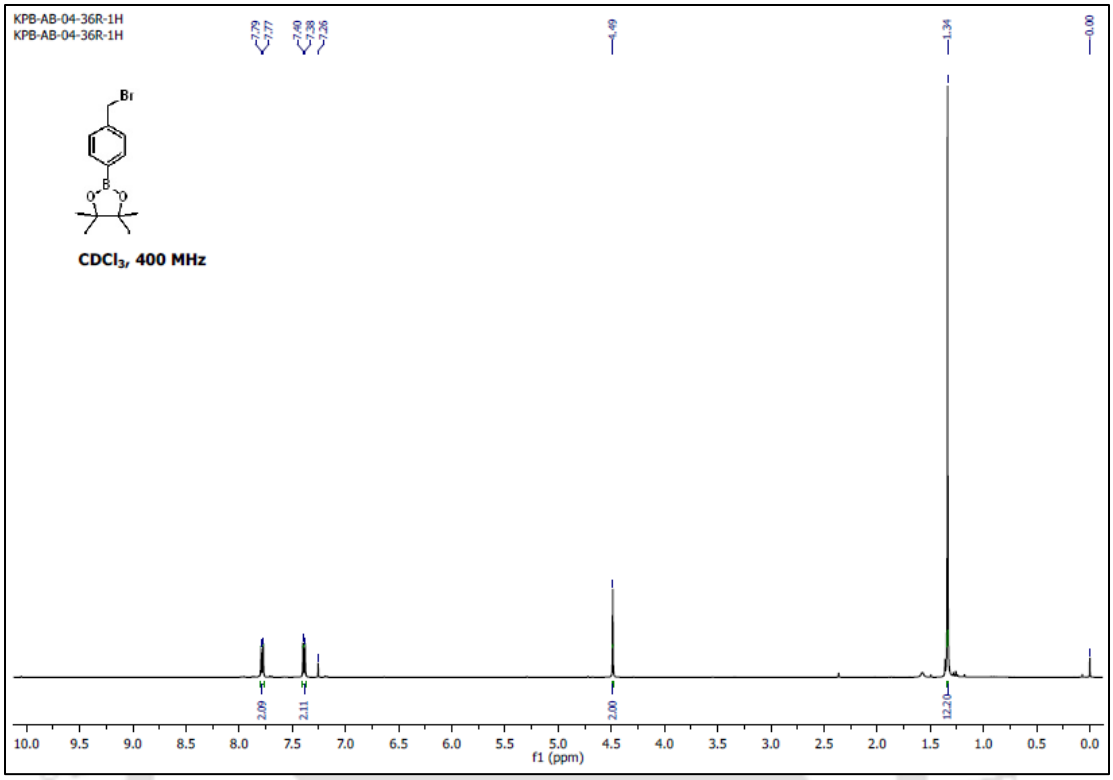

Figure A3.5: ^{1}H NMR spectrum ($CDCl_3$, 400 MHz) of compound **2.19**.

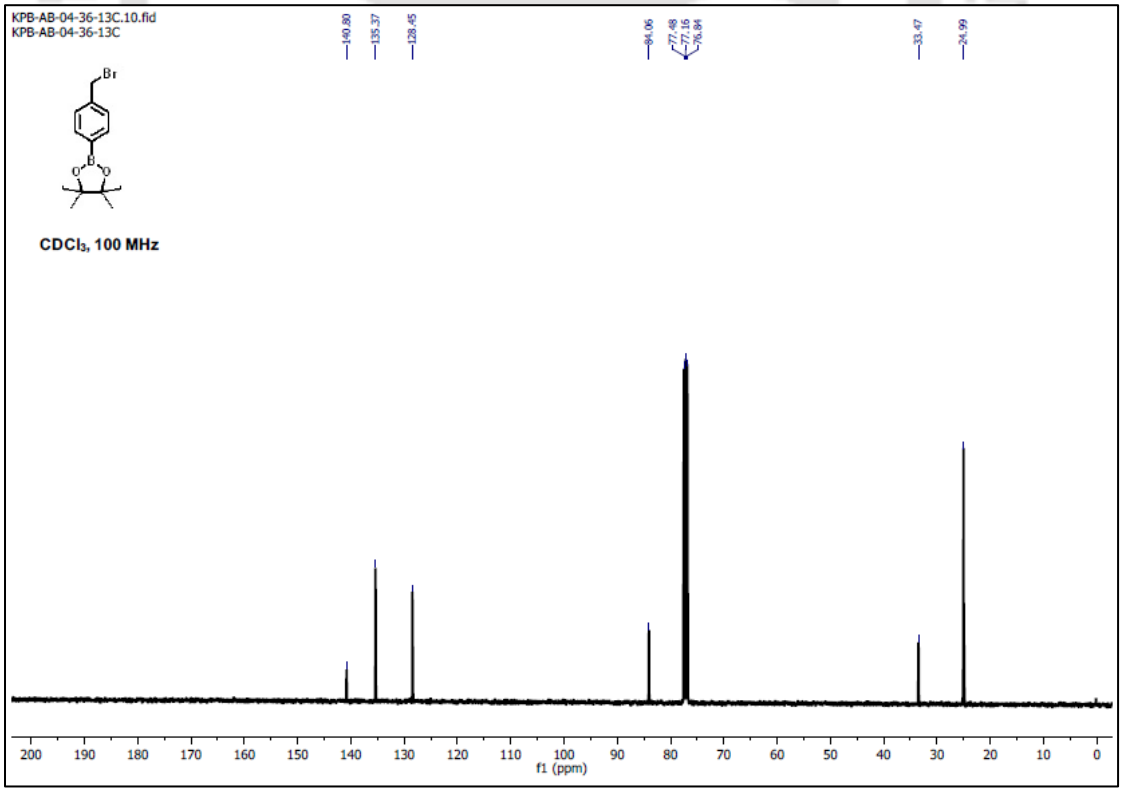

Figure A3.6: ^{13}C NMR spectrum ($CDCl_3$, 100 MHz) of compound **2.19**.

TH-3161_176122050

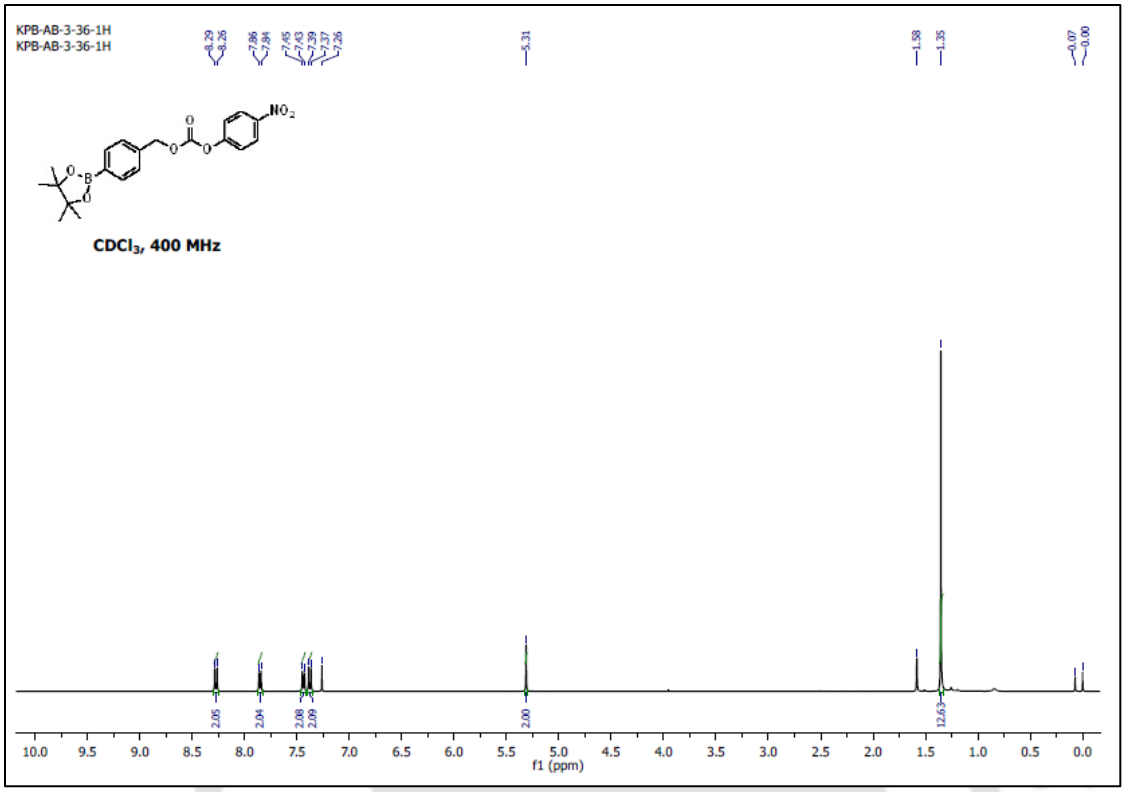

Figure A3.7: ^{1}H NMR spectrum ($CDCl_3$, 400 MHz) of compound **2.20**.

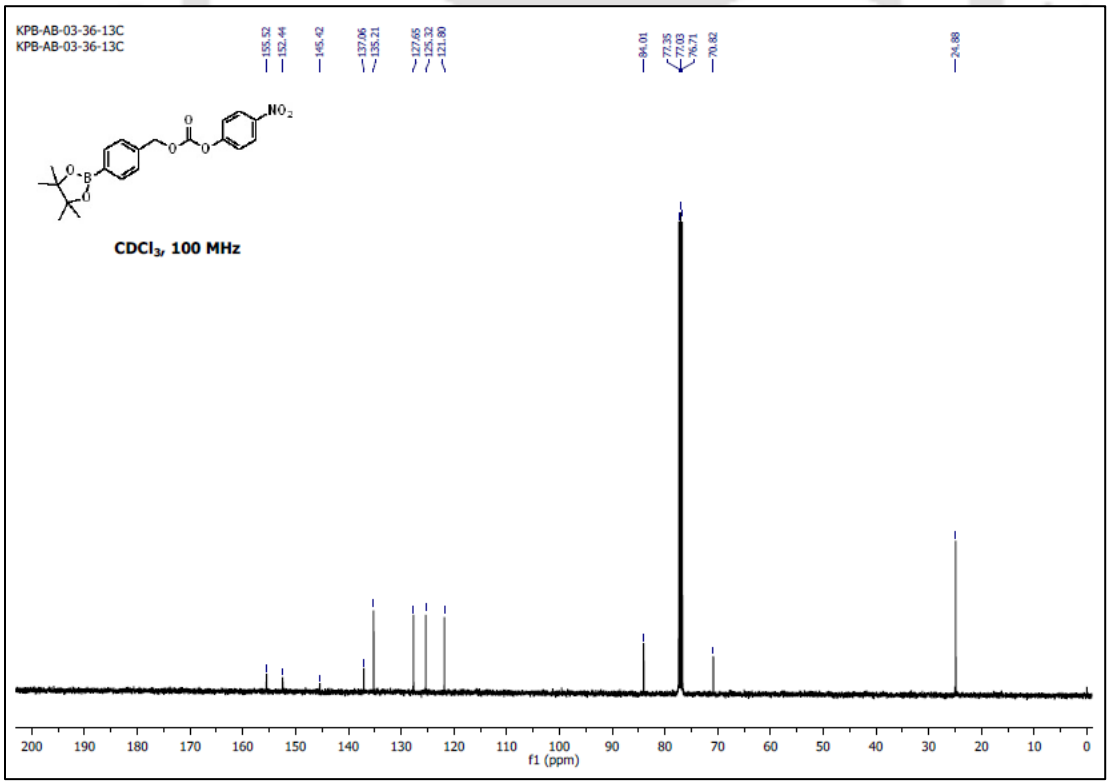

Figure A3.8: ^{13}C NMR spectrum ($CDCl_3$, 100 MHz) of compound **2.20**.

TH-3161_176122050

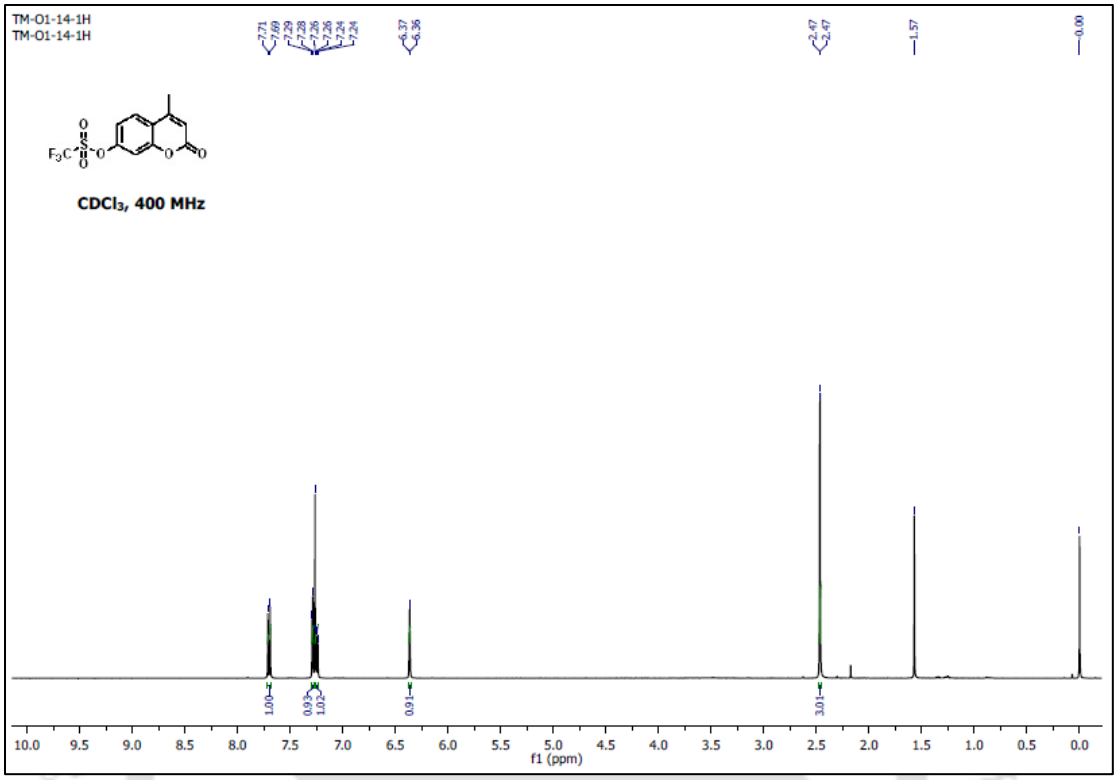

Figure A3.9: ^{1}H NMR spectrum ($CDCl_3$, 400 MHz) of compound **2.21**.

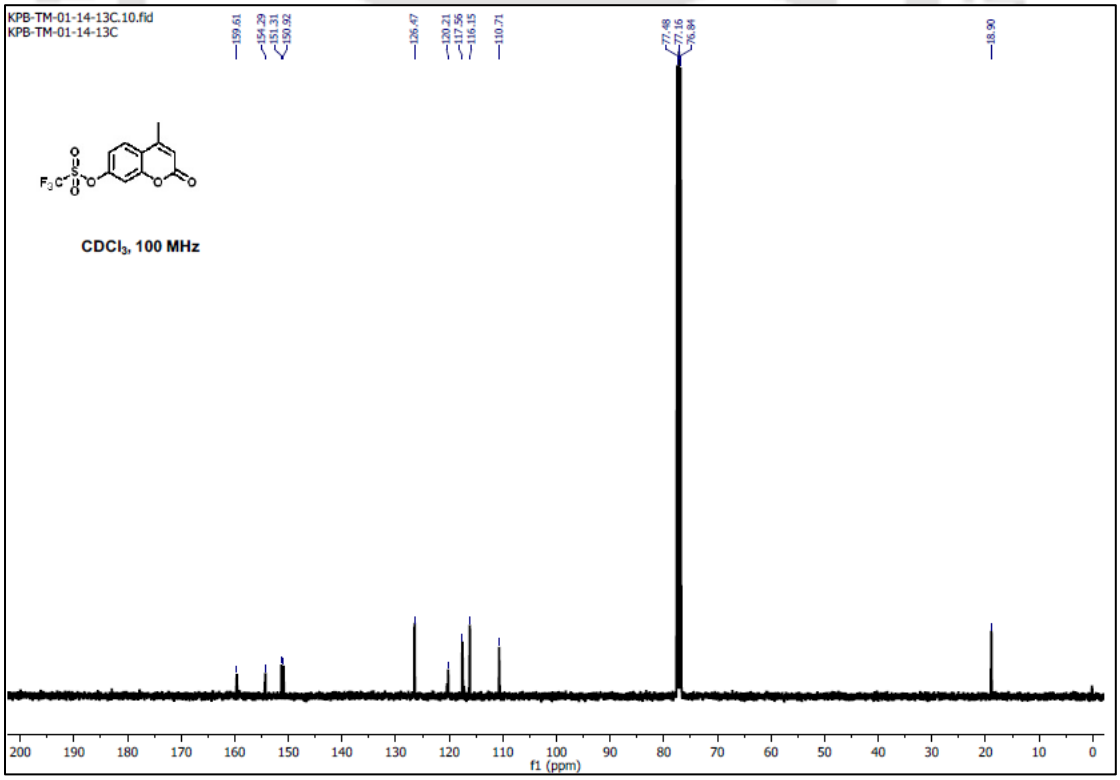

Figure A3.10: ^{13}C NMR spectrum ($CDCl_3$, 100 MHz) of compound **2.21**.

TH-3161_176122050

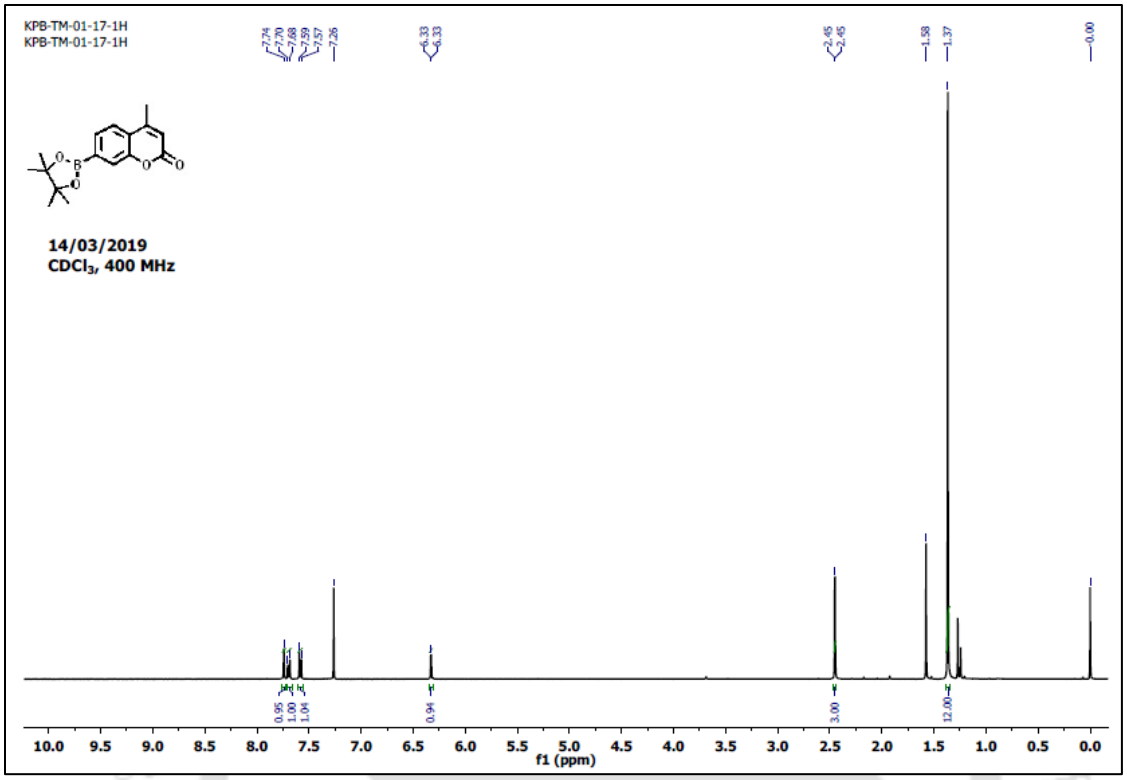

Figure A3.11: ^{1}H NMR spectrum ($CDCl_3$, 400 MHz) of compound **2.1**.

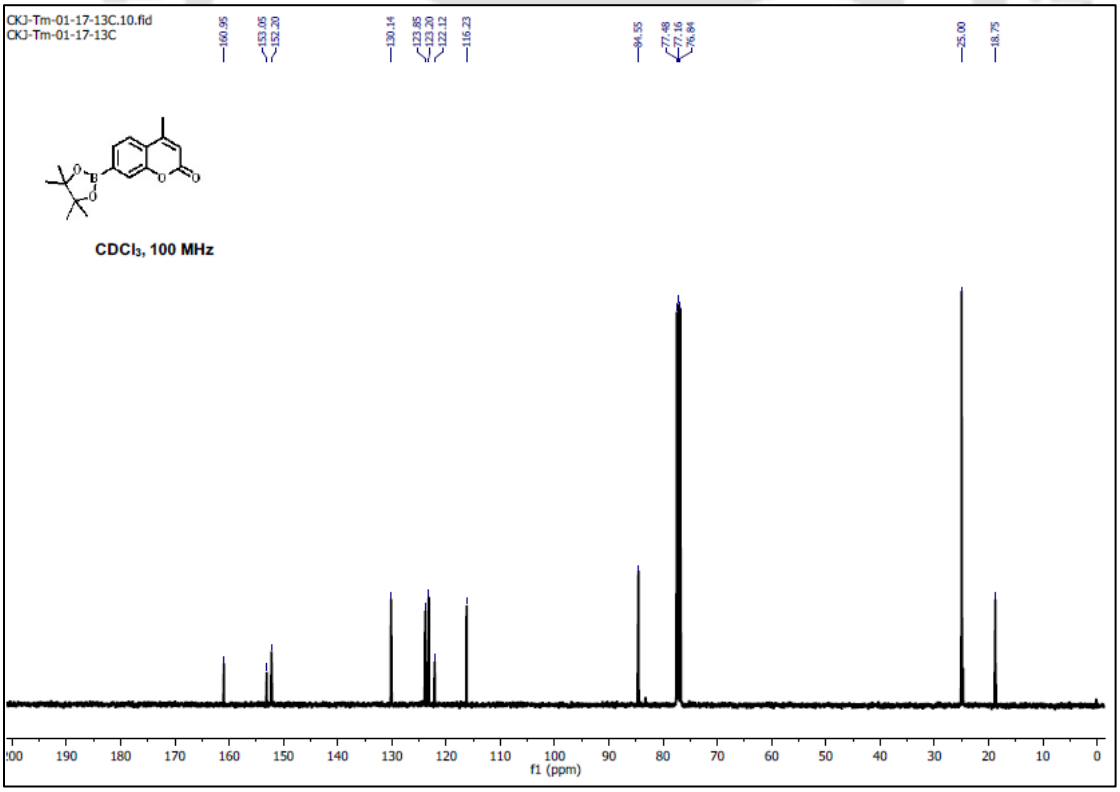

Figure A3.12: ^{13}C NMR spectrum ($CDCl_3$, 100 MHz) of compound **2.1**.

TH-3161_176122050

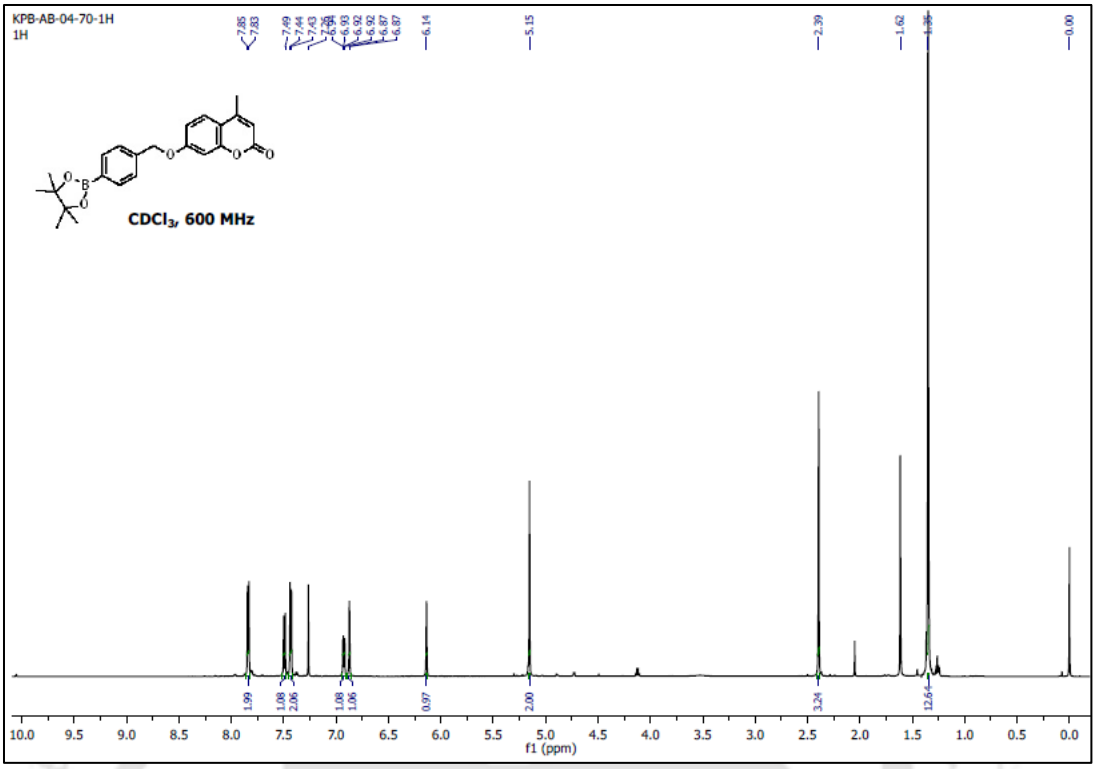

Figure A3.13: ^{1}H NMR spectrum ($CDCl_3$, 600 MHz) of compound **2.2**.

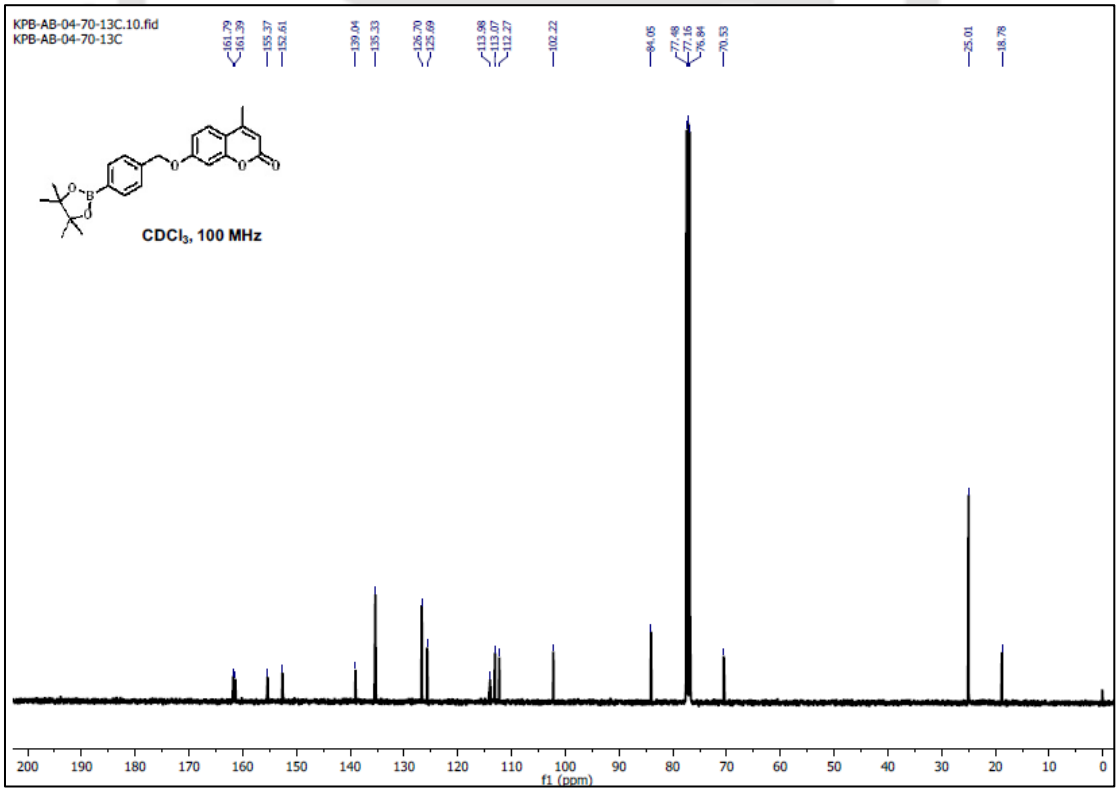

Figure A3.14: ^{13}C NMR spectrum ($CDCl_3$, 100 MHz) of compound **2.2**.

TH-3161_176122050

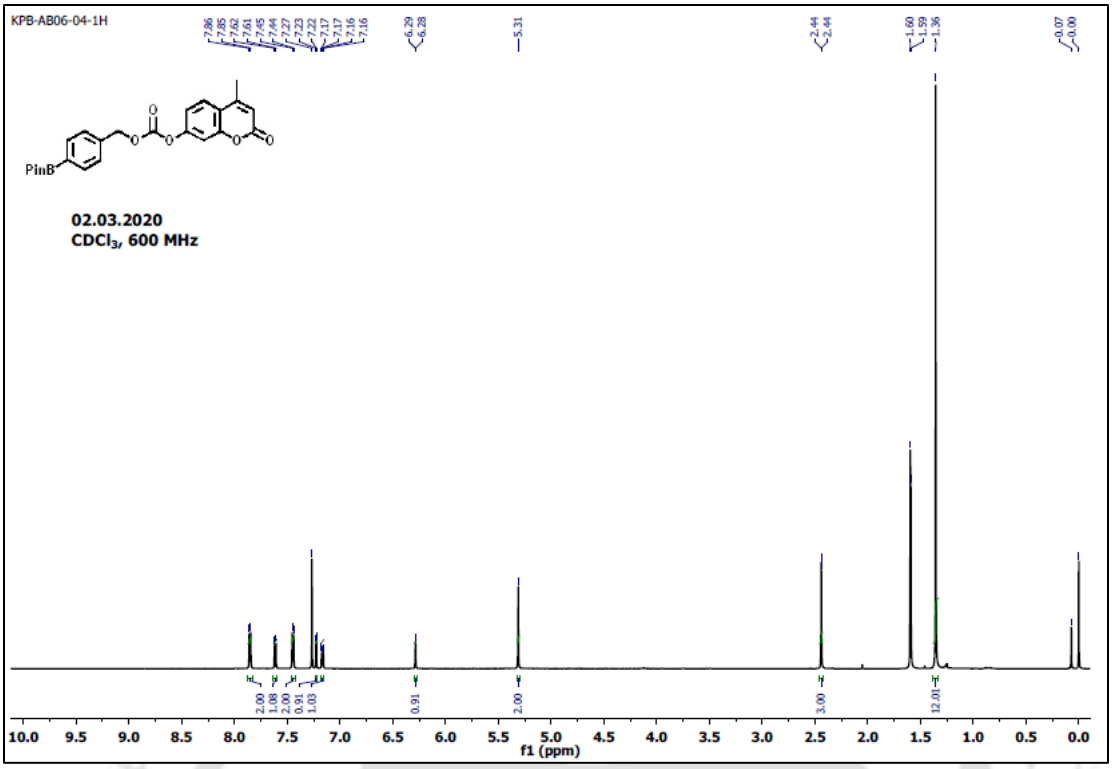

Figure A3.15: ^{1}H NMR spectrum ($CDCl_3$, 600 MHz) of compound **2.3**.

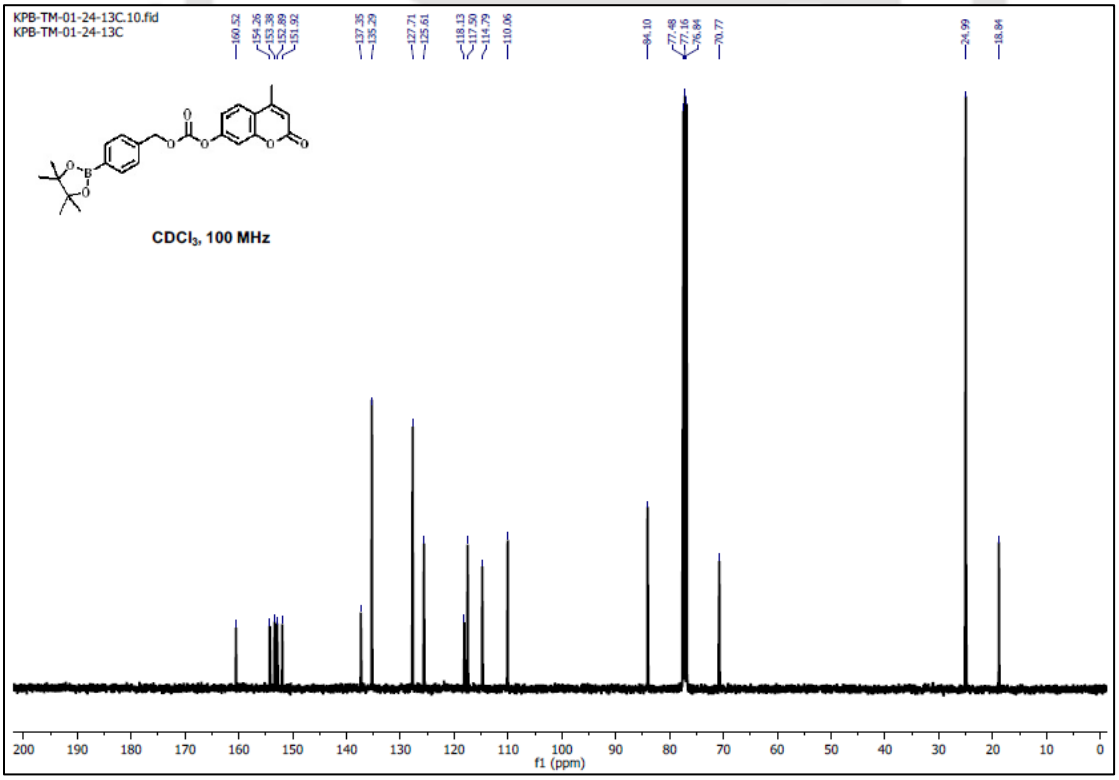

Figure A3.16: ^{13}C NMR spectrum ($CDCl_3$, 100 MHz) of compound **2.3**.

TH-3161_176122050

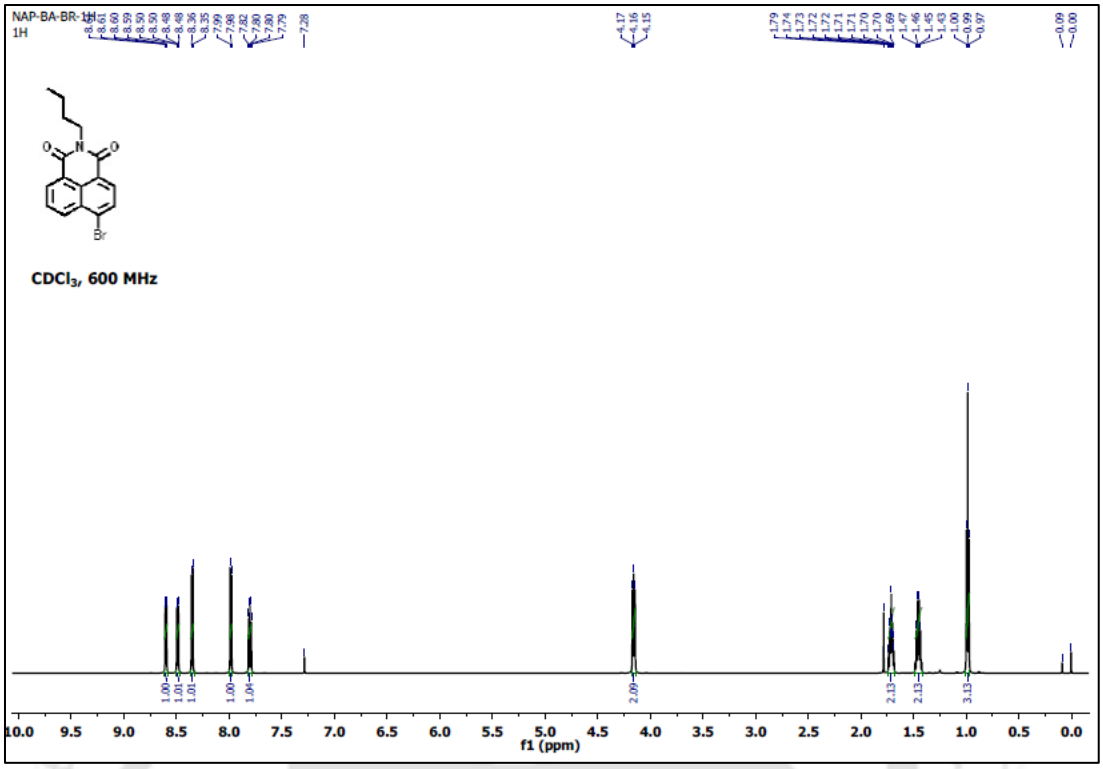

Figure A3.17: ^{1}H NMR spectrum ($CDCl_3$, 600 MHz) of compound **2.23**.

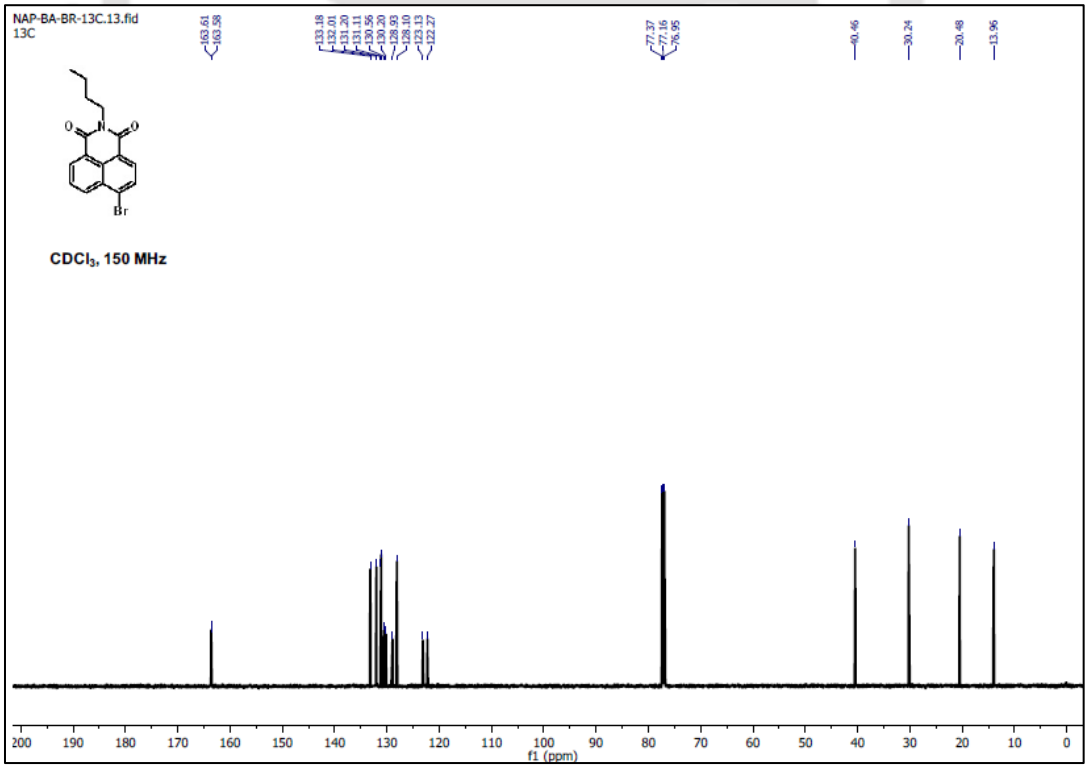

Figure A3.18: ^{13}C NMR spectrum ($CDCl_3$, 150 MHz) of compound **2.23**.

TH-3161_176122050

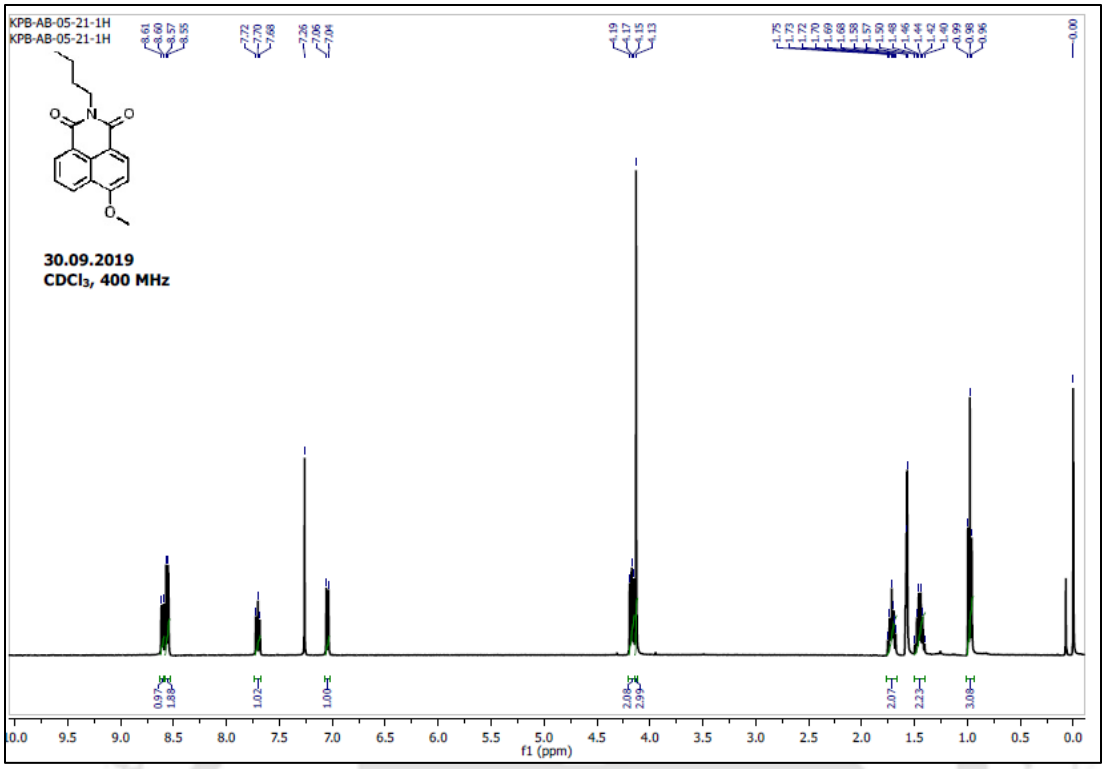

Figure A3.19: ^{1}H NMR spectrum ($CDCl_3$, 400 MHz) of compound **2.24**.

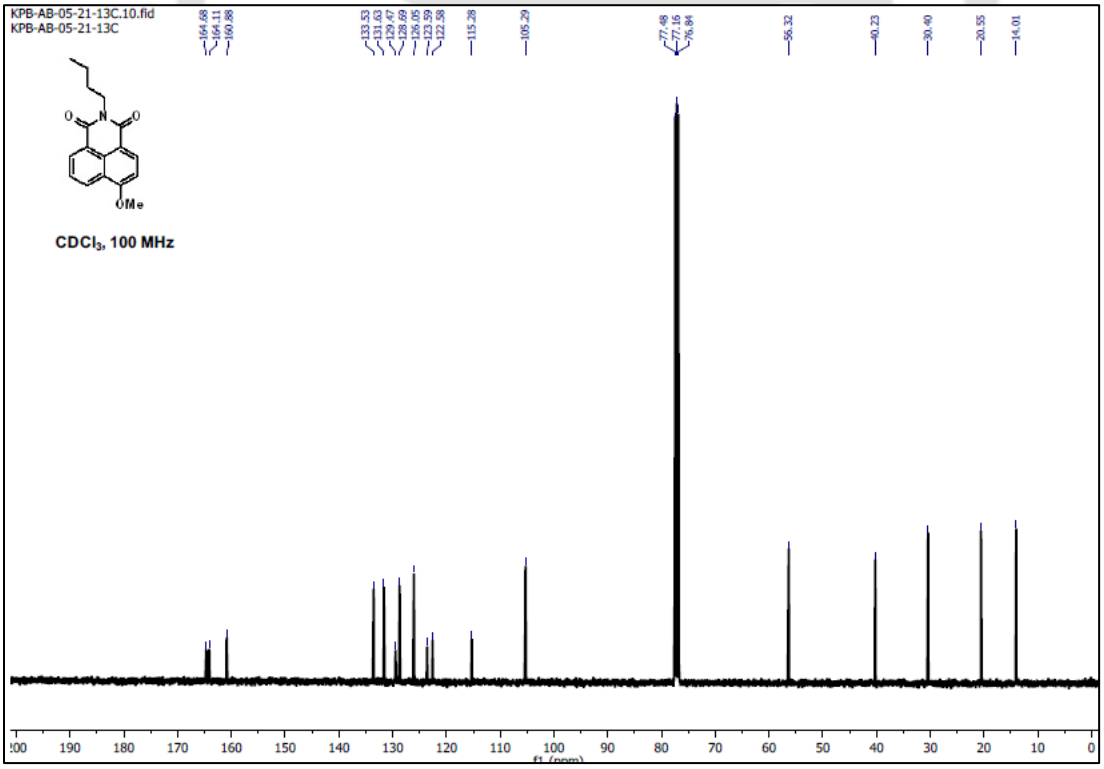

Figure A3.20: ^{13}C NMR spectrum ($CDCl_3$, 100 MHz) of compound **2.24**.

TH-3161_176122050

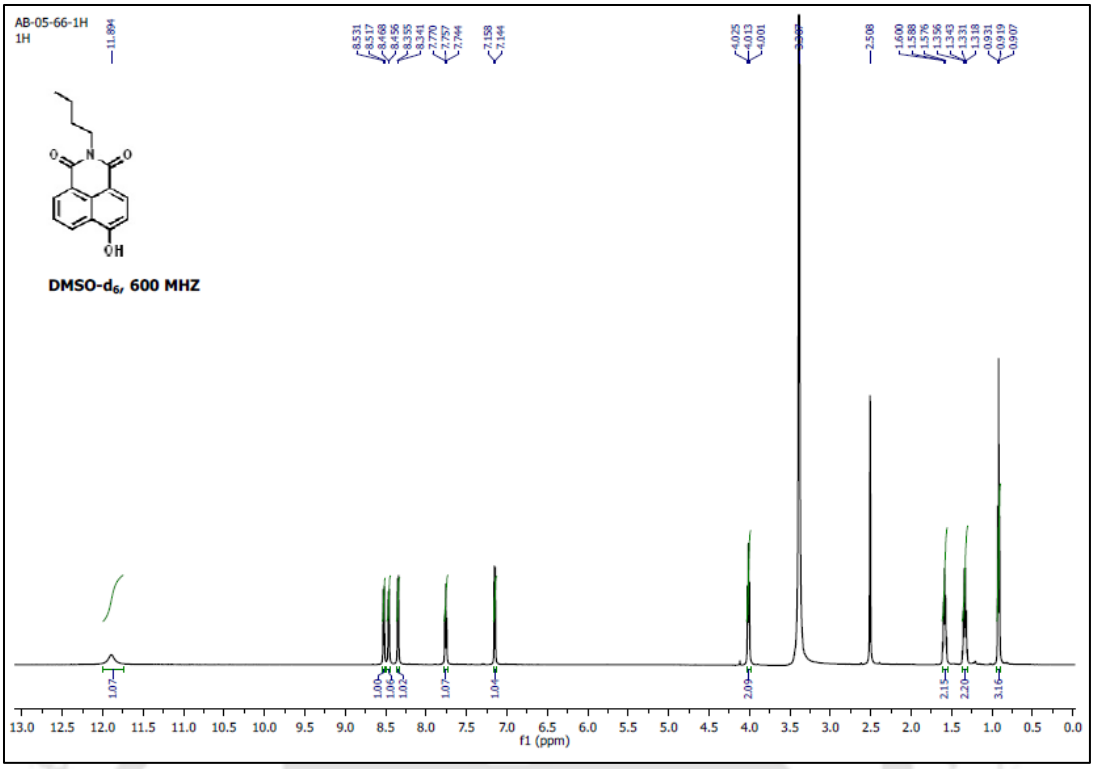

Figure A3.21: ^{1}H NMR spectrum (DMSO-d_6, 600 MHz) of compound **2.11**.

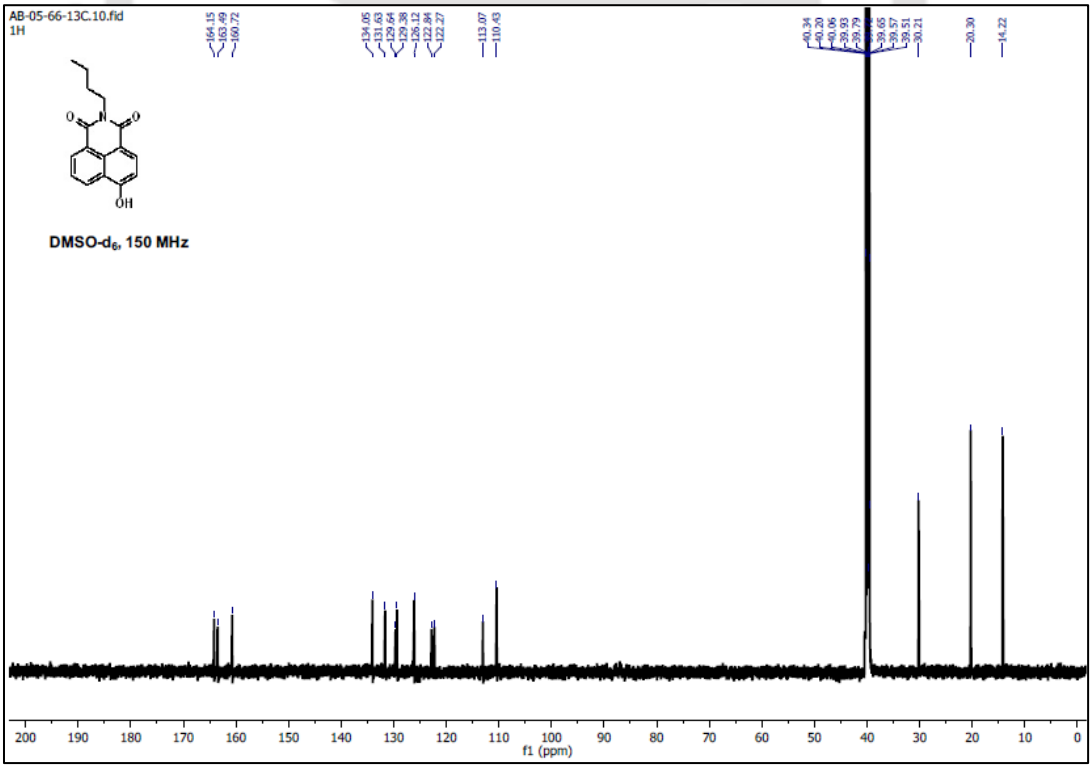

Figure A3.22: ^{13}C NMR spectrum (DMSO-d_6, 150 MHz) of compound **2.11**.

TH-3161_176122050

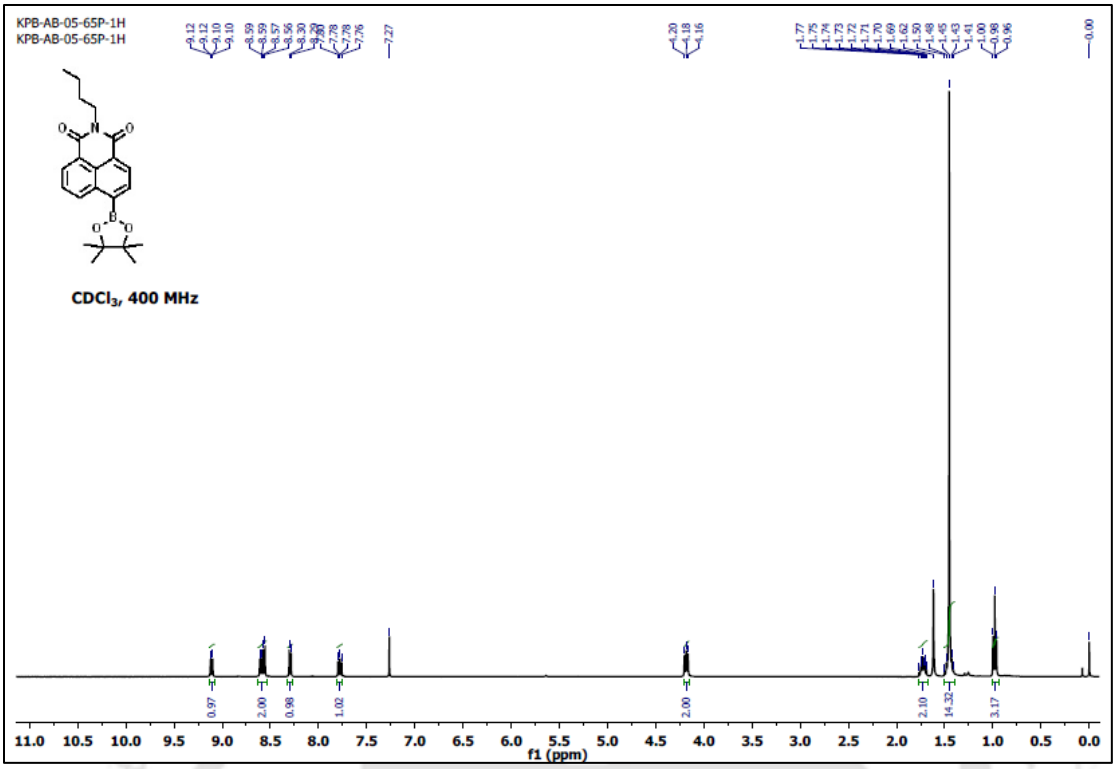

Figure A3.23: ^{1}H NMR spectrum ($CDCl_3$, 400 MHz) of compound **2.4**.

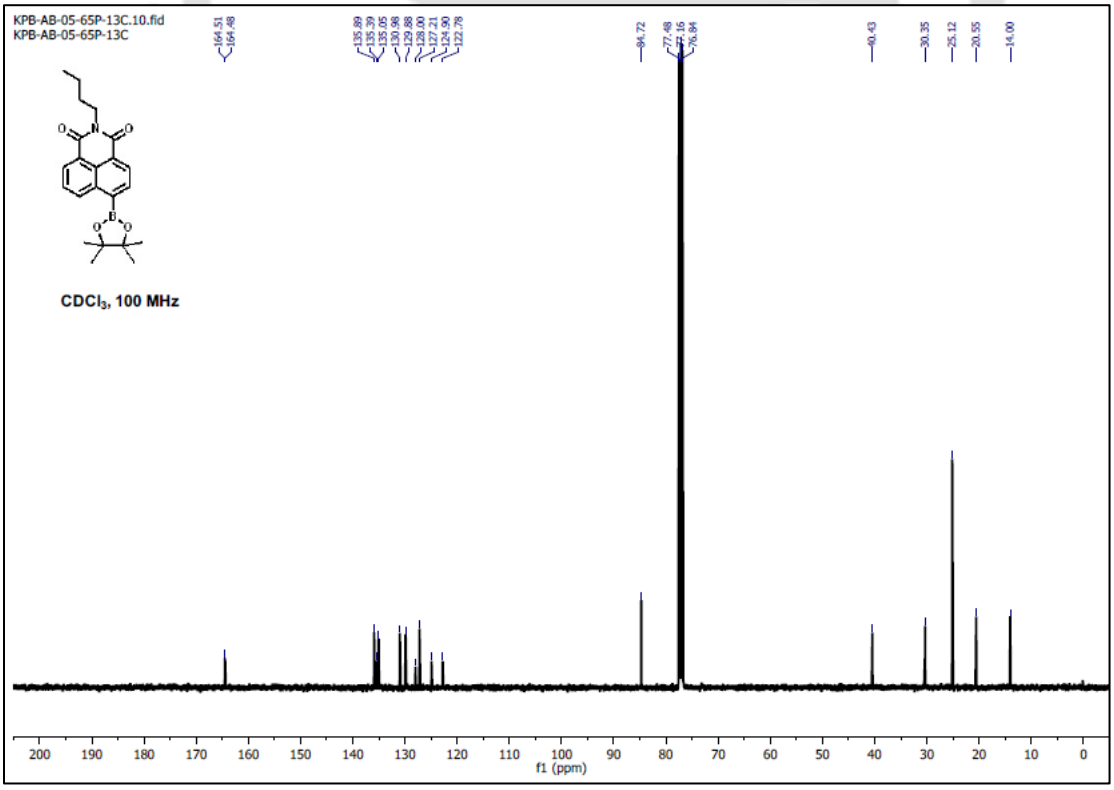

Figure A3.24: ^{13}C NMR spectrum ($CDCl_3$, 100 MHz) of compound **2.4**.

TH-3161_176122050

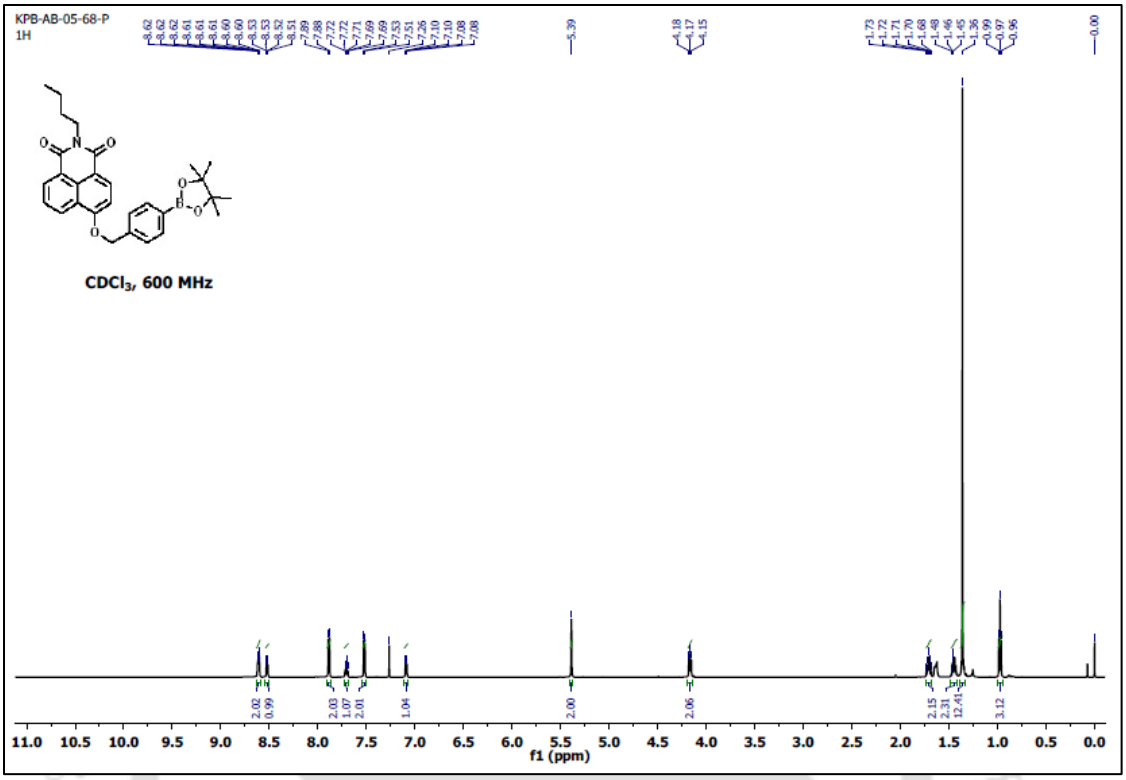

Figure A3.25: ^{1}H NMR spectrum ($CDCl_3$, 600 MHz) of compound **2.5**.

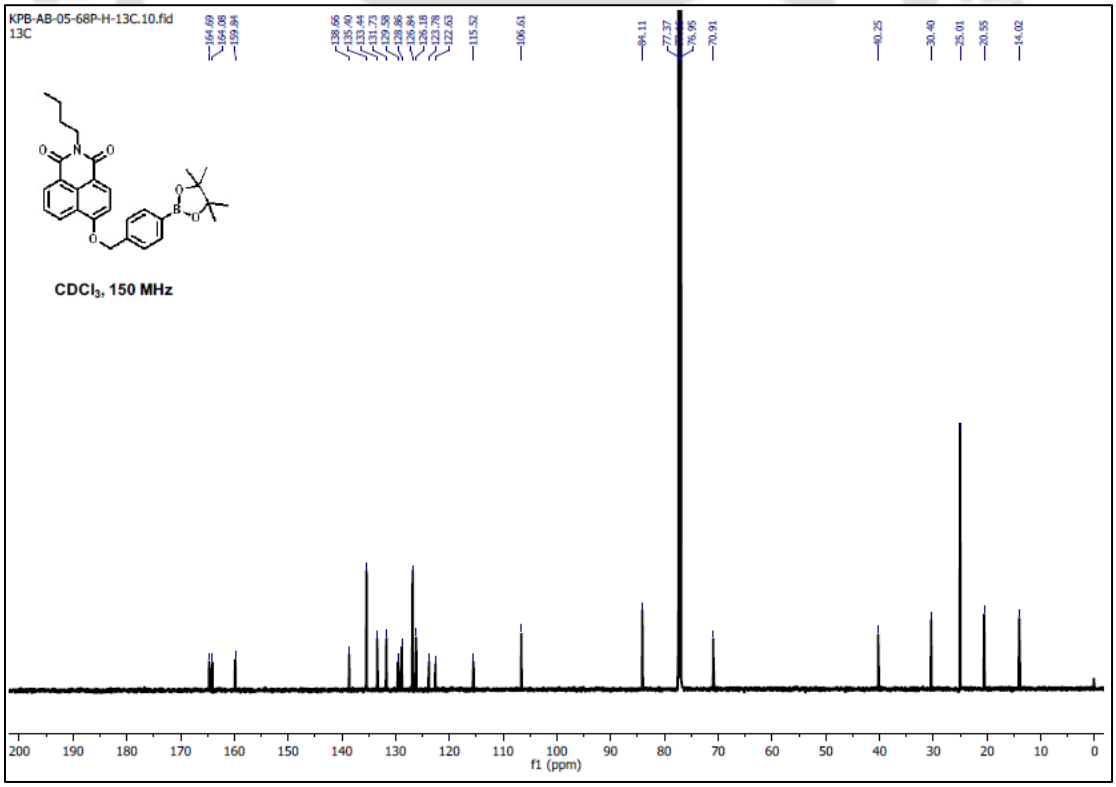

Figure A3.26: ^{13}C NMR spectrum ($CDCl_3$, 150 MHz) of compound **2.5**.

TH-3161_176122050

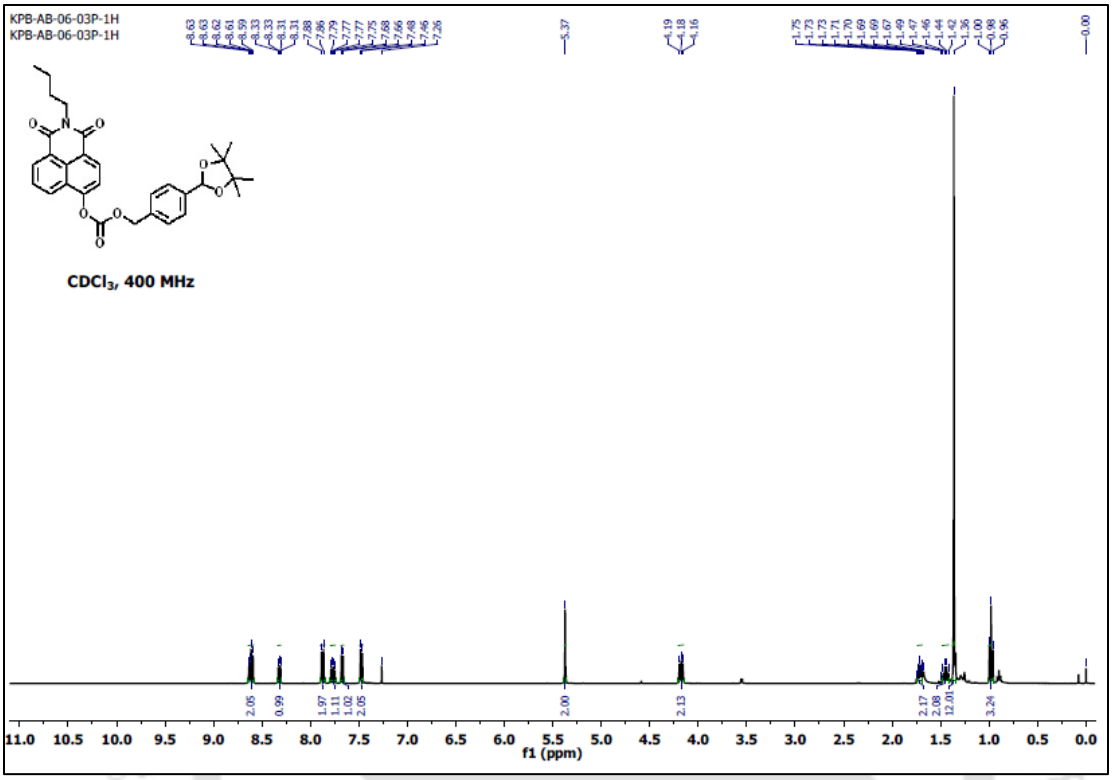

Figure A3.27: ^{1}H NMR spectrum ($CDCl_3$, 400 MHz) of compound **2.6**.

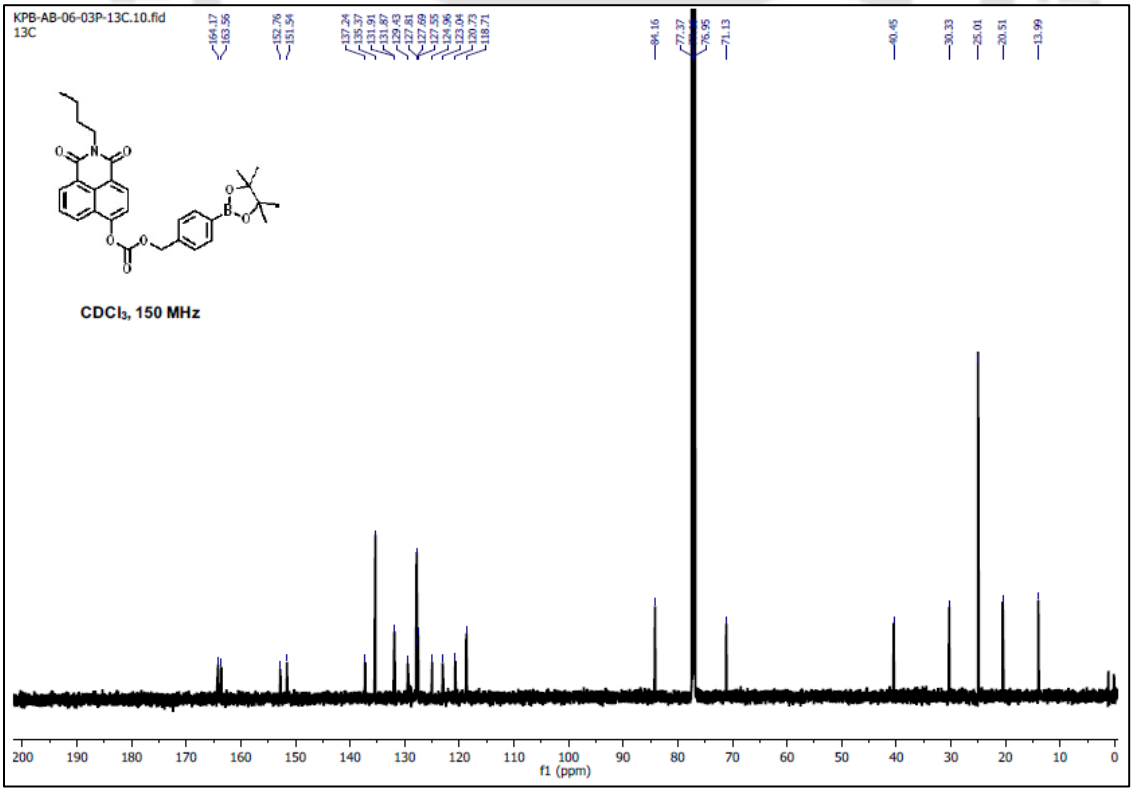

Figure A3.28: ^{13}C NMR spectrum ($CDCl_3$, 150 MHz) of compound **2.6**.

TH-3161_176122050

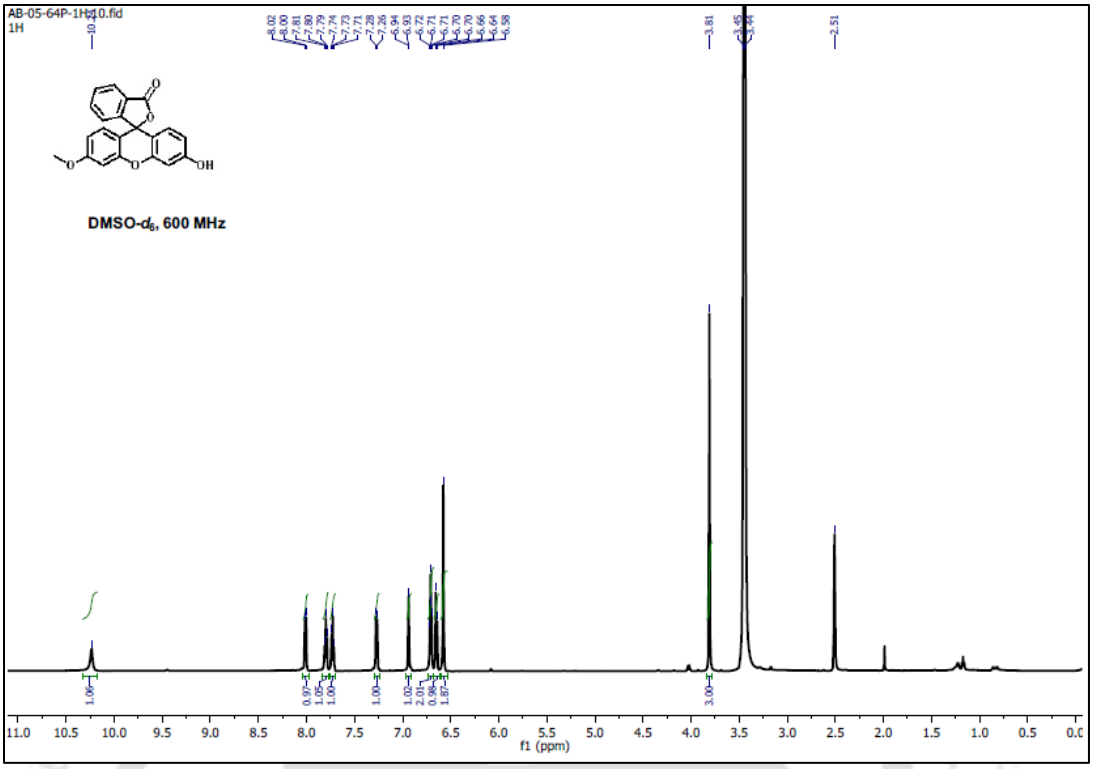

Figure A3.29: ^{1}H NMR spectrum (DMSO-d_6, 600 MHz) of compound **2.12**.

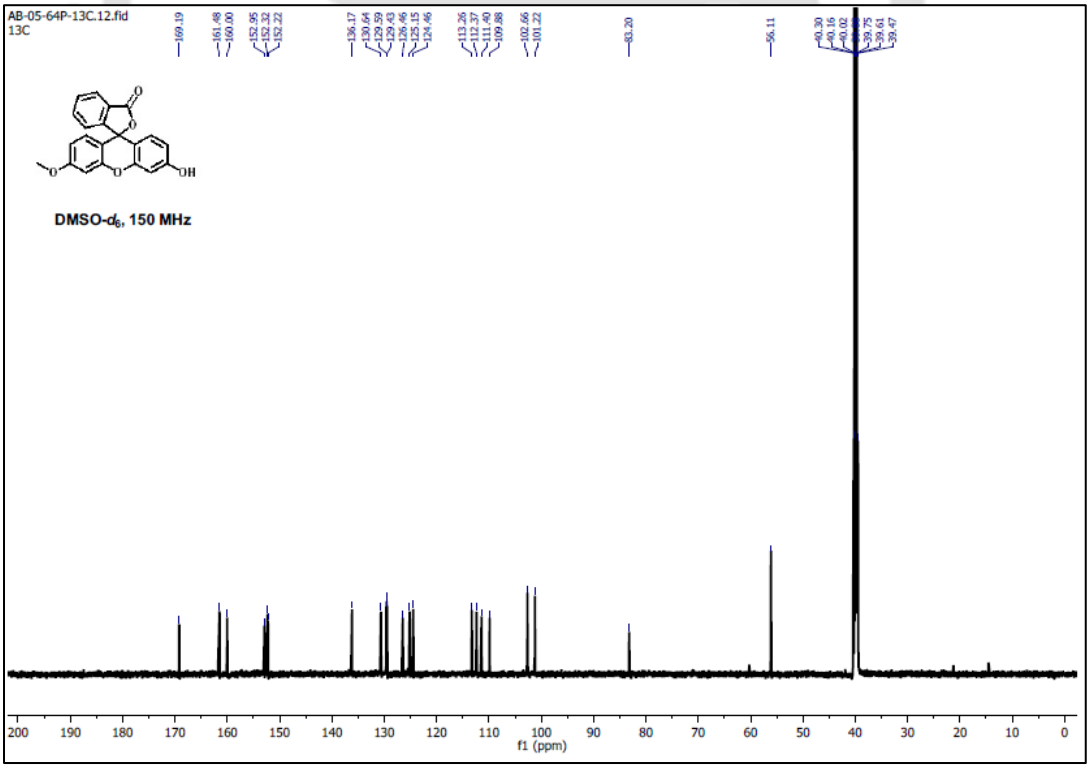

Figure A3.30: ^{13}C NMR spectrum (DMSO-d_6, 150 MHz) of compound **2.12**.

TH-3161_176122050

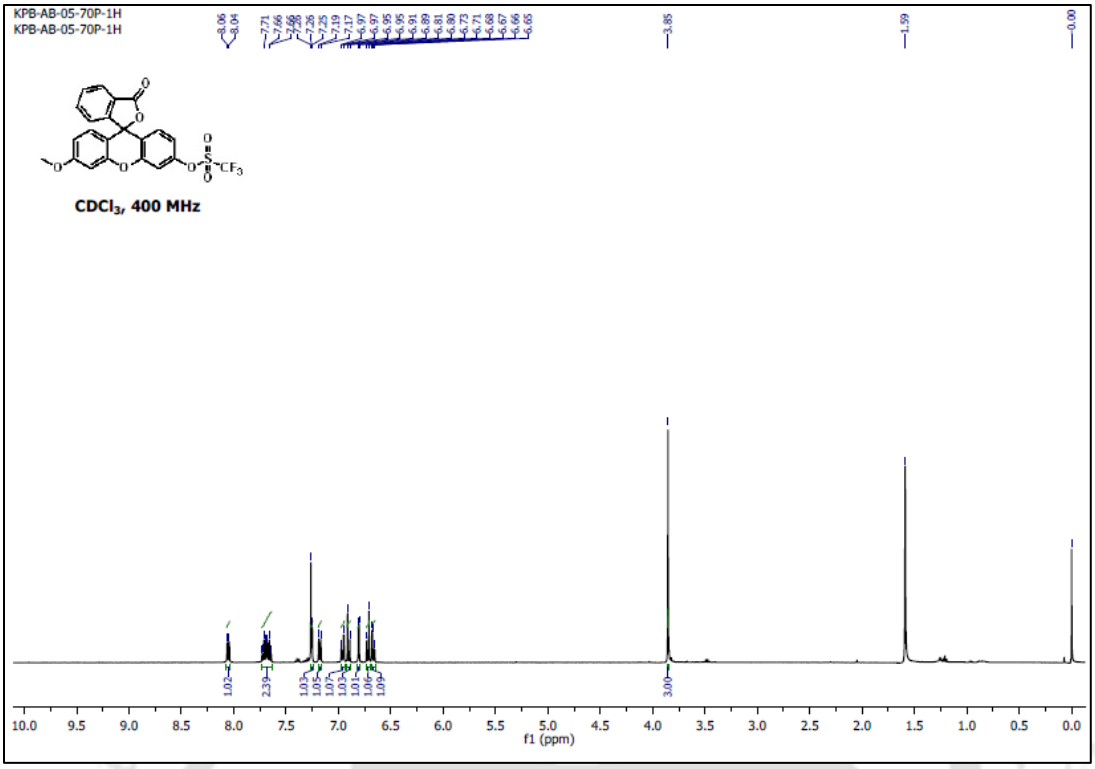

Figure A3.31: ^{1}H NMR spectrum ($CDCl_3$, 400 MHz) of compound **2.26**.

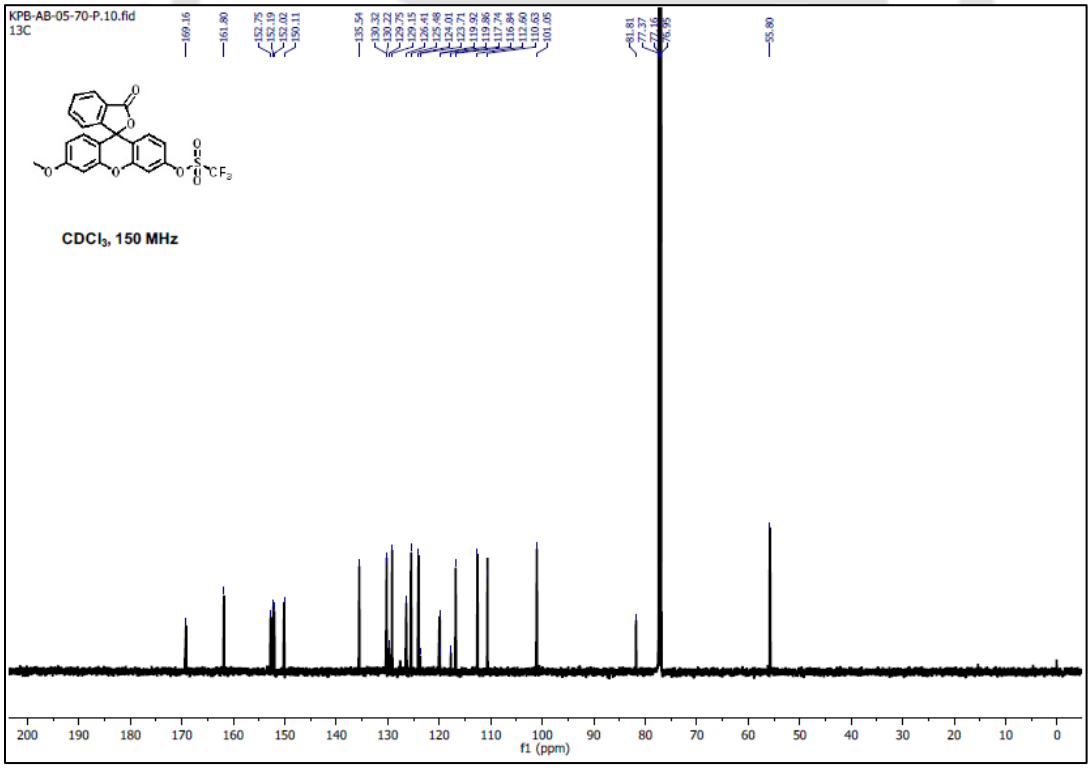

Figure A3.32: ^{13}C NMR spectrum ($CDCl_3$, 150 MHz) of compound **2.26**.

TH-3161_176122050

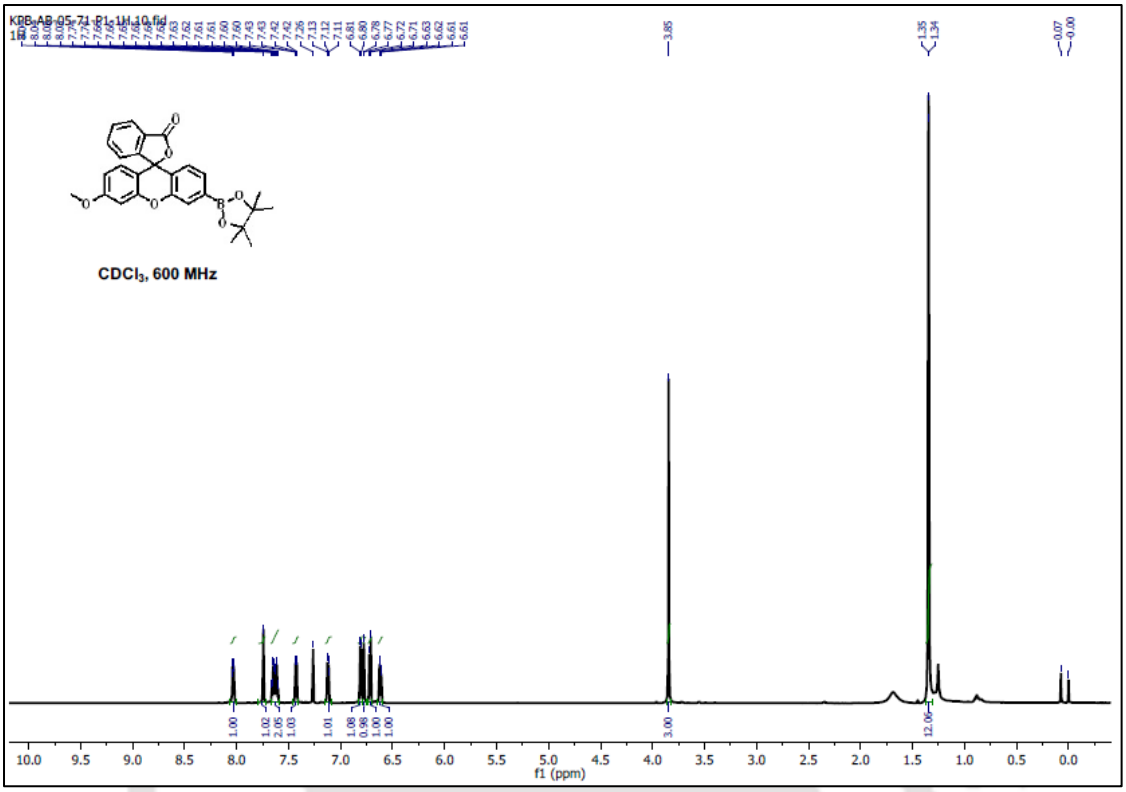

Figure A3.33: ^{1}H NMR spectrum ($CDCl_3$, 600 MHz) of compound **2.7**.

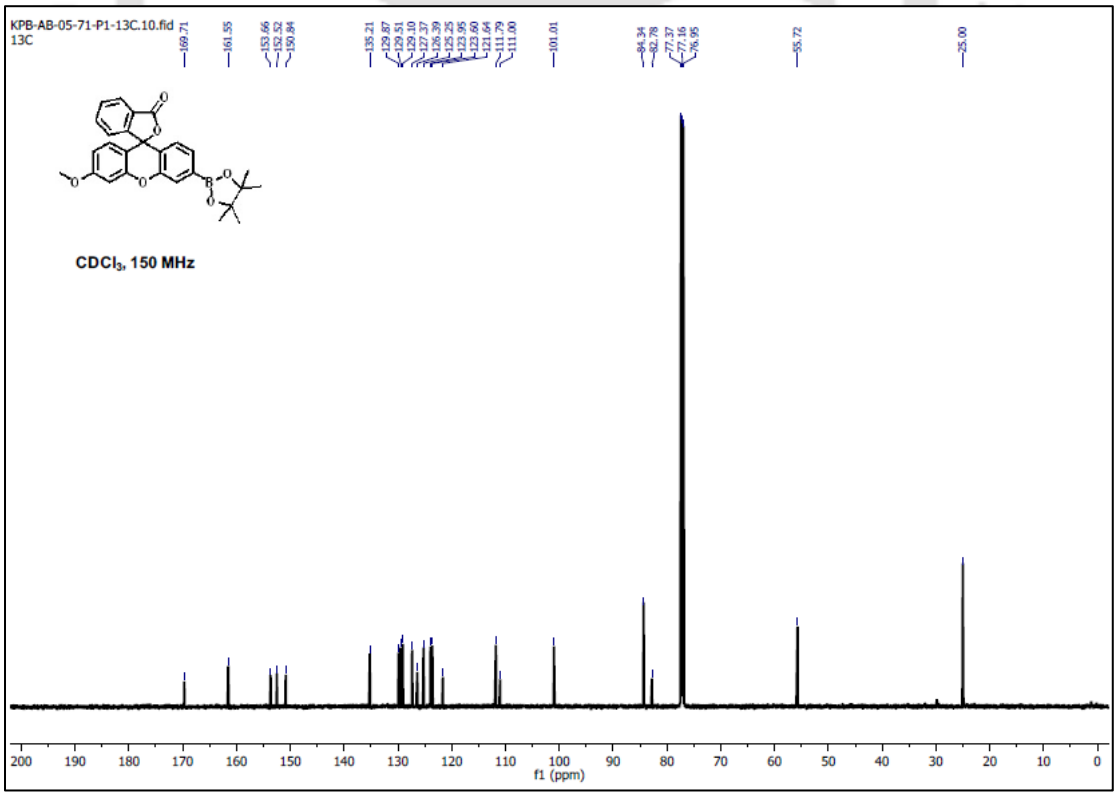

Figure A3.34: ^{13}C NMR spectrum ($CDCl_3$, 150 MHz) of compound **2.7**.

TH-3161_176122050

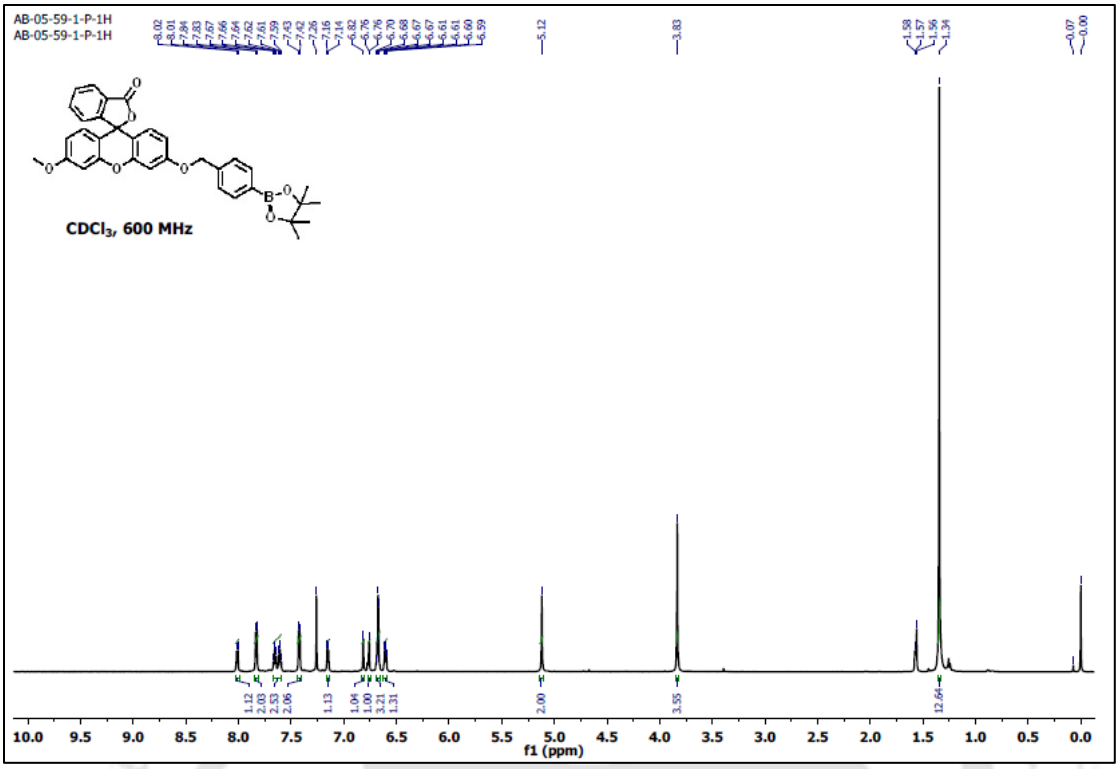

Figure A3.35: ^{1}H NMR spectrum ($CDCl_3$, 600 MHz) of compound **2.8**.

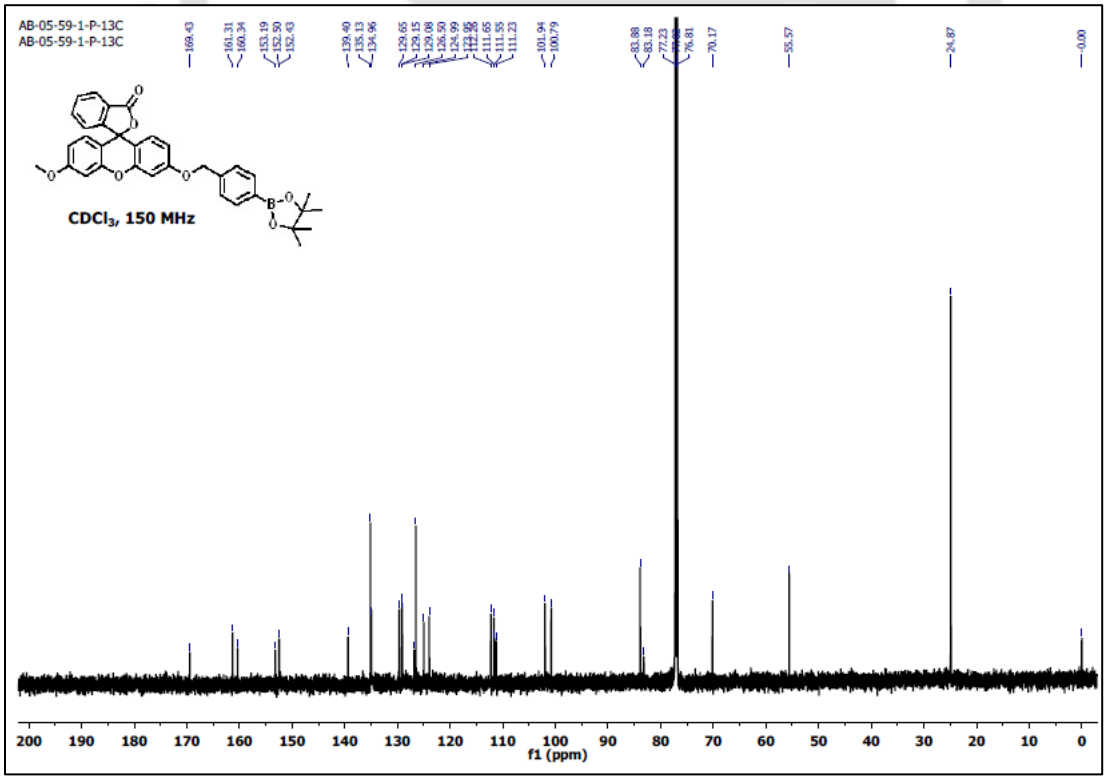

Figure A3.36: ^{13}C NMR spectrum ($CDCl_3$, 150 MHz) of compound **2.8**.

TH-3161_176122050

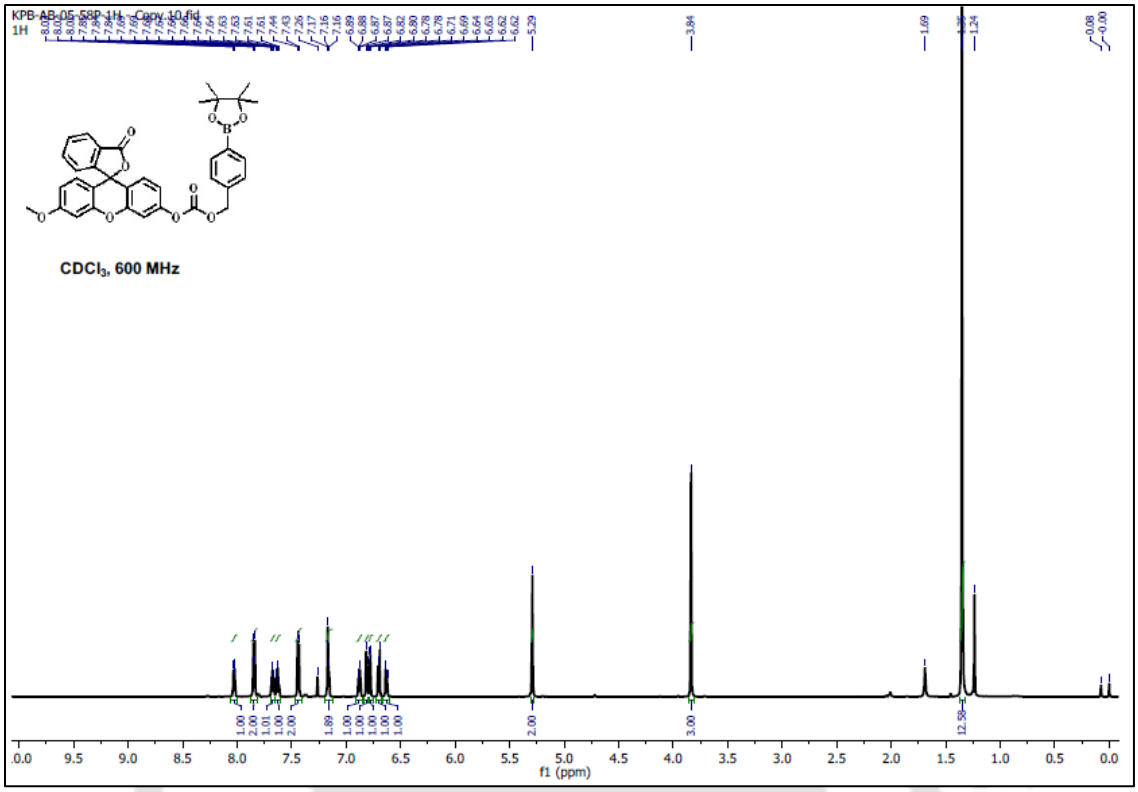

Figure A3.37: ^{1}H NMR spectrum ($CDCl_3$, 600 MHz) of compound **2.9**.

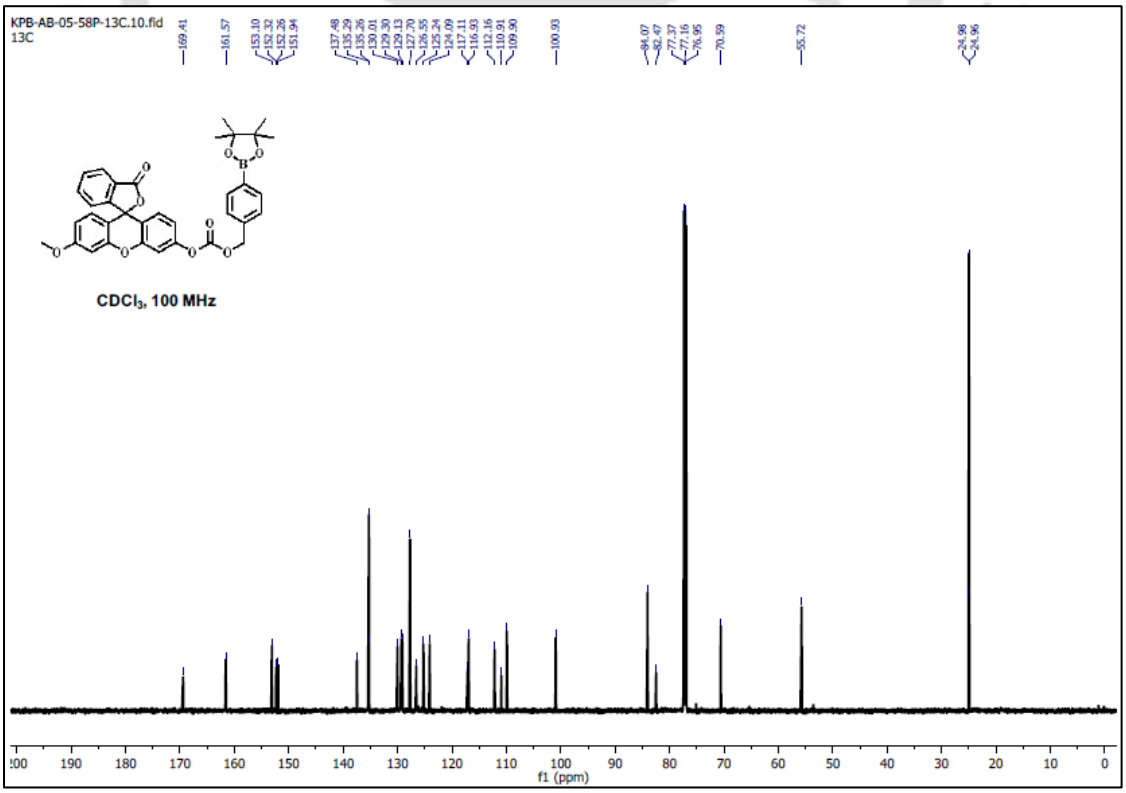

Figure A3.38: ^{13}C NMR spectrum ($CDCl_3$, 100 MHz) of compound **2.9**.

TH-3161_176122050

TH-3161_176122050

Supplementary data of chapter 3

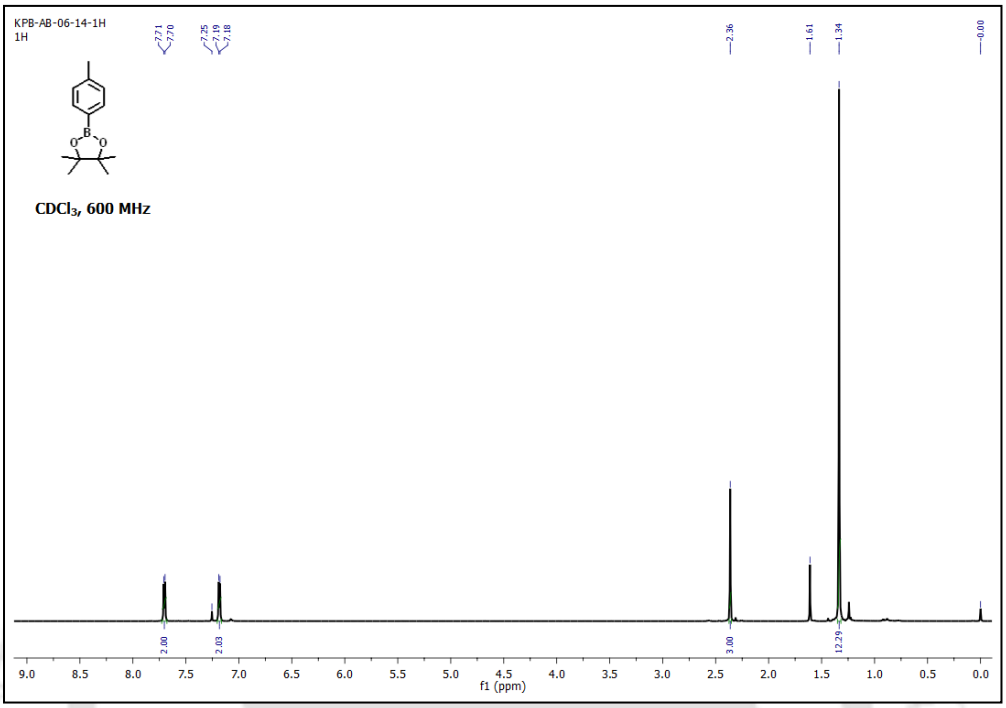

Figure A4.1: ^{1}H NMR spectrum ($CDCl_3$, 600 MHz, ppm) of compound **3.2**.

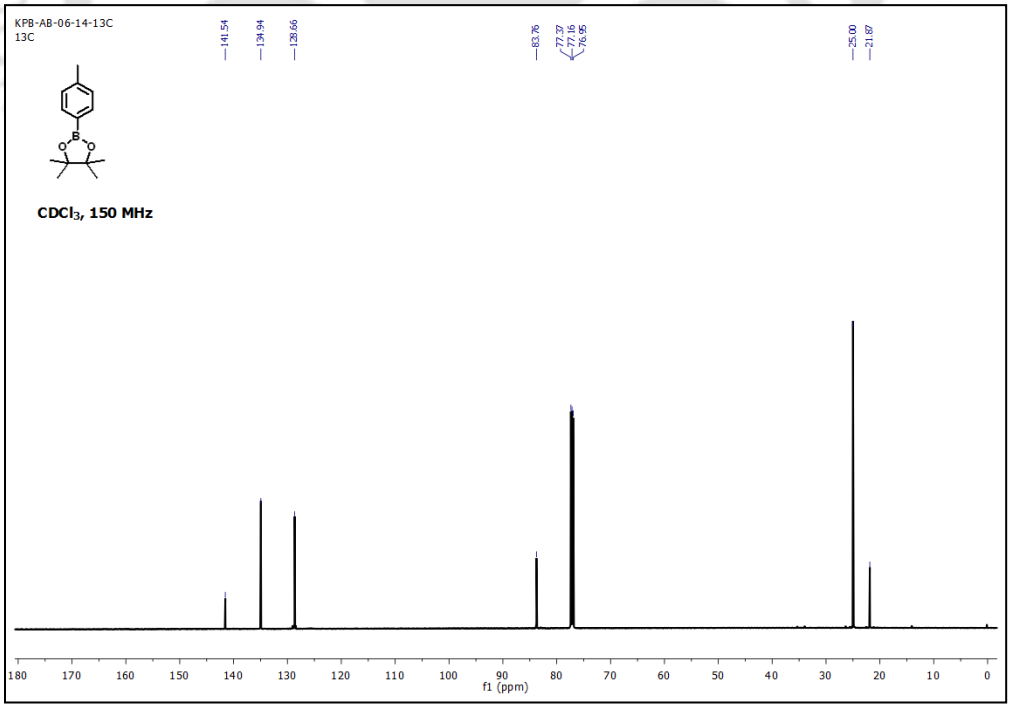

Figure A4.2: ^{13}C NMR spectrum ($CDCl_3$, 150 MHz, ppm) of compound **3.2**.

TH-3161_176122050

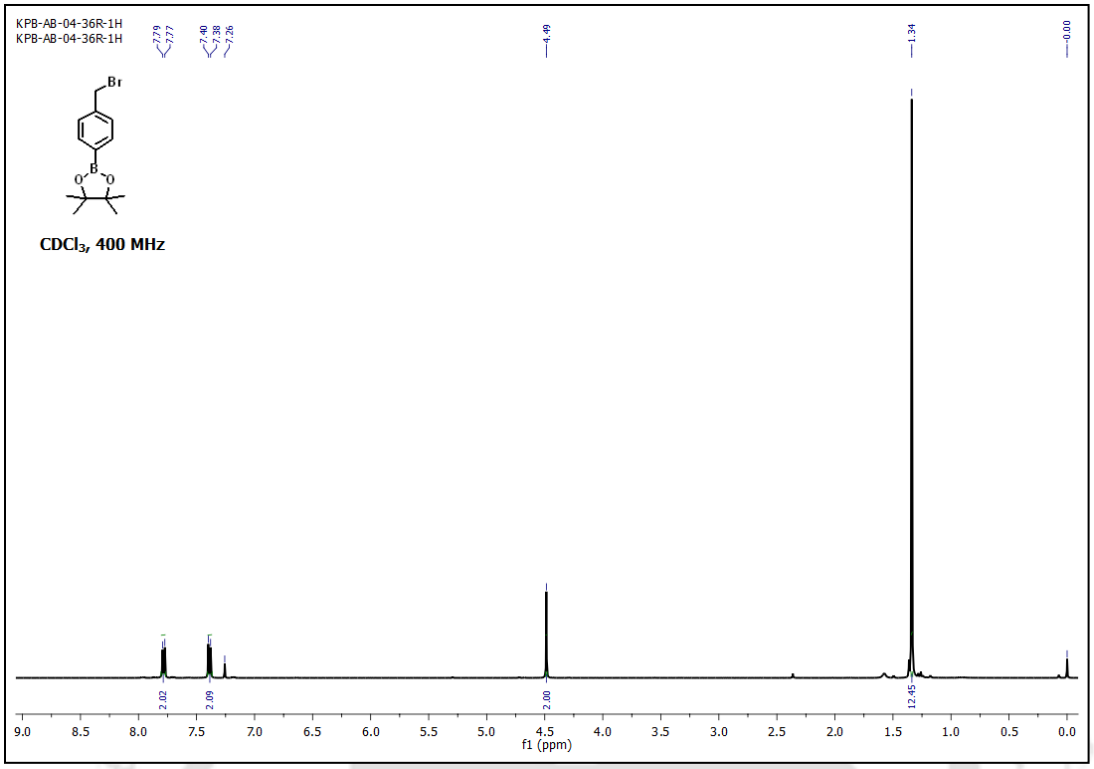

Figure A4.3: ^{1}H NMR spectrum ($CDCl_3$, 400 MHz, ppm) of compound **3.3**.

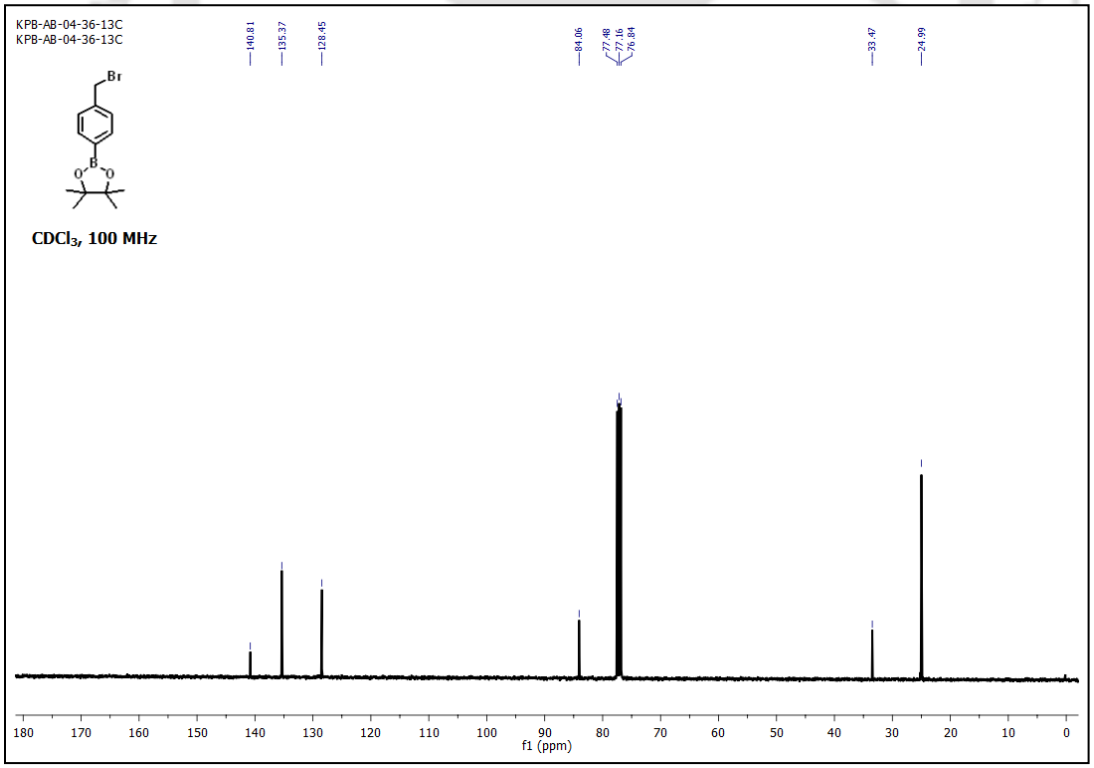

Figure A4.4: ^{13}C NMR spectrum ($CDCl_3$, 100 MHz, ppm) of compound **3.3**.

TH-3161_176122050

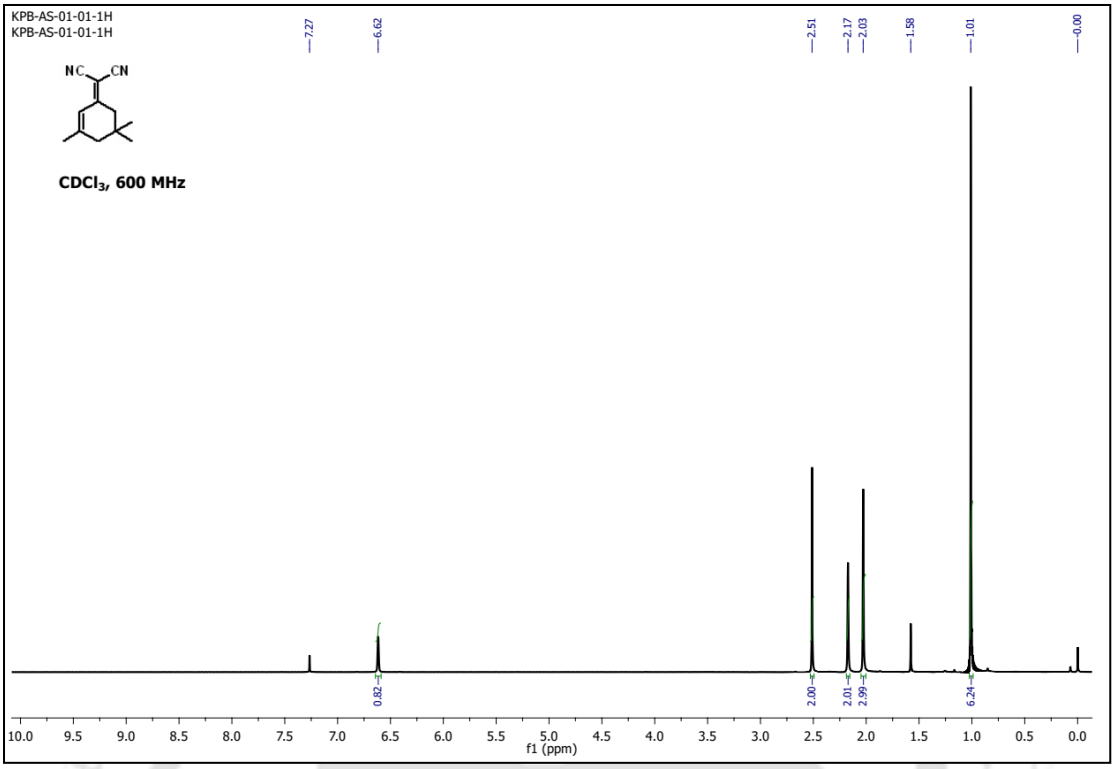

Figure A4.5: ^{1}H NMR spectrum ($CDCl_3$, 600 MHz) of compound **3.5**.

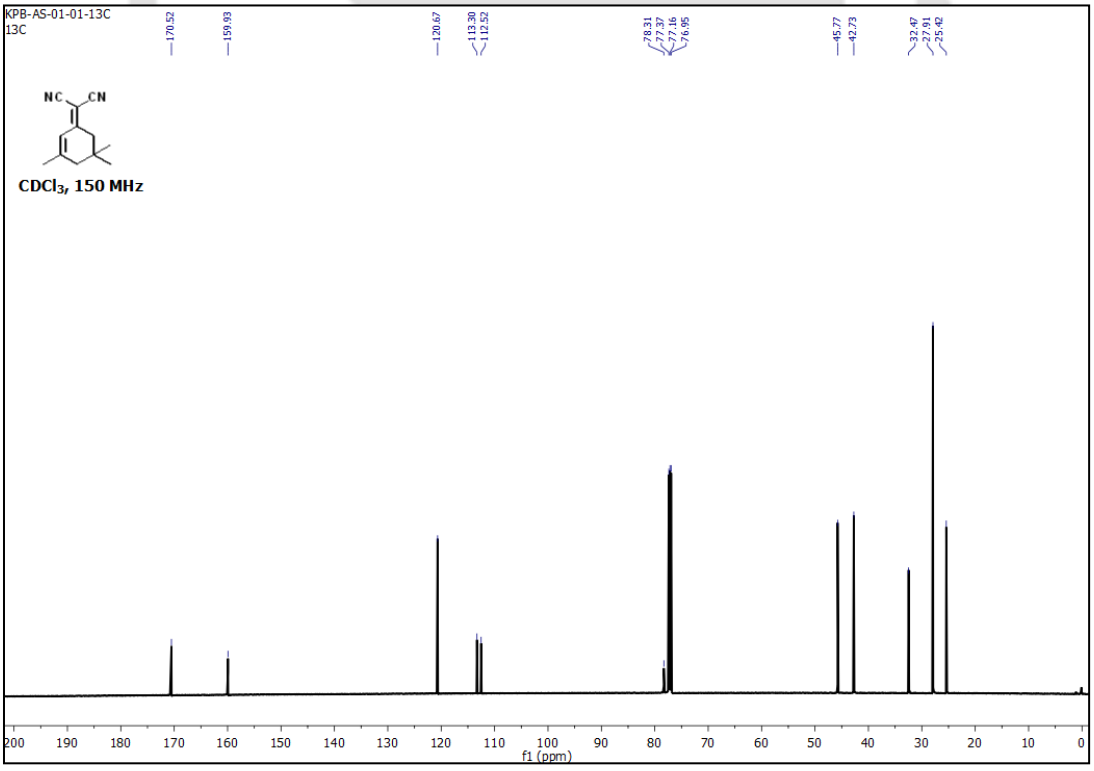

Figure A4.6: ^{13}C NMR spectrum ($CDCl_3$, 150 MHz) of compound **3.5**.

TH-3161_176122050

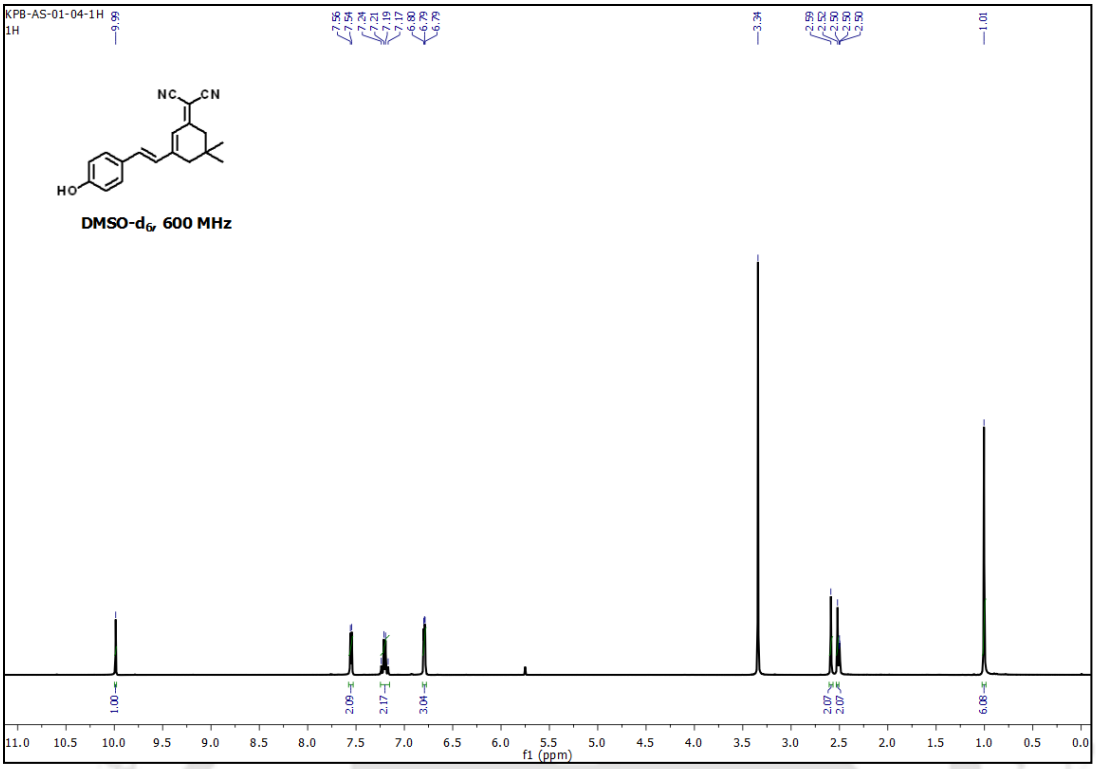

Figure A4.7: ^{1}H NMR spectrum (DMSO-*d*$_6$, 600 MHz) of **DCI-OH**.

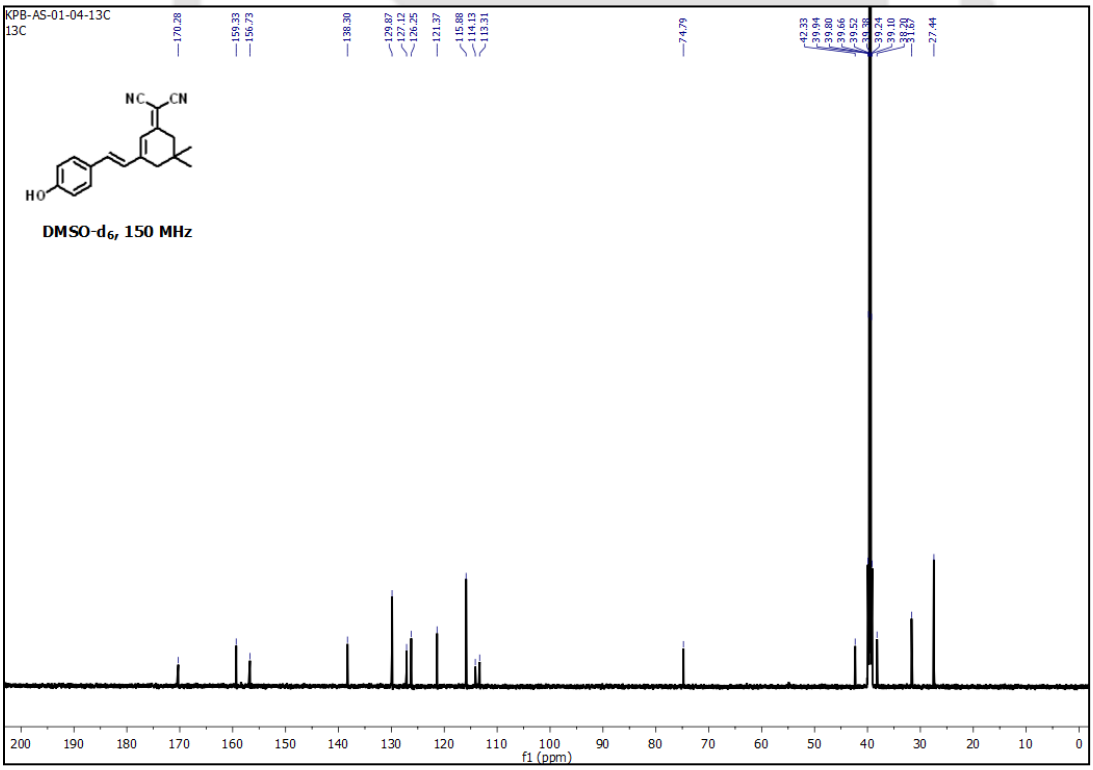

Figure A4.8: ^{13}C NMR spectrum (DMSO-*d*$_6$, 150 MHz) of **DCI-OH**.

TH-3161_176122050

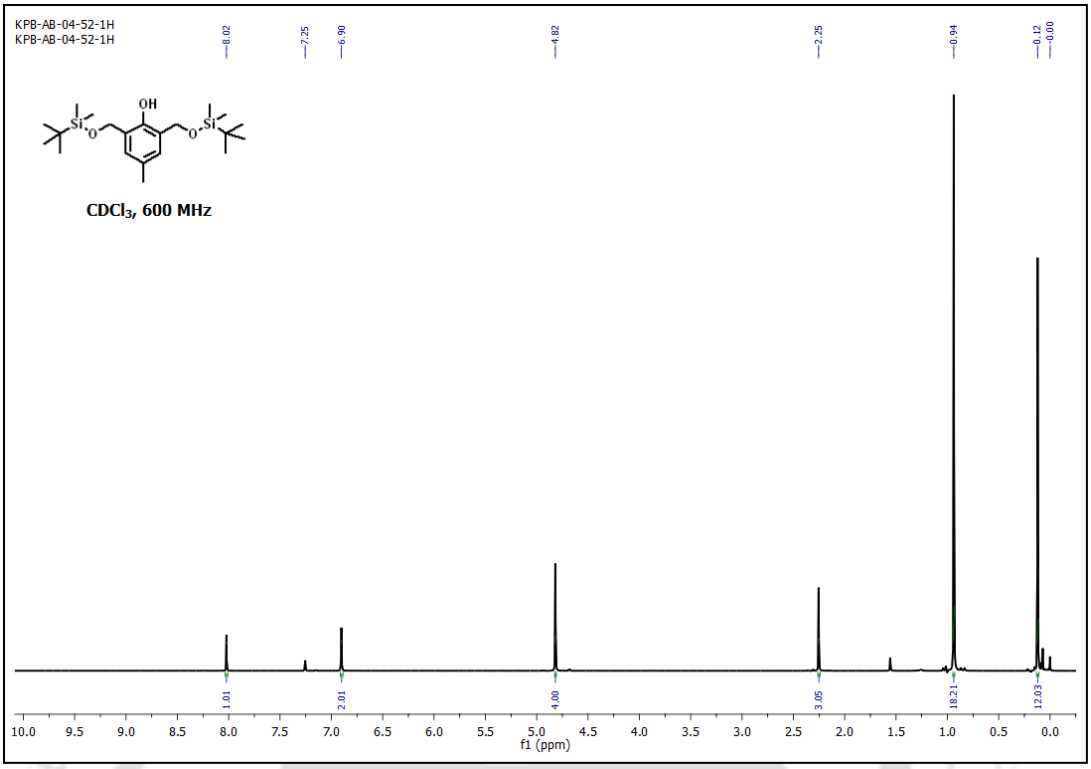

Figure A4.9: ^{1}H NMR spectrum ($CDCl_3$, 600 MHz) of compound **3.7**.

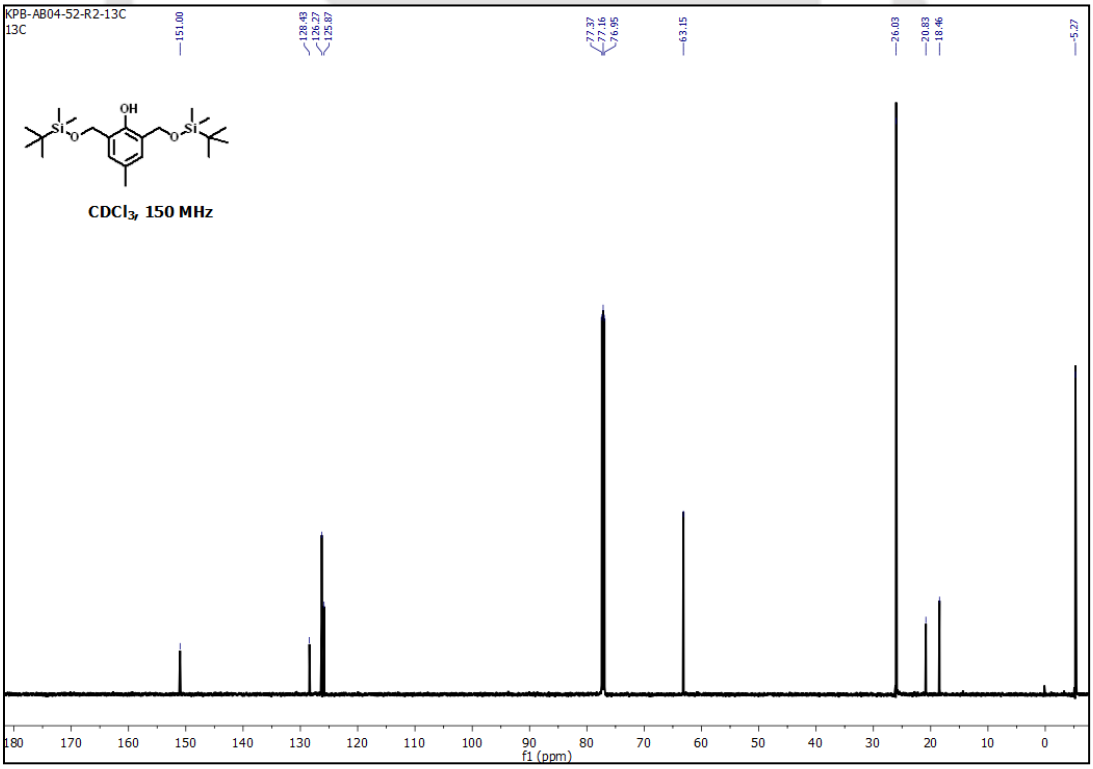

Figure A4.10: ^{13}C NMR spectrum ($CDCl_3$, 150 MHz) of compound **3.7**.

TH-3161_176122050

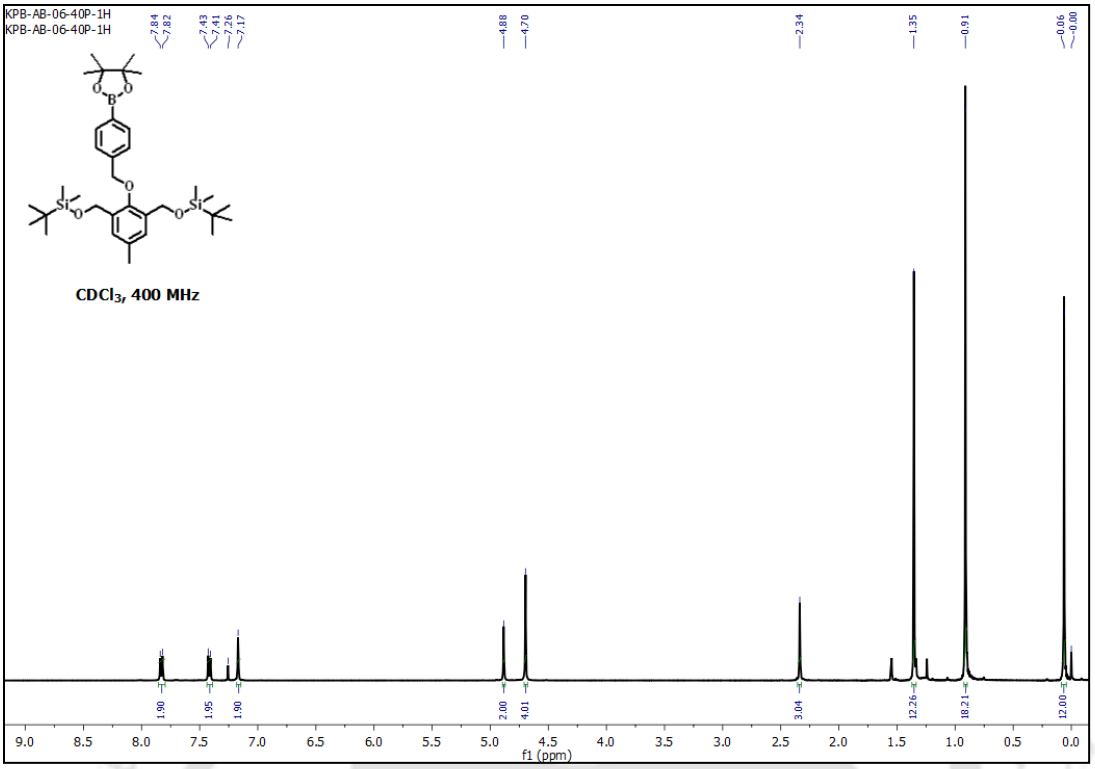

Figure A4.11: ^{1}H NMR spectrum ($CDCl_3$, 400 MHz) of compound **3.8**.

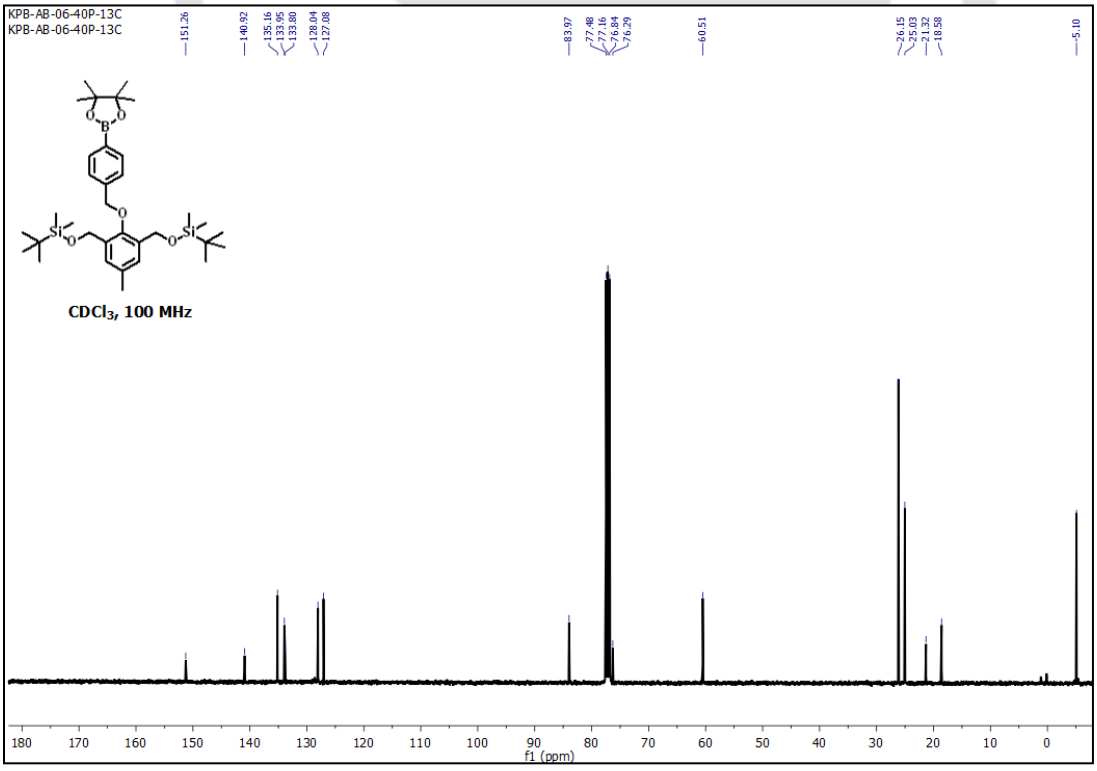

Figure A4.12: ^{13}C NMR spectrum ($CDCl_3$, 100 MHz) of compound **3.8**.

TH-3161_176122050

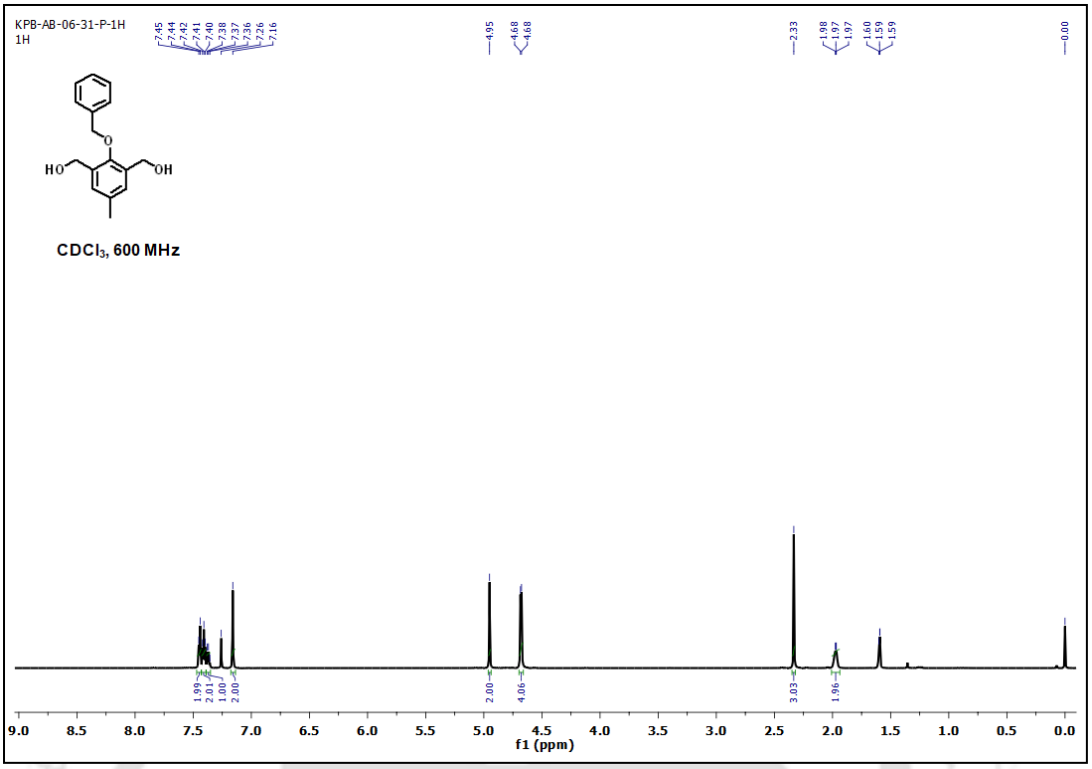

Figure A4.13: ^{1}H NMR spectrum ($CDCl_3$, 600 MHz) of compound **3.9**.

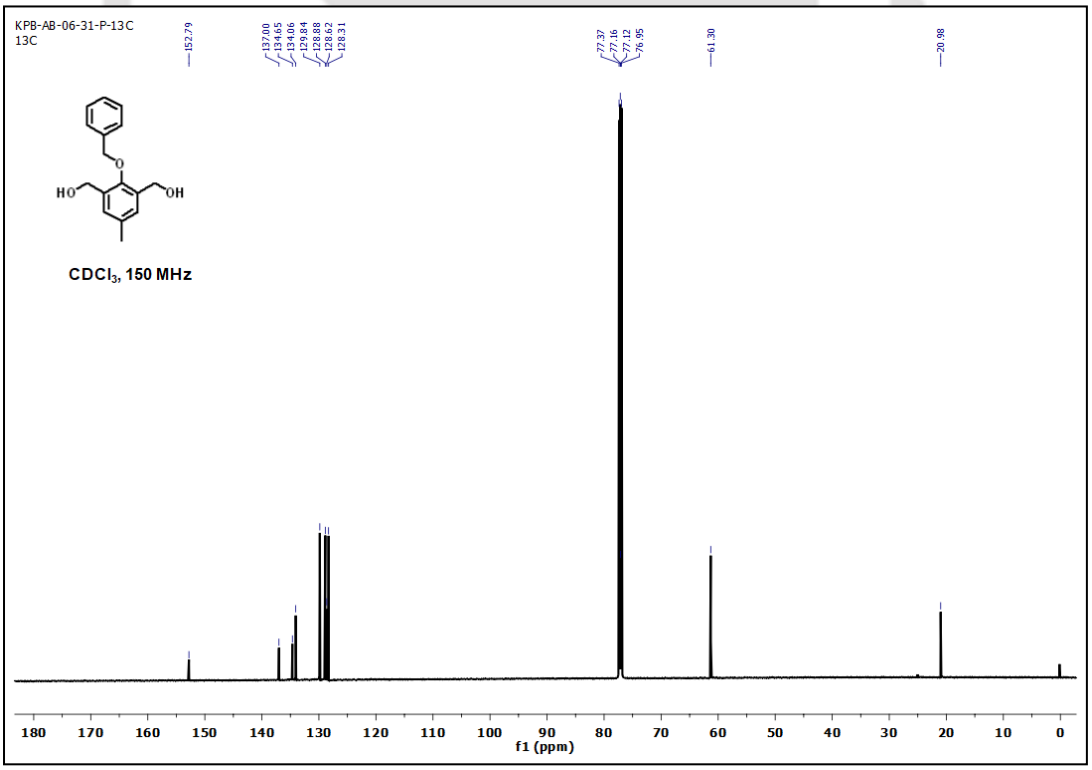

Figure A4.14: ^{13}C NMR spectrum ($CDCl_3$, 150 MHz) of compound **3.9**.

TH-3161_176122050

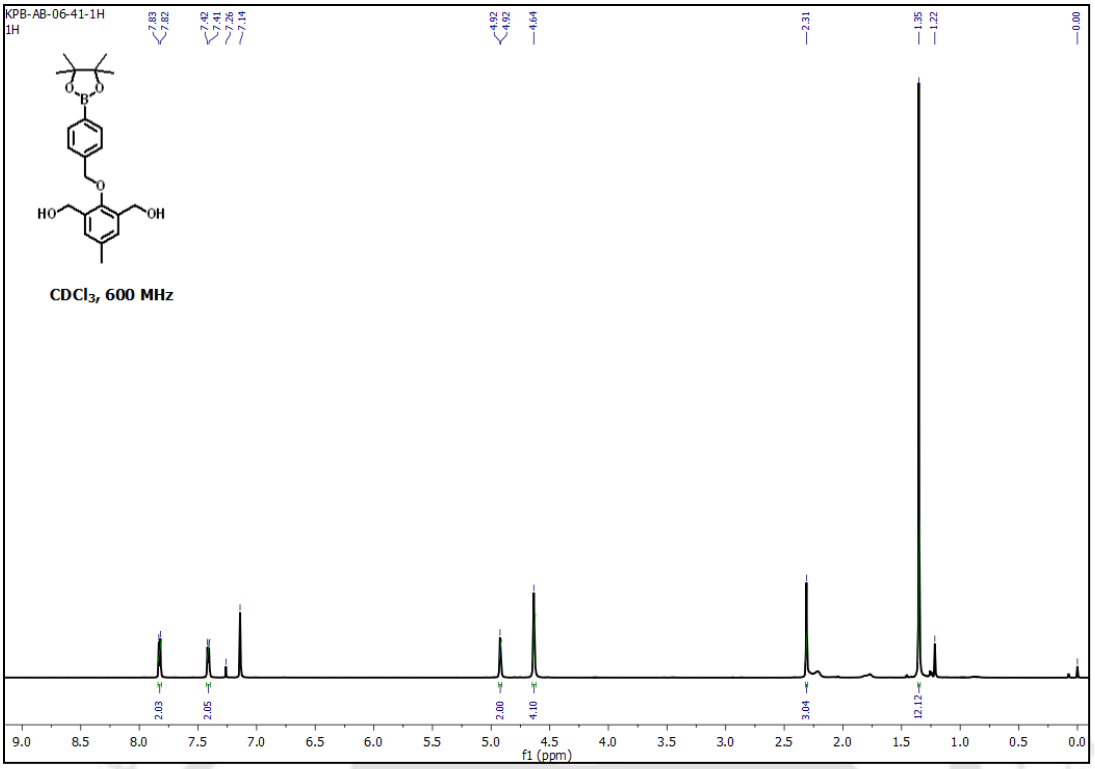

Figure A4.15: ^{1}H NMR spectrum ($CDCl_3$, 600 MHz) of compound **3.10**.

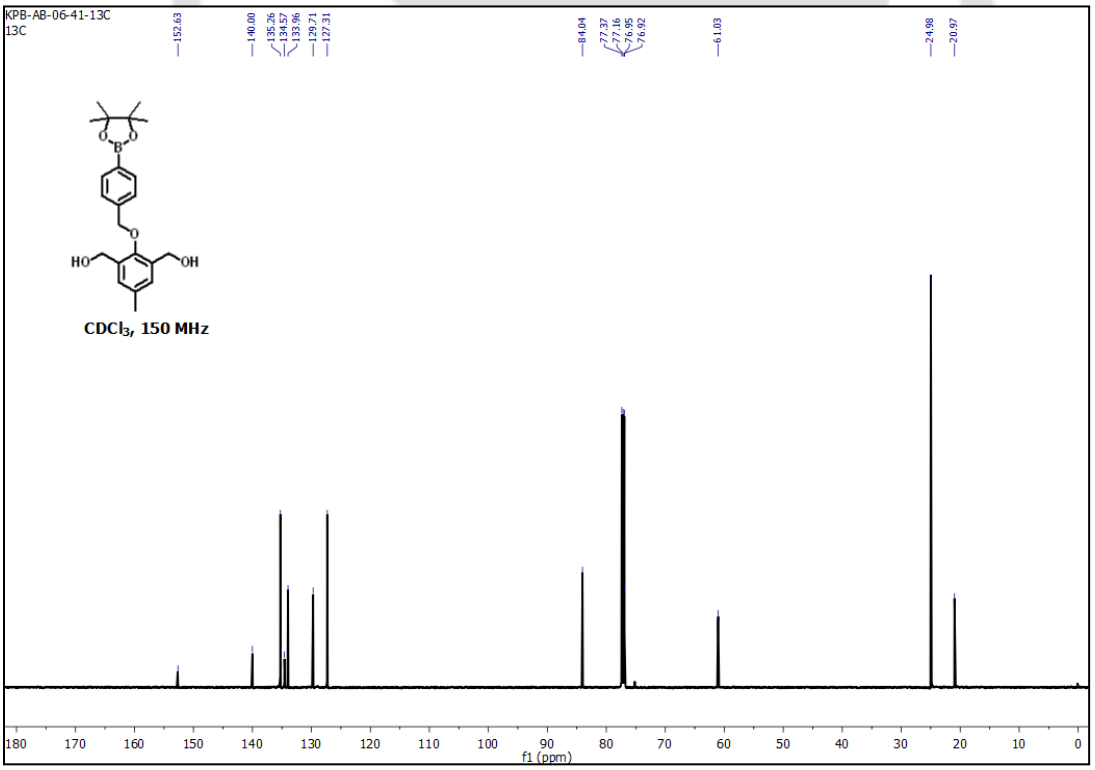

Figure A4.16: ^{13}C NMR spectrum ($CDCl_3$, 150 MHz) of compound **3.10**.

TH-3161_176122050

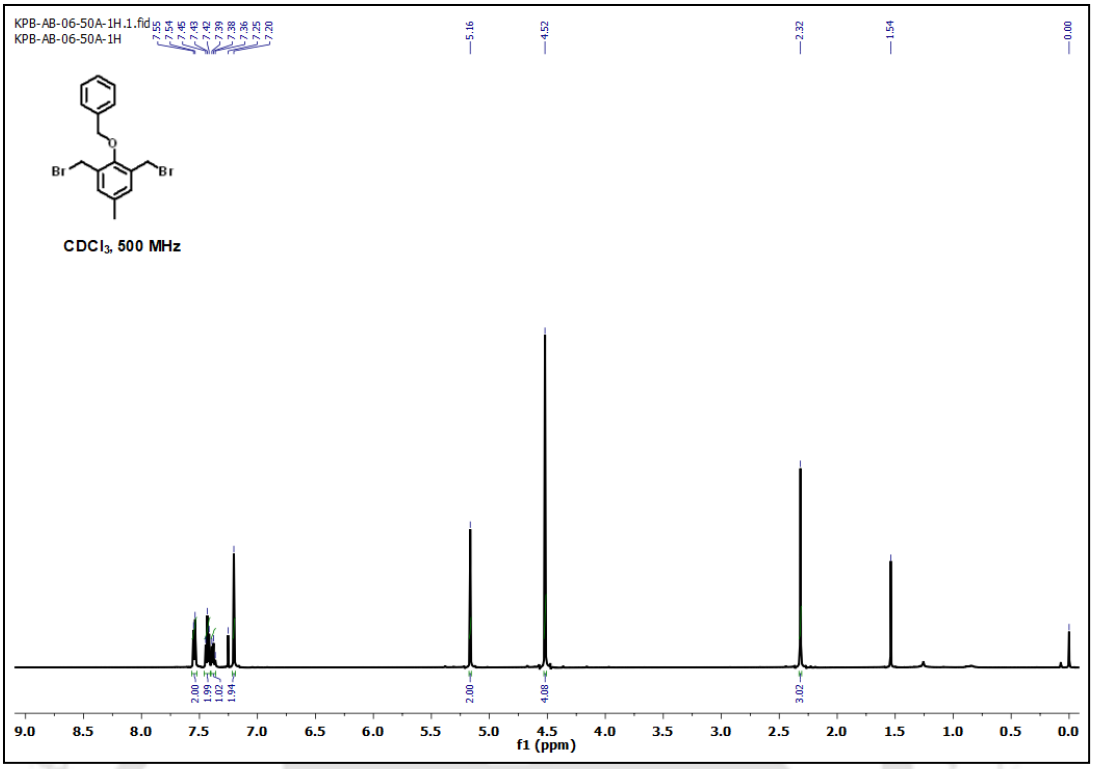

Figure A4.17: ^{1}H NMR spectrum ($CDCl_3$, 500 MHz) of compound **3.11**.

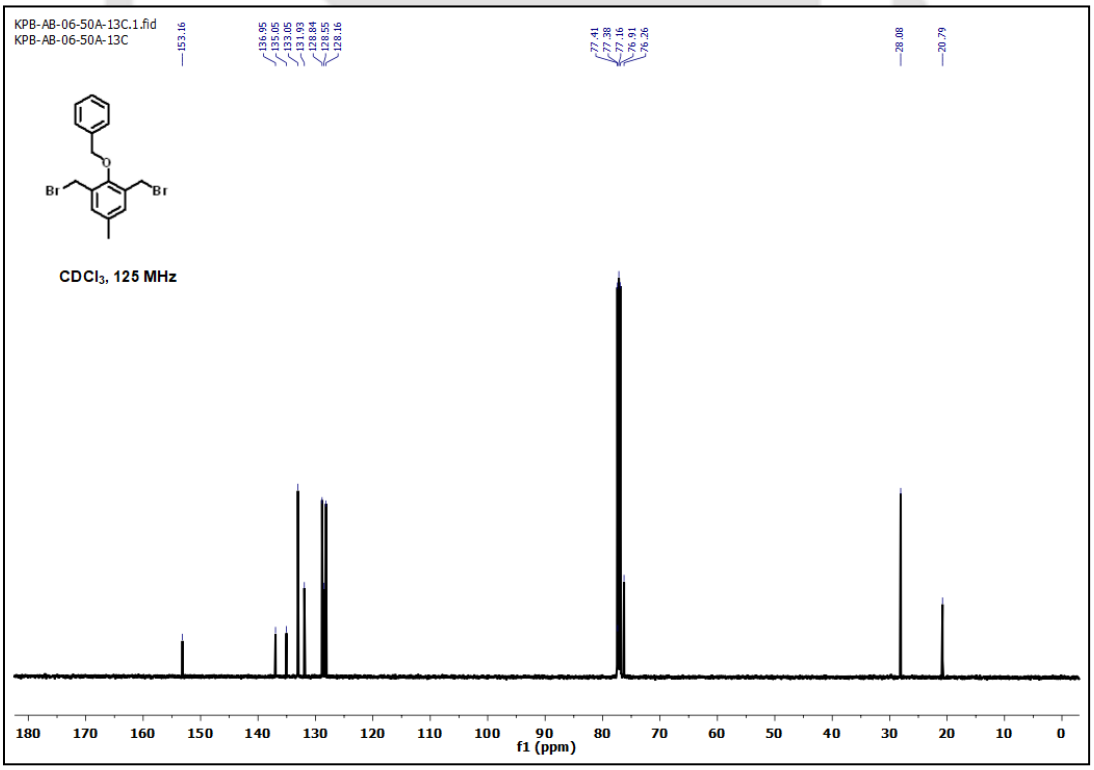

Figure A4.18: ^{13}C NMR spectrum ($CDCl_3$, 125 MHz) of compound **3.11**.

TH-3161_176122050

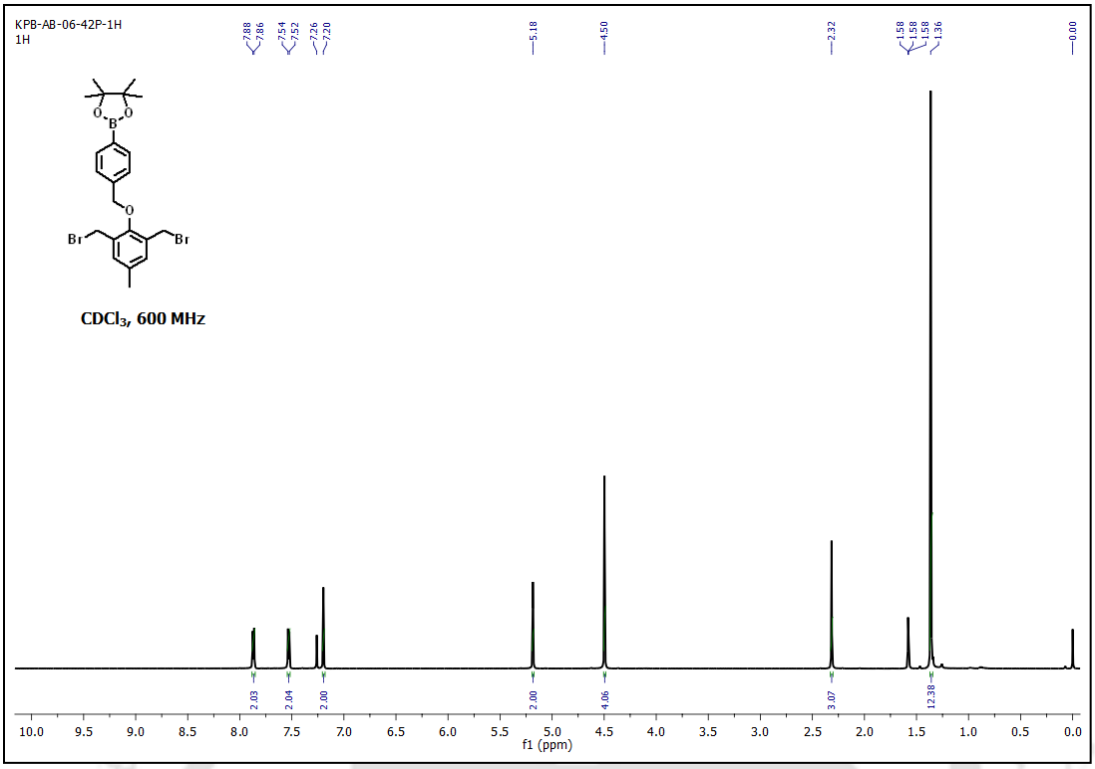

Figure A4.19: ^{1}H NMR spectrum ($CDCl_3$, 600 MHz) of compound **3.12**.

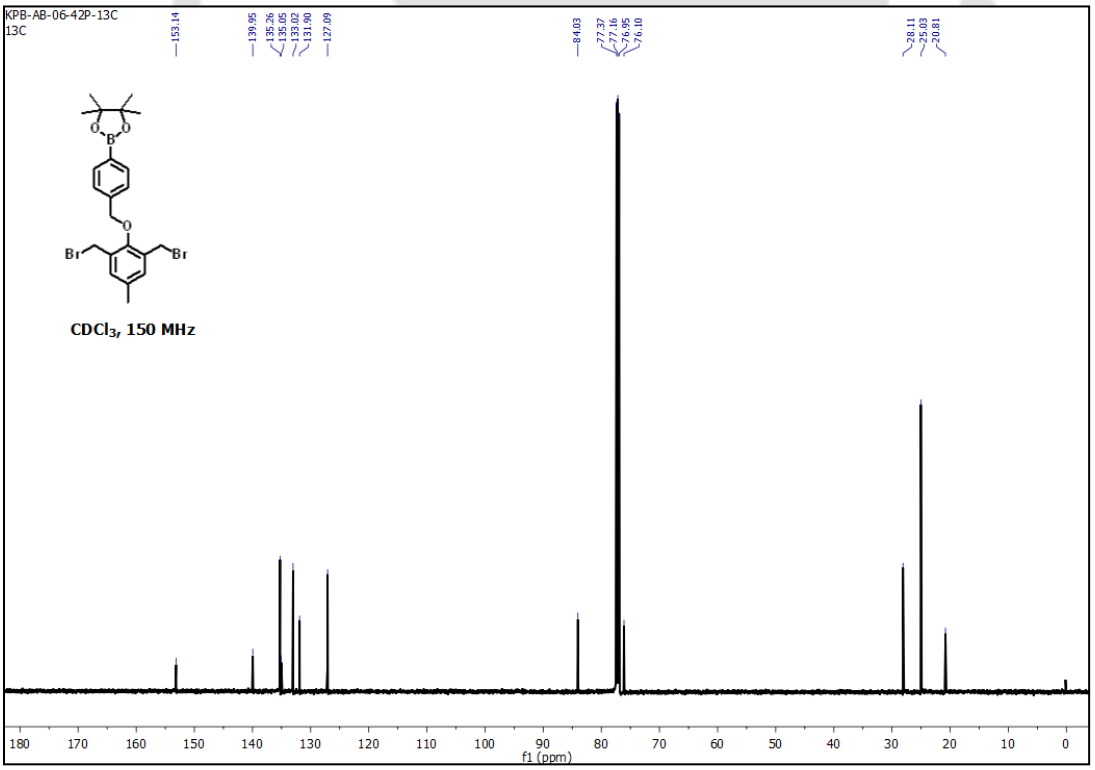

Figure A4.20: ^{13}C NMR spectrum ($CDCl_3$, 150 MHz) of compound **3.12**.

TH-3161_176122050

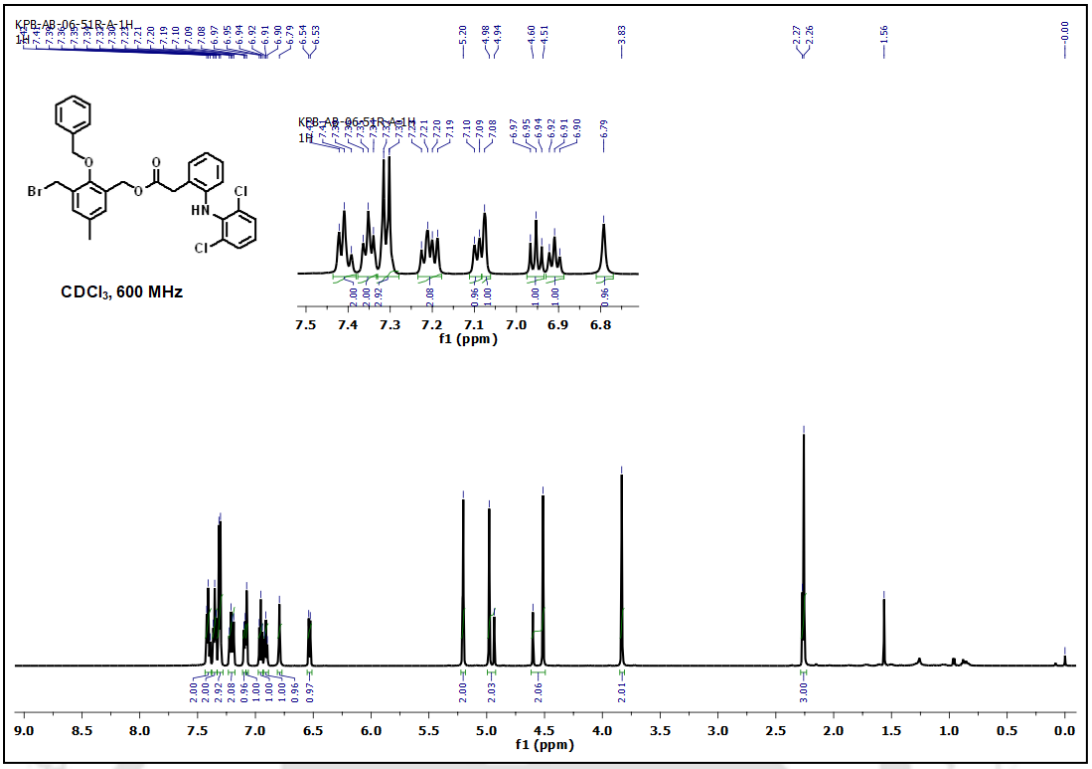

Figure A4.21: ^{1}H NMR spectrum ($CDCl_3$, 600 MHz) of compound **3.13**.

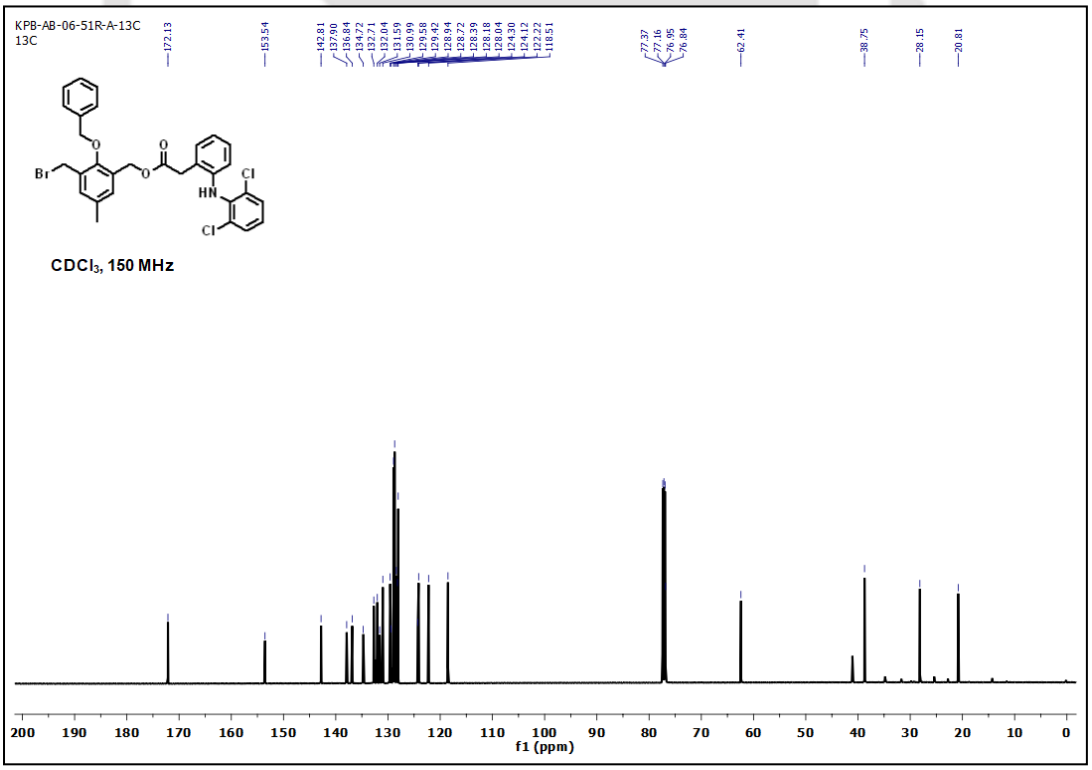

Figure A4.22: ^{13}C NMR spectrum ($CDCl_3$, 150 MHz) of compound **3.13**.

TH-3161_176122050

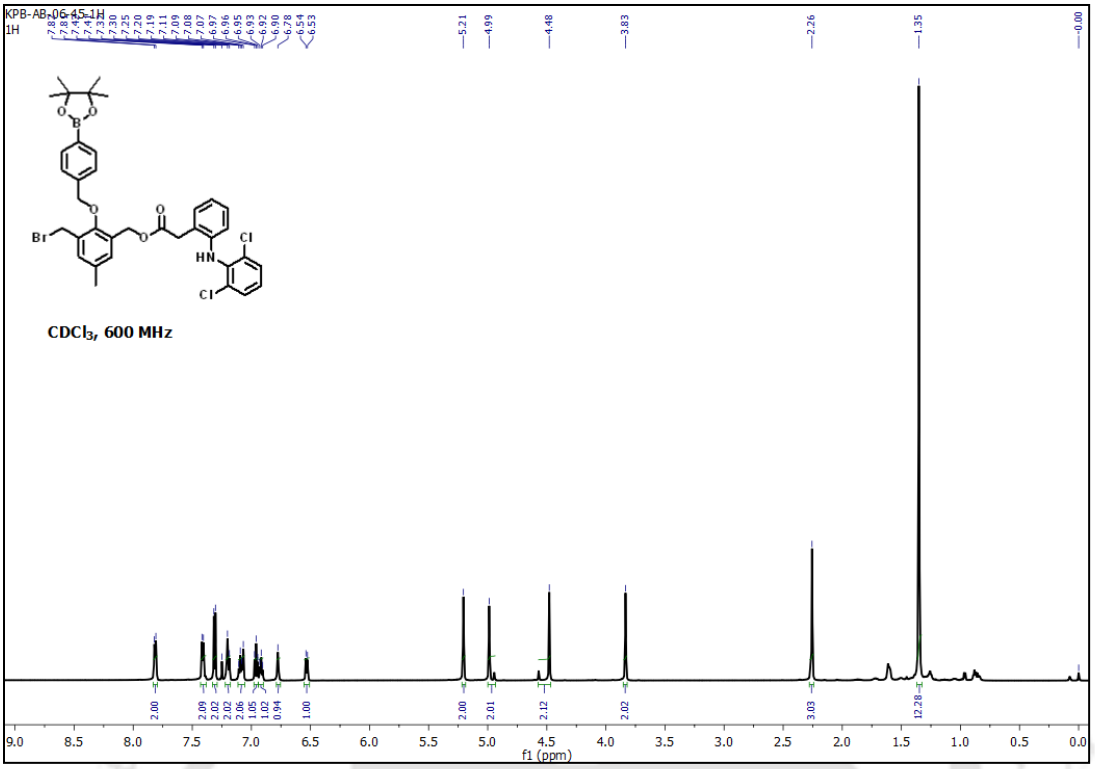

Figure A4.23: ^{1}H NMR spectrum ($CDCl_3$, 600 MHz) of compound **3.14**.

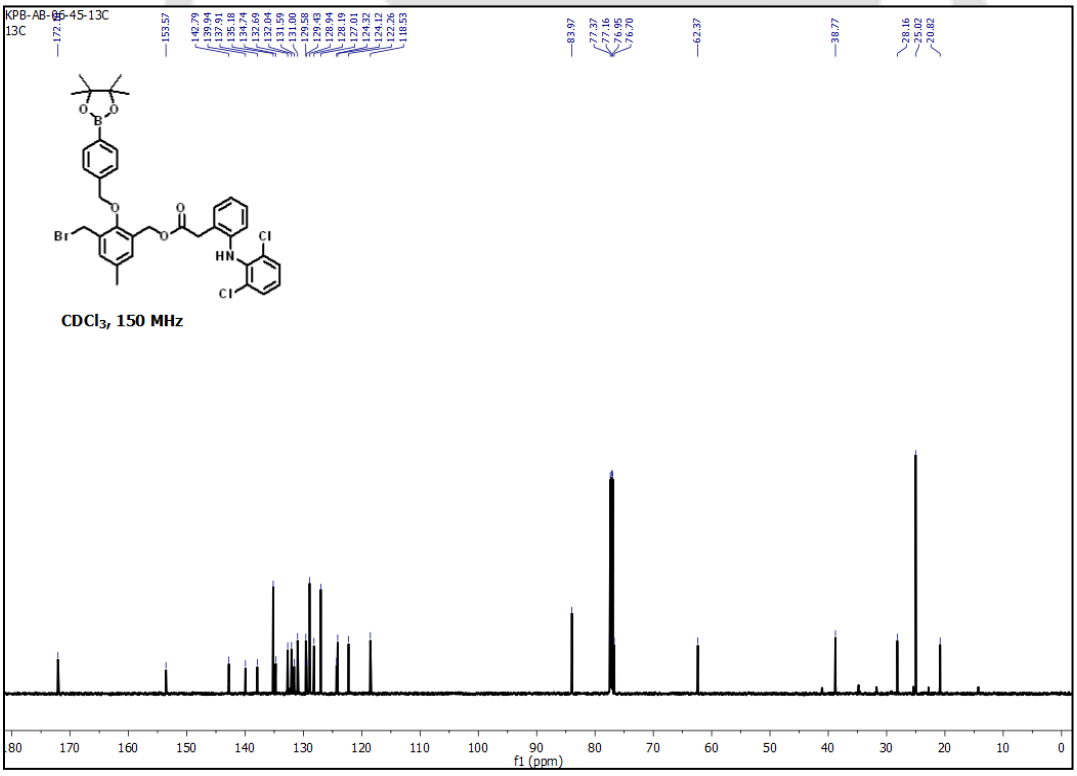

Figure A4.24: ^{13}C NMR spectrum ($CDCl_3$, 150 MHz) of compound **3.14**.

TH-3161_176122050

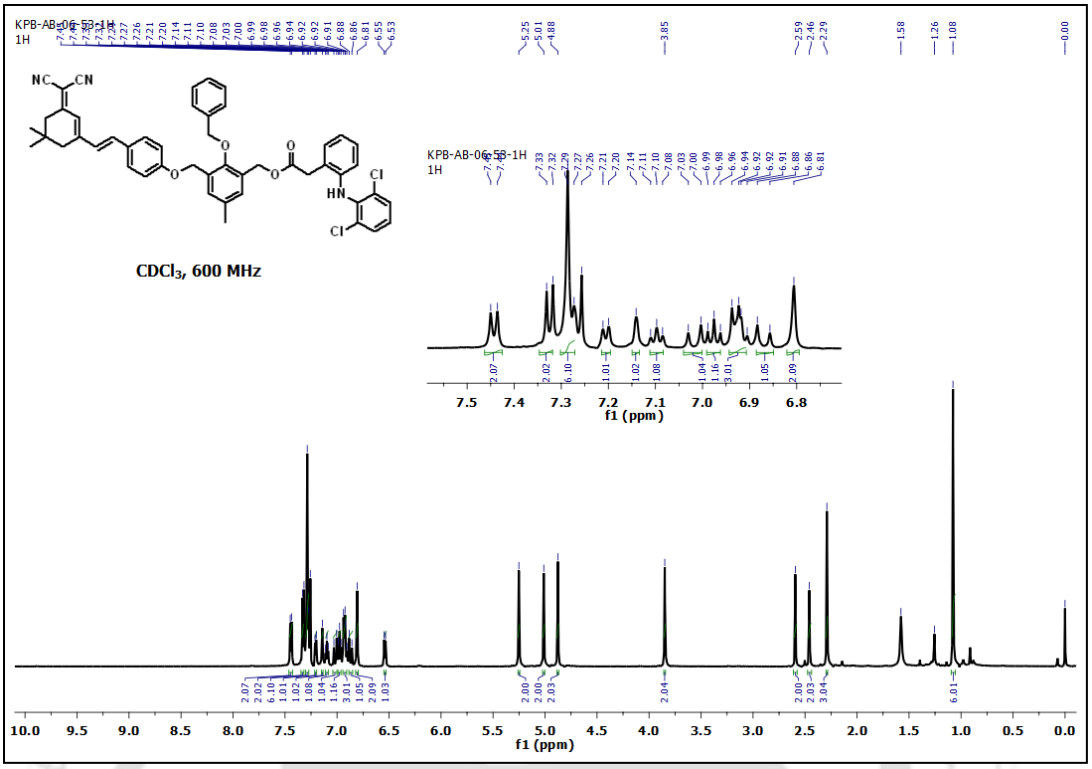

Figure A4.25: ^{1}H NMR spectrum ($CDCl_3$, 600 MHz) of **DCI-Con**.

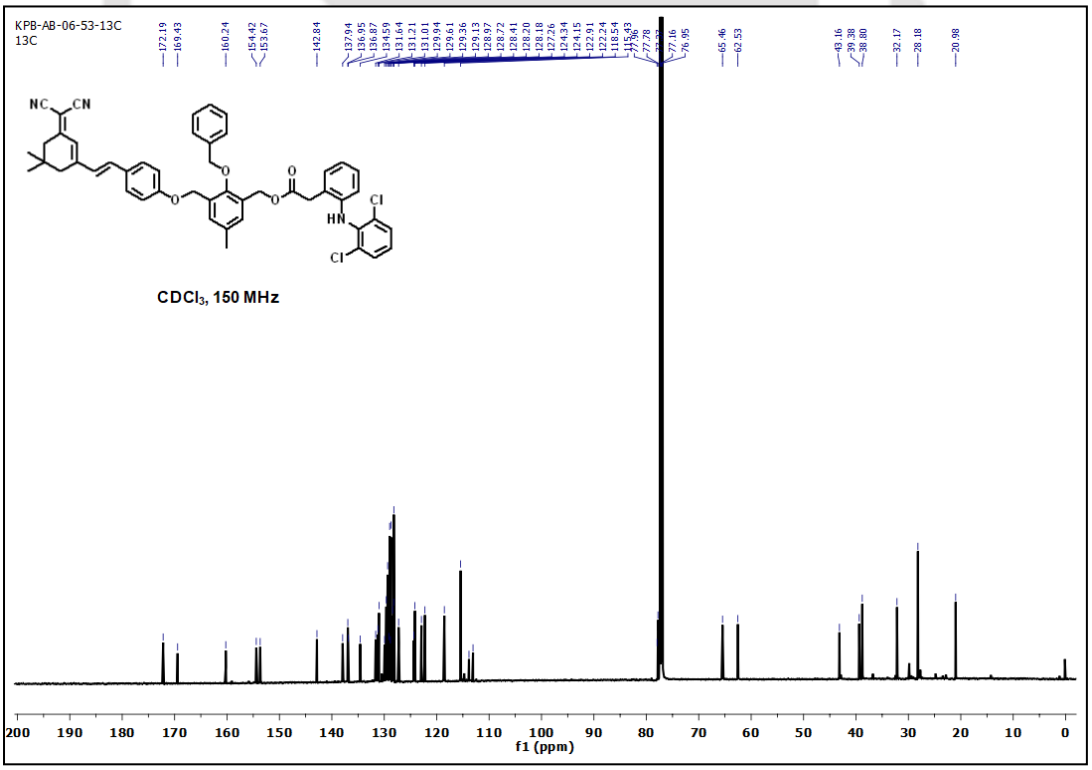

Figure A4.26: ^{13}C NMR spectrum ($CDCl_3$, 150 MHz) of **DCI-Con**.

TH-3161_176122050

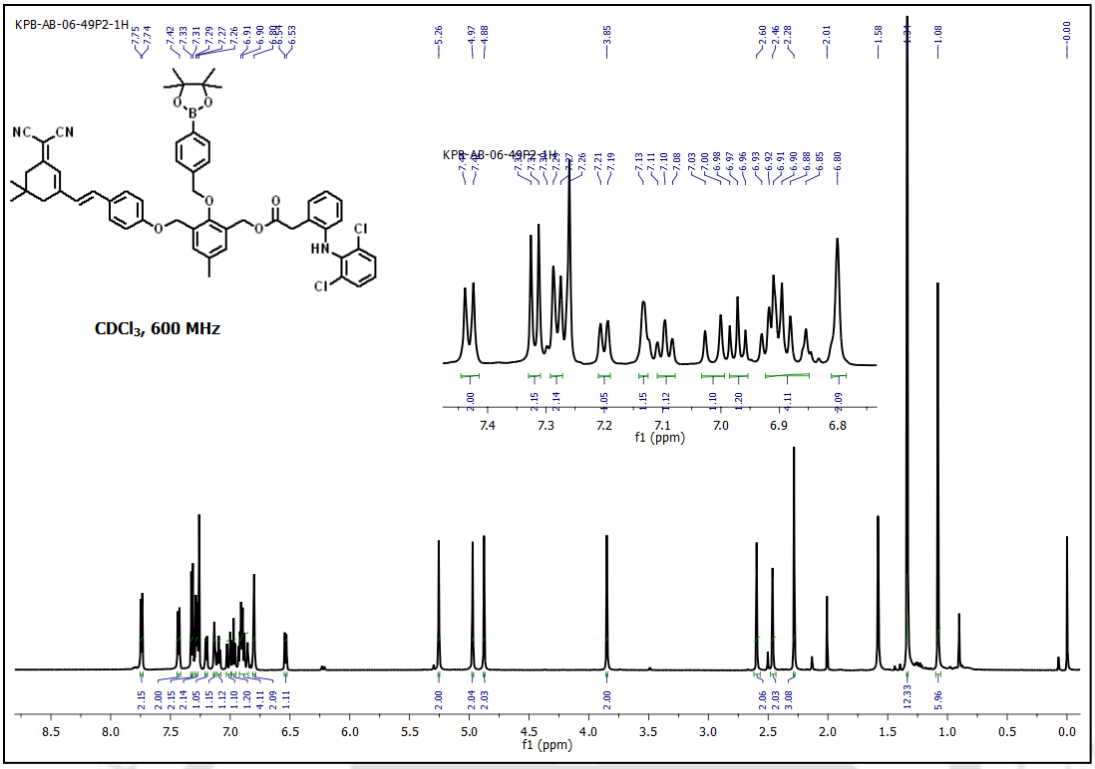

Figure A4.27: ^{1}H NMR spectrum ($CDCl_3$, 600 MHz) of **DCI-ROS**.

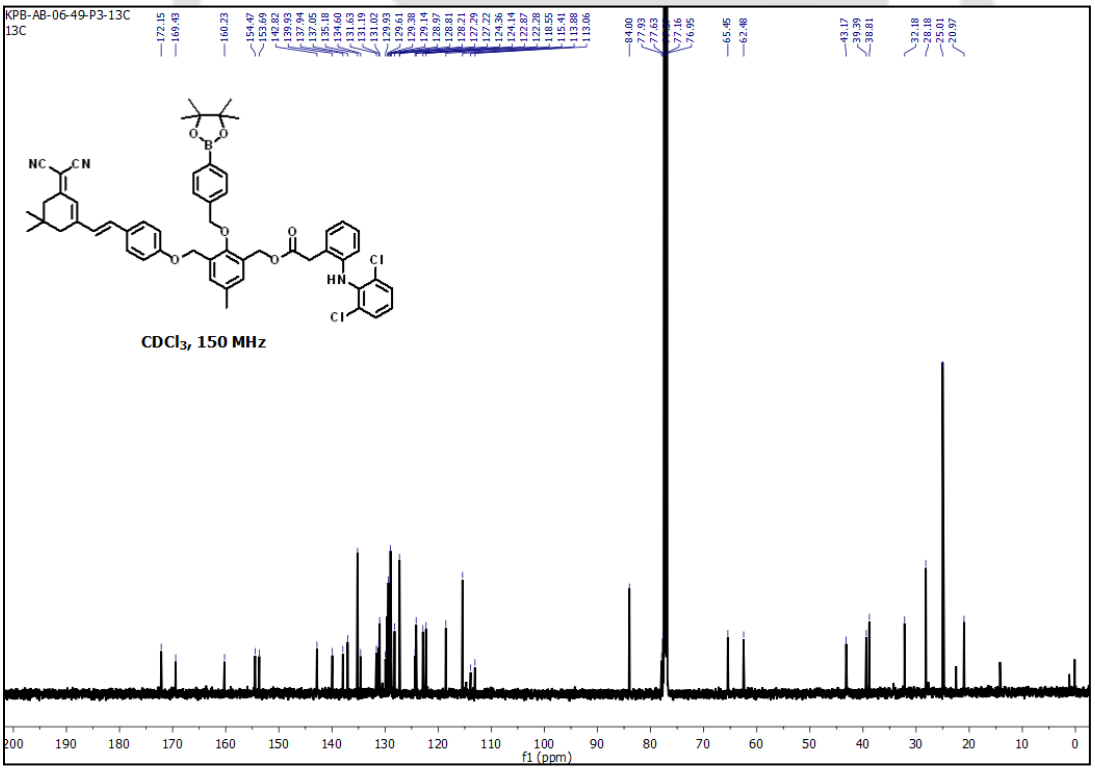

Figure A4.28: ^{13}C NMR spectrum ($CDCl_3$, 150 MHz) of **DCI-ROS**.

TH-3161_176122050

Supplementary data of chapter 4

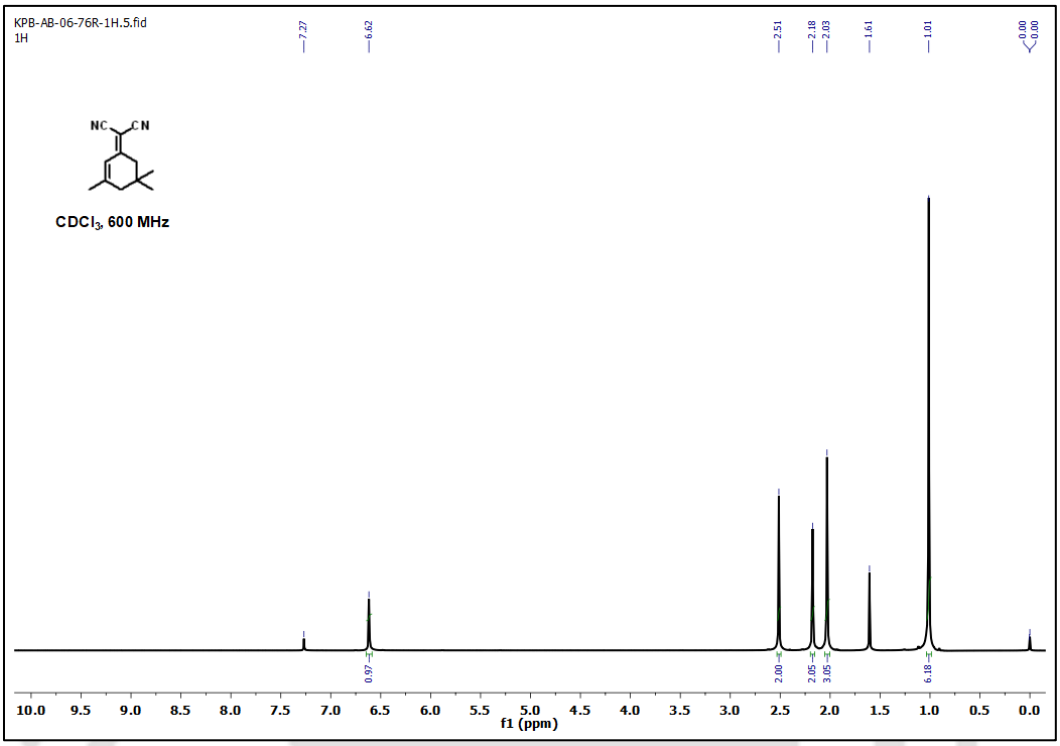

Figure A5.1: ^{1}H NMR spectrum ($CDCl_3$, 600 MHz, ppm) of compound **4.2**.

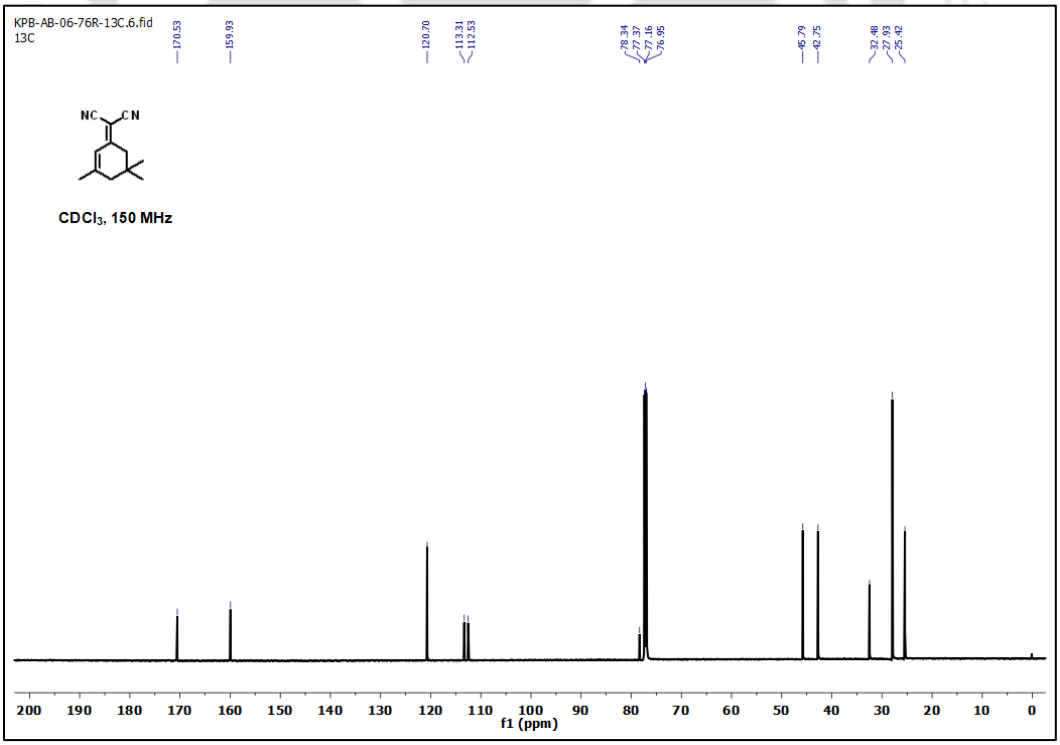

Figure A5.2: ^{13}C NMR spectrum ($CDCl_3$, 150 MHz, ppm) of compound **4.2**.

TH-3161_176122050

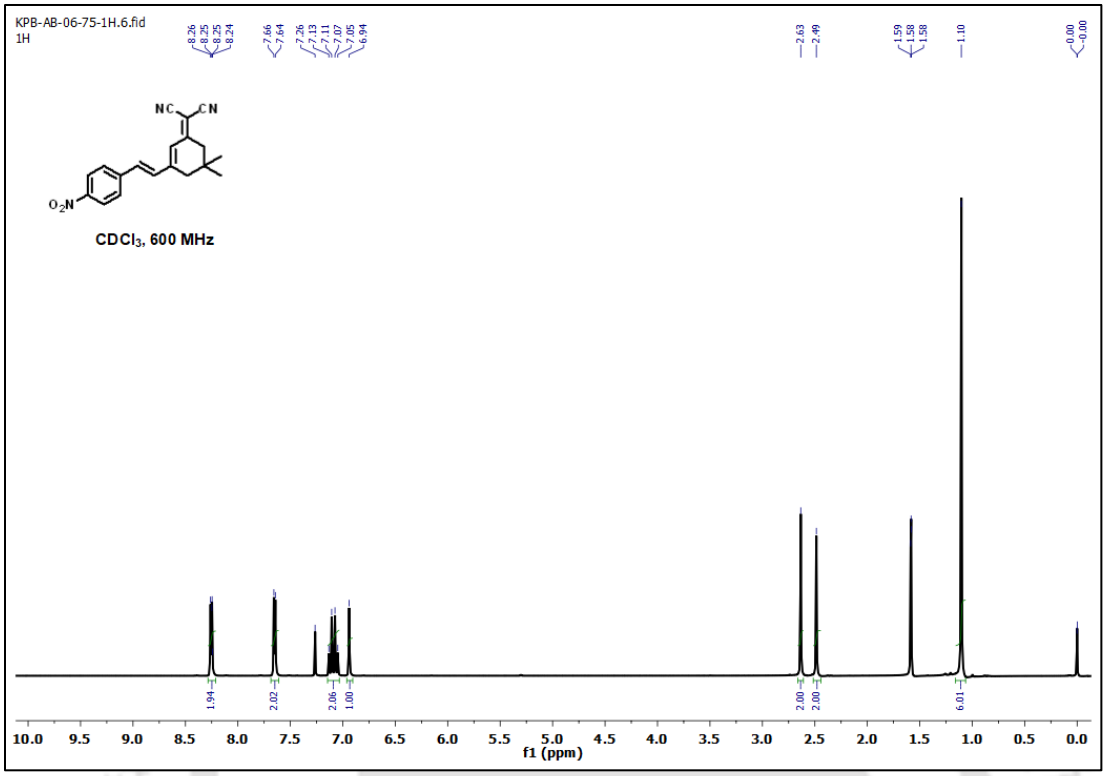

Figure A5.3: ^{1}H NMR spectrum ($CDCl_3$, 600 MHz, ppm) of compound **4.3**.

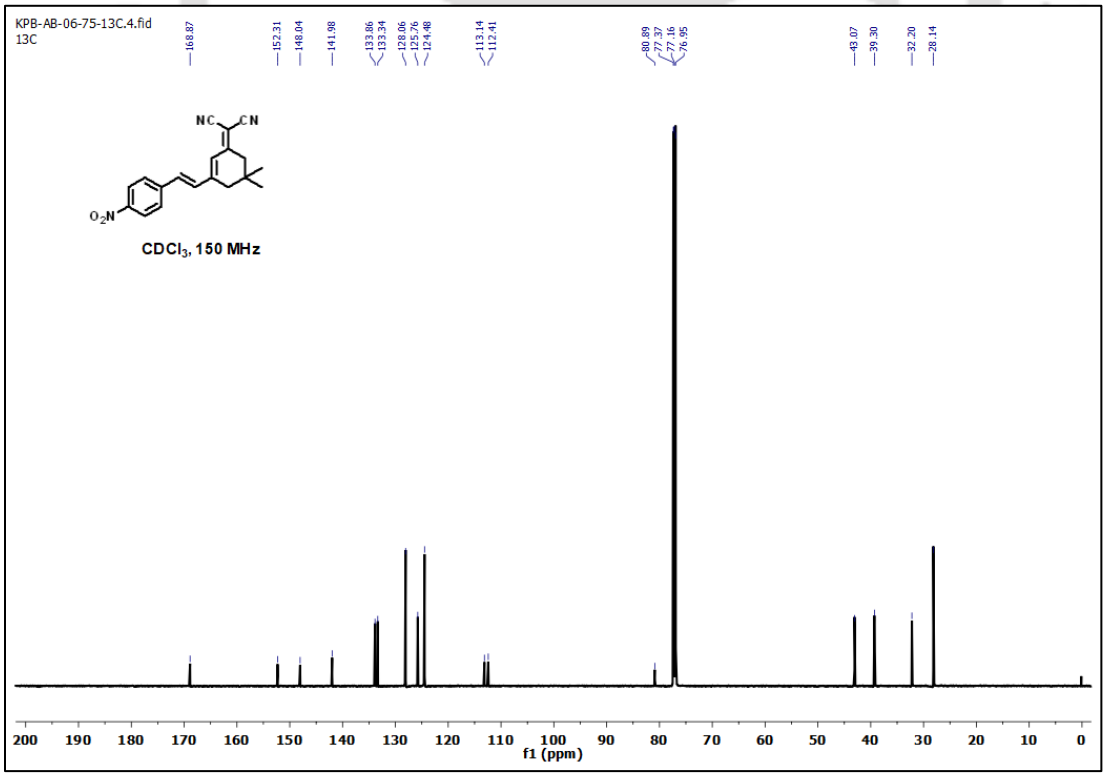

Figure A5.4: ^{13}C NMR spectrum ($CDCl_3$, 150 MHz, ppm) of compound **4.3**.

TH-3161_176122050

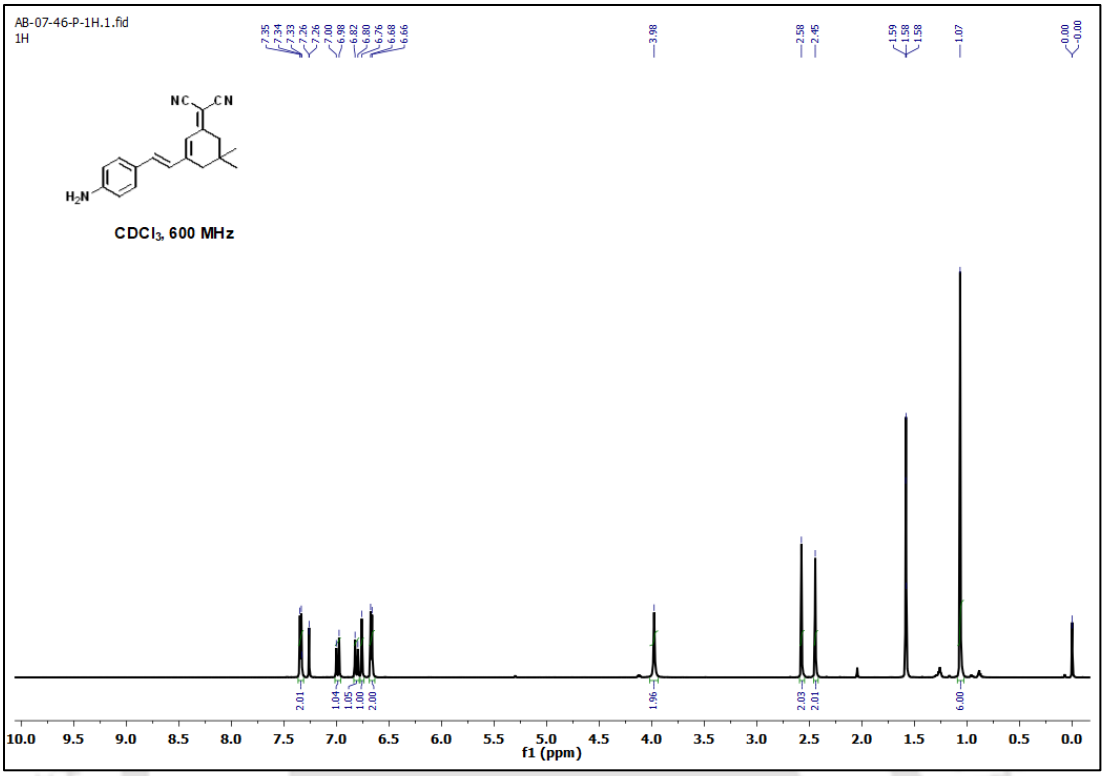

Figure A5.5: ^{1}H NMR spectrum ($CDCl_3$, 600 MHz, ppm) of **DCI-NH$_2$**.

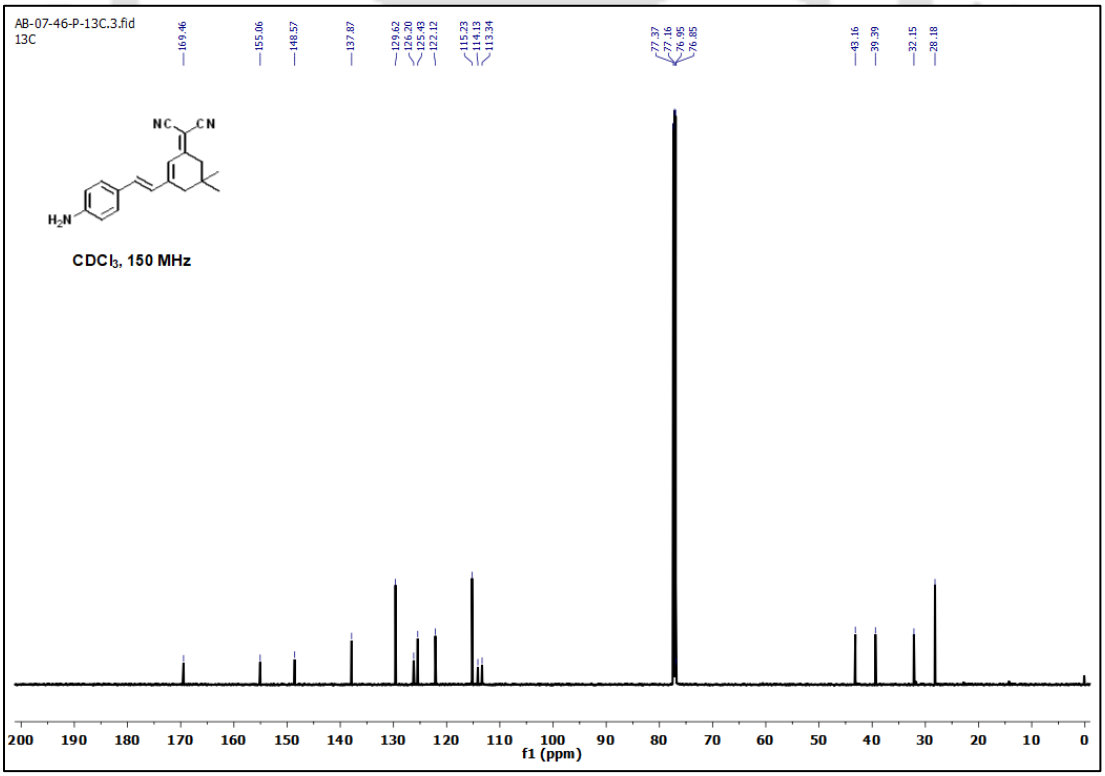

Figure A5.6: ^{13}C NMR spectrum ($CDCl_3$, 150 MHz, ppm) of **DCI-NH$_2$**.

TH-3161_176122050

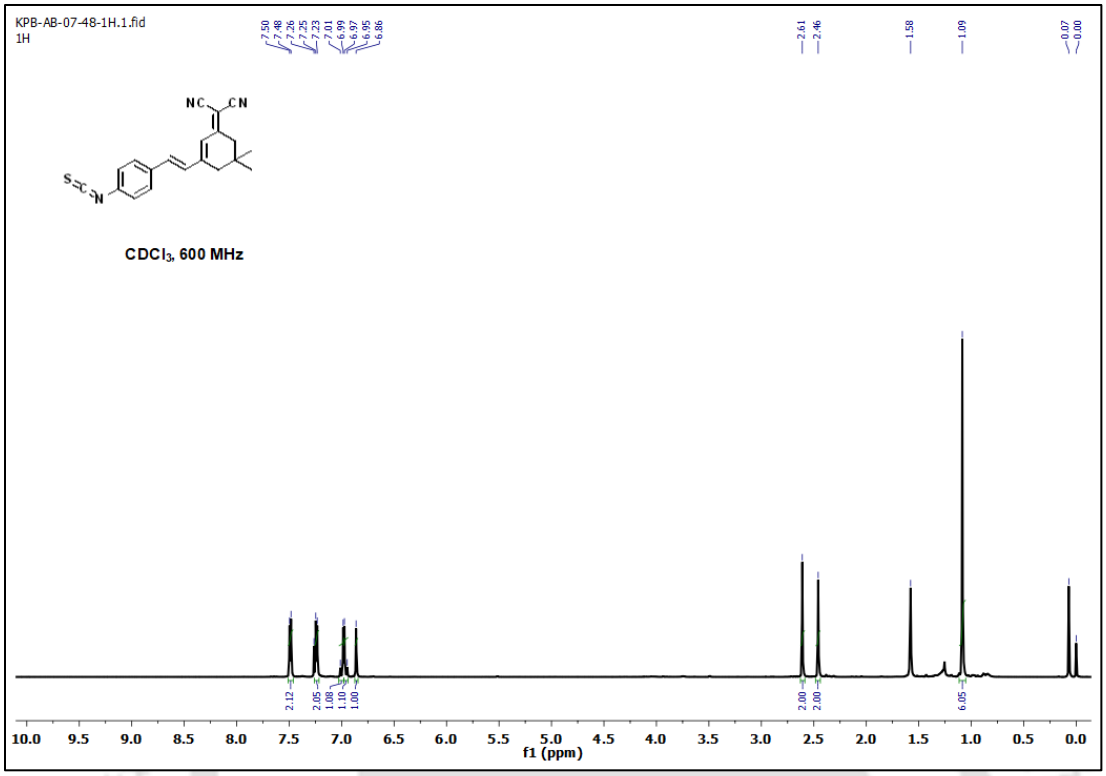

Figure A5.7: ^{1}H NMR spectrum ($CDCl_3$, 600 MHz, ppm) of **DCI-NCS**.

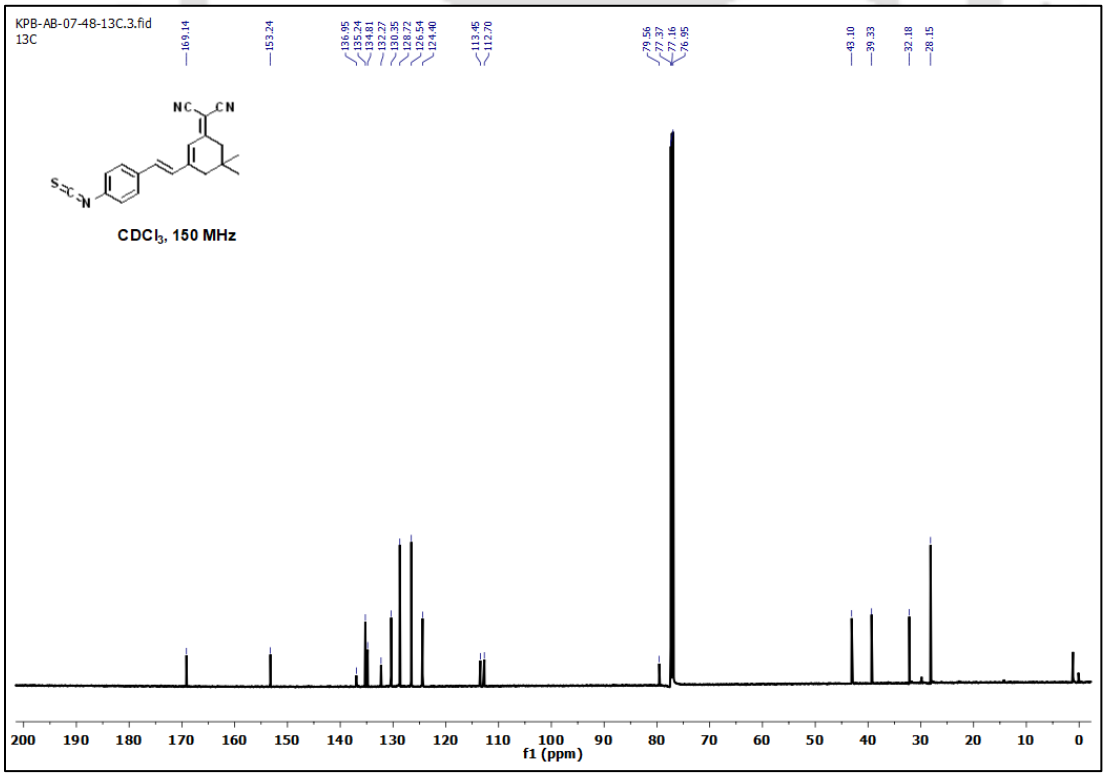

Figure A5.8: ^{13}C NMR spectrum ($CDCl_3$, 150 MHz, ppm) of **DCI-NCS**.

TH-3161_176122050

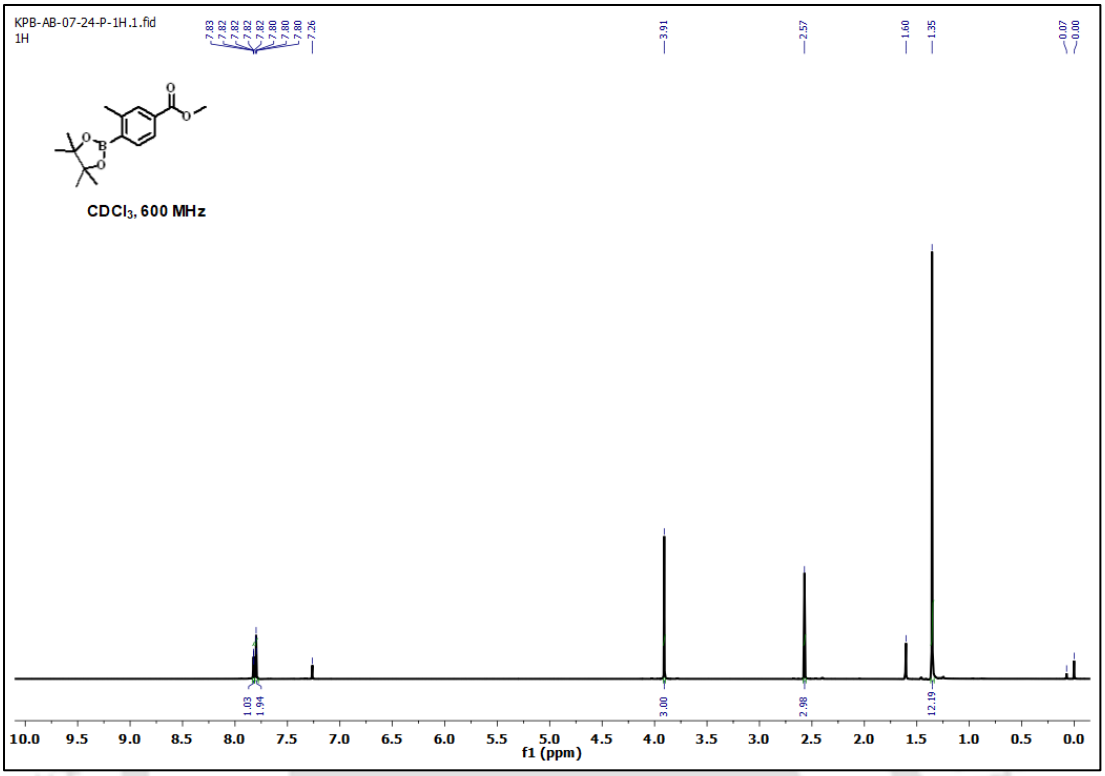

Figure A5.9: ^{1}H NMR spectrum ($CDCl_3$, 600 MHz, ppm) of compound **4.5**.

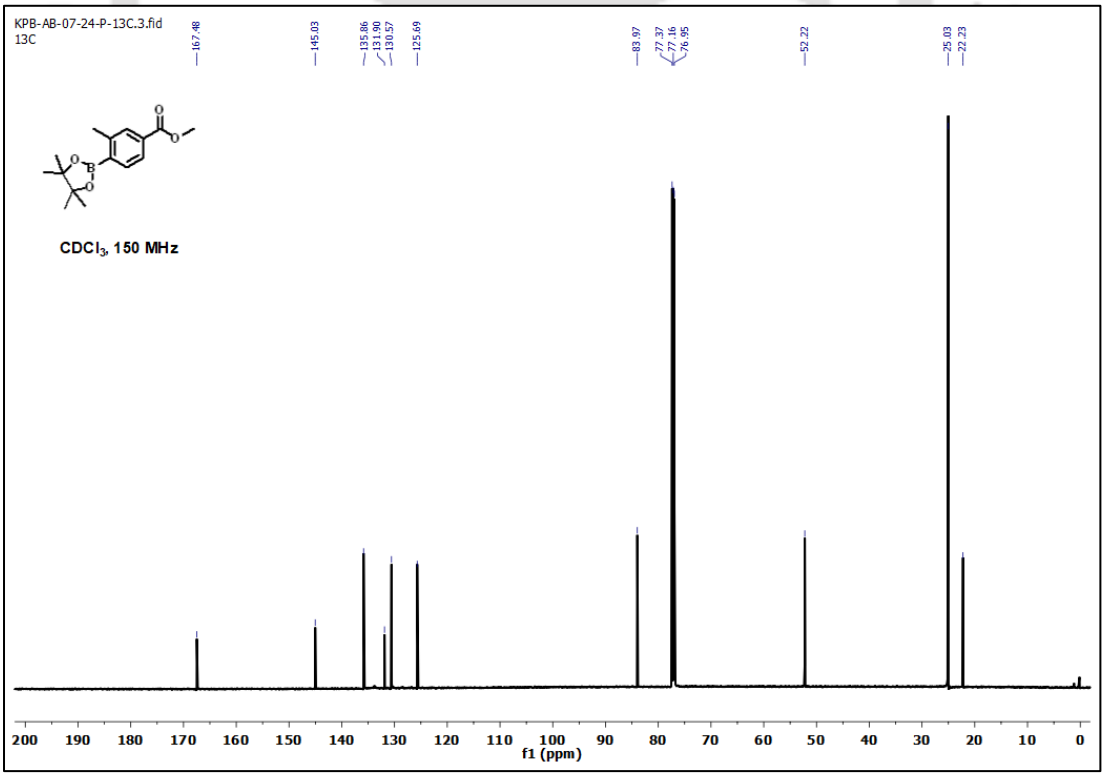

Figure A5.10: ^{13}C NMR spectrum ($CDCl_3$, 150 MHz, ppm) of compound **4.5**.

TH-3161_176122050

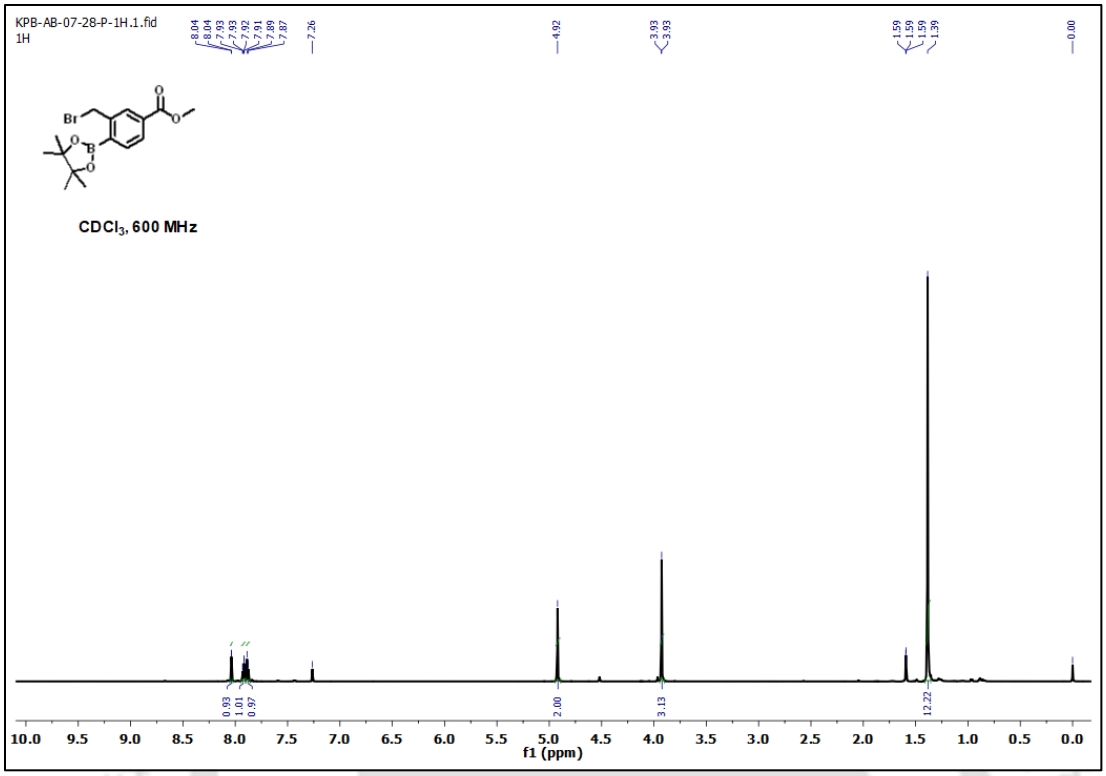

Figure A5.11: ^{1}H NMR spectrum ($CDCl_3$, 600 MHz, ppm) of compound **4.6**.

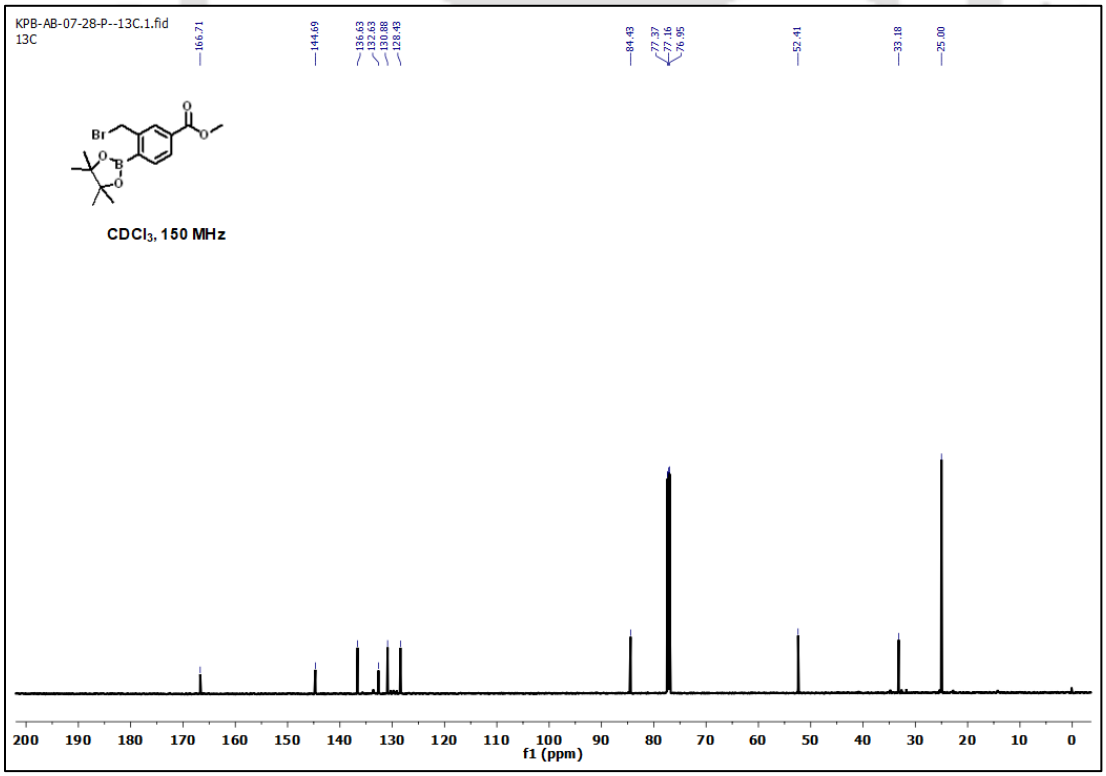

Figure A5.12: ^{13}C NMR spectrum ($CDCl_3$, 150 MHz, ppm) of compound **4.6**.

TH-3161_176122050

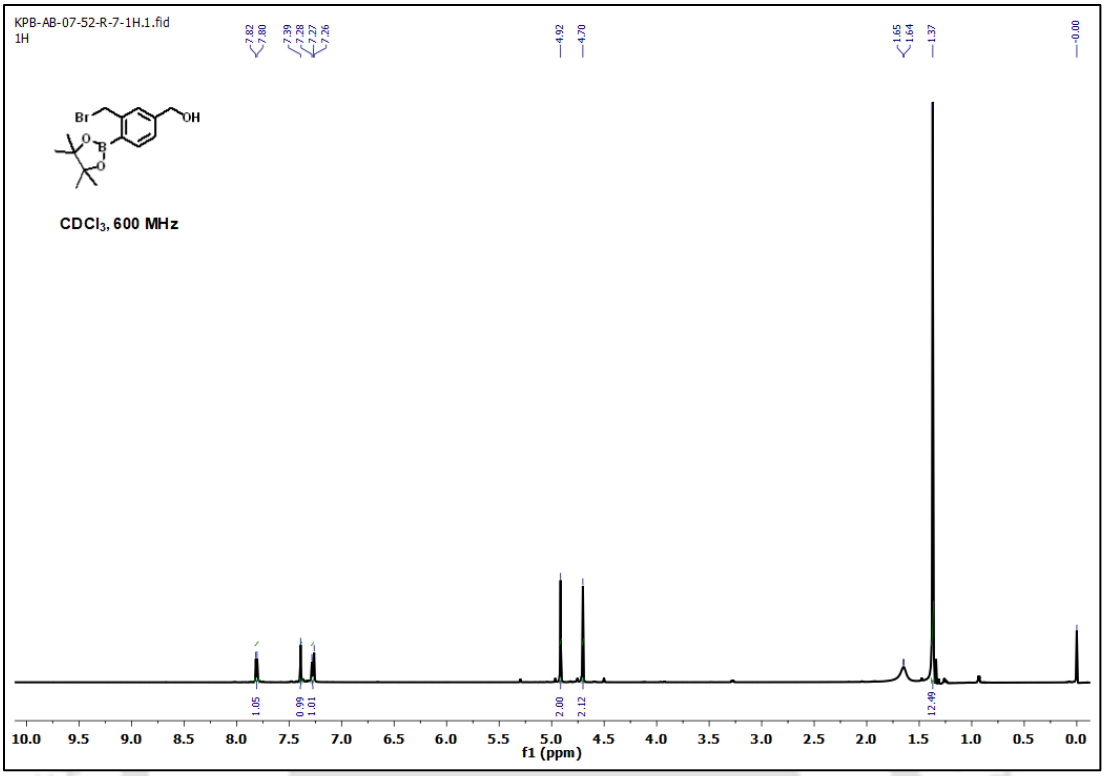

Figure A5.13: ^{1}H NMR spectrum ($CDCl_3$, 600 MHz, ppm) of compound **4.7**.

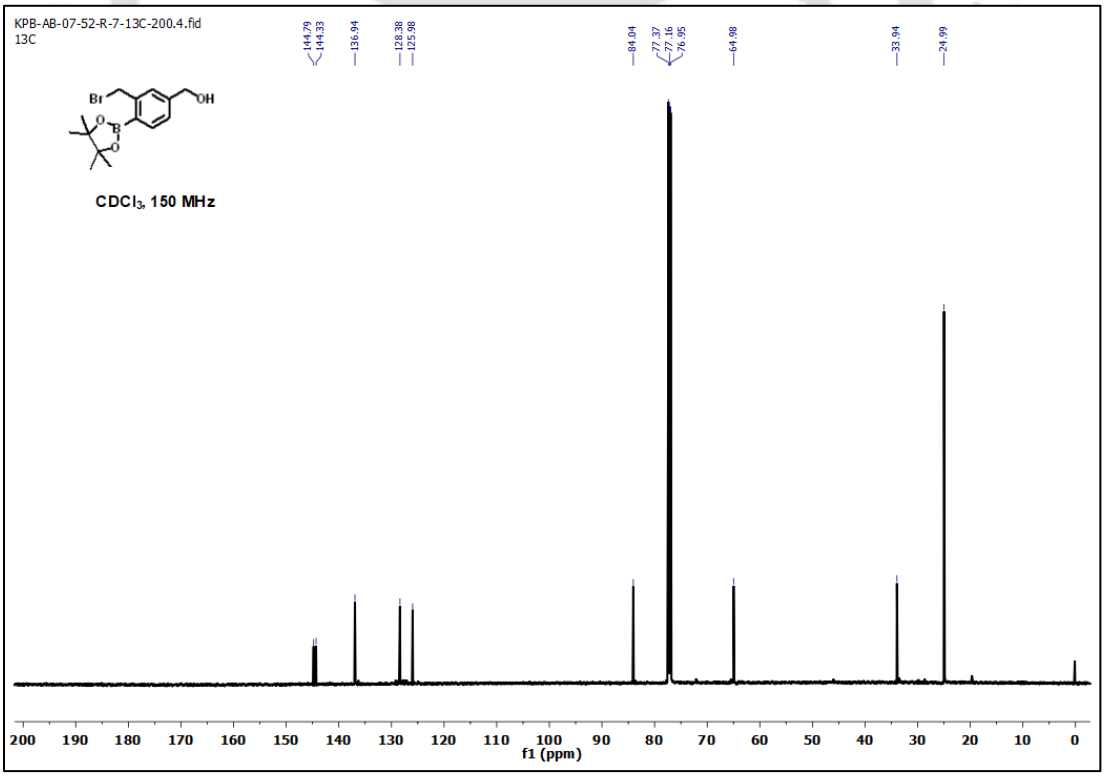

Figure A5.14: ^{13}C NMR spectrum ($CDCl_3$, 150 MHz, ppm) of compound **4.7**.

TH-3161_176122050

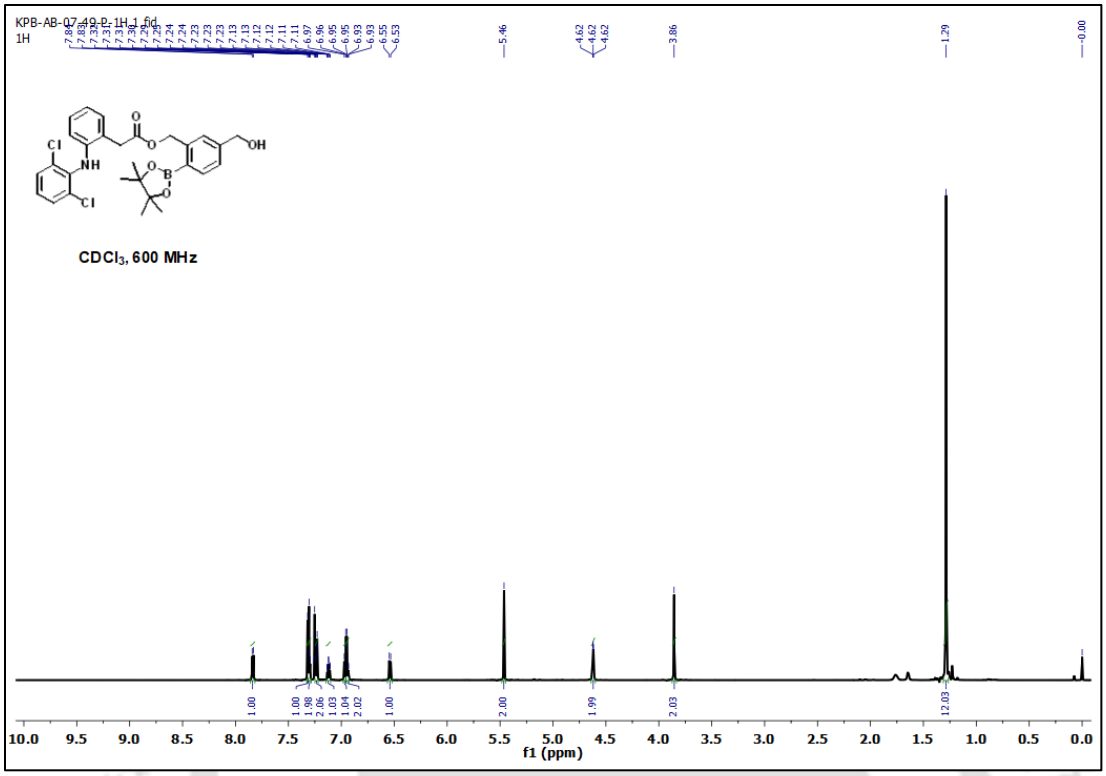

Figure A5.15: ^{1}H NMR spectrum ($CDCl_3$, 600 MHz, ppm) of compound **4.8**.

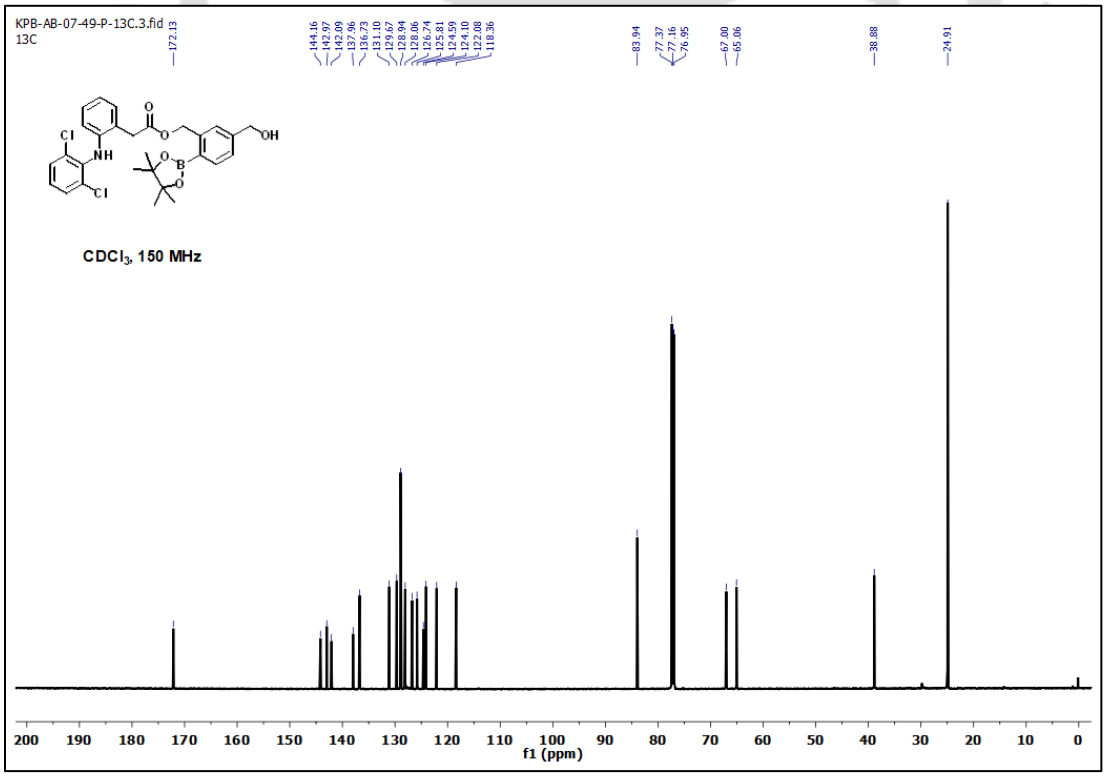

Figure A5.16: ^{13}C NMR spectrum ($CDCl_3$, 150 MHz, ppm) of compound **4.8**.

TH-3161_176122050

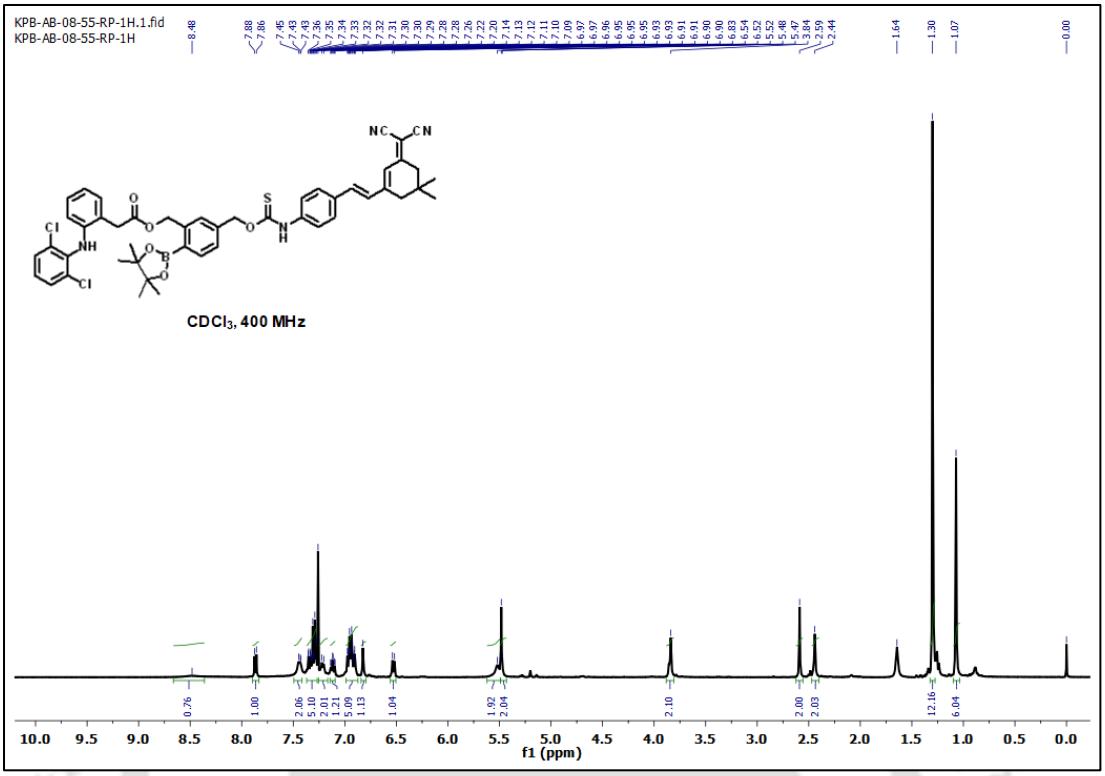

Figure A5.17: ^{1}H NMR spectrum ($CDCl_3$, 400 MHz, ppm) of **DCF-HS**.

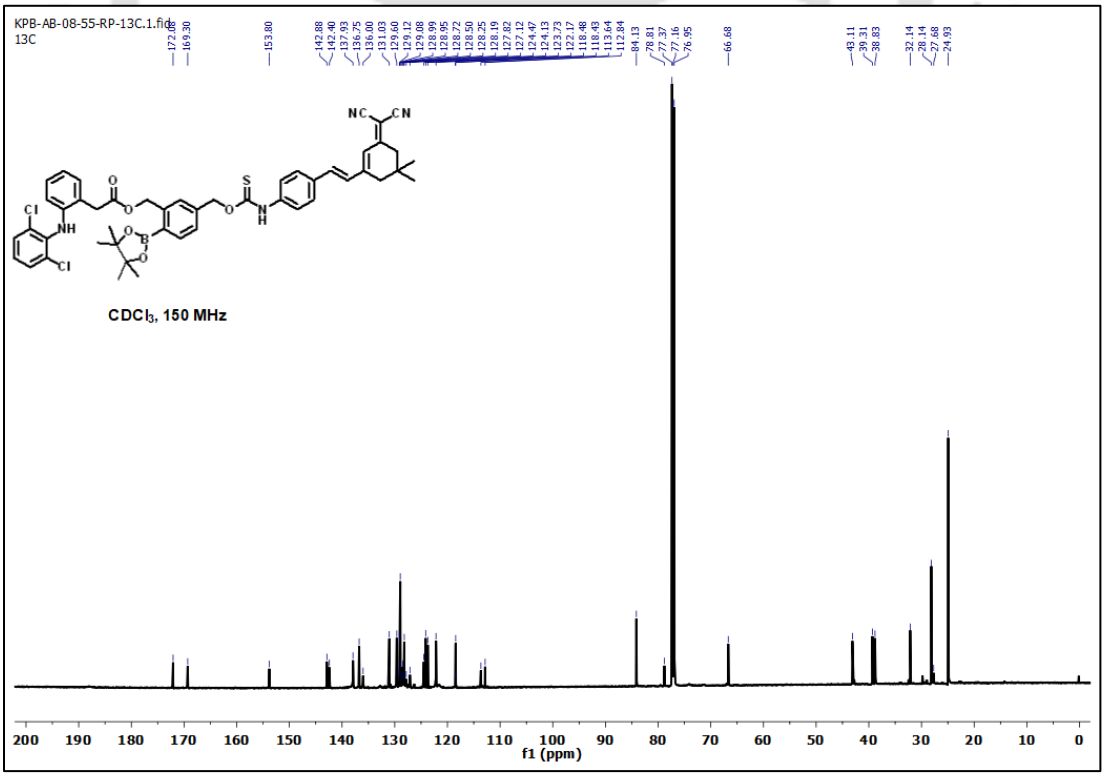

Figure A5.18: ^{13}C NMR spectrum ($CDCl_3$, 150 MHz, ppm) of **DCF-HS**.

TH-3161_176122050

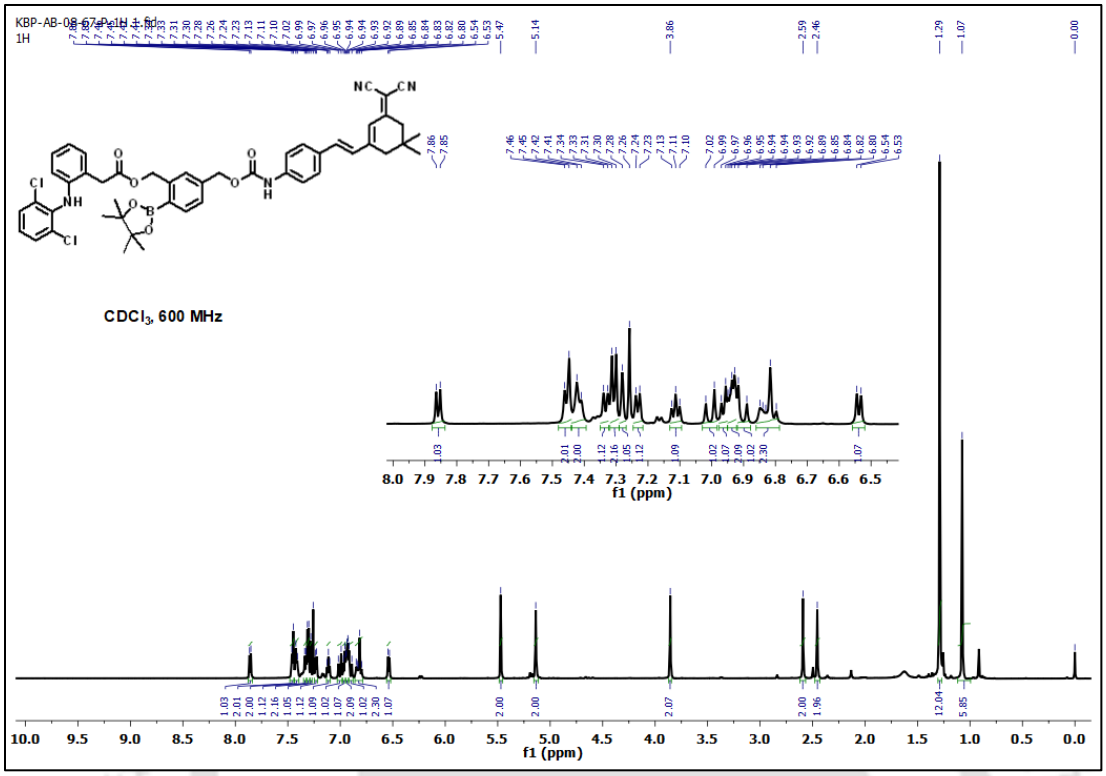

Figure A5.19: ^{1}H NMR spectrum ($CDCl_3$, 600 MHz, ppm) of **DCF-Con**.

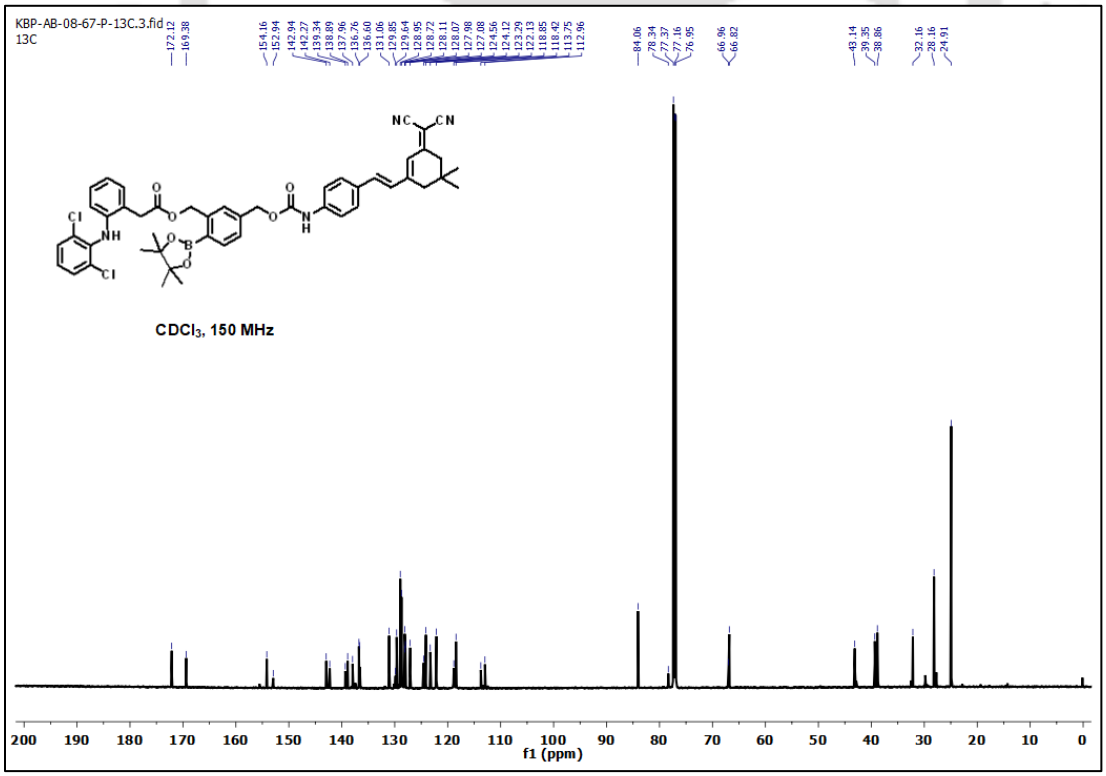

Figure A5.20: ^{13}C NMR spectrum ($CDCl_3$, 150 MHz, ppm) of **DCF-Con**.

TH-3161_176122050

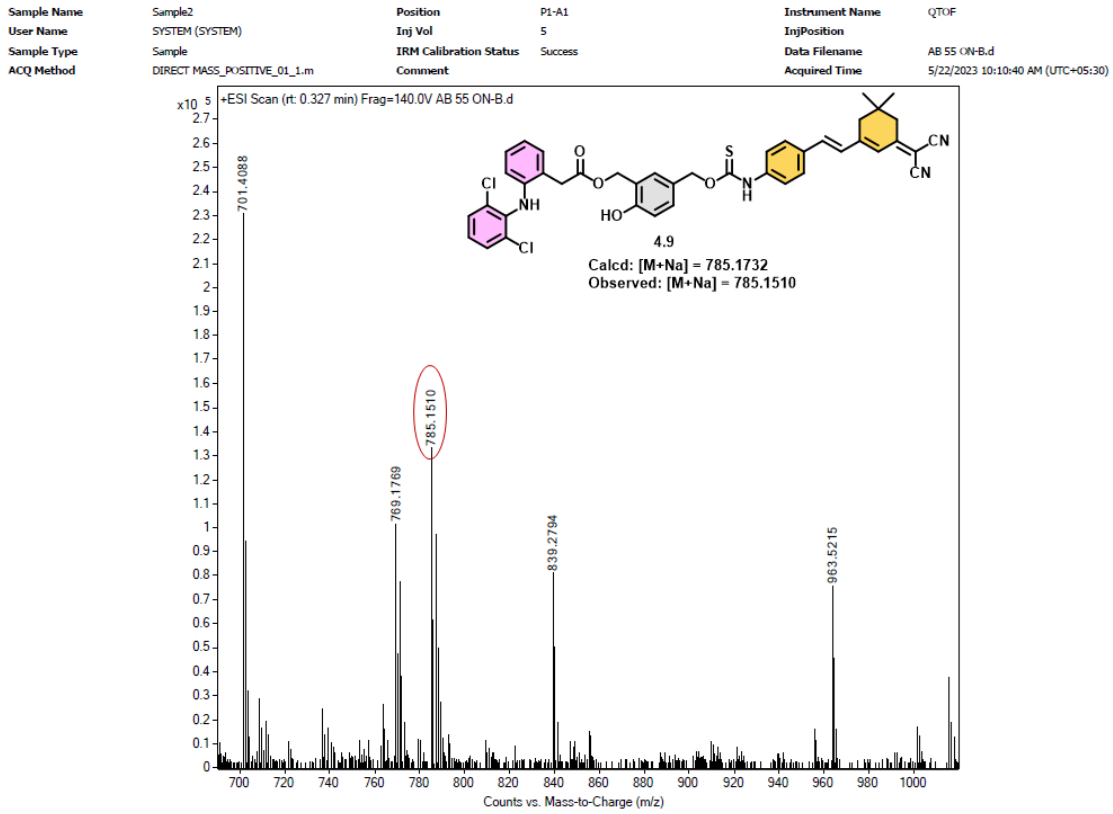

Figure A5.21. ESI-MS spectrum of the reaction mixture of **DCF-HS** with H_2O_2 showing the presence of intermediate **4.9**. ESI-MS (+ve) *m/z* calcd for $C_{42}H_{36}Cl_2N_4NaO_4S$ $[M + Na]^+$: 785.1732; observed = 785.1510.

TH-3161_176122050

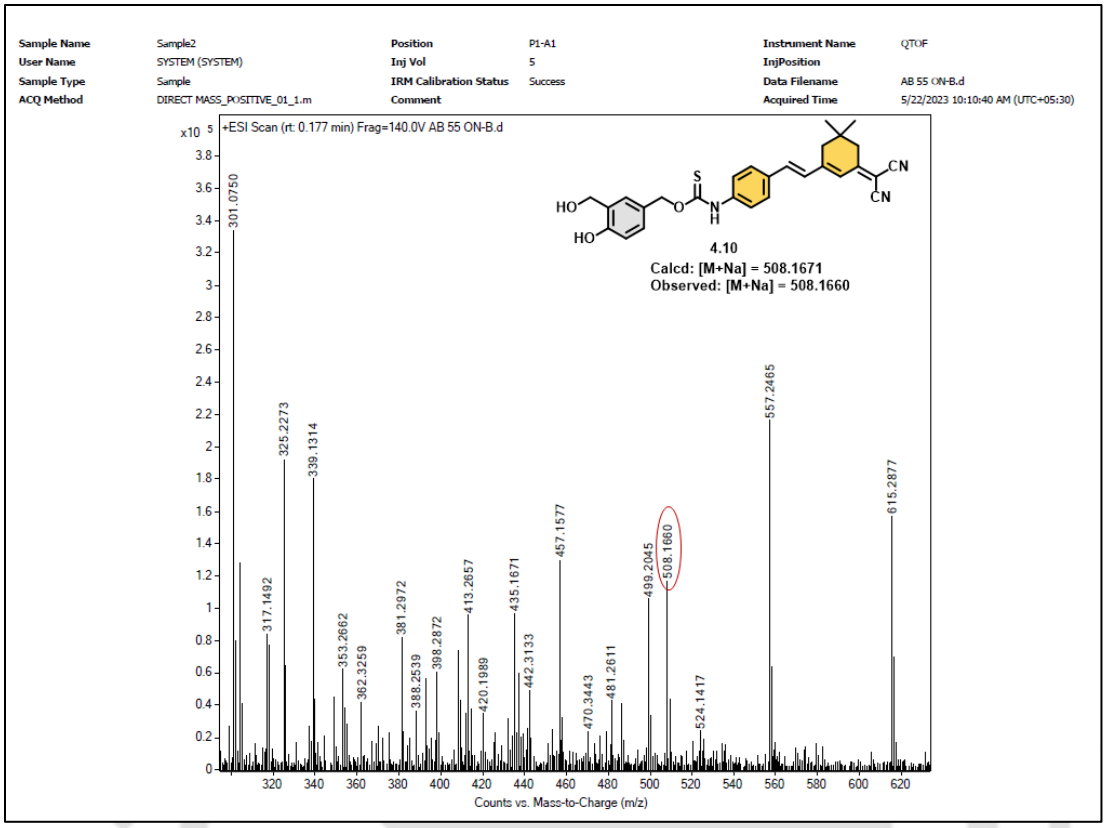

Figure A5.22. ESI-MS spectrum of the reaction mixture of **DCF-HS** with H_2O_2 showing the presence of intermediate **4.10**. ESI-MS (+ve) *m/z* calcd for $C_{28}H_{27}N_3NaO_3S$ $[M + Na]^+$: 508.1671; observed = 508.1660.

TH-3161_176122050

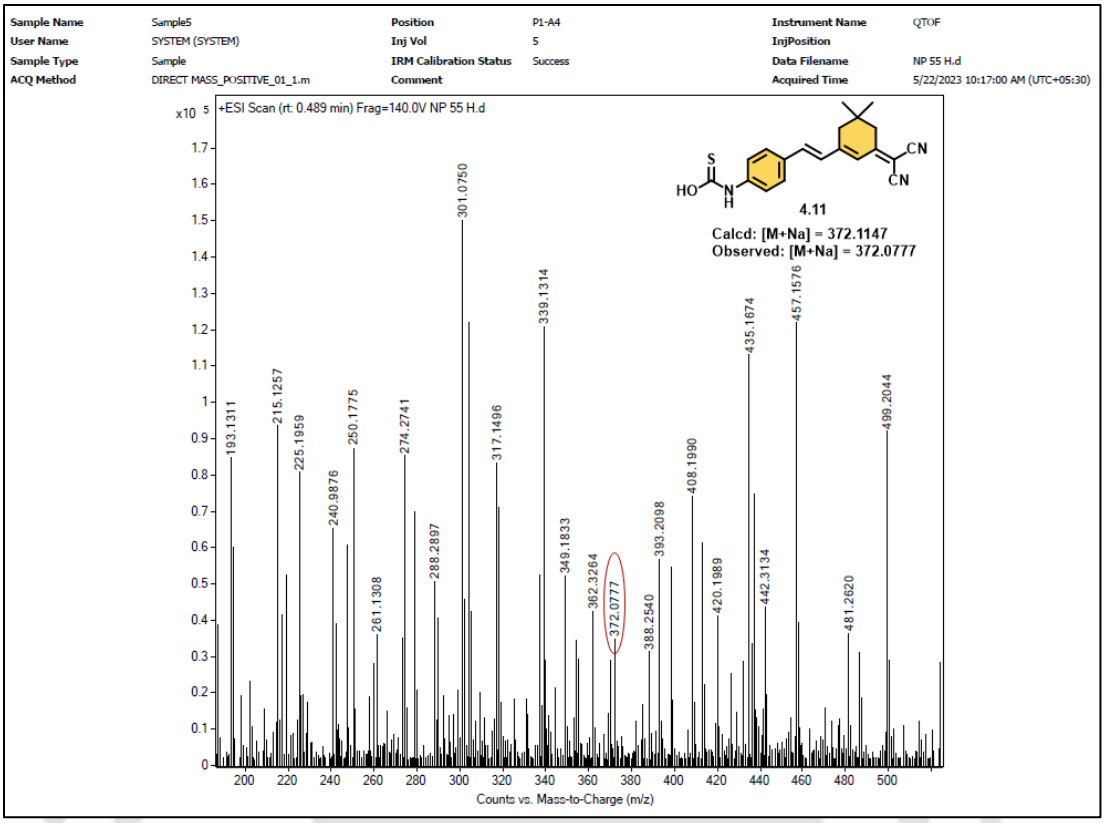

Figure A5.23. ESI-MS spectrum of the reaction mixture of **DCF-HS** with H_2O_2 showing the presence of intermediate **4.11**. ESI-MS (+ve) *m/z* calcd for $C_{20}H_{19}N_3NaOS$ $[M + Na]^+$: 372.1147; observed = 372.0777.

TH-3161_176122050

TH-3161_176122050

Supplementary data of chapter 5

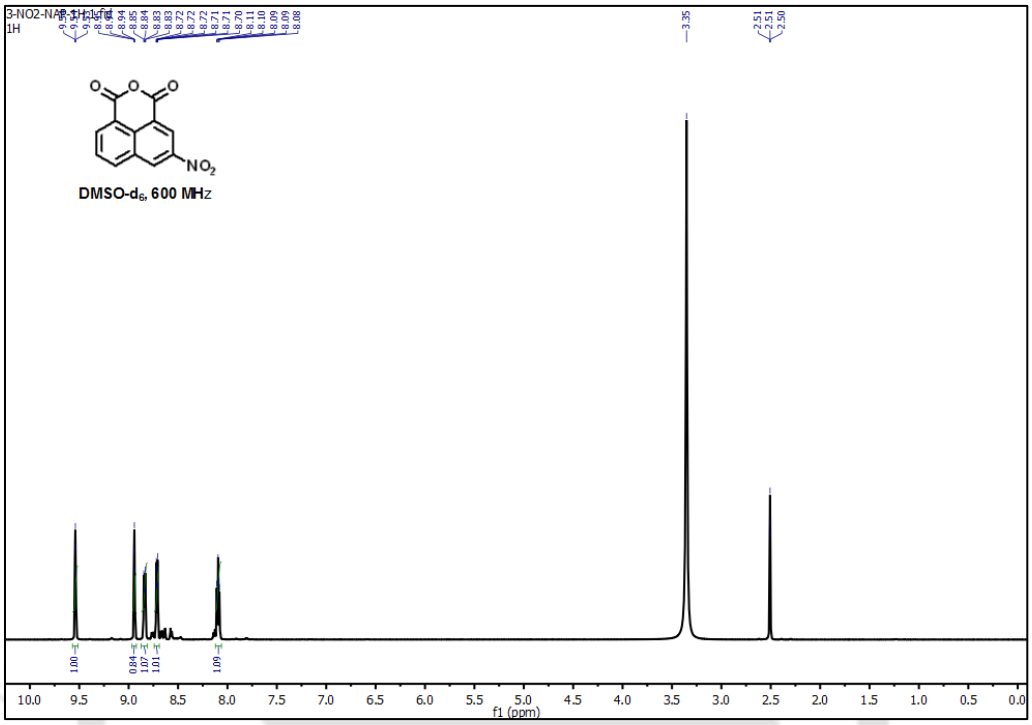

Figure A6.1: ^{1}H NMR spectrum (DMSO-d$_6$, 600 MHz, ppm) of compound **5.5**.

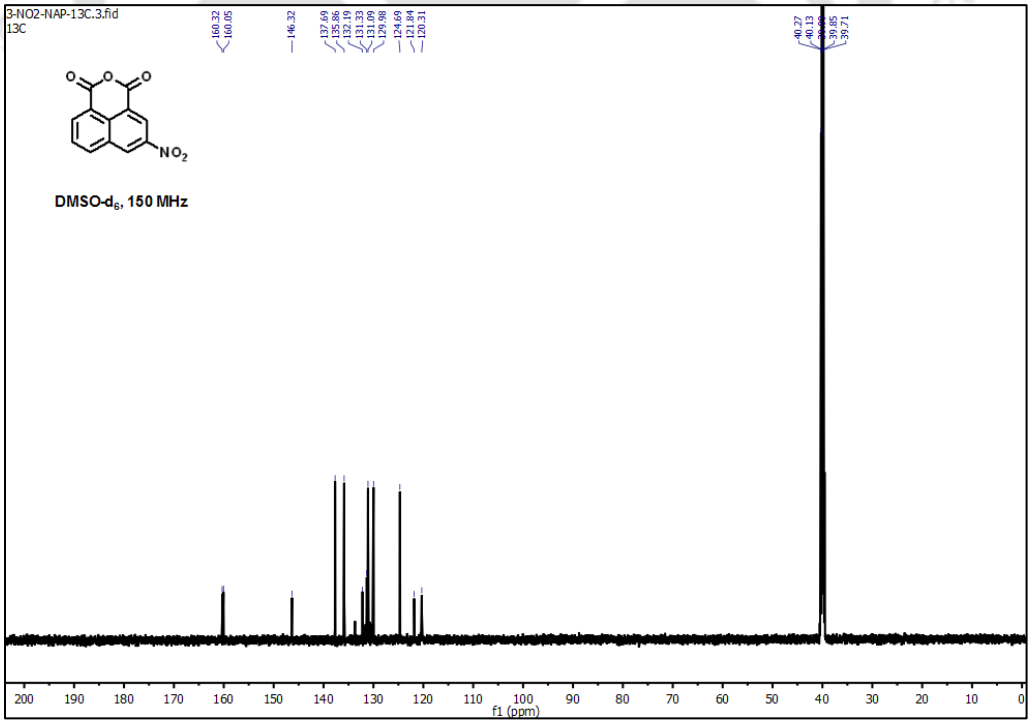

Figure A6.2: ^{13}C NMR spectrum (DMSO-d$_6$, 150 MHz, ppm) of compound **5.5**.

TH-3161_176122050

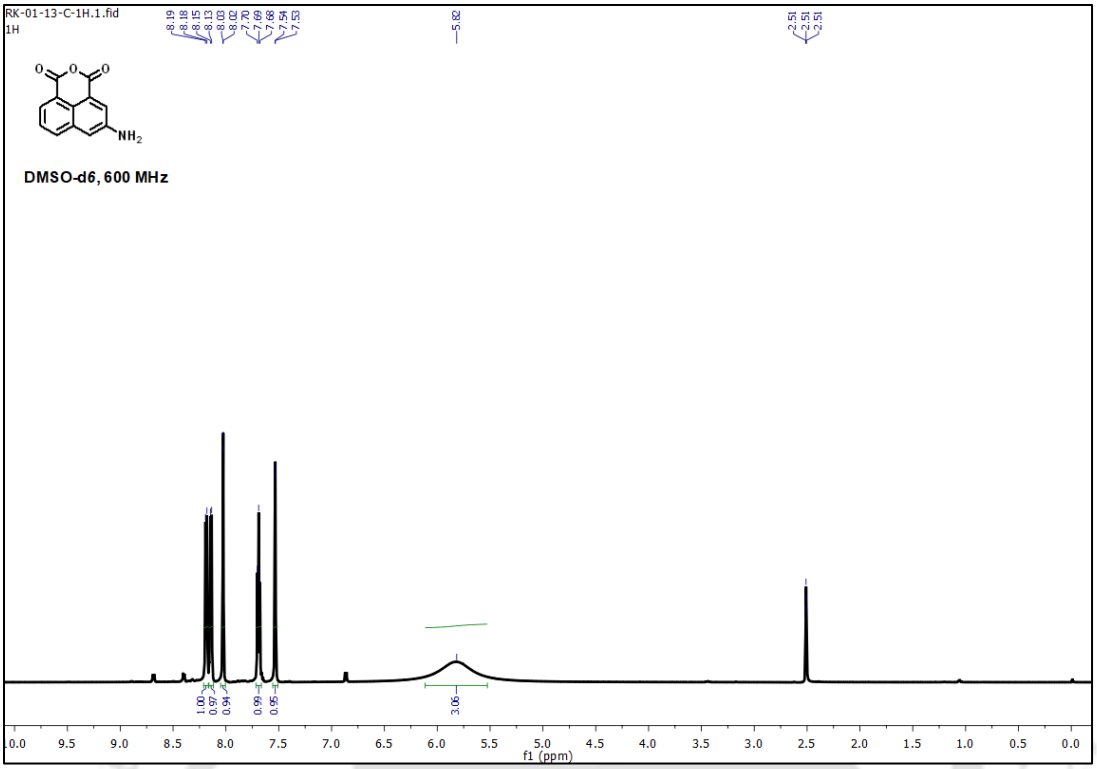

Figure A6.3: ^{1}H NMR spectrum (DMSO-d$_6$, 600 MHz, ppm) of compound **5.6**.

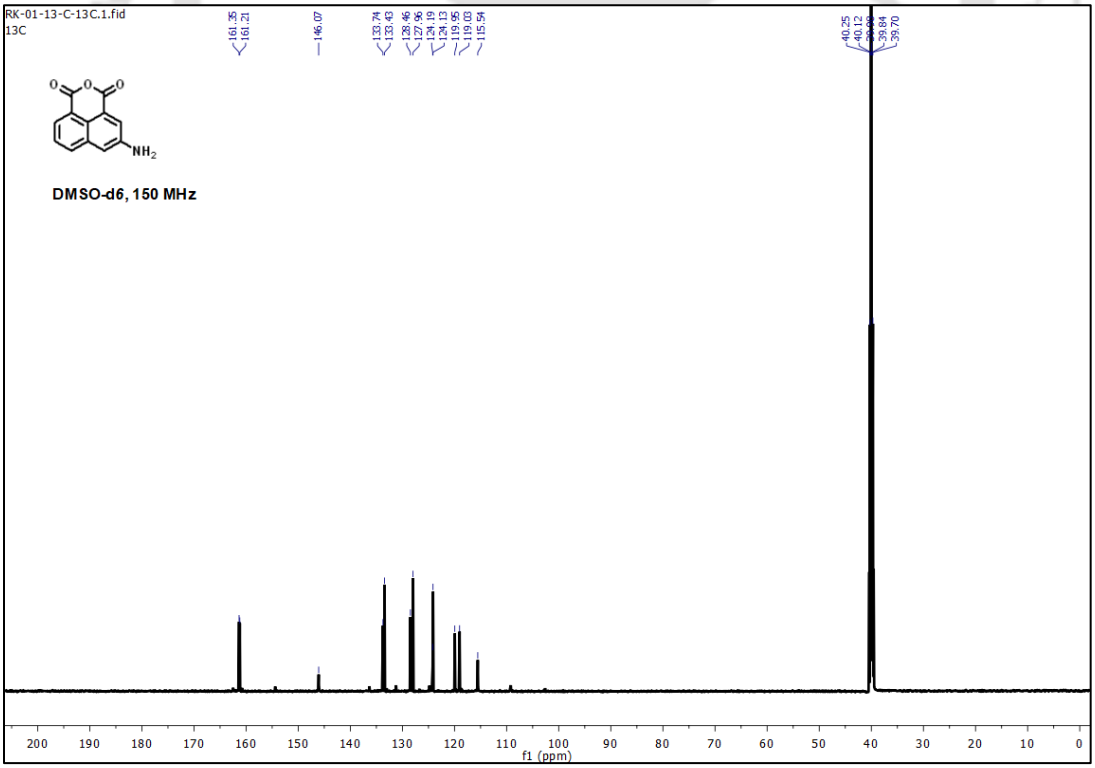

Figure A6.4: ^{13}C NMR spectrum (DMSO-d$_6$, 150 MHz, ppm) of compound **5.6**.

TH-3161_176122050

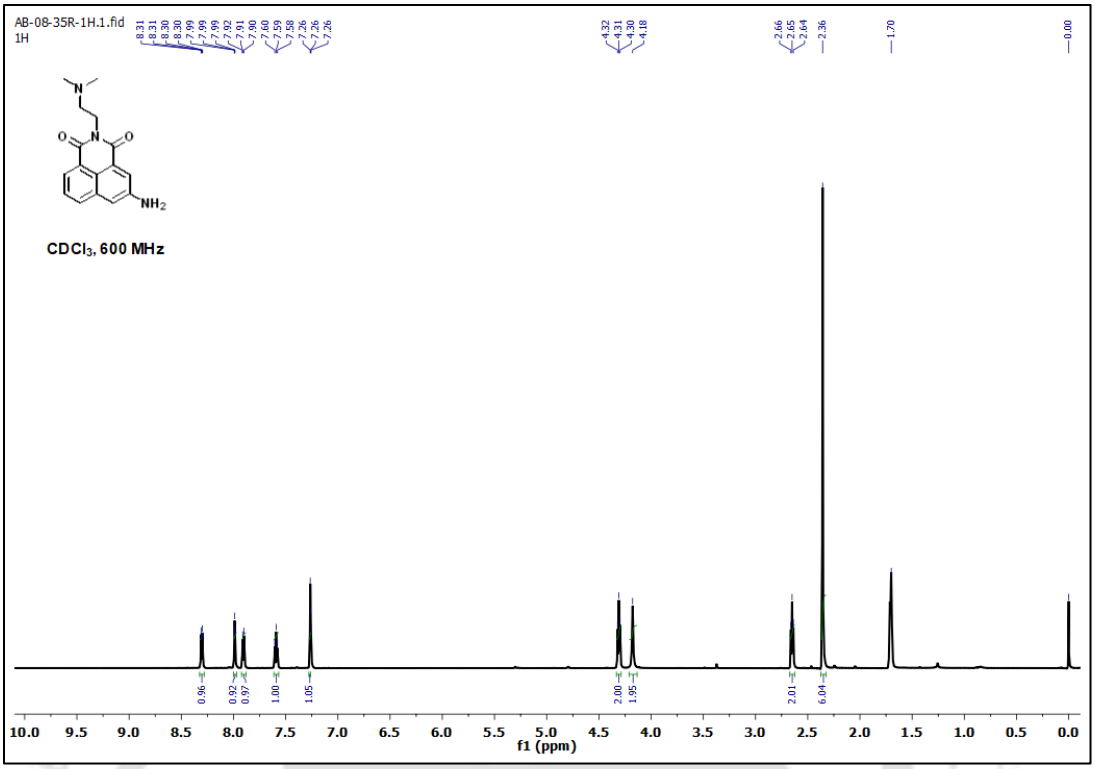

Figure A6.5: ^{1}H NMR spectrum ($CDCl_3$, 600 MHz, ppm) of amonafide.

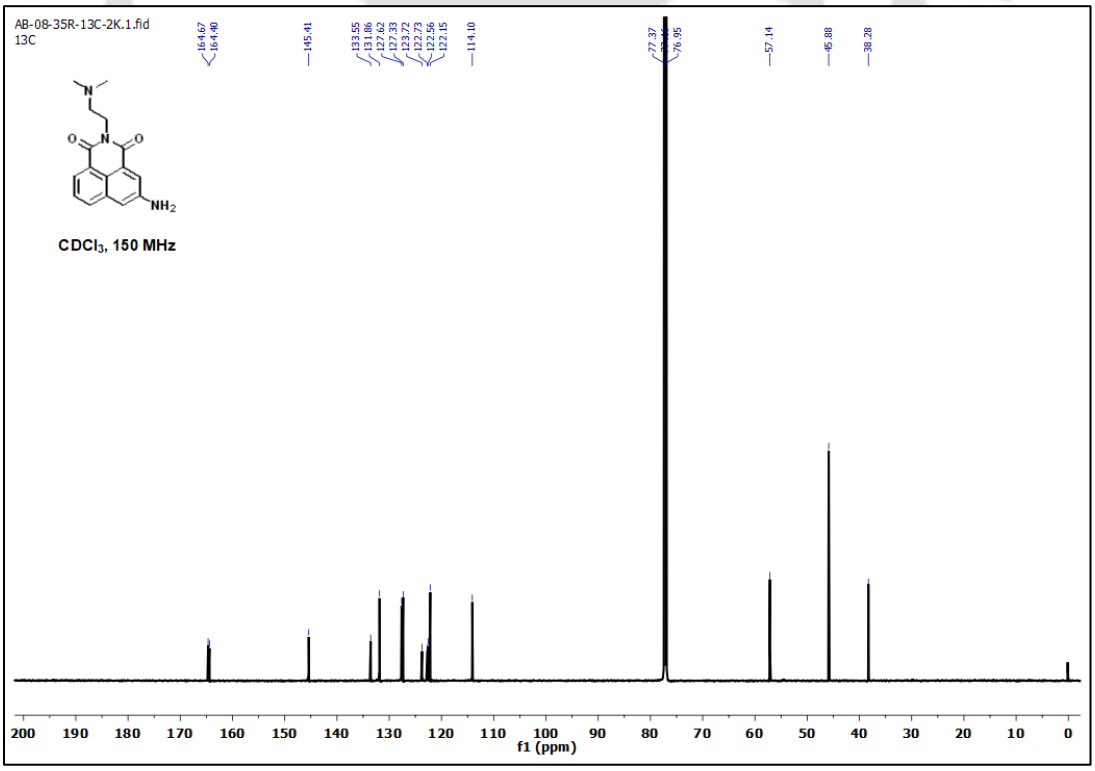

Figure A6.6: ^{13}C NMR spectrum ($CDCl_3$, 150 MHz, ppm) of amonafide.

TH-3161_176122050

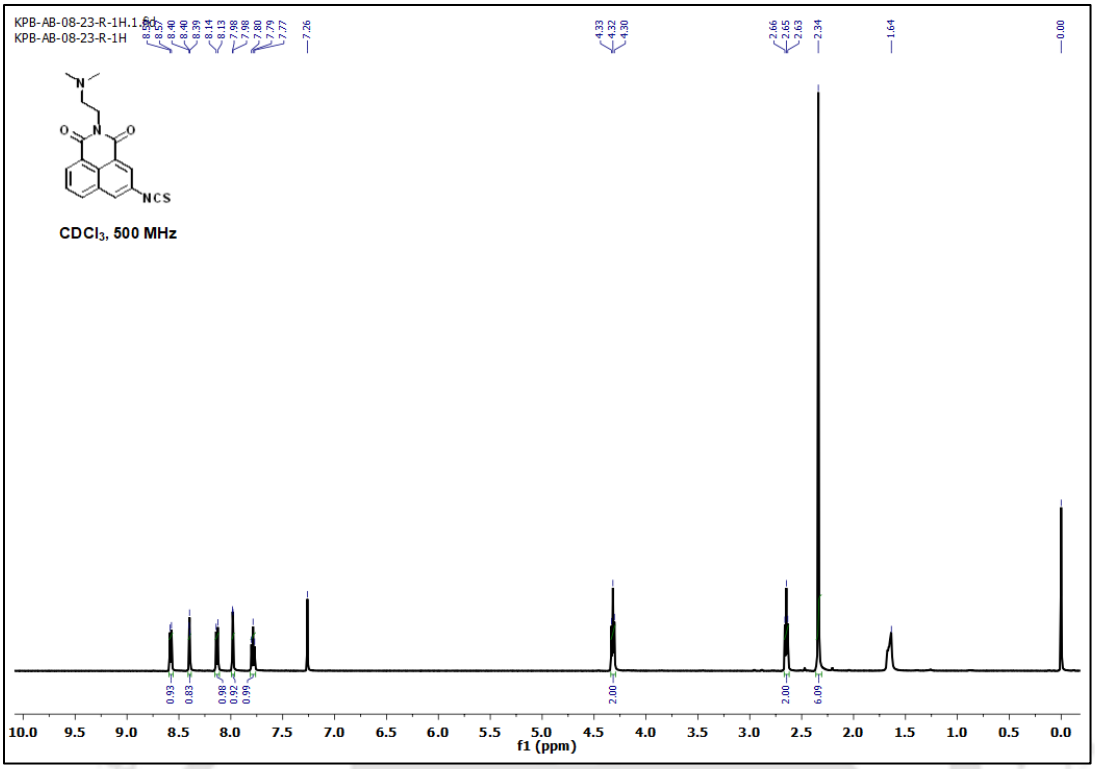

Figure A6.7: ^{1}H NMR spectrum ($CDCl_3$, 500 MHz, ppm) of compound **5.7**.

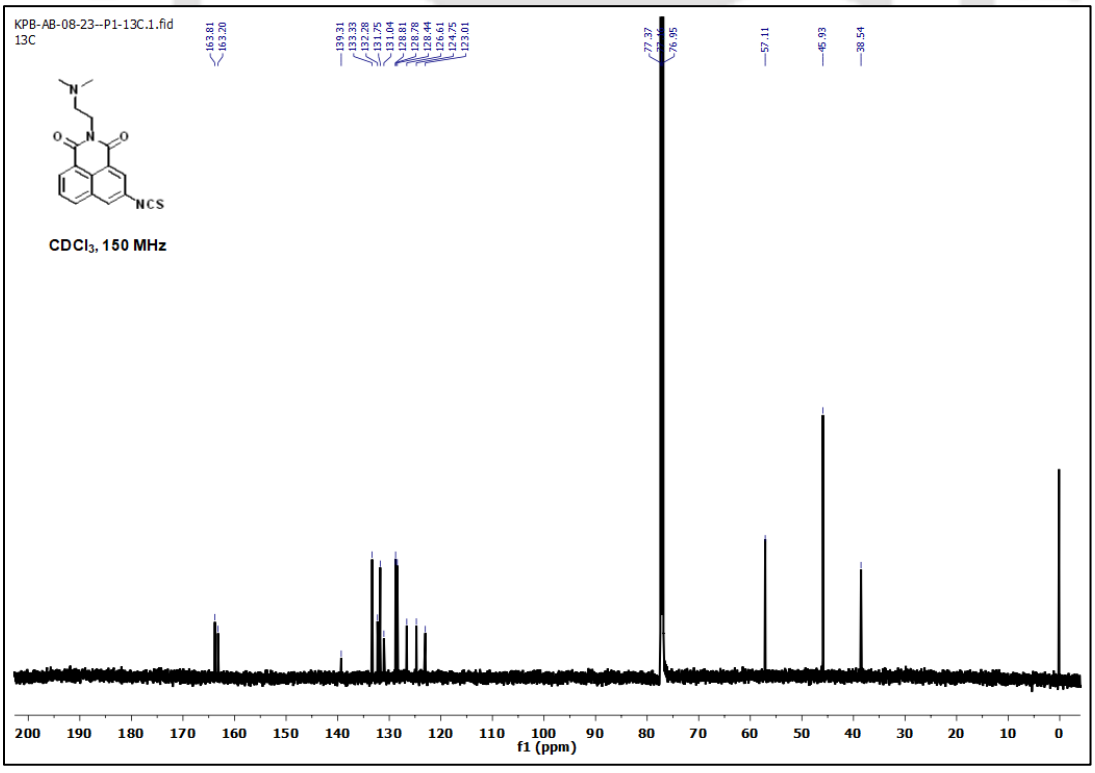

Figure A6.8: ^{13}C NMR spectrum ($CDCl_3$, 150 MHz, ppm) of compound **5.7**.

TH-3161_176122050

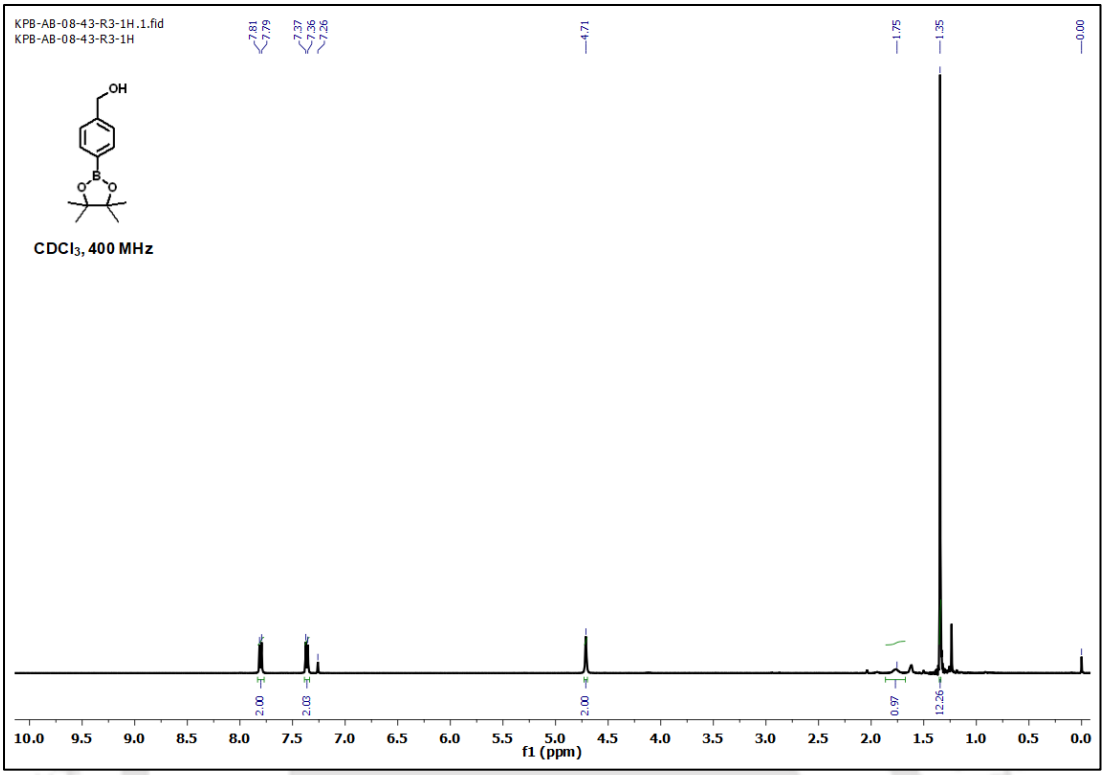

Figure A6.9: ^{1}H NMR spectrum ($CDCl_3$, 400 MHz, ppm) of compound **5.9**.

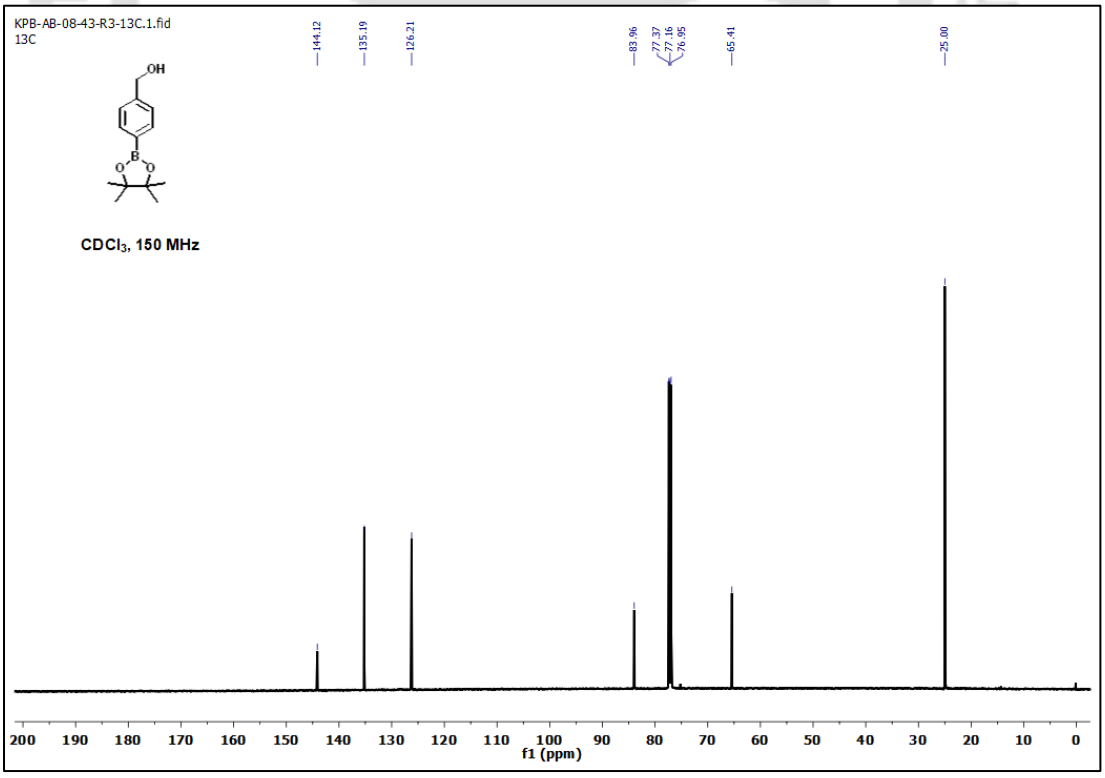

Figure A6.10: ^{13}C NMR spectrum ($CDCl_3$, 150 MHz, ppm) of compound **5.9**.

TH-3161_176122050

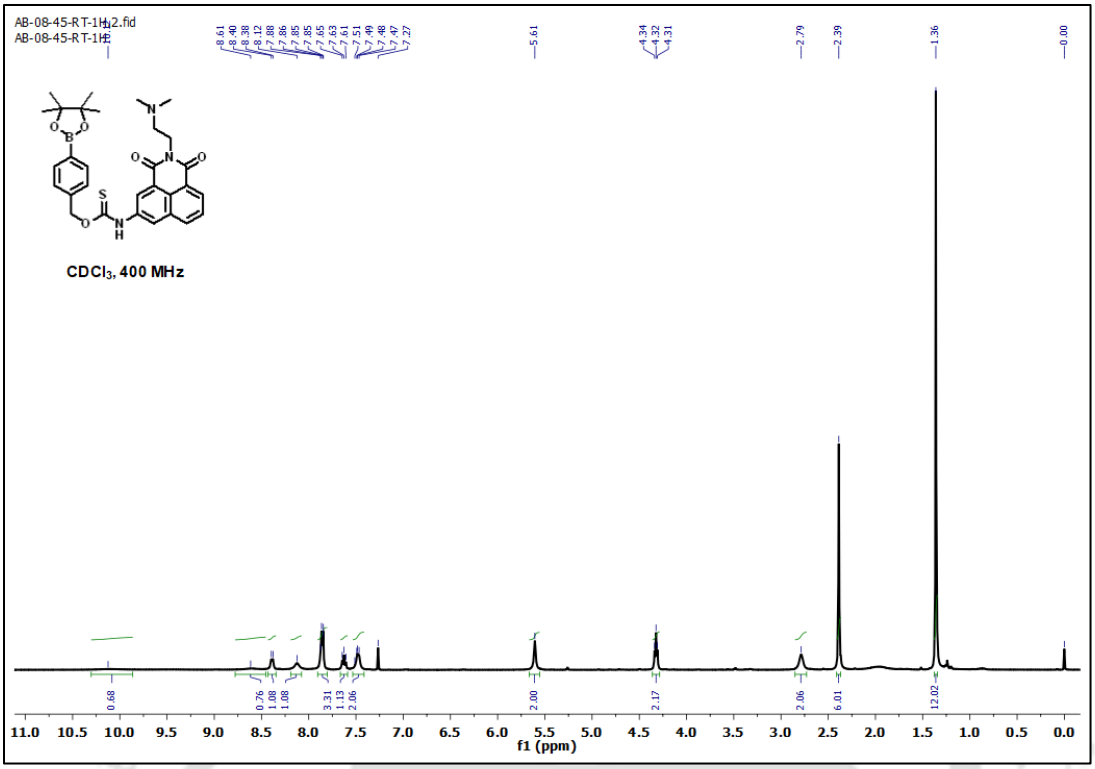

Figure A6.11: ^{1}H NMR spectrum ($CDCl_3$, 400 MHz, ppm) of **AM-TCB**.

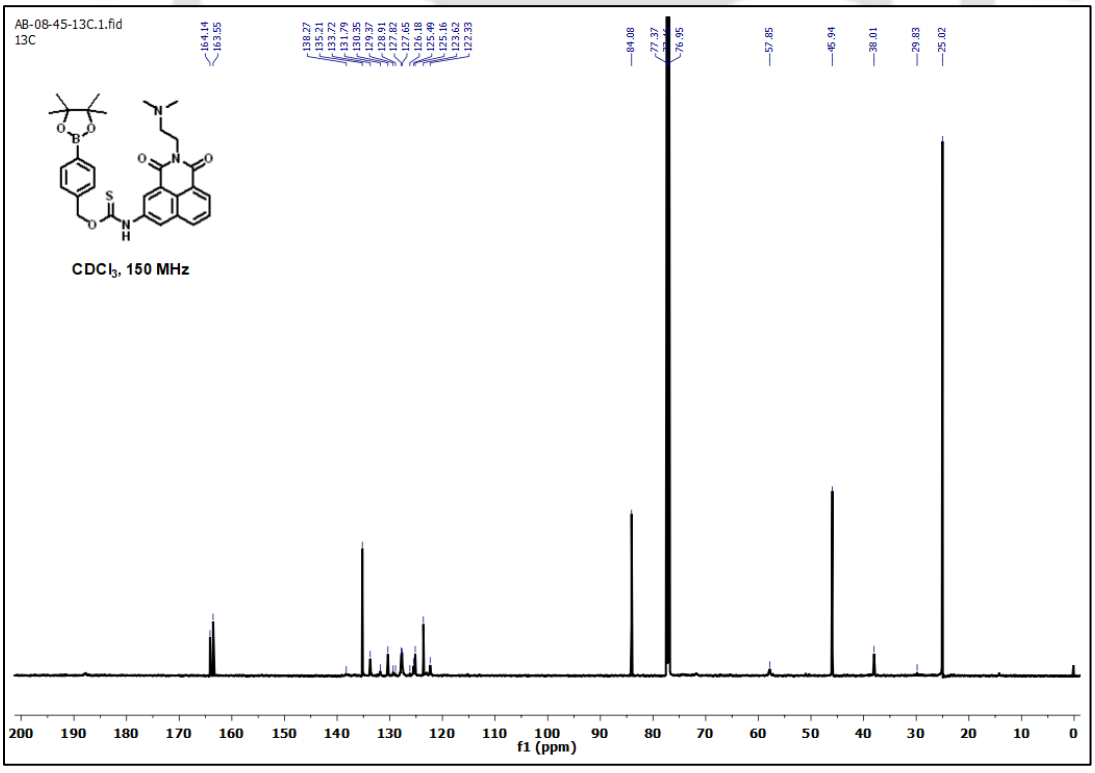

Figure A6.12: ^{13}C NMR spectrum ($CDCl_3$, 150 MHz, ppm) of **AM-TCB**.

TH-3161_176122050

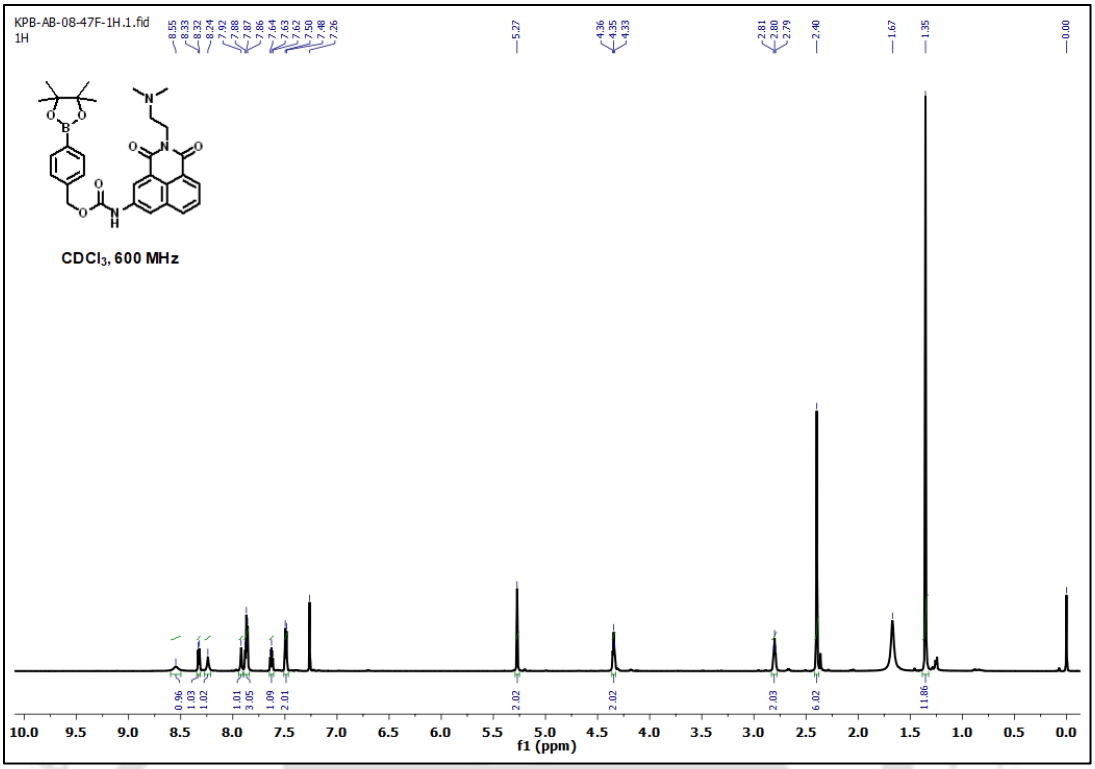

Figure A6.13: ^{1}H NMR spectrum ($CDCl_3$, 600 MHz, ppm) of **AM-CB**.

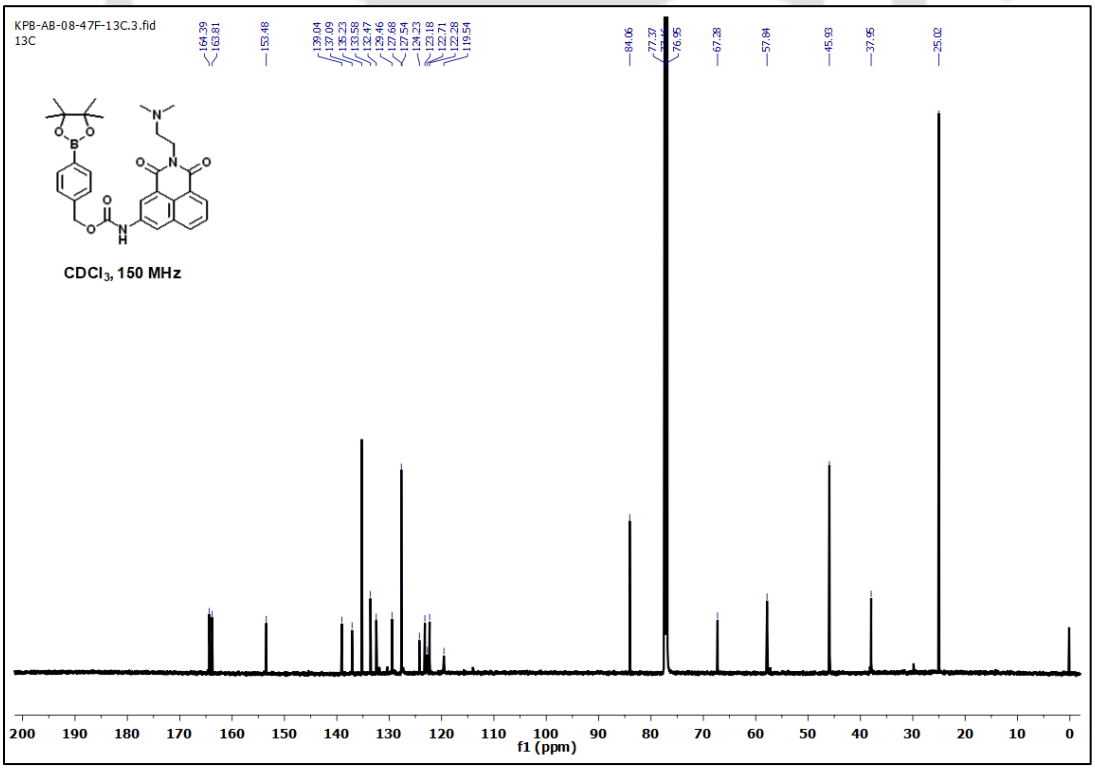

Figure A6.14: ^{13}C NMR spectrum ($CDCl_3$, 150 MHz, ppm) **AM-CB**.

TH-3161_176122050

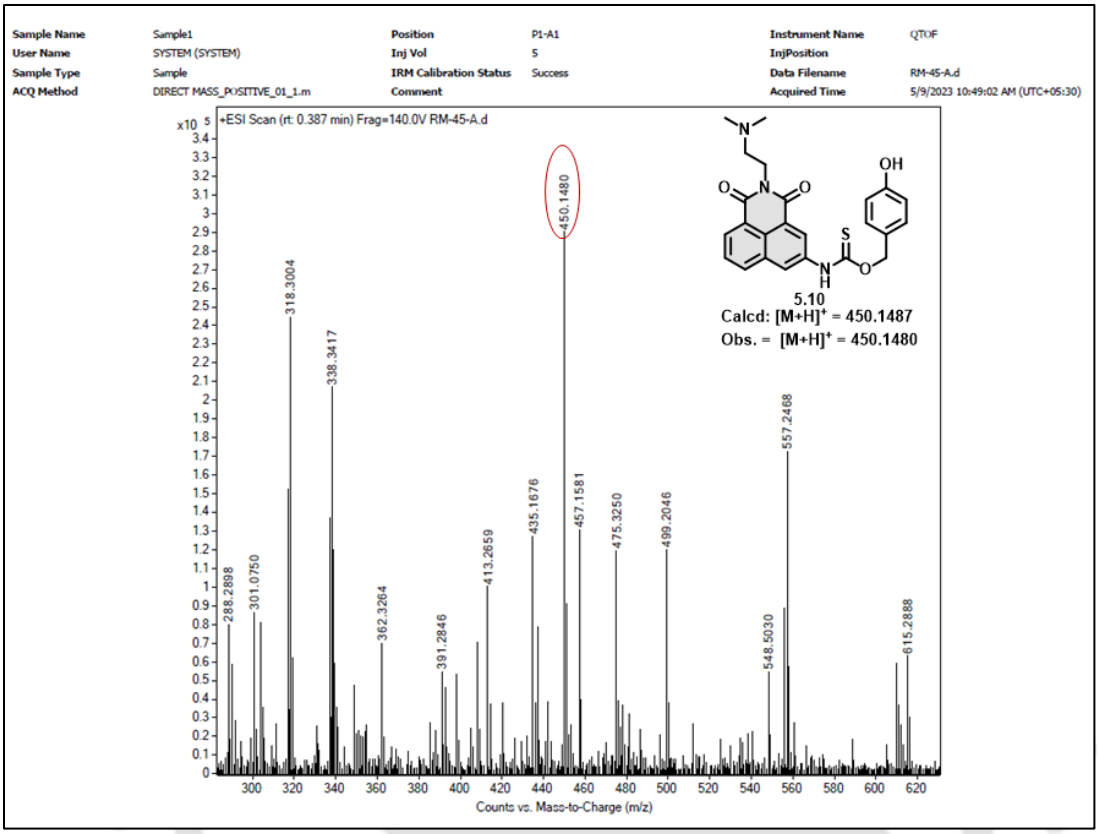

Figure A6.15. ESI-MS spectrum of the reaction mixture of **AM-TCB** with H_2O_2 showing the presence of intermediate **5.10**. ESI-MS (+ve) *m/z* calcd for $C_{24}H_{24}N_3O_4S$ $[M + H]^+$: 450.1487; observed = 450.1480.

TH-3161_176122050

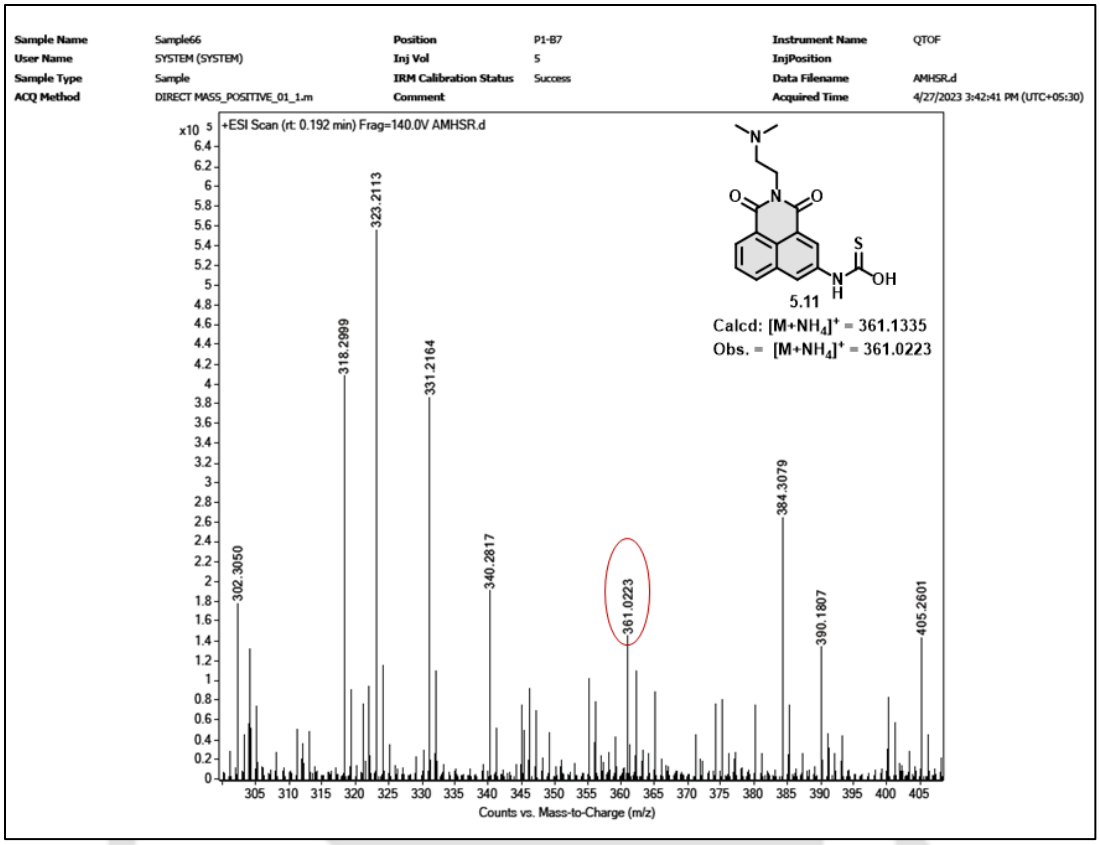

Figure A6.16. ESI-MS spectrum of the reaction mixture of **AM-TCB** with H_2O_2 showing the presence of intermediate **5.11**. ESI-MS (+ve) *m/z* calcd for $C_{17}H_{21}N_4O_3S$ $[M + NH_4]^+$: 361.1335; observed = 361.0223.

TH-3161_176122050